HAL
open science

Determination of the cosmological parameters in the framework of the Friedmann-Lemaître model

Dyaa Chbib

To cite this version:

Dyaa Chbib. Determination of the cosmological parameters in the framework of the Friedmann-Lemaître model. Physics [physics]. Aix-Marseille Université, Faculté des Sciences – Luminy, Centre de Physique Théorique - UMR 7332, 2017. English. NNT : . tel-01851540

HAL Id: tel-01851540

https://theses.hal.science/tel-01851540

Submitted on 30 Jul 2018

HAL is a multi-disciplinary open access archive for the deposit and dissemination of scientific research documents, whether they are published or not. The documents may come from teaching and research institutions in France or abroad, or from public or private research centers.

L'archive ouverte pluridisciplinaire **HAL**, est destinée au dépôt et à la diffusion de documents scientifiques de niveau recherche, publiés ou non, émanant des établissements d'enseignement et de recherche français ou étrangers, des laboratoires publics ou privés.

AIX-MARSEILLE UNIVERSITÉ
ECOLE DOCTORALE 352
FACULTÉ DES SCIENCES - LUMINY
CENTRE DE PHYSIQUE THÉORIQUE-UMR 7332

Thèse présentée pour obtenir le grade universitaire de docteur

Discipline : Physique et Sciences de la Matière
Spécialité : Astrophysique et cosmologie

Dyaa Chbib

Détermination des paramètres cosmologiques dans le cadre du modèle de Friedmann-Lemaître

Soutenue le 15/12/2017 devant le jury :

Marc Lachièze-Rey	Université de Paris 7	**Rapporteur**
Pierre Astier	Université de Paris 7	**Rapporteur**
Roser Pello	Université de Paul Sabatier	**Examinateur**
Anne Ealet	Université d'Aix-Marseille	**Examinateur**
André Tilquin	Université d'Aix-Marseille	**Invité**
Thomas Schücker	Université d'Aix-Marseille	**Invité**
Roland Triay	Université d'Aix-Marseille	**Directeur de thèse**

Résumé

Un siècle après le modèle d'univers de Friedmann-Lemaître, les observations le confortent avec une constante cosmologique Λ et une composante de matière sombre (noire) sans pression (poussière) et froide dominant celle baryonique, que l'on désigne par modèle ΛCDM ou encore modèle standard. L'accélération de l'expansion de l'Univers confirmée par le diagramme de Hubble des supernovae en 1998 impose une valeur strictement positive à la constante cosmologique.

Mes travaux de thèse se focalisent sur l'estimation des valeurs de paramètres cosmologiques du modèle standard en utilisant la technique de corrélation nulle. Cette approche présente l'avantage d'être plus robuste que les techniques usuelles. En particulier, il n'est pas requis de préciser la fonction de luminosité, celle-ci est déduite par cette méthode. De plus, elle prend en compte le biais de Malmquist due à la limitation en magnitude apparent. Ce travail a consisté aussi à modéliser des échantillons de l'événement quasar ainsi que l'événement supernova, une extrapolation adaptée du premier. Ce qui a permis de générer des échantillons conformes aux hypothèses des modèles, afin de valider les approches statistiques. Nous avons exploité les données du Sloan Digital Sky Survey (SDSS) pour les quasars, et celles du SuperNova Legacy Survey (SNLS) et du SDSS-II pour les supernovae. Les inférences statistiques ont conduit à un univers spatialement fermé et une présence de matière noire plus faible.

Dans le cadre d'une prochaine application de cette technique, elle sera utilisée pour contraindre les modèles d'énergie noire. De même, l'utilisation des amas de galaxies observées grâce à l'effet de Sunyaev Zel'dovich, servira d'échantillon cosmologique. Une telle étude pourra contribuer à apporter un élément de réponse à la validité du rôle supposé des neutrinos massifs dans la formation des amas dans l'ère primordiale de l'Univers.

Mots Clés : Cosmologie, Matière noire, Énergie noire, paramètres cosmologiques, statistiques, simulation, quasars, supernovæ, diagramme de Hubble.

Abstract

A century after the Universe model of Friedmann-Lemaître, the observations comfort it with a cosmological constant Λ and a dark matter component without pressure (dust) and cold dominating the baryonic one, which is denoted by ΛCDM model or standard model. The acceleration of the expansion of the Universe confirmed by the Hubble diagram of the supernovae in 1998 imposes a strictly positive value on the cosmological constant.

My thesis work focuses on the estimation of the cosmological parameters values of the standard model using the null correlation technique. This approach has the advantage of being more robust than the usual techniques. In particular, it is not necessary to specify the luminosity function, it is derived from the data analysis. In addition, it accounts for the Malmquist bias due to selection effects on apparent magnitude. This work deals with modelling samples of the quasar event and the supernova event, which enables us to generate samples in order to validate the statistical approaches. We used data from the Sloan Digital Sky Survey (SDSS) for quasars, and the SuperNova Legacy Survey (SNLS) and SDSS-II for supernovae. The Statistical inferences suggest a Universe spatially Closed and a weaker presence of dark matter than that in the Standard model.
Such a statistical analysis can be used to constrain dark energy models.

Application of this technique might be useful for analyzing of clusters of galaxies observed through the effect of Sunyaev Zel'dovich, in view of deriving the cosmological model and provide an answer to the question of the contribution of massive neutrinos in the formation of clusters in the primordial era of the Universe.

Key Words: Cosmology, dark matter, dark energy, cosmological parameters, statistics, simulation, quasars, supernovæ, Hubble diagram.

Remerciements

Je tiens à remercier mon directeur de thèse Roland Triay pour m'avoir proposé un sujet de thèse en cosmologie. Je souhaite remercier tous les membres de jury de thèse pour avoir accepté de donner de leur temps pour évaluer mes travaux. En particulier, les deux rapporteurs, Pierre Astier et Marc Lachièze-Rey, pour leurs retours sur le manuscrit. Je souhaite aussi remercier Thierry Martin, directeur de l'unité de recherche UMR7332, qui a accepté de m'accueillir dans leur unité pour effectuer cette thèse.

Je souhaite également exprimer mes remerciements à l'ancien responsable d'informatique du labo, Vincent Bayle, pour son aide d'installation de plusieurs modules au début de ma thèse.

Je remercie mes colocs (Nadim, Jérôme, Ibtisem, Marie, Michelle) avec qui j'ai passé des belles années à Marseille, je n'oublie pas les bonnes soirées au vieux port après un long jour de travail, et aussi les belles randonnées dans les calanques pendant les weekends! Je vous souhaite la réussite dans vos vies personnelles et professionnelles.

Je remercie particulièrement ma famille pour son soutien pendant toute la durée de mes études et surtout dans les derniers moments de ma thèse. Merci pour vos sentiments, confiances, conseils, aides... À tout moment difficile vous étiez là pour me soutenir, grand merci. Je souhaite le meilleur pour chacun de vous dans sa carrière et sa vie.

Pour finir, je remercie ma fiancée, qui était toujours présente et proche pour rendre ma vie joyeuse et m'aider à dépasser toutes les difficultés. Merci pour la joie que tu fais dans ma vie et pour les bons moments qu'on a passés ensemble ! Merci pour tous les projets qu'on a rêvé à réaliser dans notre future !

Contents

1 Basics of Observational Cosmology **3**

1.1 Introduction 4
1.2 Newtonian cosmology 4
1.3 Einstein's cosmology 5
1.4 The Friedmann-Lemaître-Gamow model 6
1.4.1 The Friedmann's equations 7
1.4.2 Primordial Universe 8
1.5 Contents of the Universe 9
1.6 Baryonic Acoustic Oscillations 13
1.7 Dark matter 13
1.8 The Dark Energy 14
1.8.1 Models with Scalar Fields 15
1.8.2 The Cosmological Constant 16
1.9 Hubble diagram and measure of distances 16
1.9.1 The Comoving Distance 18
1.9.2 The Age and the Conformal Time 20
1.9.3 The Luminosity Distance 20
1.10 The Magnitude Systems 21
1.10.1 The Apparent Magnitude 21
1.10.2 The Vega System 21
1.10.3 The AB System 21
1.11 Constrain the cosmological parameters 22
1.12 Conclusion 22

2 Quasars samples **23**

2.1 Introduction 23
2.2 Spectrum of quasar 24

2.3 Events in the space-time diagram 24
2.4 The selection effect 27
2.5 Modelling a sample of quasars 28
2.5.1 Statistical modelling 29
2.5.2 Simulation technique 29
2.5.3 The k-correction 34
2.6 Conclusion 35

3 The null correlation technique 37
3.1 Introduction 37
3.2 Weighting factors 40
3.3 Luminosity function and selection function 44
3.4 Kolmogorov-Smirnov test 46
3.5 The V/V_{max} test 47
3.5.1 Calculation of the V/V_{max} terms 48
3.6 Conclusion 50

4 Application to quasars data 51
4.1 Introduction 51
4.2 The Sloan Digital Sky Survey data 52
4.2.1 The k-correction 53
4.3 Results 54
4.3.1 The null correlation test 54
4.3.2 The V/V_{max} test 57
4.3.3 Estimation of the luminosity function and the selection function 60
4.4 Inferences on cosmological expansion based on QSOs 61
4.5 Conclusion 79

5 Application to supernovae type Ia sample 81
5.1 Introduction 81
5.2 Type Ia Supernovae as standard candles 82
5.2.1 The lightcurve of type-Ia SN 83
5.2.2 Standardisation of type-Ia SN 84
5.2.3 Modelling of the Supernova event 86
5.2.4 Sampling the light curve of type-Ia SN and selection effects 88
5.2.5 Calibration statistics 90
5.2.6 Simulation 94
5.3 The null correlation test on the supernova sample 98
5.3.1 Luminosity function and Selection function 100
5.3.2 Precision and error 101
5.4 Application to the JLA sample 101
5.4.1 Description of samples 102

5.4.2 Results 103
5.5 Conclusion 107

6 Résumé en français **113**
6.1 La cosmologie moderne 115
6.2 Simulation d'échantillon de quasar 118
6.3 La technique de corrélation nulle 120
6.4 Résultats avec les données quasars 121
6.5 Modélisation d'échantillon de supernova et résultats sur les données de SDSS-II/SNLS3 122

Appendices **127**

A Probability density functions **129**

B Calculation of the weighting factor **131**

C Calculation of V(M) **133**

D Code Python **135**

List of Figures

1.1 This image shows the Cosmic Microwave Background as seen by ESA's Planck satellite (upper right half) and by its predecessor, NASA's Wilkinson Microwave Anisotropy Probe (lower left half). The colors represent the temperature fluctuations. Red (res. blue) corresponds to warm (resp. cold) regions. Image taken from the website of ESA and the Planck Collaboration . . 9

1.2 The CMB power spectrum obtained with Planck 2015. Top: Agreement of the flat standard model of cosmology ΛCDM with the observation data from the temperature release of the Planck satellite. Residuals with respect to this model are shown in the bottompanel [Planck Collaboration XIII (2015)]. 10

1.3 Scale at which the hypothesis of a spatial uniform distribution of gravitation sources becomes valid is roughly above 100 Mpc, according to the distribution of a large number of galaxies with 2dF survey. The figure shows the large-scale structures, which are less visible with distance from the orbserver. The Milky Way is located at the intersection of the two slices of the observed sky [M. Colless 2003]. 11

1.4 The spatial distribution of the quasars of the BOSS catalog shows a radial stratification due to four distinct phases of observations, and in each of sub-samples a decrease in the number of objects as the radius increases. By taking into account this selection effect, one can safely guess that this distribution is uniform. Figure credit: universetoday website. 11

1.5 Confidence contours in the $(\Omega_M, \Omega_\Lambda)$ plan obtained by the Supernova Cosmology Project with observations of 42 SNe Ia [S. Perlmutter et al. 1999]. 15

1.6 Evolution of the densities of radiation Ω_γ, of radiation Ω_m, and of the cosmological constant Ω_Λ with respect to the expansion factor. The different periods indicated by the dashed lines correspond to the Planck scale, the electroweak symmetry breaking (EW), the Big Bang nucleosynthesis (BBN) and the present epoch (Now). Credit: [S. Carroll 2004]. 17

1.7 The Hubble diagram showing the expansion of the Universe. The radial velocity of stars, corrected for solar motion plotted against the distance estimated from the stars and the average of brightness of galaxies in a cluster. Credit: [E. Hubble 1929]. 18

1.8 The Hubble diagram of the Supernovae samples with the SNLS, SDSS, HST and several low-z surveys. Credit: [Betoule, M. et al 2014]. 19

1.9 From top left to bottom right: The comoving distance, the luminosity distance, the distance modulus and the comoving volume versus the redshift for six different cosmological models. 22

2.1 Diagram unifying different astrophysical types of AGN (blazars, quasars, seyfert galaxies) depending on the inclination angle with respect to the line of sight of the dust torus surrounding the same central engine (Noted in green). The various components of AGN (noted in white): A luminous accretion disk which surrounds the central black hole. Broad emission lines which are due to clouds orbiting above the disk. A thick dusty torus which obscures the broad-line region from transverse lines-of-sight. Narrow emission lines which are originated from irradiated clouds so far from the central source. Credit: [C. M. Urry, P. Padovani, 1995] 25

2.2 Spectrum of quasar at rest frame determined by the SDSS survey. The dashed thin and thik lines are the power-law fits to the estimated continuum flux. Credit: [D. Berk, et al 2001]. . . 26

2.3 Spectrum of quasar SDSS 1044-0125 at redshift 5.8. The optical Lyman-α emission (1215 Å) is shifted into near Infra-Red $\sim$ 8230 Å. 26

2.4 The spacetime diagram (conformal time η versus comoving space) : The red filled circle stands for our present position. The world lines of sources are vertical (perennial - black) and (ephemeral - blue), they cross the past light cone of the observer for observed objects. These ones are characterized by an absolute magnitude M and a comoving volume V for the perenial ones, and also by a lifetime duration $\Delta\eta$ for ephemeral ones. 27

2.5 Similar to Fig.2.4 showing the appearance (blue)/disappearance (green) of new/existing supernovae due to the intersection/out of intersection of the light cone with their limited lifetime. . . . 28
2.6 The blue curve gives the maximum volume $v_{max}(M)$ around the observer up to which an object with absolute magnitude M can be observed by using a device that detects up to a limiting apparent magnitude m_{lim}. 31
2.7 Simulation of a QSOs sample complete up to a limiting apparent magnitude. The blue curve caracterizes the threshold on apparent magnitude. The distribution of simulated sources (red) is uniform with respect to comoving volume (V) and Gaussian with respect to absolute magnitude (M). 32
2.8 A complete sample up to redshift z_{max} with $(\Omega_\circ, \lambda_\circ = 0.3, 0.7)$. A uniform distribution appears in vertical axis and a Gaussian distribution in the horizontal axis. 33
2.9 Distributions of a complete sample up to redshift z_{max} and limiting magnitude m_{lim}, by disentangling the visible objects (blue) from those that are not visible (red). A): Histogram of absolute magnitudes. B): M-V diagram. 34
2.10 A typical quasar spectrum at redshift z =5. The QSO can be observed in two bands thanks to the Lyα emission line which is in the i' band and the Lyα forest which is along of the r' band. Figure credit: [R. Sharp et al 2001]. 34

3.1 The distribution of the sample in both (x, y) and (X, Y) frames. 38
3.2 Searching the zero value of the weighted covariance of X and Y. The equation $\Gamma(\theta) = 0$ shows two solutions, the first one ($\theta = \frac{\pi}{4}$) matches the one used for simulation. 39
3.3 Data distribution in the (M, V) frame and (M, m) frame. 40
3.4 The inverse of the correlation function versus redshift for a given cosmological model. 41
3.5 The percentage of the lost of the statistical information (left: for $\mathcal{L}_1$, right: for $\mathcal{L}_0$) with respect to the parameter β. 42
3.6 The weighting factor with respect to the redshift for a given cosmological model. 42
3.7 Left to right, top to bottom. The values of the weighted covariance with respect to cosmological model. The null values of the NCC are found by horizontal and vertical interpolations in the covariance grid. The NCC in the ($\Omega_\circ$, $\lambda_\circ$) plane retrieve the initial simulation model (the filled red circle). 43
3.8 The shape of the NCC of two simulated samples with different sizes and different apparent magnitude limits. 43

3.9 The dependence of cosmological model on the NCC appears in these curves when we use two samples with same characteristics but with different cosmological models. 43
3.10 The precision of the method is shown obviously by increasing the size of the sample. From left to right and from top to bottom, the size of the sample increases from 35 to 350 to 2000 respectively. We see that the statistical fluctuations decrease with the increasing of the number of objects. 44
3.11 Statistics of the luminosity function (upper panels) and the selection function (lower panels) 45
3.12 Similar to Fig.3.11 but with a Gumbel distribution for the luminosity function. 46
3.13 Three cdf testing uniform distribution with Kolmogorov-Smirnov test. 46
3.14 The redshift range is not connected for this model with positive curvature $\kappa_\circ = 0.4$. The distance modulus $\zeta(z)$ of a source with absolute magnitude M has most likely two solutions and it cannot be observed in the hatched area. 49
3.15 Kolmogorov- Smirnov test (Likelihood of candidates). Search for the minimum of D_{max} (top left) as a function of $\lambda_\circ$, and (bottom right) as a function of $\Omega_\circ$, on the NCC (top right). . . . 50

4.1 The Sloan foundation 2.5m telescope Ritchey-Chretien type located at Apache Point Observatory, in south east New Mexico. . 52
4.2 Left: The k-correction of the SDSS-DR3 sample in the i-band including both the emission-line and continuum components, normalized at $z = 2$ with a fixed spectral index $\alpha_\nu = -0.5$. Right: The numerical derivative of k-correction with respect to the redshift z. 54
4.3 The null correlation curves corresponding to EDR, DR1, DR3, DR7 samples and DR3 subsamples. The curves are located in the region with positive curvature $\kappa_\circ > 0$ (above the straight line). All the curves give close candidate values for cosmological parameters excepted the one of EDR sample (red curve). 55
4.4 The absolute magnitude-volume diagram of the EDR sample. The left panel with $\Omega_\circ = 0.076$, $\lambda_\circ = 1.211$. The right panel with $\Omega_\circ = 0.3$, $\lambda_\circ = 0.7$. The domains corresponding to limiting magnitudes $i = 15$, 19.1, 20.5 and 21.78 are delimited by the corresponding curves (yellow, blue, green and black). The second ordinate axis represents the redshift values. . 55
4.5 Similar to Fig.4.4: the absolute magnitude-volume diagram of the DR1 sample. 55
4.6 Similar to Fig.4.4: the absolute magnitude-volume diagram of the DR3 sample. 55

4.7 Similar to Fig.4.4: the absolute magnitude-volume diagram of the uniform statistical subsample of the DR3 (SUBDR3). 55
4.8 Similar to Fig.4.4: the absolute magnitude-volume diagram of the SDSS-DR7 sample. 56
4.9 The absolute magnitude-volume diagram of a simulated sample which consists of 46,420 objects with a Gaussian luminosity function with $M_0 = -25$, $\sigma_M = 1.2$, a limiting magnitude $m_{lim} = 19.1$, and a maximum redshift $z_{max} = 13.6$ in the model $\Omega_\circ = 0.076$, $\lambda_\circ = 1.211$. 56
4.10 The volume-redshift diagram in the model $\Omega_\circ = 0.076$, $\lambda_\circ = 1.211$. The graduation on the ordinate is translated into angular distance on the right hand side axis. 56
4.11 The distance modulus $\zeta(z)$-redshift diagram in the model $\Omega_\circ = 0.076$, $\lambda_\circ = 1.211$, showing the angular distance on the right hand side axis. The maximum of $\zeta(z)$ corresponds to $\tilde{\tau} = \frac{2\pi}{3}$. 56
4.12 Weighting factor applied to DR3 sample and simulation sample without (left) and with (right) k-correction. Red curve with ($\lambda_\circ = 1.275$, $\Omega_\circ = 0.132$) and blue with ($\lambda_\circ = 1.229$, $\Omega_\circ = 0.132$). The disturbed shape of the curve is due to the contribution of the emission lines. 57
4.13 We represent the apparent magnitude limits on the FS diagram of the homogeneous statistical subsample, SUBDR3, chosen to apply the V/V_{max}: $18.65 < m < 19.1$ 59
4.14 The cdf of V/V_{max} compared to a uniform distribution, for a SUBDR3 subsample with $\Omega_\circ = 0.076$ and $\lambda_\circ = 1.211$. 59
4.15 Distance between the empirical cdf and theoretical cdf (D_{max}), testing a uniform distribution of V/V_{max} values, for candidates cosmological models on the NCC corresponding to SUBDR3. Left panel: D_{max} as a function of $\lambda_\circ$. Right panel: D_{max} as a function of $\Omega_\circ$. In both panels, the values of D_{max} on the ordinate axis is translated into significance level on the right hand side axis. 59
4.16 The cdf of V/V_{max} compared to a uniform distribution, for a DR7 subsample with ($\Omega_\circ = 0.0169$ and $\lambda_\circ = 1.079$). 59
4.17 Similar to Fig.4.15 : D_{max} with respect to $\lambda_\circ$ (left) and ($\Omega_\circ$ (right) as candidates given by the null correlation curve of DR7. 59
4.18 Contribution of measurement errors to NCC corresponding to DR3 79
4.19 The luminosity function $f(M)$ of the subsample of SUBDR3 with ($\Omega_\circ = 0.0305$, $\lambda_\circ = 1.1180$). 79
4.20 The selection function $\phi(m)$ of the SUBDR3 subsample with ($\Omega_\circ = 0.0305$, $\lambda_\circ = 1.1180$). The upper panel is an enlargement of the area in which the function is most constant. 79

5.1 The supernova classification tree. 82
5.2 The light curves of different types of SNe in the blue band: the type Ia, Ib, II-L, II-P, and SN 1987A. The Curve of the SN Ia is brighter than all other SN types. Figure courtesy: [Wheeler 1990]. 83
5.3 The supernova spectral Types. The gravitational supernovae is the progenitor of the supernovae type Ib, Ic and II. The progenitor of SN type Ia is a thermonuclear explosion of white dwarfs. Figure courtesy: Supernova Cosmology Project (SCP). 83
5.4 An artistic image of a white dwarf and a red geant star. Figure courtesy: STFC/David Hardy. 83
5.5 Spectra of three Type Ia supernovae, SN 1987D, SN 1987N, and SN 1990N, about one week after the maximum of their LC. Figure courtesy: [A. V. Filippenko 1997] 83
5.6 UBVRI light curves for SN 1998bu (Figure courtesy: [N. B. Suntzeff 1999]) 84
5.7 Light curve standard obtained. The B-band light-curves for a low-redshift SNe Ia from the Calan-Tololo survey (Figure courtesy: Hamuy et al. [1996a]) 85
5.8 Correlation between the absolute magnitude with the decline rate Δm_{15} of the light-curve for low-redshift SN Ia from the Calan-Tololo survey (Figure courtesy: Hamuy et al. [1996a]) . . 85
5.9 Left: a schematic of intrinsic light curve of a SN. Right: the interception of the world-line of the SN with the past light cone. 87
5.10 Light curve of SN SNLS-04D3gx. This figure shows a light curve well sampled by observations which help to characterize its parameters (x_0, t^*_{obs}, x_1, c) without biases. Figure courtesy: [Astier P. et al, 2006] 91
5.11 A representative figure of the SN Ia light curves in the aim to explain the selection effects. The dashed curve represents the master curve where the entire light curves must coincide. The highest blue curve represents the light curve of the SN Ia brighter, broader, slower and bluer than the master curve. The cyan curve (the lowest) represents the light curve of the SN Ia fainter, narrower, faster and less bluer than the master curve. The t_1 and t_2 are two observation dates for which a candidate of SN is detected by subtracting the images taken at these dates. 91
5.12 The selection of SNe depends on two characteristics: the maximum of luminosity m^* and the decline rate Δm_{15}. The lowest light curve is the threshold light curve characterized by m^*_{lim} and $\Delta m_{15,lim}$ which are used as the selection criteria. A SN with a decline rate $\Delta m_{15} < \Delta m_{15,lim}$ is observed as long as its apparent magnitude at maximum luminosity $m^* < m^*_{lim}$. 92

5.13 Two SNe with the same intrinsic characteristics at different redshifts. Although the light curve of the SN of the highest redshift ($z = 1.5$) has a small decline rate $\Delta m_{15}^2 < \Delta m_{15,lim}$ due to the dilation of time, this SN will not be considered in the sample because it has not a sufficient time to have a good sampling of its light curve. The selection of SN is done only if $m^* < m^*_{lim}$. . 93
5.14 The brighter-slower relation (absolute magnitude versus shape parameter) 93
5.15 Absolute magnitude-volume diagram of simulated samples (A) (left) and (B) (right). 96
5.16 Hubble diagram of simulated samples (A) (left) and (B) (right). 97
5.17 Four dimensional diagrams of characteristics of sample (A). . . . 97
5.18 Four dimensional diagrams of characteristics of sample (B). . . . 97
5.19 The NCC corresponding to (A) sample (left) and the one corresponding to (B) sample (right). 99
5.20 Shape of the NCC with respect to the characteristics of sample and cosmological model. 99
5.21 NCC of ten randomly generated samples with the same characteristics in the standard cosmological model. 100
5.22 Search for the minimum of KS test, D_{max}, (top left) as a function of $\lambda_\circ$, and (bottom right) as a function of $\Omega_\circ$, on the NCC (top right). 100
5.23 Statistics of the luminosity function (upper panels) and the selection function (lower panels) 101
5.24 Similar to Fig.5.23 101
5.25 The NCCs of the 500 simulated samples. 102
5.26 Set of the best candidates of the cosmological model with the likelihood contours (top left). The probability density functions with respect to $\lambda_\circ$ (top right) and with respect to $\Omega_\circ$ (left bottom). 102
5.27 The FS diagram of JLA sample build with the model: $\Omega_\circ = 0.3$, $\lambda_\circ = 0.7$. The red dots represent the SDSS-II data, and the blue ones represent those of SNLS3. The rest is represented with multicolor. 103
5.28 The FS diagram of HST sample build with the model ($\Omega_\circ = 0.3$, $\lambda_\circ = 0.7$). 104
5.29 The FS diagram of low-z sample build with the model ($\Omega_\circ = 0.3$, $\lambda_\circ = 0.7$). 105
5.30 The FS diagram of SDSS-II sample build with the model: $\Omega_\circ = 0.3$, $\lambda_\circ = 0.7$. 106
5.31 The FS diagram of SNLS3 sample build with the model: $\Omega_\circ = 0.3$, $\lambda_\circ = 0.7$. 107

5.32 Similar to Fig.5.17 for SNLS3 sample with calibration of standardization coefficients with respect to the low-z sample. 107
5.33 The null correlation curve in the $\lambda_\circ - \Omega_\circ$ diagram corresponding to SNLS3 sample. 108
5.34 The null correlation curves in the ($\Omega_\circ$, $\lambda_\circ$) diagram that correspond to QSO samples and SNLS3 sample (the highest). 108
5.35 D_{max} with respect to $\lambda_\circ$ (left) and $\Omega_\circ$ (right) as candidates given by the NCC of SNLS3. 108
5.36 The FS diagram of SDSS-II sample build with the model ($\Omega_\circ = 0.11$, $\lambda_\circ = 1.32$). 109
5.37 The FS diagram of SNLS3 sample build with the model ($\Omega_\circ = 0.11$, $\lambda_\circ = 1.32$). 110
5.38 Luminosity function (left panel) and selection function (right panel) built with the model ($\Omega_\circ = 0.11$, $\lambda_\circ = 1.32$), corresponding to SNLS3 sample. 110
5.39 Similar to Fig.5.26 110

6.1 Le diagramme de Hubble des échantillons de Supernovae avec SNLS, SDSS, HST et plusieurs sondages low-z. Figure tirée de [Betoule, M. et al 2014] 118
6.2 Le diagramme magnitude absolue-volume de l'échantillon simulé présenté en rouge. La courbe bleue est le volume en fonction de la magnitude absolue à une magnitude apparente limite donnée. Cet échantillon a été généré avec un univers plat ($\Omega_\circ, \lambda_\circ = 0.3, 0.7$). Une répartition uniforme apparaît sur l'axe vertical et une distribution gaussienne sur l'axe horizontal tel qu'ils ont été choisi initialement dans la simulation. 119
6.3 La courbe de corrélation nulle dans le plan ($\Omega_\circ, \lambda_\circ$). La courbe retrouve le modèle cosmologiques utilisé pour effectuer la simulation de l'échantillon. 121
6.4 Les courbes de corrélation nulles dans le diagramme($\Omega_\circ$, $\lambda_\circ$) correspondant aux échantillons EDR, DR1, DR3, DR7 et aux sous-échantillons DR3. Les courbes sont situées dans la région avec une courbure positive $\kappa_\circ > 0$ (au-dessus de la ligne droite). Toutes les courbes sont en accord et proches l'une de l'autre, sauf la courbe rouge qui correspond à l'échantillon EDR. 121
6.5 Les courbes de corrélation nulles dans le diagramme ($\Omega_\circ$, $\lambda_\circ$) qui correspondent aux échantillons QSO et à l'échantillon SNLS (le plus élevé). 124

Introduction

The understanding of the Universe was started in the XVIth epoch when the polish Copernicus suggested a heliocentric model of solar system, leading to the idea: no special place for Earth in the Universe. This revolution was followed by a second and major one dated for 1687, where Isaac Newton offers the first real theory of gravitation. This theory explained for the first time the movement of the stars in the sky as well as falling bodies on Earth, giving a description of the gravitational interaction as a force that spreads instantly. However, this theory was not able to explain the anomalous precession of Mercury's perihelion by 42.7 arcseconds per century. The questions that formed the weaknesses of Newton's theory, have been answered with the new theory of gravitation given by Einstein in 1905-1915. A new description of gravity is given by the Einstein Field Equations, which can be summed up in words as follows: matter modify the curvature of space-time, and the curvature of space-time maps the movement of matter.
It is worth to mention that Einstein added to his equations a cosmological constant Λ searching a solution of a static cosmic Universe. Both Friedmann (1922) and Lemaître (1927), independently, proved that the Einstein's theory has cosmological solutions of an expanding, non static Universe. It was not until 1929, the era of modern cosmology began with the discovery of Hubble of the expansion of the Universe [E. Hubble 1929]. This discovery marked a milestone and a major progress in cosmological studies. One generally believes that this is the reason why Einstein withdrew the constant Λ claiming that its introduction was a great mistake. Later, this constant was proposed as a solution to explain the expansion of the Universe. Recently, the Hubble diagram of type-Ia supernovae agrees with a positive value of the cosmological constant, what interprets as an acceleration of the cosmological expansion [A. G. Riess et al. 1998], [S. Perlmutter et al. 1999].

Actually, the usual statistical approach in the analysis of the Hubble diagram is faced to the systematic biases, assuming hypotheses on the luminosity function and the selection function. On the other hand, a robust statistical approach requires a weaker number of hypotheses.
This thesis, introduces simulation methods of quasar and supernova samples, as well as a robust statistical technique with the aim to constrain formal values of the cosmological parameters.
In Chap.1, I present a brief description of the observational cosmology represented by the Friedmann-Lemaître-Gamow model. I present in Chap.2 the probability laws which describe the characteristics of quasar samples, and the simulation methods in which my work is part. The third chapter is devoted to describing the robust statistical method. The application of this method on the quasar data from SDSS survey and the results are exhibited in Chap.4. Finally, A new modelling of supernova sample is presented in Chap.5. A data processing of supernovae of SDSS-II and SNLS3 surveys is described as well in this chapter.

CHAPTER 1

Basics of Observational Cosmology

Contents

1.1 Introduction **4**

1.2 Newtonian cosmology **4**

1.3 Einstein's cosmology **5**

1.4 The Friedmann-Lemaître-Gamow model **6**

1.4.1 The Friedmann's equations 7

1.4.2 Primordial Universe 8

1.5 Contents of the Universe **9**

1.6 Baryonic Acoustic Oscillations **13**

1.7 Dark matter **13**

1.8 The Dark Energy **14**

1.8.1 Models with Scalar Fields 15

1.8.2 The Cosmological Constant 16

1.9 Hubble diagram and measure of distances **16**

1.9.1 The Comoving Distance 18

1.9.2 The Age and the Conformal Time 20

1.9.3 The Luminosity Distance 20

1.10 The Magnitude Systems **21**

1.10.1 The Apparent Magnitude 21

1.10.2 The Vega System 21

1.10.3 The AB System 21

1.11 Constrain the cosmological parameters 22
1.12 Conclusion 22

1.1 Introduction

Many centuries after Newton (1643 - 1727), who introduced the first universal gravitational theory, the cosmology follows Newton's theories and principles[1], searching for ways to understand the laws that control the Universe [E. Harrison 2000].
The Universe, during Newton's time, was thought to consist of only the solar system and the stars. It was unclear how far the latter were from Earth, since no direct measurement of the distances could be performed due to the quality of the astronomical instrumentation at that time. It was not until the nineteenth century, that the first direct measurement of the distance of a star was performed by Bessel [T. Plotner 2008]. After Bessel's parallax[2] in 1837, it was obvious that the size of the solar system was infinitesimal compared to that of the Universe. Luckily, the spectroscopy, a device which measures the chemical composition of stars and estimates their fluxes and luminosities, was developed in 1842 by Alexandre Becquerel (1820-1891) [I. Appenzeller 2013]
By the end of that century, the Universe was recognized as an enormous galaxy, the Milky Way where we belong, with a huge number of stars [L. Gerrit 1937]. The stars are distributed in a chaotic order in the sky, however, in some times they are accumulated in clusters. The latter are known as diffuse nebula or planetary nebula [J. B., Kaler 1976]. These observations arise a lot of questions such as: What is the nature of these clusters and how do they perform? Those questions remained unanswered until the twentieth century when in 1925, Edwin Hubble discovered a Cepheid in the brightest spiral nebula, Andromeda. Using the period-luminosity relation of Henrietta Leavitt (1908) for the calibrated Cepheids [J. D. Fernie 1969], Hubble discovered the extragalactic nature of Andromeda. This nebula is more than 2 million light years away from our galaxy [I. Ribas 2005]. Hubble, then, concluded that the Universe is not restricted to the Milky Way, and it is populated by millions of galaxies...

1.2 Newtonian cosmology

Despite the success of the Newtonian theory in explaining the gravitational laws on earth and between planets and their motion in the solar system, it

[1] Principle of inertia, fundamental principle of dynamics and principle of reciprocal actions
[2] Due to the source or observer movement, two different lines of sight illustrate two positions of the source with an angle that allows to measure distance using geometry.

fails to describe the Universe at a large scale.
The Newtonian theory predicts a non stable Universe [M.S. Longair 2013]. Assuming two objects of different masses are separated by a distance d, these objects, in the Newtonian concept, cannot remain in their positions indefinitely considering their mutual attraction. According to this theory, these objects undergo a gravitational force which leads to shorten the distance between them. Consequently, a Universe which surrounds a center of mass is doomed to collapse on itself. In the Newtonian theory, to obtain such a cosmological model without a center, one must consider a cloud filling the Universe uniformly with a constant density. However, according to Halley in 1720, in an infinite Universe containing an infinite number of stars, the night sky should be as bright as the day. This conflict between the darkness of the night sky and the assumption of an infinite and eternally static universe is the major problem of the Newtonian cosmology, known by "Olberts' paradox" [E. R. Harrison 1989]. This paradox has been resolved later through the modern cosmology (described in the next section) which shows that the Universe is expanding. Due to this expansion, the light emitted from distant stars and galaxies is "redshifted". Thus, the emission spectra of those objects appear to us as veering gradually to the light frequencies that we cannot see (typically in infrared). This interpretation explains the darkness of our night sky.

1.3 Einstein's cosmology

The modern cosmology began hundred years ago (1915) where Albert Einstein published his theory of general relativity (GR). This theory links the distribution of the energy density that fills the Universe and its geometry through the Einstein field equations (EFE):

$$R_{\mu\nu} - \frac{1}{2}Rg_{\mu\nu} = 8\pi G T_{\mu\nu} \tag{1.1}$$

Where $R_{\mu\nu}$ is the Ricci tensor, $g_{\mu\nu}$ is the metric tensor used with the convention signature $(+,-,-,-)$, R is the Ricci scalar, $T_{\mu\nu}$ is the energy-momentum tensor and G is the Newtonian constant. In GR, the units are so that the speed of light in a vacuum, $c = 1$ [3]. In 1917, Einstein introduced the cosmological constant Λ for obtaining a static Universe. Eq.1.1 becomes:

$$R_{\mu\nu} - \frac{1}{2}Rg_{\mu\nu} + \Lambda g_{\mu\nu} = 8\pi G T_{\mu\nu} \tag{1.2}$$

In 1922, the Russian meteorologist and engineer, Alexander Friedmann proved that the EFE also allow dynamical worlds [H. Nussbaumer 2014]. However, it took Einstein a few years to recognize the relevance of Friedmann's remarks.

[3] $c = 1$, i.e. time can be measured in unit of length, 1s = 2.999792458 $\times 10^8 m$

Independently, in 1927, the Belgian canon, Georges Lemaître published a paper [G. Lemaitre 1927] in which he established the same equations as Friedmann and interpreted them. Lemaître also predicted the "Hubble Law" even before the Hubble observations (getting a "correct" estimation for the Hubble constant of 625 $km.s^{-1}.Mpc^{-1}$)[4]. In 1931, he published his theory of the "primitive atom" in which he introduced the concept of the time zero.
It was not until 1929 that Hubble discovered the famous linear relationship between the distance and the velocity (Sect.1.9) of distant galaxies with the help of a telescope of 2.54 meters in diameter placed at Mount Wilson [E. Hubble 1929]. In 1931, Hubble showed Einstein the observational evidence of a redshifted nebular spectra convincing Einstein that the Universe is expanding. Einstein acknowledged, therefore, that there was no reason to maintain his idea of a finite static Universe. He abandoned the cosmological constant, describing it as "the greatest mistake of his life". In 1932, Einstein published with de Sitter his euclidean infinite cosmological model of the Universe [A. Einstein and W. de Sitter 1932]. The concept of an expanding Universe later acquired the term, "Big Bang" theory. This term was coined by Fred Hoyle, one of the proponents of the stationary model, who introduced Lemaître to his colleagues in 1950 with the words: "This is the Big Bang man!".
By the end of the 70's, [H. Fliche & J. M. Souriau 1979] reconsidered the gravitational equations with the cosmological constant in their statistical analysis of the Hubble diagram of QSOs. This allowed to estimate a positive value of Λ. Later, [Triay, R. et al. 1990], statistical investigation on the brightest cluster led to similar results which shows the acceleration of the cosmological expansion. Eight years later, [A. G. Riess et al. 1998] and [S. Perlmutter et al. 1999] pointed out the evidence of cosmic acceleration by measuring the accurate distances to distant type-Ia supernovae, used as standard candles. Since then, the use of Λ become the dilemma of the century.

1.4 The Friedmann-Lemaître-Gamow model

The framework of the modern cosmology is based on the cosmological principle. It supports the hypotheses of the homogeneity and the isotropy of the universe. According to the Copernican principle, there is no privileged place in the Universe. Furthermore, assuming the isotropy of this latter, which means that each point in the Universe has identical properties in different directions, thus, the Universe would look homogeneous[5]. As a matter of fact, observing the universe at a given length in different directions with the same opening

[4]Mpc: $10^6\times$ pc. A parsec (pc) is a unit of measurement of distance outside the solar system and it is used to express the measuring of the cosmological distances. It is equivalent to 3.26 light years: $1pc = 3.08 \times 10^{16}$m.

[5]Isotropy from every point implies homogeneity [Robert M. Wald 1984]

solid angle must lead to an identical result independent of the chosen direction. This characteristic implies that, on a large scale, we can describe the observable universe as being spatially homogeneous and isotropic. This brings us to the description of space-time with the Friedmann-Lemaître-Robertson-Walker (FLRW) metric. Despite the inhomogeneity of the Universe at small scales as shown in the map of 2df survey in Fig.1.3, the FLRW metric describes the space-time at large scales, more than 100 Mpc, where the cosmological hypotheses are valid as seen in Fig.1.4.

1.4.1 The Friedmann's equations

The FLRW metric illustrates the cosmological principle mathematically. It is defined in spherical coordinates (r, Θ, φ) as:

$$ds^2 = dt^2 - a^2(t)[\frac{dr^2}{1-kr^2} + r^2(d\Theta^2 + sin^2\Theta d\varphi^2)] \tag{1.3}$$

where t is the cosmic time, $a(t)$ is the (dimensionless) *expansion parameter*, its present value is $a_\circ = a(t_\circ) = 1$, and k is the sign of curvature of space which determines the type of geometric topology: $k = -1$ for an open Universe, $k = 0$ for a flat Universe and $k = 1$ for a closed Universe. The derivation of the FLRW metric is purely geometrical, subject to the constraints of homogeneity. An alternative form of the metric is given by taking into account the representation of the fixed coordinates. We can write the alternative FLRW metric as:

$$ds^2 = dt^2 - a^2(t)[d\chi^2 + S_k^2(\chi)(d\Theta^2 + sin^2\Theta d\varphi^2)] \tag{1.4}$$

where $d\chi$ reads:

$$d\chi = \frac{dr}{\sqrt{1-kr^2}} \tag{1.5}$$

and $S_k(\chi)$:

$$S_k(\chi) = \begin{cases} \sin(\chi) & \text{if } k = 1 \\ \chi & \text{if } k = 0 \\ \sinh(\chi) & \text{if } k = -1 \end{cases} \tag{1.6}$$

In a homogeneous Universe, the energy-momentum tensor $T_{\mu\nu}$ accounts for a perfect fluid of density ρ and pressure P. Using the $T_{\mu\nu}$ tensor with the metric in Eq.1.3, one can derive the Friedmann equations:

$$H^2 = \left(\frac{\dot{a}}{a}\right)^2 = \frac{8\pi G}{3}\rho - \frac{k}{a^2} + \frac{\Lambda}{3} \tag{1.7}$$

$$\frac{\ddot{a}}{a} = -\frac{4\pi G}{3}(\rho + 3P) + \frac{\Lambda}{3} \tag{1.8}$$

where $\dot{a}$ stands for the time derivative of a(t). H is the *Hubble parameter*, its present value is $H_\circ = 67.8 \pm 0.9\ km.s^{-1}.Mpc^{-1}$ [Planck Collaboration I (2015)].

1.4.2 Primordial Universe

Until the late thirties, the formation of elements in the Universe was a subject of debates. In 1942, George Gamow mentioned for the first time the idea of a primordial nucleosynthesis. In 1948, Gamow, Alpher and Herman predicted the cosmic microwave background, working on a model of a hot Big Bang assuming a primordial Universe composed only of neutrons (which subsequently disintegrate into protons) [P. J. E. Peebles 2014], [V. Alpher 2014]. In this model of Big Bang Nucleosynthesis (BBN), the original Universe was made up of an extremely hot and dense plasma of photons, fermions and quarks. The Universe then expanded, and its density and temperature decreased, fostering primordial nucleosynthesis i.e. the formation of the first weak nuclei (hydrogen, helium, deuterium, lithium). When the temperature became low enough ($\sim$ 3000°K) for the first atoms to form through a process called recombination. At that time, the baryons decoupled the photons and the light began to spread freely. This radiation, which was simply cooled during the Universe evolution, is known as the Cosmic Microwave Background (CMB). The baryons and cold dark matter (Sect.1.7) evolved in an attached way under the force of gravity, and formed the structures that we are currently seeing, i.e. clusters, galaxies and stars.
Interestingly, two main observations confirmed the BBN model. The first one was established in 1965, when Penzias and Wilson detected the cosmic microwave background. The natural explanation for the presence of this radiation is that the Universe passed through a warm and dense phase before the recombination happened and the radiation was emitted. This radiation has almost a perfect black body spectrum with an average temperature of 2.73°K produced by the photons of the primordial Universe and its spectrum peaks in the microwave frequency range of 160.2 GHz corresponding to a wavelength of 1.9 mm. The temperature of CMB is isotropic and homogeneous down to variations of 10^{-5} (see Fig.1.1).
The measures abundance of the weak elements in the Universe, as a second proof, are in excellent agreement with the predictions of the primordial nucleosynthesis [G. Steigman 2004]. This includes the mass abundance of Helium He4 predicted between 23% and 30%, in a perfect agreement with observations [C. A. Bertulani, et al. 2016].

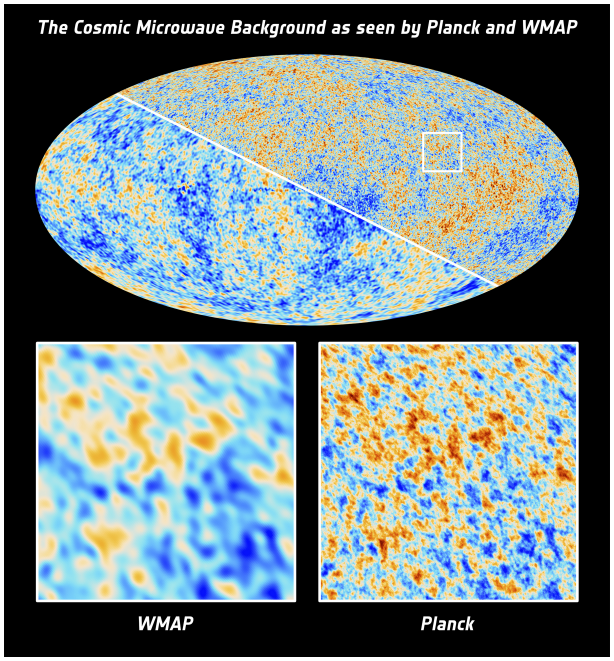

Figure 1.1: This image shows the Cosmic Microwave Background as seen by ESA's Planck satellite (upper right half) and by its predecessor, NASA's Wilkinson Microwave Anisotropy Probe (lower left half). The colors represent the temperature fluctuations. Red (res. blue) corresponds to warm (resp. cold) regions. Image taken from the website of ESA and the Planck Collaboration

1.5 Contents of the Universe

The perfect fluid is characterized by the properties of the energy-momentum tensor with pressure P and density of energy in the Universe ρ. It satisfies an (empirical) equation of state:

$$P = w\rho \tag{1.9}$$

where $w = -1$ for a cosmological constant (vacuum energy density) and $w < -\frac{1}{3}$ for dark energy models such as quintessence.
Combining Eqs.1.7 and 1.8 we get:

$$\dot{\rho} + 3(\rho + P)\frac{\dot{a}}{a} = 0 \tag{1.10}$$

From the derivation of Eqs.1.7 and 1.8, we obtain:

$$d(\rho a^3) = -P da^3 \tag{1.11}$$

using Eq.1.10, one can define the evolution in time of the energy density

$$\rho(t) \propto a(t)^{-3(1+w)} \tag{1.12}$$

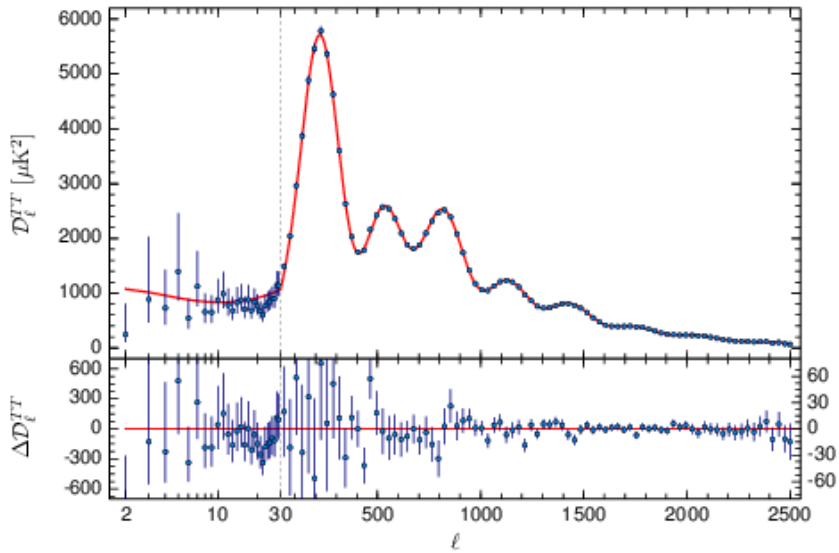

Figure 1.2: The CMB power spectrum obtained with Planck 2015. Top: Agreement of the flat standard model of cosmology ΛCDM with the observation data from the temperature release of the Planck satellite. Residuals with respect to this model are shown in the bottompanel [Planck Collaboration XIII (2015)].

For the several components of gravitational sources in the Universe, this energy density is written as:

$$\rho_i(t) \propto a(t)^{-3(1+w_i)} \tag{1.13}$$

with $w_\gamma = 1/3$ for the radiation and $w_m = 0$ for the non-relativistic matter. Equating Eq.1.13, we get:

$$\rho_\gamma a^4 \propto const. \tag{1.14}$$

$$\rho_m a^3 \propto const. \tag{1.15}$$

For relativistic matter such as neutrinos, w_γ is not constant and varies depending on the era, but this component can be neglected for recent periods.
By neglecting this term, Eq.1.7 becomes:

$$H^2 = \frac{8\pi G}{3}(\rho_m + \rho_\gamma) - \frac{k}{a^2} + \frac{\Lambda}{3} \tag{1.16}$$

With the following notation :

$$\rho_k = \frac{-3k}{8\pi G a^2} \tag{1.17}$$

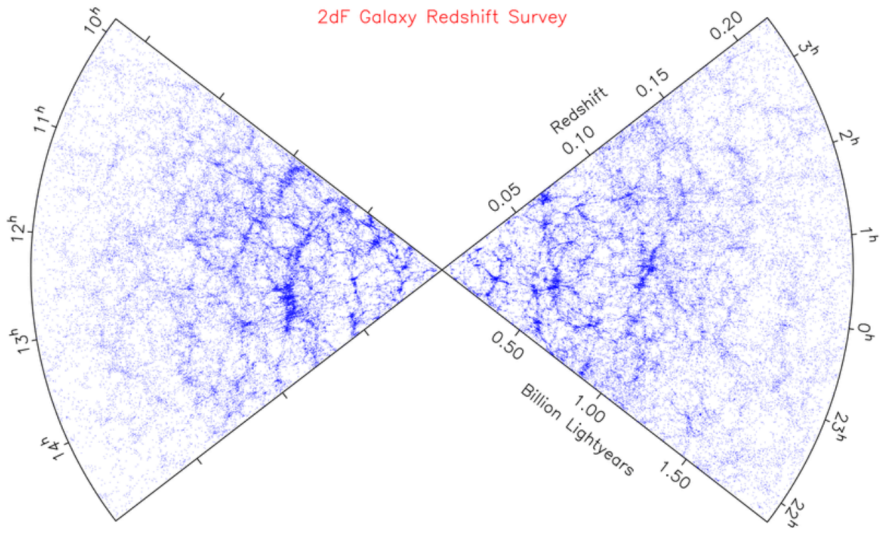

Figure 1.3: Scale at which the hypothesis of a spatial uniform distribution of gravitation sources becomes valid is roughly above 100 Mpc, according to the distribution of a large number of galaxies with 2dF survey. The figure shows the large-scale structures, which are less visible with distance from the orbserver. The Milky Way is located at the intersection of the two slices of the observed sky [M. Colless 2003].

we can express Eq.1.16 as follows:

$$H^2 = \frac{8\pi G}{3}(\rho_m + \rho_\gamma + \rho_\Lambda + \rho_k) \tag{1.18}$$

where

$$\rho_c = \frac{3H^2}{8\pi G} \tag{1.19}$$

With the dimensionless parameters:

$$\Omega_m = \frac{\rho_m}{\rho_c}, \quad \Omega_\gamma = \frac{\rho_\gamma}{\rho_c}, \quad \Omega_\Lambda = \frac{\rho_\Lambda}{\rho_c}, \quad \Omega_k = \frac{\rho_k}{\rho_c} \tag{1.20}$$

named cosmological parameters, Eq.1.18 becomes:

$$\frac{H^2}{H_\circ^2} = \frac{\rho_m}{\rho_{c,\circ}} + \frac{\rho_\gamma}{\rho_{c,\circ}} + \frac{\rho_\Lambda}{\rho_{c,\circ}} + \frac{\rho_k}{\rho_{c,\circ}} \tag{1.21}$$

Using Eqs. 1.14 and 1.15, we obtain:

$$\frac{H^2}{H_\circ^2} = \frac{\rho_m}{\rho_{c,\circ}}\left(\frac{a_\circ}{a}\right)^3 + \frac{\rho_\gamma}{\rho_{c,\circ}}\left(\frac{a_\circ}{a}\right)^4 + \frac{\rho_\Lambda}{\rho_{c,\circ}} + \frac{\rho_k}{\rho_{c,\circ}}\left(\frac{a_\circ}{a}\right)^2 \tag{1.22}$$

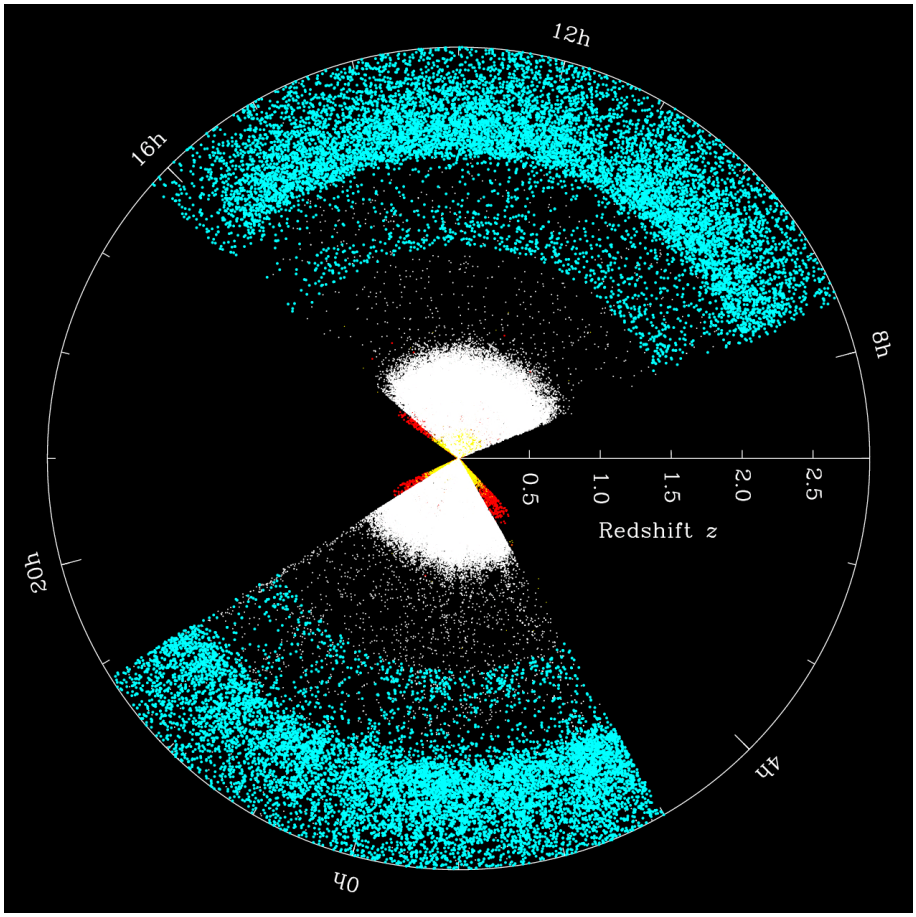

Figure 1.4: The spatial distribution of the quasars of the BOSS catalog shows a radial stratification due to four distinct phases of observations, and in each of sub-samples a decrease in the number of objects as the radius increases. By taking into account this selection effect, one can safely guess that this distribution is uniform. Figure credit: universetoday website.

Since $a_\circ = 1$, therefore:

$$\frac{H^2}{H_\circ^2} = \Omega_m a^{-3} + \Omega_\gamma a^{-4} + \Omega_\Lambda + \Omega_k a^{-2} \tag{1.23}$$

where these dimensionless parameters satisfiy:

$$\Omega_m + \Omega_\gamma + \Omega_\Lambda + \Omega_k = 1 \tag{1.24}$$

The above notations of cosmological parameters are the usual notations, but they are substituted by $\Omega_\Lambda \equiv \lambda_\circ = \frac{\Lambda}{3H_\circ^2}$, $\Omega_k \equiv -\kappa_\circ = \frac{k_\circ}{H_\circ^2}$, $\Omega_m \equiv \Omega_\circ = \frac{8\pi G\rho_{m,\circ}}{3H_\circ^2}$ and $\Omega_\gamma \equiv \alpha_\circ = \frac{8\pi^3 \mathrm{G}(\mathrm{k}T_\circ)^4}{45\hbar^3 H_\circ^2} \propto 10^{-5}$ which are more appropriated because these quantities show different behaviors with time. Let us define the polynomial:

$$P(a) = \lambda_\circ a^4 - \kappa_\circ a^2 + \Omega_\circ a + \alpha_\circ \tag{1.25}$$

$$P(1) = 1; \quad \lambda_\circ - \kappa_\circ + \Omega_\circ + \alpha_\circ = 1 \tag{1.26}$$

In our statistcal analysis, we estimate the parameters $\lambda_\circ$ and $\Omega_\circ$.

1.6 Baryonic Acoustic Oscillations

The properties of the CMB guarantee the existence of a scale from which the universe becomes isotropic and homogeneous, as well as the measurement of the velocity of our galaxy with respect to the referential that it defines. Even though the temperature of the CMB is extremely uniform throughout the sky, the COBE satellite (Cosmic Background Explorer) detected tiny fluctuations or temperature anisotropies in the CMB in 1992. The WMAP (Wilkinson Microwave Anisotropy Probe) satellite, launched in 2001, confirmed the COBE observation and mapped the temperature fluctuations with a much higher resolution. More recently, the Planck satellite mapped the CMB anisotropy with even higher accuracy (see Fig.1.1). In general agreement with the observation, the anisotropy in the CMB grew from the gravitational tension of small fluctuations existent in the early Universe. These perturbations gave rise to acoustic oscillations in the photon-baryon fluid before the recombination. During that period, the gravitational attraction between baryons tended to collapse the system and compress the photon-baryon fluid whereas the photon pressure provided an opposite restoring force. This created sound waves that propagate in the fluid of the primordial Universe. At the time of recombination, the photons were diffused freely and these oscillations outlined in the CMB. A modelling of the dynamics of these structures in the primordial plasma makes it possible to interpret the angular fluctuations of its temperature, which are observed by means of a spectral analysis, which provides estimates of cosmological parameters. Moreover, these features have an imprint on baryonic structures at every stage of the evolution of the Universe called Baryonic Acoustic Oscillations (BAO). It is believed that the high density areas associated with the acoustic waves in the CMB condense to create the current structures. The size of structures, can be used to trace back the cosmological parameters [W. Hu 1997]. Fig.1.2 shows the power spectrum of the CMB obtained by Planck satellite.

1.7 Dark matter

Dark matter is an ad hoc ingredient used in the modelling of a gravitational structure to interpret observations. It does not interact electromagnetically and therefore cannot be detected directly with telescopes. Its properties are deducted from gravitational effects on visible matter. It is believed that only

less than 10% of the energy density of the Universe comes from baryonic and in principle, visible matter. [E. Hubble 1934] proposed the first measure of the density of (visible) matter in the Universe based on an average of the measured galactic mass (6 - 8) $\times$ 10^8 $M_\odot$. The existence of such matter was derived by Jan Oort in 1932 who studied the orbits of stars in the galaxy and concluded that the Milky Way should contain more matter than what was visible [J. H. Oort 1932]. Soon after, Zwicky measured the dispersion of the radial velocities of eight galaxies in the Coma supercluster and found a surprisingly large value [F. Zwicky 1933]. Applying the virial theorem, he found that the total mass of the supercluster should be 400 times greater than the mass of visible matter [F. Zwicky 1937]. He resolved the problem by introducing a hidden mass distributed in the cluster.
In the 1970s, Vera Rubin measured the rotational curves of spiral galaxies and discovered that the radial velocity of the galaxy Andromeda (M31) remains constant until at least 30 kpc using the 21 cm line of Hydrogen [Rubin et al. 1970]. In disagreement with the expected keplerian rotational curve, this study has given rise an evidence of the existence of dark matter in the galaxies. Since then, the modelling of several observations are in agreement with the existence of dark matter in the universe such as the dynamics of galaxies and clusters, the gravitational lensing and the temperature distribution of hot gas in the galaxy clusters as well as cosmological probes such as the CMB, BAO and Type Ia Supernovae.
Three different types of dark matter have been defined: cold dark matter (CDM), warm dark matter (WDM) and hot dark matter (HDM). The neutrino is the best candidate for hot matter while its mass is not yet well constrained. Concerning the cold dark matter, the best candidates are the WIMPs (Weak Interacting Massive Particles), which are predicted by many supersymmetric theories, and MACHO (Massive Compact Halo Astronomical Object). The decoupling date of these particles intervenes in the formation of large structures in the Universe. A Universe dominated by hot dark matter would have a "top-down" scenario of structure formation: the formation of superclusters of galaxies which then break up into clusters, then galaxies, and so forth. Conversely, a Universe dominated by cold dark matter scenario would be a "bottom-up": formation of galaxies (from clouds of gas) which are grouped into clusters and then into superclusters. Nowadays observations agree with the theory of cold dark matter despite some cluster observations suggest that they have formed previously.

1.8 The Dark Energy

Since the end of 90s, acceleration of cosmic expansion has been detected by using Hubble diagram of type-Ia supernovae thanks to Supernova Cosmology

Project (SCP) [S. Perlmutter et al. 1999] and the High-Z supernova [A. G. Riess et al. 1998]. According to FLG model, such an acceleration results from either a positive zero cosmological constant or the an unknown gravitational source, an ad hoc alternative motivated by the cosmlogical constant problem in High Energy Physics. These two interpretations being integrated in a single one named "Dark Energy". Fig.1.5 presents the confidence contours of Ω_m and Ω_Λ (see Sect.1.5) obtained by SCP using 42 SNe Ia. This section outlines the two frequent approaches used to explain this acceleration.

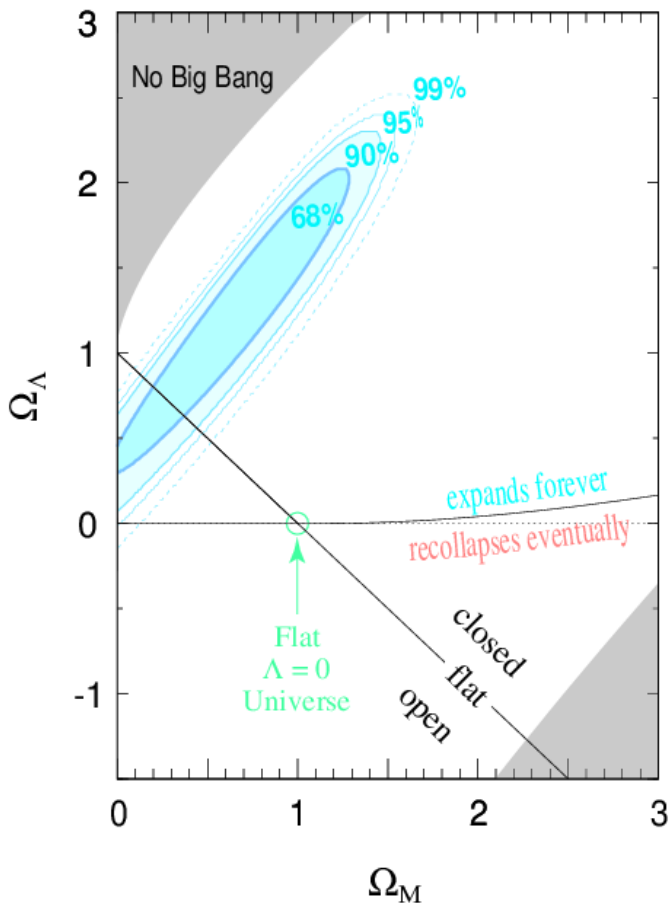

Figure 1.5: Confidence contours in the (Ω_M, Ω_Λ) plan obtained by the Supernova Cosmology Project with observations of 42 SNe Ia [S. Perlmutter et al. 1999].

1.8.1 Models with Scalar Fields

To sketch the approach to this issue, we limit to describe models which are behind several dark energy models. The first models of this class are the

quintessence models [B. Ratra 1988, C. Wetterich 1988] in which the dark energy is described by a scalar field in a slow rolling plan, in a way quite similar to inflation. The dynamics of dark energy by that of a scalar field which is characterized by potential that has to fit to observational constraints. The quintessence models appear interesting when considering that The main issue with these models is the determination of the potential to obtain a value of dark energy density close to the measured energy density. To solve this problem, other scalar fields have been proposed as a phantom field [R. Caldwell 2002, 2003] and K-essence model [T. Chiba et al. 2000, C. Armendariz-Picon 2000, 2001]. But these models suffer from similar problems.

1.8.2 The Cosmological Constant

While in GR, the cosmological constant stands for a universal constant. From the point of view of particle physics, it would be the energy density of quantum fluctuations of vacuum. Hence, two major obstacles appear: the cosmological constant problem and the problem of coincidence.

The Cosmological constant problem

According to the particle physics, the value of the energy density of the vacuum is estimated:

$$\rho_\Lambda^{vacuum} \sim (10^{18} GeV)^4 \sim 2.10^{110} erg/cm^3 \tag{1.27}$$

On the other hand, observations of type-Ia SNe and CMB fluctuations, the observed energy density is of order:

$$\rho_\Lambda^{obs} \sim (10^{-12} GeV)^4 \sim 2.10^{-10} erg/cm^3 \tag{1.28}$$

Therefore, the expected value is $\sim$ 120 order of magnitude larger than the observed energy density [S. Weinberg 1989], [S. Carroll 2001]:

$$\rho_\Lambda^{vacuum} \sim 10^{120} \rho_\Lambda^{obs} \tag{1.29}$$

This disagreement is known as the “Cosmological constant problem”.

The coincidence problem

The observed energy densities of the vacuum and of matter are of the same order of magnitude, as seen in Fig.1.5, while, the energy densities of the components of the Universe ($\alpha_\circ$, $\Omega_\circ$, and $\lambda_\circ$) evolve differently as shown in Fig.1.6. This figure shows that the vacuum energy initially had a negligible quantity with respect to the two other densities, then it becomes dominant in the present time. We also see that the transitions between the dominant components are

fairly short, particularly between matter and energy of the vacuum. It is intriguing that this transition happens today which makes the present day a privileged time in cosmic history. It is, therefore, interesting to ask whether the observed dark energy is a form of energy having a state equation variable with time. Hence, a new model has been introduced by adding a scalar field

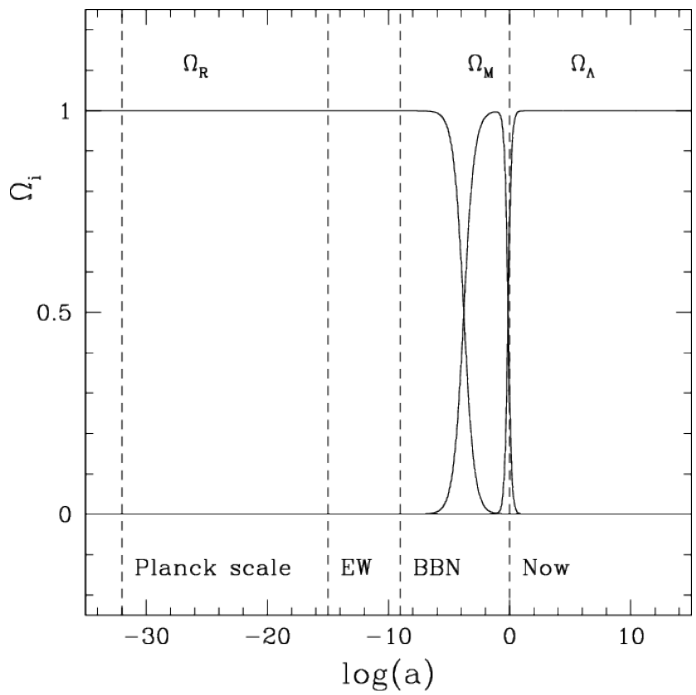

Figure 1.6: Evolution of the densities of radiation Ω_γ, of radiation Ω_m, and of the cosmological constant Ω_Λ with respect to the expansion factor. The different periods indicated by the dashed lines correspond to the Planck scale, the electroweak symmetry breaking (EW), the Big Bang nucleosynthesis (BBN) and the present epoch (Now). Credit: [S. Carroll 2004].

slowly varying with time (see Sect1.8.1).

1.9 Hubble diagram and measure of distances

What Hubble did that led to the discovery of his law was the measure of both the distance and the velocity of galaxies in the nearby Universe (see Fig.1.7). He showed that galaxies recede with a velocity that increases proportionally with their distance, what gives the Hubble's law:

$$v = H_\circ d \tag{1.30}$$

where the recession velocity of galaxies v and their distance d. The constant of proportionality $H_\circ$ is called the Hubble constant. Since its discovery, the

Hubble diagram became a major tool for retrieving of cosmological information. The distribution of type-Ia supernovae in this diagram is used with (large samples of type-Ia supernovae) detected from surveys such as the SNLS, SDSS, HST and low-z surveys (Fig.1.8). The spectra of a source is seen redshifted

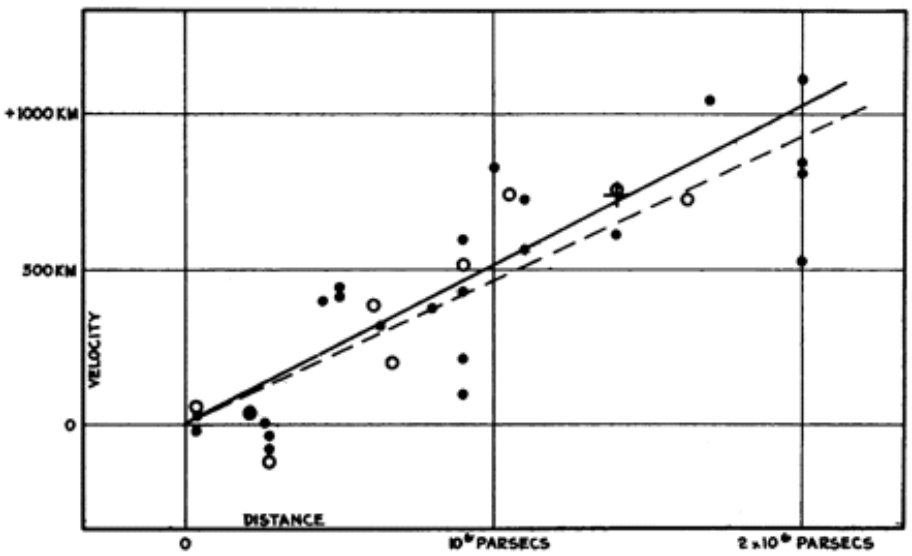

Figure 1.7: The Hubble diagram showing the expansion of the Universe. The radial velocity of stars, corrected for solar motion plotted against the distance estimated from the stars and the average of brightness of galaxies in a cluster. Credit: [E. Hubble 1929].

by an observer, due to the expansion of the Universe. The redshift z is defined as follows:

$$1 + z = \frac{\lambda_o}{\lambda_e} = \frac{a(t_o)}{a(t_e)} = \frac{1}{a(t)} \tag{1.31}$$

where $a_o = 1$. Therefore, the formula of the expansion factor at time t is expressed as:

$$a(z) = \frac{1}{1+z} \tag{1.32}$$

1.9.1 The Comoving Distance

In the comoving space, the galaxies have fixed coordinates and the *comoving distance* τ^* between the observer and the source of light at redshift z. Using

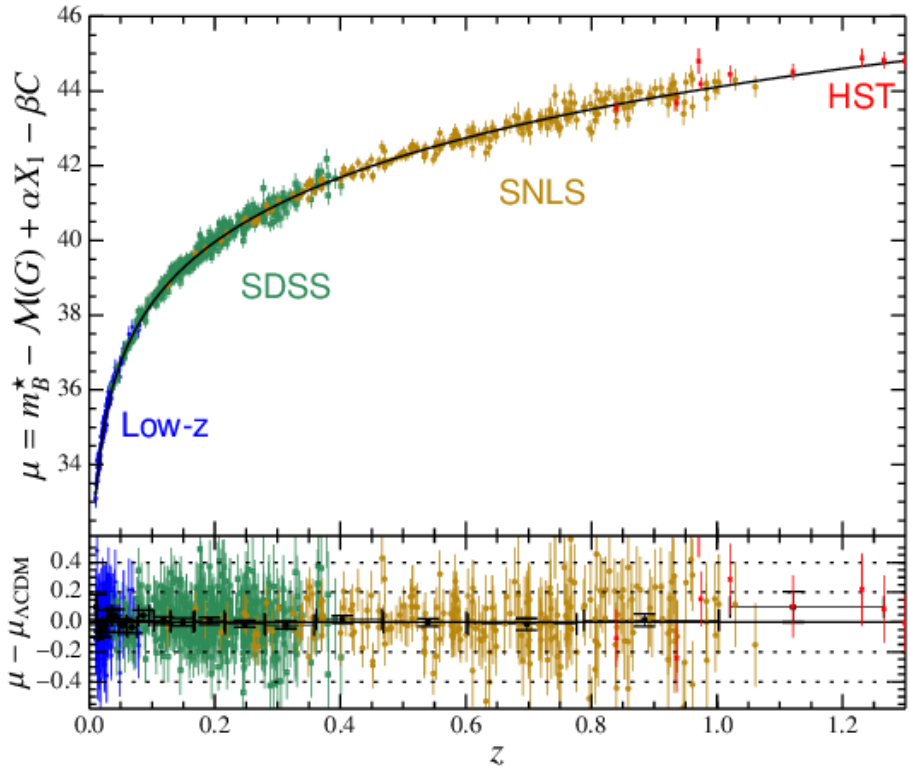

Figure 1.8: The Hubble diagram of the Supernovae samples with the SNLS, SDSS, HST and several low-z surveys. Credit: [Betoule, M. et al 2014].

Eqs 1.7, 1.23 and 1.25, one obtains:

$$\tau^*(z) = \int_{t_e}^{t_o} \frac{dt}{a(t)} \tag{1.33}$$

$$= \int_{a_e}^{a_\circ} \frac{da}{H_\circ\sqrt{\lambda_\circ a^4 - \kappa_\circ a^2 + \Omega_\circ a + \alpha_\circ}} \tag{1.34}$$

$$= \frac{1}{H_\circ}\int_{\frac{1}{1+z}}^{1} \frac{1}{\sqrt{P(a)}}\,\mathrm{d}a \tag{1.35}$$

Hereafter, we use the dimensionless comoving distance:

$$\tau(z) = \int_{\frac{1}{1+z}}^{1} \frac{\mathrm{d}a}{\sqrt{P(a)}} \tag{1.36}$$

The dimensionless comoving volume $V(z)$ is the volume of a sphere of radius $\tau(z)$ centered on the observer's location. It is defined by the following formula:

$$V(z) = \begin{cases} \frac{\pi}{\kappa_\circ^{\frac{3}{2}}}(2\tilde{\tau} - \sin(2\tilde{\tau})) & \text{if } \kappa_\circ > 0 \\ \frac{4\pi}{3}\tau^3 & \text{if } \kappa_\circ = 0 \\ \frac{\pi}{|\kappa_\circ|^{\frac{3}{2}}}(\sinh(2\tilde{\tau}) - 2\tilde{\tau}) & \text{if } \kappa_\circ < 0 \end{cases} \tag{1.37}$$

where $\tilde{\tau} = \tau\sqrt{\mid \kappa_\circ \mid}$ is the angular distance.

1.9.2 The Age and the Conformal Time

The lookback time can be measured from the observer at $z = 0$ (time $t_\circ$) back to redshift z (*time* t) [6]. It is given by:

$$t(z) = \frac{1}{H_\circ}\int_{\frac{1}{1+z}}^{1} \frac{a\mathrm{d}a}{\sqrt{P(a)}} \tag{1.38}$$

For a flat cosmological model ($\lambda_\circ = 0.7, \Omega_\circ = 0.3$) and $H_\circ = 70\ km.s^{-1}.Mpc^{-1}$, the age of the Universe today is estimated at:

$$t_\circ = \frac{978\ \text{Gyr}}{H_\circ}\int_0^1 \frac{a\mathrm{d}a}{\sqrt{P(a)}} = 13.4698\ \text{Gyr} \tag{1.39}$$

The *conformal time* η^* reads:

$$d\eta^* = \frac{dt}{a(t)} \tag{1.40}$$

and then, we obtain:

$$\eta^*_{(z)} = \frac{1}{H_\circ}\eta_{(z)} \tag{1.41}$$

where η is the dimensionless conformal time (see Eq.1.36).

1.9.3 The Luminosity Distance

The emitted light of a source is received by the observer as he is on a surface element of a sphere of radius d_L, the luminosity distance, centered on the light source. The received light per unit of time represents the flux and the apparent

[6] In a common language (poor), it is the time taken by the emitted light to travel from an object at redshift z to the observer [K. Krisciunas 1993].

brightness of this source which decreases with the square of the distance, by the known inverse square law:

$$f = \frac{L}{4\pi d_L^2} \tag{1.42}$$

where L is the intrinsic luminosity of an object. It turns out that the luminosity distance is related to the comoving distance and can be written as follows:

$$d_L = \frac{c}{H_\circ}(1+z).T(\tau_{(z)}) \tag{1.43}$$

With:

$$T(\tau_{(z)}) = \begin{cases} \frac{sin(\tilde{\tau})}{\sqrt{\kappa_0}} & \text{if } \kappa_0 > 0 \\ \tau & \text{if } \kappa_0 = 0 \\ \frac{sinh(\tilde{\tau})}{\sqrt{|\kappa_0|}} & \text{if } \kappa_0 < 0 \end{cases} \tag{1.44}$$

1.10 The Magnitude Systems

In astronomy, the magnitude system is frequently used to describe the brightness of an object. The magnitude is a scale used to classify the stars depending on their brightness. The brightest stars have the lowest magnitude for which one degree of magnitude corresponds to a difference of 2.51 times in brightness.

1.10.1 The Apparent Magnitude

This magnitude corresponds to the perception of a star's luminosity in the eyes of an observer. Perception through the human eye is non-linear and is sensitive to relative differences of luminosity between stars, therefore the observed magnitude is presented in logarithmic scale. The apparent magnitude m of an object, is defined as its flux, f, measured in a given observational filter, and the one of a reference object (for example Vega star which has null magnitude), f_0 , in the same filter.

$$m = -2.5\log_{10}\left(\frac{f}{f_0}\right) \tag{1.45}$$

The magnitude of the reference star is null what defines the origin of magnitude by defining the *zero point* notion (ZP) as:

$$ZP = -2.5\log_{10}(f_0) \tag{1.46}$$

one has:

$$m = -2.5\log_{10}(f) + ZP \tag{1.47}$$

There are two magnitude systems: the Vega and AB systems.

1.10.2 The Vega System

For this system, Vega (α lyr) is the reference star and its magnitude should be null in all filters. Because it is not always the case, corrections of Vega magnitude for the filters $UBVRI$ are required, e.g., [Johnson and Morgan 1953]: give $V = 0.03$, $B - V = 0.0$, $U - B = -0.01$, and others: $V - R = 0.0$ and $R - I = 0.006$ are given by [B. J. Taylor 1986] in accordance with the Vega spectrum [D. S., Hayes et al. 1985] and [Bohlin et al. 2004].

1.10.3 The AB System

The AB magnitude system is based on spectral flux densities which correspond to measurements that are calibrated in absolute units. This system links the magnitude to physical units directly. It is introduced by [J. B. Oke et al. 1983] and developed by [Fukugita et al. 1996] under the SDSS program. The magnitude in this system is defined as:

$$m_{AB} = -2.5 \log_{10} \frac{\int d(\log \nu) f_\nu T_\nu}{d(\log \nu) T_\nu} - 48.6 \tag{1.48}$$

with f_ν the flux in units of frequency, of unit erg.s^{-1}.cm^{-2}.Hz^{-1}, and T_ν is the transmission of the filter used (dimensionless). The constant 48.6 is chosen so that $AB = V$ for an object whose spectrum is flat. This reference system is based on four dwarf stars of type F.

1.11 Constrain the cosmological parameters

Using the definition of apparent magnitude, we can introduce the absolute magnitude M of an object. This latter is a measure of the intrinsic brightness of the object and is defined as it would appear to a hypothetical observer at a distance of 10pc. The apparent magnitude for an object at redshift z is related to the absolute magnitude (following Eq.1.42), we can write:

$$m(z) = -2.5 \log_{10} \left(\frac{L}{4\pi (10pc)^2} \right) + 5 \log_{10} \left(\frac{d_L(z)}{10pc} \right) \tag{1.49}$$

$$m(z) = M + 5 \log_{10} \left(\frac{d_L(z)}{10pc} \right) \tag{1.50}$$

The difference between the two magnitudes is called *distance modulus* $\zeta(z)$ (Fig.1.9) and is defined as:

$$\zeta(z) = 5 \log_{10} \left(\frac{d_L(z)}{10pc} \right) \tag{1.51}$$

The best measurement or estimation of this latter represents the clue of constraining the Hubble diagram pearls, the cosmological parameters $\lambda_\circ$ and $\Omega_\circ$.

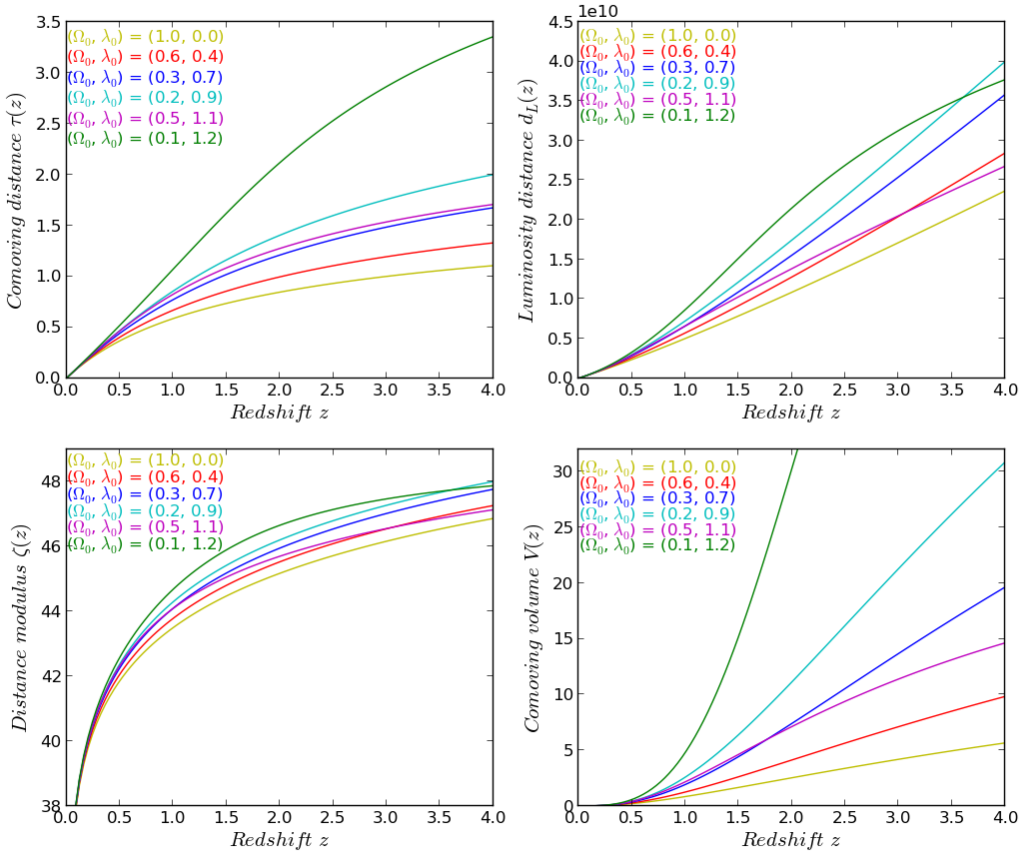

Figure 1.9: From top left to bottom right: The comoving distance, the luminosity distance, the distance modulus and the comoving volume versus the redshift for six different cosmological models.

1.12 Conclusion

In this Chapter, we have presented the standard cosmological model ΛCDM based on the Friedmann-Lemaître-Gamow model. In the framework, we will seek the more appropriated values of the cosmological parameters using statistical techniques.

CHAPTER 2

Quasars samples

Contents

2.1 Introduction **23**

2.2 Spectrum of quasar **24**

2.3 Events in the space-time diagram **24**

2.4 The selection effect **27**

2.5 Modelling a sample of quasars **28**

2.5.1 Statistical modelling 29

2.5.2 Simulation technique 29

2.5.3 The k-correction 34

2.6 Conclusion **35**

2.1 Introduction

Quasars were discovered in the late 1950's using the radio telescopes with no observation of corresponding visible objects. The first one was tied to an optical object was the radio source. Surprisingly, the spectrum of this object had many unidentified broad emission lines. Soon after, it was discovered by the Dutch astronomer Maarten Schmidt that these lines were not so strange, as they were just redshifted. Believing he was observing a star, Schmidt discovered the radio quasar, 3C 273, in 1963 and identified its emission lines of hydrogen and showed that they were shifted to larger wavelengths [M. Schmidt 1963]. It resembled a star, because it was seen as a point source through the

telescope. But unlike the stars, the spectrum of this point source had a strong radio emission. More objects of the same type were soon observed. In the absence of the explanation of the astrophysical nature of these objects, they were called quasi-stellar radio sources, the name which has been subsequently abbreviated as "quasars".

Quasars are considered a subset of the population of active galactic nuclei (AGN) (e.g. see [R. Antonucci 1993]). Fig.2.1 represents a AGN which consists of a super-massive black hole in the center surrounded by an accretion disk. It is formed due to the surrounding materials which fall under the huge gravity of the black hole. While falling, these materials release their potential energy as a result of the friction generated between them. Through different turbulent phenomena, these materials generate high energy particles channeled by the magnetic field lines of the AGN. These particles are later released in the form of two collimated jets from the magnetic poles. The accretion disk is surrounded by a thick torus of dust.
An AGN whose jet of particles collimates in our line of sight is called a "Blazar". If the jet tips in another direction and the host galaxy of the black hole is visible, the AGN is a Seyfert galaxy, otherwise, the AGN is a quasar. The quasar (QSO for quasi stellar objects) is the brightest class of AGNs.

2.2 Spectrum of quasar

QSOs are identified mainly by their emission lines. Lyman-α emission line ($\lambda_{Ly-\alpha} = 1215$ Å) characterizes particularly the quasars (see Fig. 2.2). Additional emission lines are also visible in their spectrum, such NV, SiIV, CIV, MgII, among other ones less important, see Spectral Lines used in SDSS table. In general a "Lyman alpha forest" is present in most of QSOs spectra, a depression of the continuum in the spectrum caused by a succession of absorption lines at smaller wavelength than the Lyman-$_\alpha$ emission line. It is caused by the the presence of neutral hydrogen located along the line of sight of the quasar. This is the âGunn-Peterson effectâ [J. Gunn and B. Peterson 1965]. Fig.2.3 represents a QSO from the SDSS survey at a redshift of 5.8. The part of the spectrum between the Lyman-β and the Lyman-γ emission lines is called the forest Lyman-β, etc... This depression of the continuum due to the superposition of absorption lines is caused by hydrogen clouds and other absorbers in front of the QSO.

2.3 Events in the space-time diagram

With the motivation in mind to use events (such as light emissions from astronomical objects) to probe the geometry of space-time, one has to specify

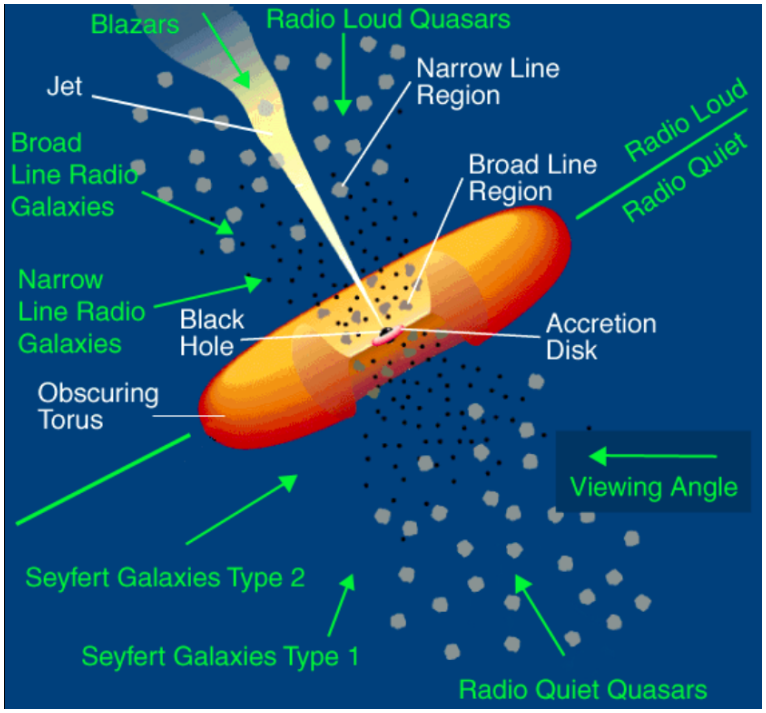

Figure 2.1: Diagram unifying different astrophysical types of AGN (blazars, quasars, seyfert galaxies) depending on the inclination angle with respect to the line of sight of the dust torus surrounding the same central engine (Noted in green). The various components of AGN (noted in white): A luminous accretion disk which surrounds the central black hole. Broad emission lines which are due to clouds orbiting above the disk. A thick dusty torus which obscures the broad-line region from transverse lines-of-sight. Narrow emission lines which are originated from irradiated clouds so far from the central source. Credit: [C. M. Urry, P. Padovani, 1995]

their intrinsic properties that characterize a single family. They are assumed to be not very different from one another in terms of their intrinsic luminosity (standard candles). Moreover, we assume that they do not show evolutionary effects and that they are uniformly distributed in space. These characteristics stand for random variables with probability densities who are defined by specific working hypotheses. The data are face to selection effects in observation, and a selection function is used at this purpose. We check the efficiency of our statistical method on simulation samples as a representation of the real data.

The main selection effect, it has been described by Malmquist (see Sect.2.4), depends only on the apparent magnitude. Therefore, a selection function must be used in the probability density in order to take it into account among other selection effects in observation.

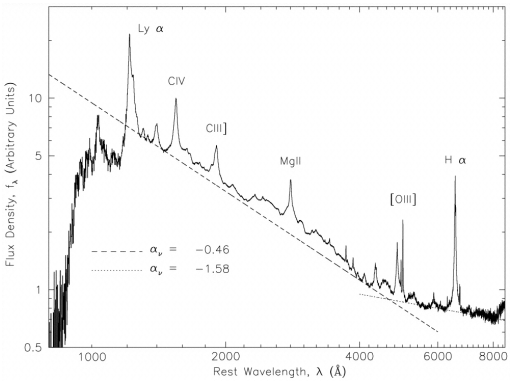

Figure 2.2: Spectrum of quasar at rest frame determined by the SDSS survey. The dashed thin and thik lines are the power-law fits to the estimated continuum flux. Credit: [D. Berk, et al 2001].

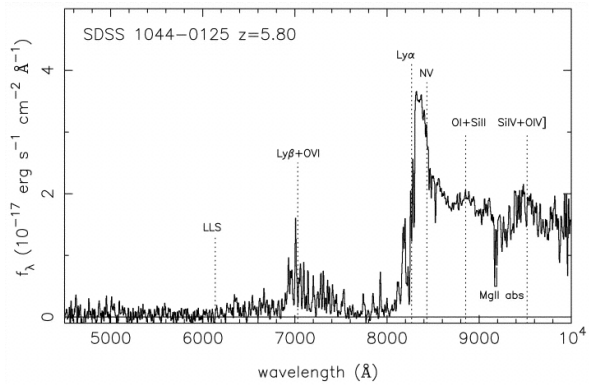

Figure 2.3: Spectrum of quasar SDSS 1044-0125 at redshift 5.8. The optical Lyman-α emission (1215 Å) is shifted into near Infra-Red $\sim$ 8230 Å.

According to working hypotheses, the objects have fixed position on the comoving space V_3 and they are expected to be uniformly distributed.
In the space-time diagram (Figs.2.4 & 2.5) as described by the direct product of the conformal time with V_3, perennial[1] sources show vertical world lines (black) while ephemeral ones (blue and green) stand for parts of those ones. By assuming that they are bright enough, they can be observed solely when the light past cone of the observer crosses that gives a date (i.e. a redshift). Two dates (the beginning) η_1 and (the end) η_2 are displayed for ephemeral events. Similarly, the duration of observation, being infinitesimal compared to cosmological scale, is magnified on the space-time diagram. On these figures, the intersection of the world lines with the past light cone of the observer (the two crossed lines at the red circle) ensures the object to be visible, if it is bright enough with respect to observation device. The objects (quasar, galaxy,...) are characterized intrinsically by the comoving distance τ and the absolute magnitude M by assuming that it is constant in time. On the other hand, the ephemeral objects are characterized by a luminosity fonction (light curve) instead of a constant absolute magnitude.

[1]A perennial object is an object which emits a stream of light and has been doing so since the inception of the observable universe, since the decoupling epoch, and for all time, such as galaxies, quasars and clusters.

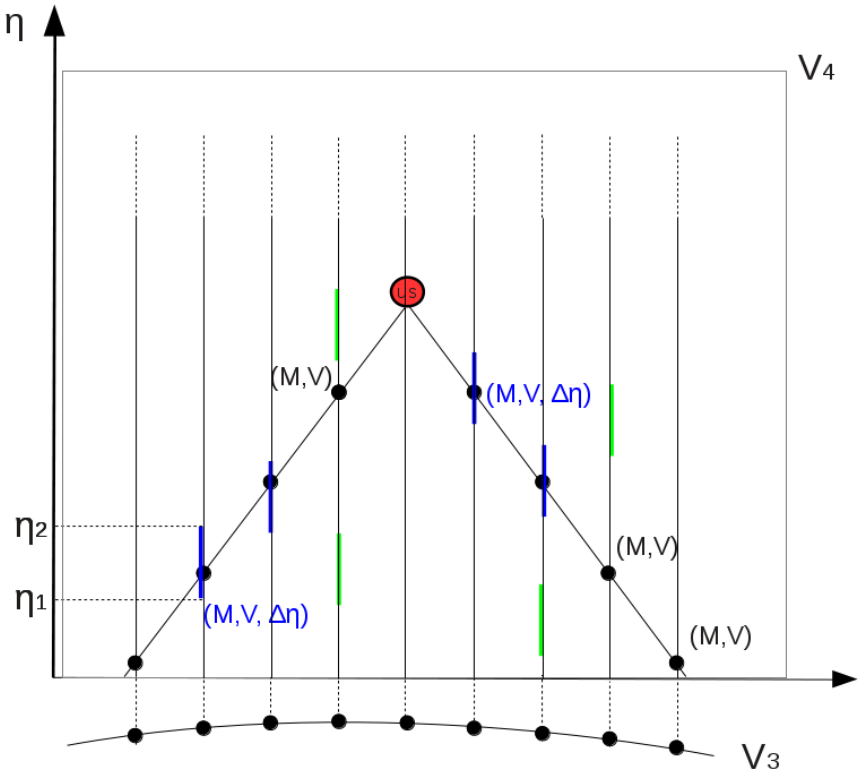

Figure 2.4: The spacetime diagram (conformal time η versus comoving space) : The red filled circle stands for our present position. The world lines of sources are vertical (perennial - black) and (ephemeral - blue), they cross the past light cone of the observer for observed objects. These ones are characterized by an absolute magnitude M and a comoving volume V for the perenial ones, and also by a lifetime duration $\Delta\eta$ for ephemeral ones.

2.4 The selection effect

With a limiting magnitude in observation, since the apparent luminosity decreases with distance, the sample average of absolute magnitudes does not provide us the mean absolute magnitude of the population, see Gunnar Malmquist (1922). This bias arises due to the limited sensitivity of instruments and telescopes, causing the over-representation of luminous objects in a magnitude-limited sample. Therefore, the average of absolute magnitude of the truncated sample will be brighter than the one of the complete sample [Binney & Merrifield, 1998]. This limitation in the apparent magnitude is the main selection effect.

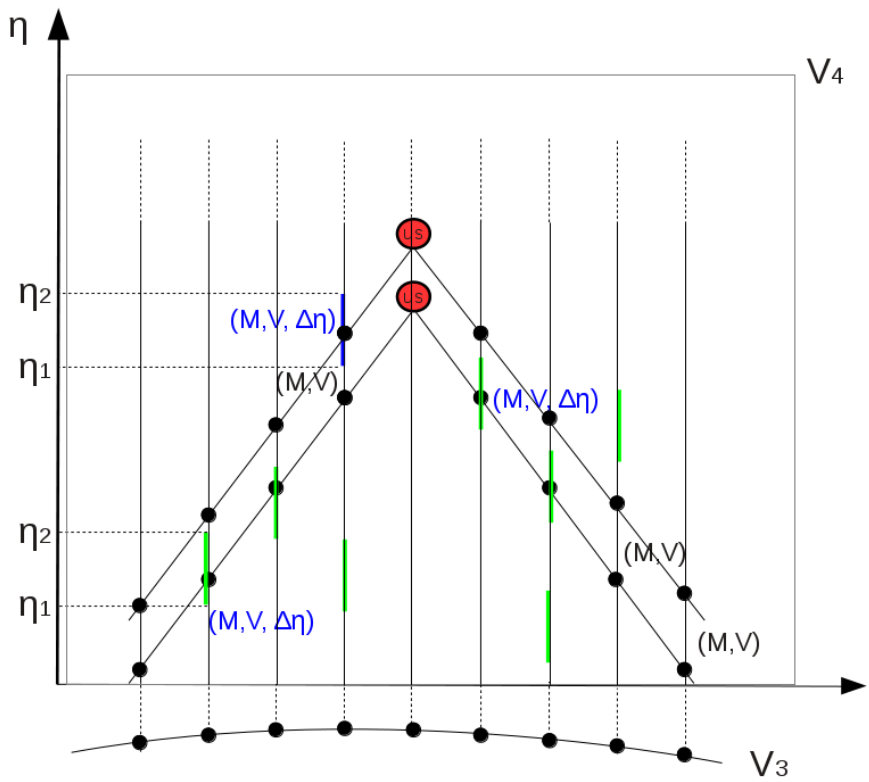

Figure 2.5: Similar to Fig.2.4 showing the appearance (blue)/disappearance (green) of new/existing supernovae due to the intersection/out of intersection of the light cone with their limited lifetime.

2.5 Modelling a sample of quasars

Given that the quasars are detected at high redshift, therefore the use of the Hubble diagram with this type of objects will be a good tool to obtain the cosmological information. The farthest quasar observed up to now is the quasar ULAS J112001.48+064124.3 detected at redshift $z = 7.085$ [E. Momjian et al 2013]. As usual, a non evolution of quasars is assumed on interpreting the non-linear Hubble diagram. In the following, we assume $H_\circ = 70\ Km.Mpc^{-1}.s^{-1}$ [D. N. Spergel et al 2013].

2.5.1 Statistical modelling

In this section, we focus on building a simulation sample of QSOs with an approach which is different than that used in the MCMC [Lewis et al 2002]. As we have noted in Sect.2.3, the QSOs are characterized intrinsically by an absolute magnitude M and a uniform distribution in the comoving space. If

the absolute magnitude M is distributed according to the luminosity function $f(M)$, then the QSO's sample is described with the product of two independent probability densities as follow:

$$dP_{th} \propto f(M)dM.dV \tag{2.1}$$

Assuming that the selection effects depend solely on m, we use a selection function $\phi(m)$ for describing the selection process in observation. Then, the probability density of the observable variables are described by:

$$dP_{obs} = \frac{\phi(m)dP_{th}}{P_{th}(\phi)} \tag{2.2}$$

where $P_{th}(\phi)$ is a normalization factor:

$$P_{th}(\phi) = \int \phi dP_{th} \tag{2.3}$$

We define the cumulative distribution function (cdf) of the random variable M as:

$$F(x) = \int_{-\infty}^{x} dP_{obs} = \frac{1}{P_{th}(\phi)} \int_{-\infty}^{x} f(M)dM\hat{V}(M) \tag{2.4}$$

where $\hat{V}(M)$ is defined as follows:

$$\hat{V}(M) = \int \phi(\zeta(z) + M)dV(z) \tag{2.5}$$

$F(x)$ is a uniform random variable between 0 and 1.

The absolute magnitude-volume diagram is a graphic representation of data that enables one to check visually any artifact in the distribution. For the true values of cosmological parameters, they are distributed uniformly along the V-axis and according to the luminosity distribution function along the M-axis. This diagram was proposed by Fliche and Souriau [H. Fliche & J. M. Souriau 1979], (hereafter named FS diagram).

2.5.2 Simulation technique

A simulation that describes a sample of QSOs in a cosmological model ($\lambda_\circ$, $\Omega_\circ$), depends on apparent magnitude m_{lim} and a luminosity function $f(M)$ (usually a Gaussian function, see appendix A.1. If the sample is "complete" up to apparent magnitude m_{lim}, then the selection function reads:

$$\phi(m) = \theta(m_{lim} - m) \tag{2.6}$$

where θ stands for a Heaviside function. For a given threshold m_{lim}, a source with absolute magnitude M is visible up to redshift z_{max}, a value that satisfies the following equation:

$$m_{lim} = \zeta(\ z_{max}) + M \tag{2.7}$$

Hence, let us define the function $v_{max}(M)$ that coincides with $\hat{V}(M)$ is this particular case:

$$\hat{V}(M) = \ v_{max}(M) = \ v(\ z_{max}) \tag{2.8}$$

Having defined a correspondence table of the cumulative distribution function $F(x)$, we can deduce by interpolation its inverse function. Hence, we generate a random uniform sample $\hat{F}$: $\hat{F}_k \in [0, 1]$ and we retrieve the corresponding absolute magnitude M_k by solving the inverse mapping :

$$M_k = F^{-1}(\hat{F}_k) \tag{2.9}$$

and hence the volume $v_{max}(M_k)$ following Eq.2.8 (or Eq.2.5 if $\phi(m)$ is not a Heaviside function). We generate a uniform random variable $\hat{V}_k$ between $[0,\ v_{max}(M_k)]$, and then we determine the redshift:

$$z_k = V^{-1}(\hat{V}_k) \tag{2.10}$$

where V^{-1} stands for the inverse fonction of the comoving volume Eq.1.37. Fig.2.6 shows the diagram v_{max} versus M for a given apparent magnitude m_{lim}. The red symbol plus is a realization of a uniform random variable distributed between 0 and $v_{max}(M_k)$. This step is done for N number of objects. Finally, we compute the apparent magnitude of each object according to Eq.1.50, to obtain a simulated sample of QSOs: $\{(z_k, m_k)\}_{k=1..N}$ (presented in Fig.2.7)[2]. We generated several samples that allowed us to validate the techniques used hereafter. We chose the standard cosmological model ($\lambda_\circ = 0.7$, $\Omega_\circ = 0.3$) and a Gaussian luminosity function of mean $M_0 = -20$ and standard deviation $\sigma_M = 0.3$, with a limiting apparent magnitude $m_{lim} = 26$.

An example of biased sample generator

Although not absolutely necessary, it is not uninteresting to describe a method of sample simulation, which can be found in the literature to estimate the correction of the bias of Malmquist, which is unfortunately erroneous. To generate a sample complete up to an apparent limiting magnitude m_{lim}, it consists on choosing ad hoc a redshift value domain so to minimize the number of objects

[2]This simulation sample is different than the one obtained by the MCMC method where the major drawback of this latter is that it is extremely time consuming [Vicent J. Martinez et al] (see COSMOMC based on MCMC approach)

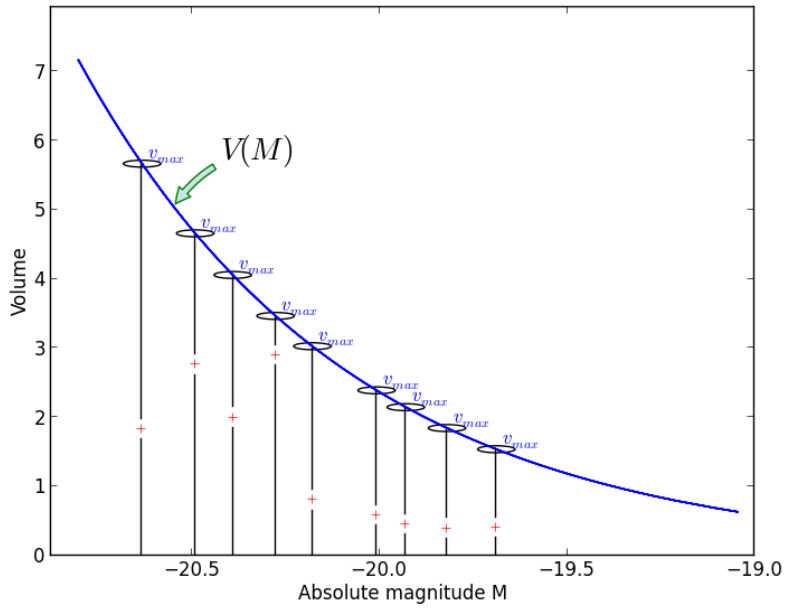

Figure 2.6: The blue curve gives the maximum volume $v_{max}(M)$ around the observer up to which an object with absolute magnitude M can be observed by using a device that detects up to a limiting apparent magnitude m_{lim}.

discarded because of the apparent magnitude threshold. Let the z_{max} be such a value, the corresponding volume reads V_{max} as given by Eq.1.37. Hence, one generates a uniform distribution of N objects between 0 and V_{max} and by assuming a Gaussian distribution of the absolute magnitude with a probability density function $g_G(M; M_0, \sigma_M)$ which gives the sample, $\{M_k,\ V_k\}_{k=1..N}$. Therefore, the redshift is determined by solving the inverse function of volume, $V^{-1}(V_k)$, and the apparent magnitude following Eq.1.50. As a result, one obtains the observed quantities $\{(z_k, m_k)\}_{k=1..N}$. Such a sample is shown in the $M-V$ diagram in Fig.2.8. We see clearly that the objects with absolute magnitude M are distributed uniformly until a maximum volume is reached. To represent the selection effects, we apply a threshold m_{lim} to the resulting sample excluding all events that have a larger value of apparent magnitude than m_{lim}; this cutoff is translated by a Heaviside function $\theta(m_{lim} - m)$. A cutoff at z_{max} is present (in the simulation), as described by a Heaviside function $\theta(z_{max} - z)$. Therefore, the probability density of the events reads:

$$dP_{obs} = \frac{1}{P_{th}(\theta_m \theta_z)} \theta(m_{lim} - m)\theta(z_{max} - z) g_G(M; M_0, \sigma_M) dM\, dV \qquad (2.11)$$

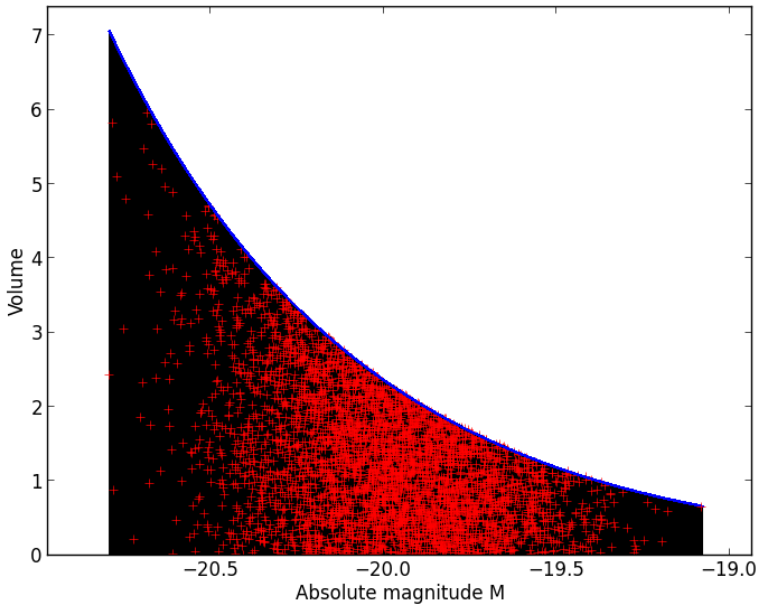

Figure 2.7: Simulation of a QSOs sample complete up to a limiting apparent magnitude. The blue curve caracterizes the threshold on apparent magnitude. The distribution of simulated sources (red) is uniform with respect to comoving volume (V) and Gaussian with respect to absolute magnitude (M).

where $P_{th}(\theta_m \theta_z)$ is a normalization factor:

$$P_{th}(\theta_m \theta_z) = \int \theta(m_{lim} - m)\theta(z_{max} - z) g_G(M; M_0, \sigma_M) dM\, dV \qquad (2.12)$$

The comparison between Fig.2.8 and Fig.2.9-B shows up the sources (red) that are not bright enough to be visible at a limiting magnitude m_{lim}. The histogram in Fig.2.9-A shows this distribution of absolute magnitudes of a complete sample up to redshift z_{max}, the red domain corresponds to sources not enough bright to be visible with a limiting apparent magnitude m_{lim}. The average of the observed sample (blue domain) is found to be brighter than the mean that characterizes the population ($\langle M \rangle = M_0 - \delta M$), appearing noticeably on the histogram. This is the effect of the Malmquist bias. The number deficit corresponds to $\approx 20\%$ of the sample. Contrary to the technique used above, determining a maximum redshift of the sample before starting the simulation is unlikely since we would lose a large number of objects, as can be observed in the empty circle in Fig.2.9-B. In other words, we applied cutoff on the redshift, in addition to the cutoff applied on the apparent magnitude, might be the cause of raising the systematic errors. Without this cutoff, the circle must contain a such number of objects. Moreover, a selection function

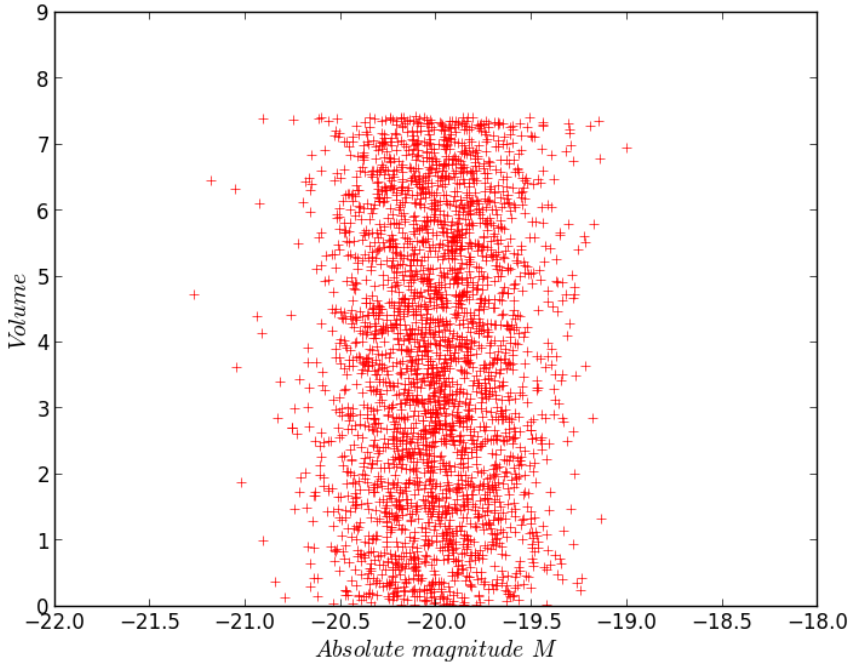

Figure 2.8: A complete sample up to redshift z_{max} with $(\Omega_\circ, \lambda_\circ = 0.3, 0.7)$. A uniform distribution appears in vertical axis and a Gaussian distribution in the horizontal axis.

depending on the redshift put an additional correlation between the variables, which is inconsistent with the hypotheses of work of the statistical test described in Chap.3. This is the main difference between this method and the simulation method described in Sect.2.5.1, which make this last the recommended method of simulation.

2.5.3 The k-correction

As we have seen in Sects.1.9 & 2.2, the cosmological expansion of the universe shifts the spectrum of QSO toward the red wavelength (Fig.2.10). Therefore, in order to have an homogeneous data sample, one needs a $k-$correction ([Humason, Mayall, & Sandage 1956]; [Oke & Sandage 1968]). Namely, one uses the absolute magnitude M at the same wavelength for all objects at any redshift and Eq.1.50 becomes:

$$m_X = M_Y + M_X - M_Y + \zeta(z) \tag{2.13}$$

$$m_X = M_Y + k_{XY}(z) + \zeta(z) \tag{2.14}$$

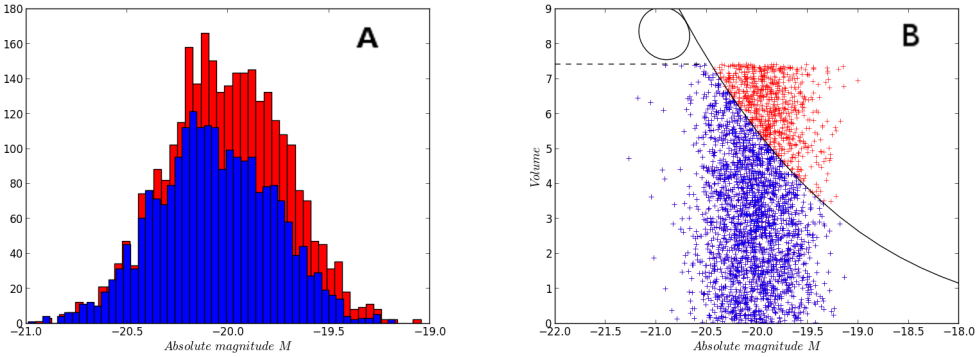

Figure 2.9: Distributions of a complete sample up to redshift z_{max} and limiting magnitude m_{lim}, by disentangling the visible objects (blue) from those that are not visible (red). A): Histogram of absolute magnitudes. B): M-V diagram.

where m_X is the apparent magnitude in the observed X band, M_Y is the absolute magnitude of the source in the rest-frame Y band and k_{XY} is the k-correction between the X and Y bands. k_{XY} is calculated through the rate of the observed flux in X band and the one measured in a "fictive" filter in the rest frame Y [Hogg, D. W. 2002]:

$$k_{XY}(z) = -2.5log_{10}(1+z) - 2.5log_{10}\left[\frac{\int \Phi(\lambda)X(\lambda)d\lambda}{\int \Phi(\frac{\lambda}{1+z})Y(\lambda)d\lambda}\frac{\int \Phi_0(\lambda)Y(\lambda)d\lambda}{\int \Phi_0(\lambda)X(\lambda)d\lambda}\right] \quad (2.15)$$

where $\Phi(\lambda)$ is the spectrum of the source and $\Phi_0(\lambda)$ is the spectrum of the reference object.

Because, quasars spectrum shows various broad emission lines, their k-correction accounts for a component due to the underlying continuum, Kcont, and another component due to the emission lines, Kem [Ross N. P. 2013]. We define the redshift's term:

$$\zeta(z) = 5\log_{10}\left(\frac{d_L(z)}{10pc}\right) + k(z) \quad (2.16)$$

Thus, Eq.2.14 is written as follows:

$$m = M + \zeta(z) \quad (2.17)$$

Because of the presence of the emission lines in the spectrum of QSO, the k-correction is not a monotonous function. Hence, the redshift's term in Eq.2.17 is no longer an invertible function.

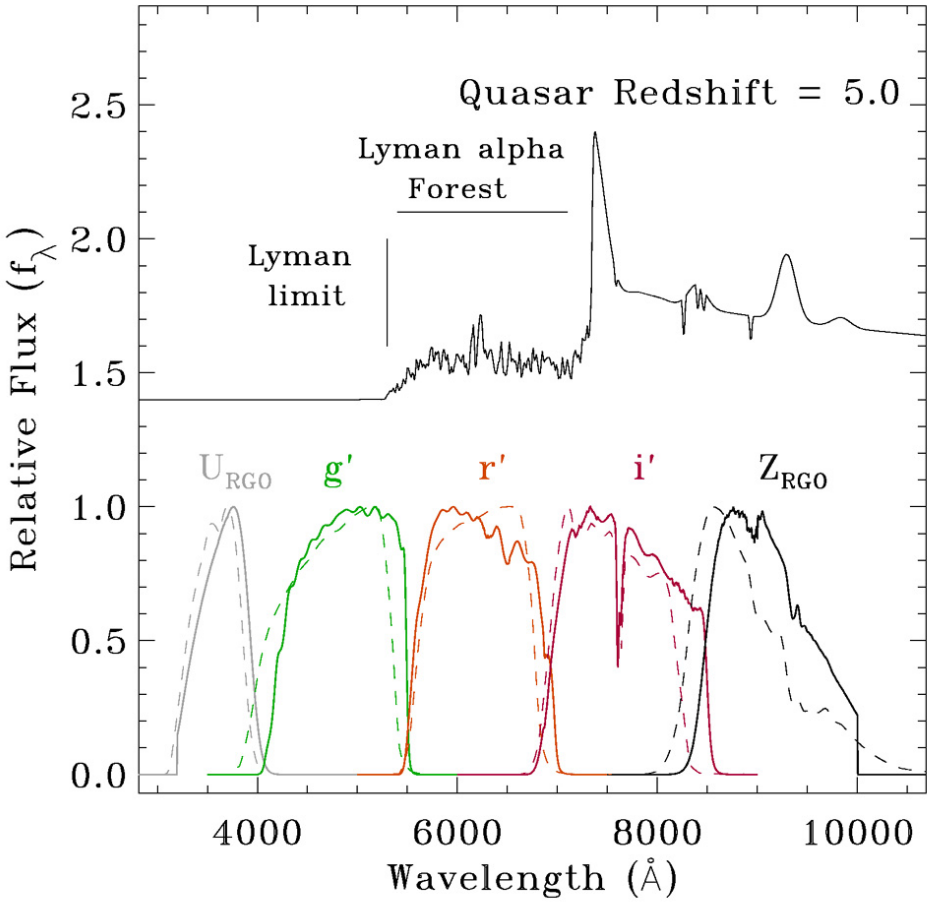

Figure 2.10: A typical quasar spectrum at redshift z =5. The QSO can be observed in two bands thanks to the Lyα emission line which is in the i' band and the Lyα forest which is along of the r' band. Figure credit: [R. Sharp et al 2001].

2.6 Conclusion

In this chapter we have described how to model a QSO sample from a theoretical to an observed probability laws that describes the events. We presented an efficient simulation method for providing samples in agreement with the working hypotheses.

CHAPTER 3

The null correlation technique

Contents

3.1 Introduction **37**

3.2 Weighting factors **40**

3.3 Luminosity function and selection function **44**

3.4 Kolmogorov-Smirnov test **46**

3.5 The V/V$_{max}$ test **47**

3.5.1 Calculation of the V/V$_{max}$ terms 48

3.6 Conclusion **50**

The correction of biased statistics requires to know the probability law of characteristics describing the sample used, such as the luminosity function and the selection effects. Hereafter, we use a robust statistical method which does not depend on the luminosity function and the selection function. These features are derived as a result of this approach. The innovative aspect of this approach is the use of the weighting factor.

3.1 Introduction

The null correlation technique was formulated by [H. Fliche & J. M. Souriau 1979] for quasar statistics and later adapted for the brightest cluster galaxies by [Triay, R. et al. 1990]. To illustrate this technique, let us describe a simple example of linear correlation with a uniform distribution on the y-axis, and a Gaussian distribution on the x-axis with mean 0 and standard deviation 0.5.

The probability density function of the Gaussian distribution:

$$\mathrm{d}P \propto g_G(x)\mathrm{d}x\, f(y)\mathrm{d}y \tag{3.1}$$

where $f(y)$ is a Heaviside function:

$$f(y) = \begin{cases} 1 & \text{if } 0 \leq y < 1 \\ 0 & \text{otherwise} \end{cases} \tag{3.2}$$

With a rotation of angle $\frac{\pi}{4}$ the distribution appears as shown in Fig.3.1. Now, let us suppose that the observer is faced to analyze such a distribution, which is described with probability law in the (X, Y) frame:

$$\mathrm{d}P \propto G(X, Y)\mathrm{d}X\, \mathrm{d}Y \tag{3.3}$$

where G stands for the probality density function of X and Y, which works as a correlation function between the random variables X and Y:

$$G(X, Y) = g_G(X\cos(\theta) - Y\sin(\theta))\, h(X, Y) \tag{3.4}$$

with

$$h(X, Y) = \begin{cases} 1 & \text{if } 0 \leq X\sin(\theta) + Y\cos(\theta) < 1 \\ 0 & \text{otherwise} \end{cases} \tag{3.5}$$

The aim is to estimate the value of θ by assuming a linear correlation between these random variables. With the usual procedure to estimate such a value by mean of a least square fitting, one is faced to the arbitrary choice of the distance (horizontal or vertical). A way to overcome such a problem is to translate this optimization into finding a way to make the random variables independents. Eq.3.3 shows that the correlation between X and Y is given by the correlation function $\rho \propto h(X, Y)\, e^{\cos(\theta)\,\sin(\theta)\,X\,Y}$ as part of the probability density function. To remove such a correlation, one can use a weighting factor $w_i = \frac{1}{\rho}$. The weighted covariance reads:

$$\Gamma(\theta) = \sum_{i=1}^{N} w_i(X_i - \langle X\rangle)(Y_i - \langle Y\rangle) \tag{3.6}$$

where:

$$\langle X\rangle = \sum_{i=1}^{N} w_i X_i \quad \text{and} \quad \langle Y\rangle = \sum_{i=1}^{N} w_i Y_i \tag{3.7}$$

is expected to be null for the true value of theta, $\Gamma(\theta) = 0$, see Fig.3.2.

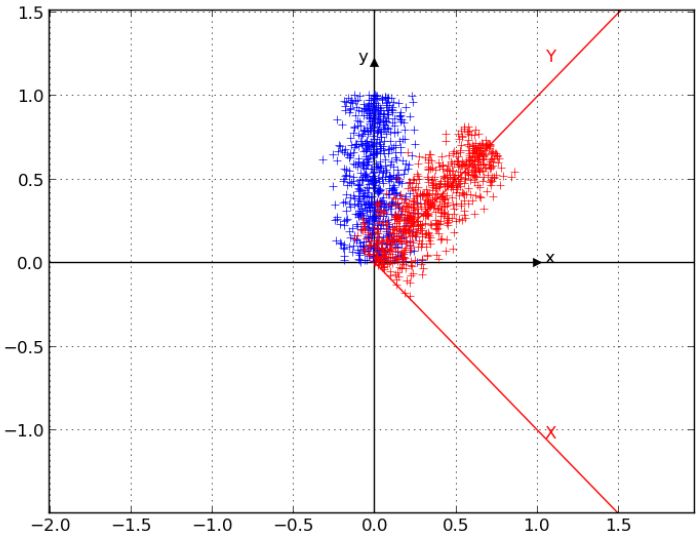

Figure 3.1: The distribution of the sample in both (x, y) and (X, Y) frames.

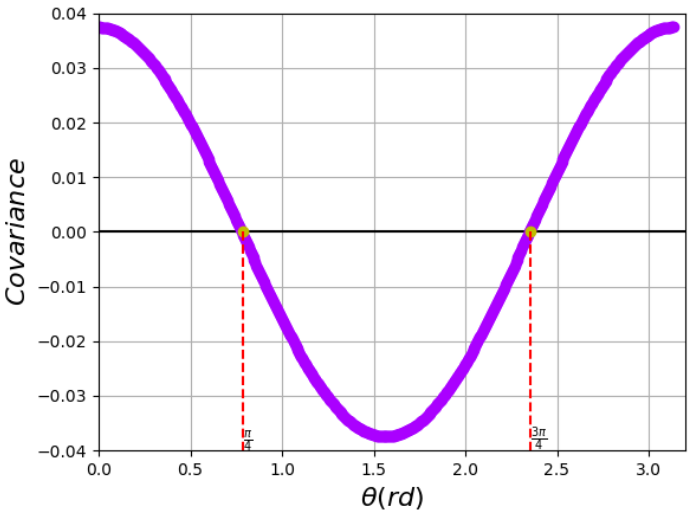

Figure 3.2: Searching the zero value of the weighted covariance of X and Y. The equation $\Gamma(\theta) = 0$ shows two solutions, the first one ($\theta = \frac{\pi}{4}$) matches the one used for simulation.

The Hubble diagram of sources at cosmological distances shows a correlation between the two observables, the redshift z and apparent magnitude m, which are not linearly dependent.

Usual statistical approach consists to fit the data to the theoretical curve by means of a least-square method, so that the values of the cosmological parameters minimize the dispersion. To know if the selection effects bias the estimates of these parameters, we must make assumptions to describe them in the probability distribution of these data.
The null correlation technique does not require to make such additional hypotheses, but solely that there is no selection effects on redshift.

According to the formula 2.2, a simulated sample under the model ($\lambda_\circ = 0.7$, $\Omega_\circ = 0.3$) is performed, we used a Gaussian luminosity function; this sample is used in this section to discuss on the statistical technique.

The observed data are descibed in the (M, m) frame by the following probability density:

$$\mathrm{d}P_{(M,m)} = \rho(z)\phi(m)f(M)\mathrm{d}M\,\mathrm{d}m; \quad \rho(z) = \frac{\partial V}{\partial m} \tag{3.8}$$

where $\rho(z)$ is a correlation function between M and m, which corresponds to the Jacobian of the transformed variables $(M, V) \to (M, m)$. The correlation of the apparent magnitude and the absolute magnitude is shown in Fig.3.3. At first glance, for the true values of the cosmological parameters $(\Omega_\circ, \lambda_\circ)$, the correlation between the random variables M and m vanish by dividing each event by the correlation function $\rho(z)$. This correlation is given by the weighted covariance of M and m, it depends on cosmological parameters and reads:

$$\Gamma(\Omega_\circ, \lambda_\circ) = \sum_{k=1}^{N} \omega_k (M_k - \langle M \rangle)(m_k - \langle m \rangle) \tag{3.9}$$

where ω_k is a weighting factor (details in Sect.3.2) which is inversely proportional to $\rho(z_k)$. The weighted averages $\langle M \rangle$ and $\langle m \rangle$ are defined as follows:

$$\langle M \rangle = \sum_{k=1}^{N} \omega_k M_k \tag{3.10}$$

$$\langle m \rangle = \sum_{k=1}^{N} \omega_k m_k \tag{3.11}$$

The solutions of equation $\Gamma(\Omega_\circ, \lambda_\circ) = 0$ are candidate values for $\Omega_\circ$ and $\lambda_\circ$, they correspond to a curve on the $(\Omega_\circ, \lambda_\circ)$ plane.

3.2 Weighting factors

The correlation function of the probability density given by Eq.3.8, depends on the Friedmann-Lemaître model:

$$w(z) = \frac{1}{\rho(z)} = \frac{1}{\frac{\partial V}{\partial m}} \tag{3.12}$$

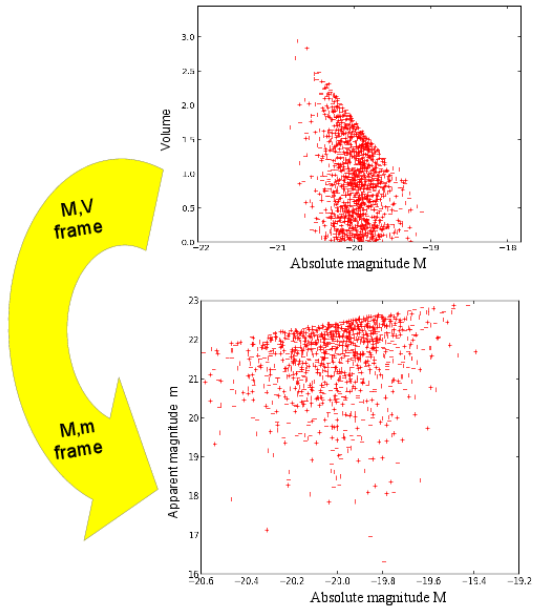

Figure 3.3: Data distribution in the (M, V) frame and (M, m) frame.

For the case of the close Universe $\kappa_0 > 0$:

We compute $\frac{\partial V}{\partial m} = \frac{\partial V}{\partial \zeta} = \frac{\partial V}{\partial z} / \frac{\partial \zeta}{\partial z}$ (the details of calculation are in the appendix **??**). Then we obtain:

- Without the k-correction term:

$$\frac{\partial V}{\partial \zeta} = \vartheta \frac{(1 - \cos(2\kappa_0^{\frac{1}{2}}\tau))}{\left[(1+z)\sqrt{P(\frac{1}{1+z})} + \kappa_0^{\frac{1}{2}} \cot(\kappa_0^{\frac{1}{2}}\tau)\right]} \tag{3.13}$$

- With the k-correction term:

$$\frac{\partial V}{\partial \zeta} = \vartheta \frac{(1 - \cos(2\kappa_0^{\frac{1}{2}}\tau))}{\left[(1+z)\sqrt{P(\frac{1}{1+z})} + \kappa_0^{\frac{1}{2}} \cot(\kappa_0^{\frac{1}{2}}\tau)\right] + \left[(1+z)^2\sqrt{P(\frac{1}{1+z})}\frac{\partial k(z)}{\partial z}\right]} \tag{3.14}$$

where $\vartheta = \frac{2\pi \ln(10)}{5\kappa_0}$.

For the case of the open Universe $\kappa_0 < 0$:

The same calculation for negative κ_0, We obtain:

- Without the k-correction term:

$$\frac{\partial V}{\partial \zeta} = \vartheta \frac{(\cosh(2|\kappa_0|^{\frac{1}{2}}\tau) - 1)}{\left[(1+z)\sqrt{P(\frac{1}{1+z})} + |\kappa_0|^{\frac{1}{2}} \coth(|\kappa_0|^{\frac{1}{2}}\tau)\right]} \tag{3.15}$$

- With the k-correction term:

$$\frac{\partial V}{\partial \zeta} = \vartheta \frac{(\cosh(2|\kappa_0|^{\frac{1}{2}}\tau) - 1)}{\left[(1+z)\sqrt{P(\frac{1}{1+z})} + |\kappa_0|^{\frac{1}{2}} \coth(|\kappa_0|^{\frac{1}{2}}\tau)\right] + \left[(1+z)^2\sqrt{P(\frac{1}{1+z})}\frac{\partial k(z)}{\partial z}\right]} \tag{3.16}$$

where $\vartheta = \frac{2\pi \ln(10)}{5|\kappa_0|}$.

For the case of the flat Universe $\kappa_0 = 0$:

- Without the k-correction term:

$$\frac{\partial V}{\partial \zeta} = \vartheta \frac{\tau^3}{\tau(1+z)\sqrt{P(\frac{1}{1+z})} + 1} \tag{3.17}$$

- With the k-correction term:

$$\frac{\partial V}{\partial \zeta} = \vartheta \frac{\tau^3}{\tau(1+z)\sqrt{P(\frac{1}{1+z})} + 1 + \tau(1+z)^2\sqrt{P(\frac{1}{1+z})}\frac{\partial k(z)}{\partial z}} \tag{3.18}$$

where $\vartheta = \frac{4\pi \ln(10)}{5}$.
The weighting factor reads:

$$\omega_k = \frac{w(z_k)}{\sum_{i=1}^{N} w(z_i)} \tag{3.19}$$

The price to pay for using the weighting factors is the partial loss of the statistical information [Triay et al 1991], mostly at high redshift as we show in Fig.3.4. It can be evaluated by measuring of the percentage of the deficit as follows:

$$\mathcal{L}_1 = 1 + \frac{1}{\ln N}\sum_{k=1}^{N} \omega_k \ln \omega_k \tag{3.20}$$

Finally, with the aim of ensuring the estimation of the $\lambda_\circ$ and $\Omega_\circ$ without depending on a particular choice of the magnitude, the weighting factor is multiplied by arbitrary functions of M and m. These functions avoid the concentration of all the weight on the near objects. We have chosen the following

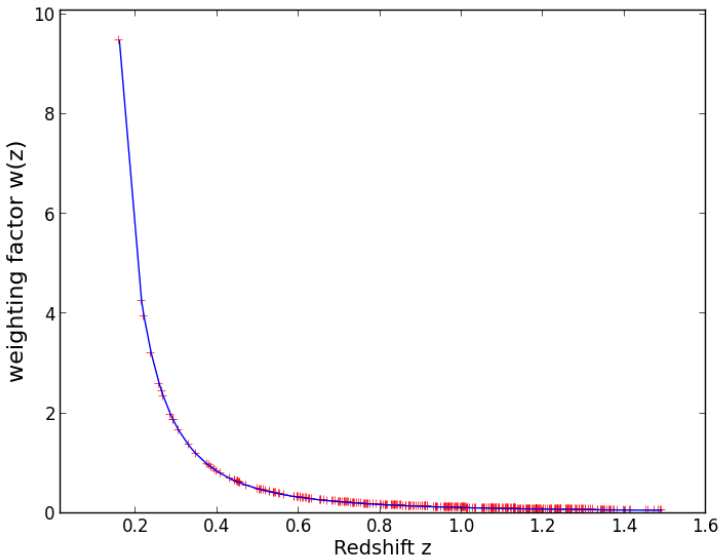

Figure 3.4: The inverse of the correlation function versus redshift for a given cosmological model.

function in particular: $10^{\frac{\beta}{5}[m-M]}$. Therefore, the weighting factor is calculated by the following formula:

$$w_\beta(z) = \frac{1}{\frac{\partial V}{\partial \zeta}} 10^{\frac{\beta}{5}[m-M]} = \frac{1}{\frac{\partial V}{\partial \zeta}} 10^{\frac{\beta}{5}\zeta} \tag{3.21}$$

where β is chosen so that weighting factors ω_k[1] are as close as possible. Its value is determined by minimizing the function over the sample:

$$\mathcal{L}_0 = Max\{w_\beta(z)\} - Min\{w_\beta(z)\} \tag{3.22}$$

Fig.3.5 shows the deficit of statitical information versus β (left panel) that can be compared to the range of weighting factors, that can be compared to the dispersion of weighting factors values (right panel). The weaker of $\mathcal{L}_1$ is, the more reliable the results. A small difference on the values of β obtained by the two methods does not have a significant impact on the estimation of the cosmological parameters. On the other hand, the simulations show that it is preferable to perform the minimization of $\mathcal{L}_0$ rather than $\mathcal{L}_1$. The latter is used loss estimator. The weighting factor versus redshift as it is shown in Fig.3.6. The use of these weighting factors favors the sources at low and high redshift compared to other, which is at the benefit to recover cosmological information, see Fig.3.4. We seek the values of cosmological parameters in the ($\Omega_\circ$,

[1] $\omega_k = \frac{w_\beta(z_k)}{\sum_{i=1}^{N} w_\beta(z_i)}$

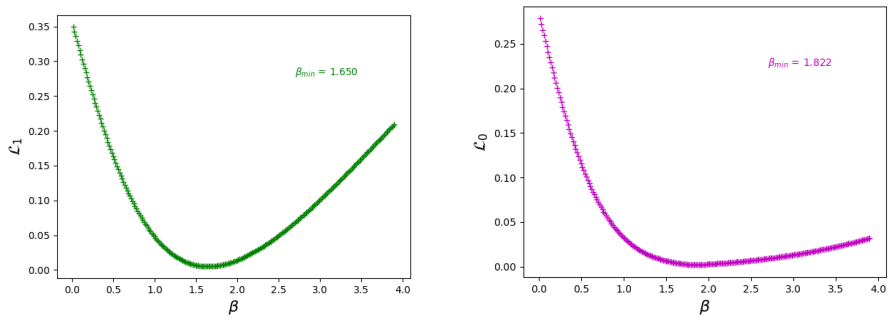

Figure 3.5: The percentage of the lost of the statistical information (left: for $\mathcal{L}_1$, right: for $\mathcal{L}_0$) with respect to the parameter β.

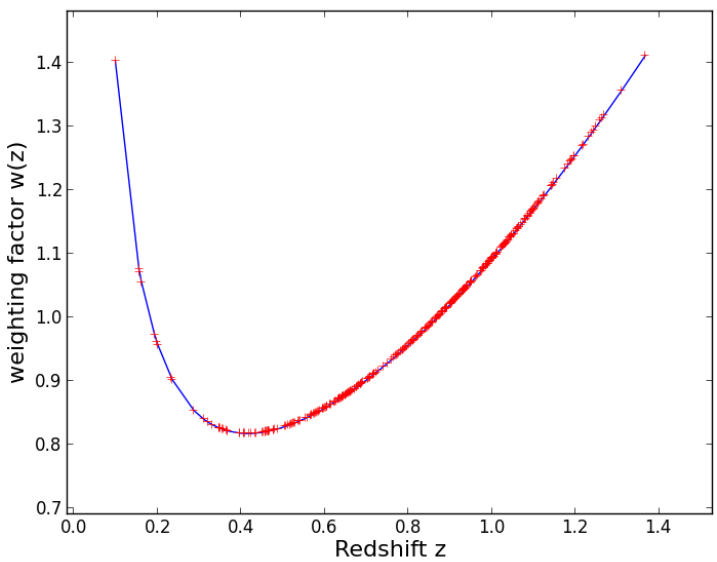

Figure 3.6: The weighting factor with respect to the redshift for a given cosmological model.

$\lambda_\circ$) diagram with a zero weighted covariance; bounced models are explicitly excluded. The statistics depend on data (m_k, z_k) and are calculated in each vertex of a grid $(\Omega_\circ^i,\ \lambda_\circ^j)_{i,j=0..n}$ according to Eqs.1.50, 3.21 and 3.9. Such a procedure separates the domain in two parts, positive covariance and negative covariance on the ($\Omega_\circ$, $\lambda_\circ$) diagram, see Fig.3.7. The roots corresponding to a zero weighted covariance, located between the negative and positive values, are determined by mean of horizontal and vertical parabolic interpolation. The set of solutions defines the null correlation curve (NCC): *the candidate values of the cosmological parameters.* Fig.3.7 shows the NCC when using the simu-

lation sample with the standard model. Note that the red circle on the curve corresponds to this model, what ensures the validity of this method.

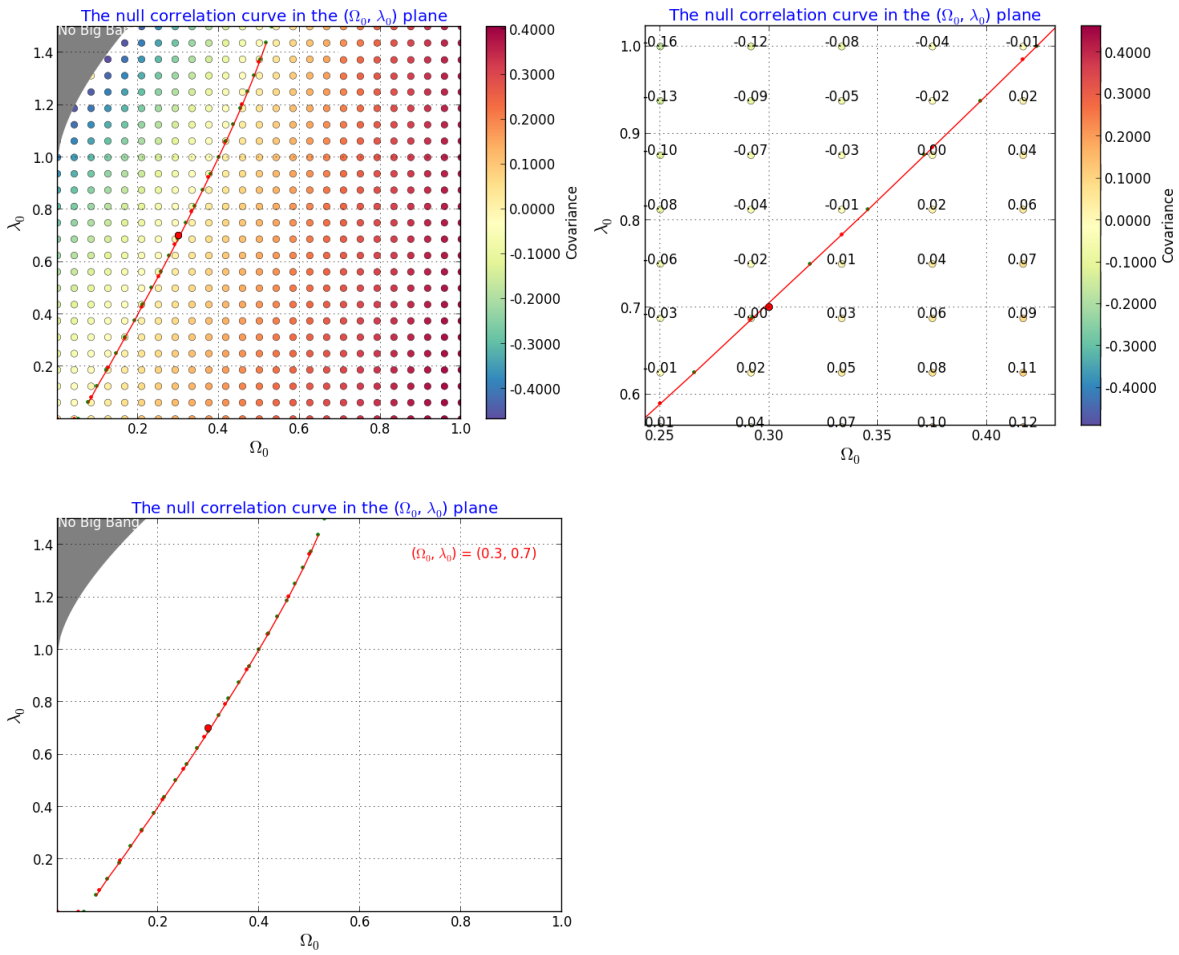

Figure 3.7: Left to right, top to bottom. The values of the weighted covariance with respect to cosmological model. The null values of the NCC are found by horizontal and vertical interpolations in the covariance grid. The NCC in the ($\Omega_\circ$, $\lambda_\circ$) plane retrieve the initial simulation model (the filled red circle).

We came by simulations to the conclusion that the NCC depends on the cosmological model and the sample features. Simulation samples were performed by assuming the standard model ($\Omega_\circ = 0.3$, $\lambda_\circ = 0.7$) and a Gaussian luminosity function $g_G(M; M_0 = -20, \sigma_M = 0.6)$ with different limiting apparent magnitude ($m_{lim} = 26$, $m_{lim} = 24$) and different sample sizes N. Fig.3.8 shows two NCCs which contain the values of cosmological parameters used to simulate the samples. Any candidate model chosen on a NCC which is different than the one used to simulate the related sample, has a different NCC. The shape of the NCC depends strongly on the chosen sample. Fig.3.9 shows the

NCC (red curve) corresponding to a simulated sample in the model ($\Omega_\circ = 0.1$, $\lambda_\circ = 1.2$). Hence, we chose the model ($\Omega_\circ = 0.19$, $\lambda_\circ = 1.4$) on this NCC to simulate another sample with the same characteristics (luminosity function, size and limited apparent magnitude). The corresponding NCC, which includes the values of the cosmological parameters used to perform the simulation, but switches around the candidate model with respect to the previous one (blue curve in Fig.3.9). The accuracy of the null correlation approach is

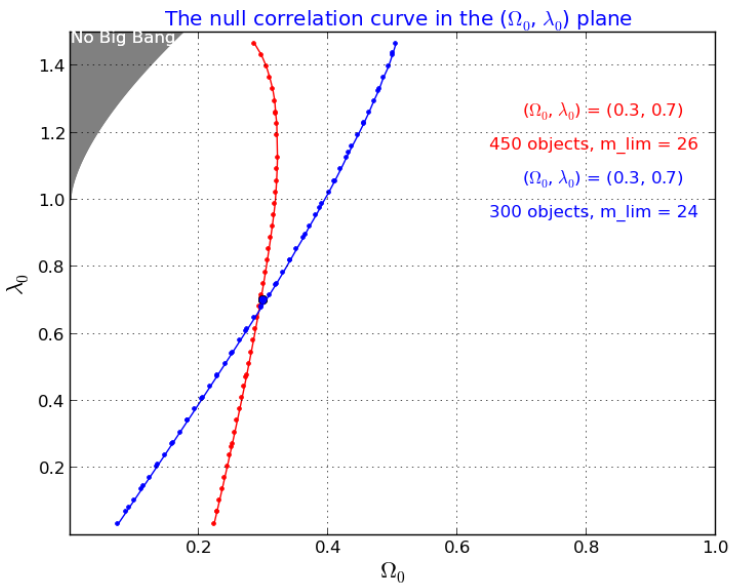

Figure 3.8: The shape of the NCC of two simulated samples with different sizes and different apparent magnitude limits.

ascertained by the study of the statistical fluctuations. Hence, one hundred random complete samples were generated according to the density defined in Eq.2.2. These samples were simulated with the same cosmological model (flat standard model), Gaussian luminosity function, size and limiting apparent magnitude. These samples provided us with one hundred NCCs for computing the statistics of Eq.3.9. The analysis was performed by varying the number of objects. It turns out that the statistical estimates are more accurate with larger number of objects. As shown in Fig.3.10, a butterfly shape is obtained by the hundredth NCCs. Fig.3.10 (top panel, left) is obtained for samples of 35 objects, (top panel, right) for samples of 350 objects and (bottom panel) for samples of 2000 objects. In the first figure, the shape of the butterfly is wide, only 30% of the curves retrieved the initial model. For 350 objects, most (98%) of the curves retrieves the initial simulated model. In the bottom panel we see clearly that the model is retrieved for all samples with high accuracy.

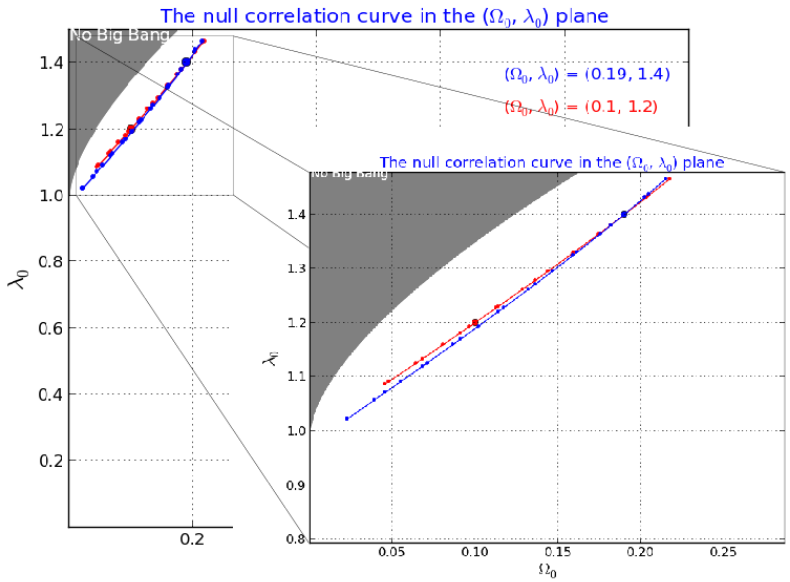

Figure 3.9: The dependence of cosmological model on the NCC appears in these curves when we use two samples with same characteristics but with different cosmological models.

3.3 Luminosity function and selection function

The null correlation approach allows us to determine the shapes of the luminosity function $f(M)$ and the selection function $\phi(m)$. For the true values of the cosmological parameters, the sample is described with the following probability density:

$$\mathrm{d}P_w = f_w(M)\mathrm{d}M\,\phi_w(m)\mathrm{d}m \tag{3.23}$$

where the functions $f_w(M)$ and $\phi_w(m)$ are defined as follows:

$$f_w(M) \propto 10^{\frac{-\beta}{5}M} f(M) \tag{3.24}$$

$$\phi_w(m) \propto 10^{\frac{\beta}{5}m} \phi(m) \tag{3.25}$$

They are evaluated from the cumulative distribution functions:

$$F_w(M) = \int_{-\infty}^{M} f_w(M)dM \tag{3.26}$$

$$\Phi_w(m) = \int_{-\infty}^{m} \phi_w(m)dm \tag{3.27}$$

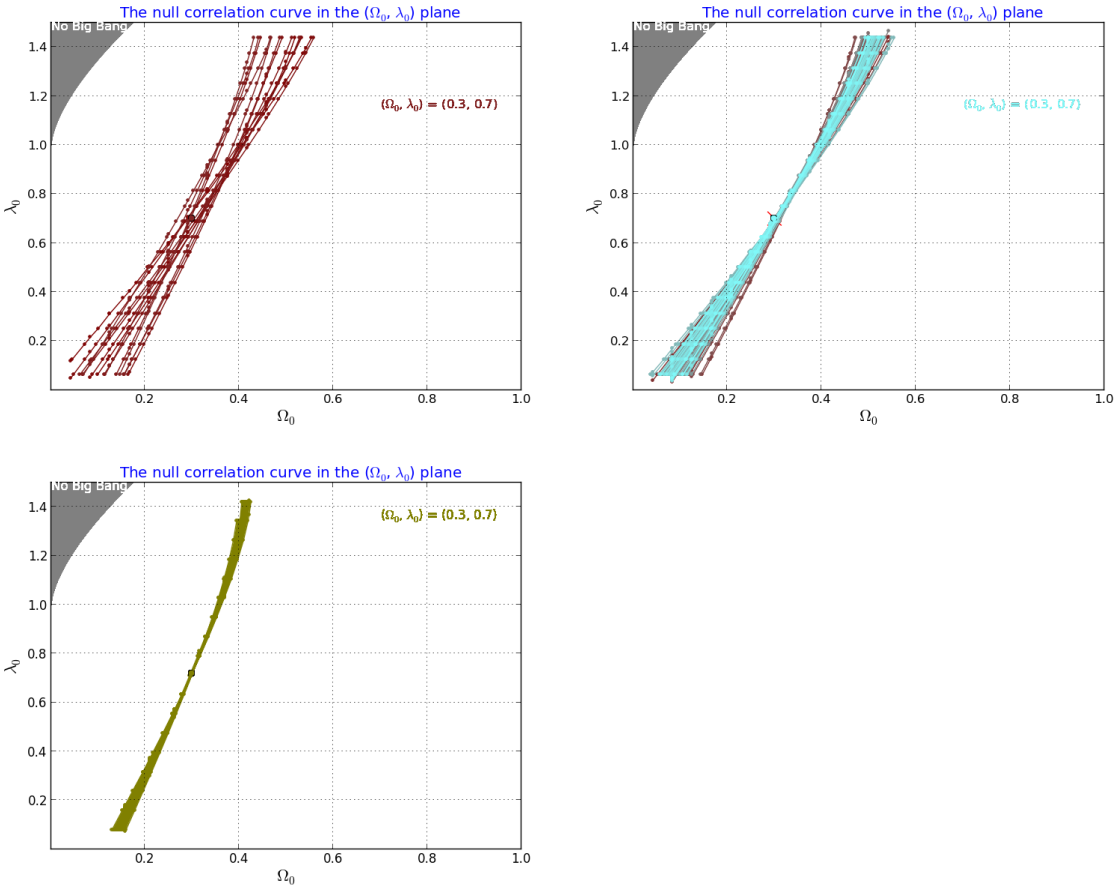

Figure 3.10: The precision of the method is shown obviously by increasing the size of the sample. From left to right and from top to bottom, the size of the sample increases from 35 to 350 to 2000 respectively. We see that the statistical fluctuations decrease with the increasing of the number of objects.

For a sufficiently large number of objects, $F_w(M)$ and $\Phi_w(m)$ can be approximated by step-functions $F_w^{st}(M)$ and $\Phi_w^{st}(m)$ as follows:

$$F_w(M) \approx F_w^{st}(M) = \sum_{k=1}^{N} \omega_k \theta(M - M_k) \tag{3.28}$$

$$\Phi_w(m) \approx \Phi_w^{st}(m) = \sum_{k=1}^{N} \omega_k \theta(m - m_k) \tag{3.29}$$

where θ is the Heaviside function. To obtain the functions $f(M)$ and $\phi(m)$, we compute $f_w(M)$ and $\phi_w(m)$ by determining the derivatives of $F_w(M)$ and $\Phi_w(m)$ and use Eqs.3.24 and 3.25. In order to avoid the arbitrary choice of

the fit, the derivatives of smooth approximations of $F_w^{st}(M)$ and $\Phi_w^{st}(m)$ are determined by the linear interpolations. Then, the luminosity function $f(M)$ and the technological function $\phi(m)$ are determined as follows:

$$\begin{cases} f(M) \propto \frac{F_w^{st}(M+\Delta_r M)-F_w^{st}(M-\Delta_l M)}{\Delta_r M+\Delta_l M} 10^{\frac{\beta}{5}M} \\ \phi(m) \propto \frac{\Phi_w^{st}(m+\Delta_r m)-\Phi_w^{st}(m-\Delta_l m)}{\Delta_r m+\Delta_l m} 10^{\frac{-\beta}{5}m} \end{cases} \tag{3.30}$$

where $\Delta_r M$ and $\Delta_l M$ are the right and left intervals of the variable M in which contain $\frac{\sqrt{N}}{2}$ values of $M_k > M$ and $M_k < M$ respectively. The intervals $\Delta_r m$ and $\Delta_l m$ also contain $\frac{\sqrt{N}}{2}$ values of $m_k > m$ and $m_k < m$ respectively. As a result of the use of linear interpolation technique, the $(\frac{\sqrt{N}}{2})$ points on the left side and the $(\frac{\sqrt{N}}{2})$ points on the right side are isolated and therefore, must be discarded in the estimation of the functions $f(M)$ and $\phi(m)$. Figs.3.11 and 3.12 show the result obtained for $f(M)$ and $\phi(m)$ with simulated samples in which $f(M)$ is a Gaussian function with an average $M_0 = -20$, a standard deviation $\sigma_M = 0.15$, a Gumbel function with mode $M_0 = -20$ and a scale parameter $\gamma_M = 1.09$ (see appendix A.2). The $\phi(m)$ function is a Heaviside function. The upper panels of these figures show the statistics of the luminosity function. The (left panel) illustrates the empirical cdf of the evaluated luminosity function represented by the green curve, it is compared to the theoretical cdf of the luminosity function represented by the red curve. The (right panel) shows the luminosity function with respect to the absolute magnitude. The red curve is the luminosity function used for the simulation of the sample and the green "plus" symbols represent the luminosity function evaluated by the interpolation technique. The lower panels show the statistics of the selection function. The (left panel) represents the empirical cdf of the evaluated selection function represented by the green curve and the theoretical cdf of the Heaviside function represented by the red curve. The (right panel) shows the technological function with respect to the apparent magnitude m. The function $\varphi(m) \equiv \phi(m)$ (the green "plus" symbols) obtained is the same as the one used in the simulation, it is evaluated as a Heaviside function (in red). These figures show that the initial luminosity and technological functions used for the simulation are retrieved perfectly by this technique with $\langle M \rangle = -20.005$ and $\sigma_M = 0.158$.

3.4 Kolmogorov-Smirnov test

The Kolmogorov-Smirnov (KS) test is a nonparametric test that allows one to check whether deviations between the theoretical cdf and the empirical (step) cdf can be considered as random fluctuations. The KS is based on the probability law of the maximum distance defined as follows:

$$D_{max} = Max(|cdf_{Theoretical} - cdf_{Empirical}|) \tag{3.31}$$

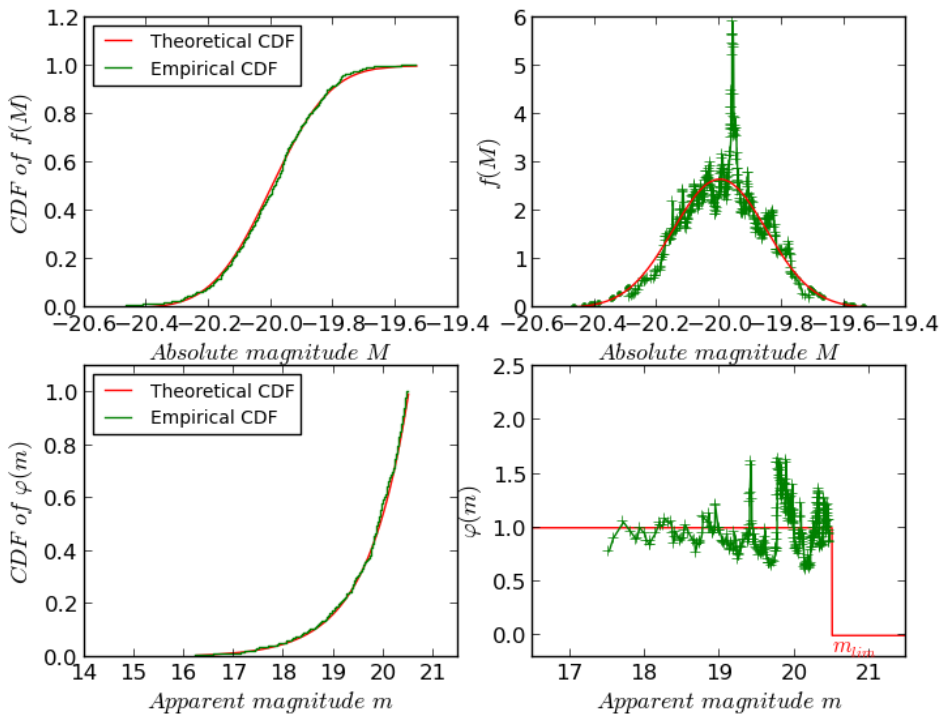

Figure 3.11: Statistics of the luminosity function (upper panels) and the selection function (lower panels)

The result of D_{max} is compared to the critical value, "$D_{max,\alpha}$", (for a significance level α) obtained from the KS table with respect to the size of the sample. It allows one to decide if the null hypothesis is accepted ($D_{max} \leq D_{max,\alpha}$) or rejected ($D_{max} \geq D_{max,\alpha}$) for a given α (by default, $\alpha = 5\%$). Fig.3.13 shows the cdf of three distributions with increasing sample size (N) (from left to right) that can be compared to the theoretical cdf of a uniform distribution (solid line). It shows how the empirical and the theoretical cdf get closer when N grows.

The KS test enables one to check whether specific functions $f(M)$ and $\phi(m)$ fit the databy comparing $F_w(M)$ with $F_w^{st}(M)$ and $\Phi_w(m)$ with $\Phi_w^{st}(m)$. For this purpose we started with the case of the luminosity function. If $f(M)$ has a Gaussian form (App.A.1), Eq.3.24 shows that $f_w(M)$ is still Gaussian with a mean $\langle M \rangle$ defined in Eq.3.11 and a standard deviation σ_M defined as the following:

$$\sigma_M^2 \approx \frac{N}{N-1} \sum_{k=1}^{N} \omega_k (M_k - \langle M \rangle)^2 \tag{3.32}$$

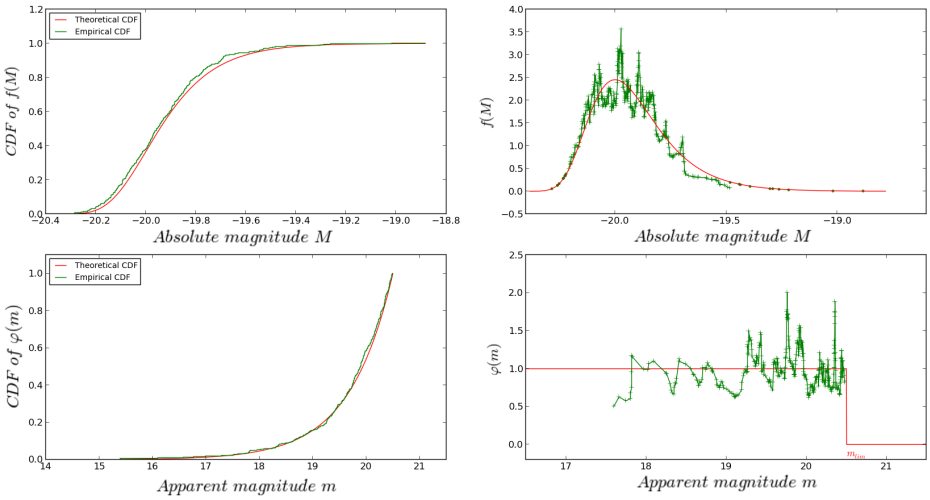

Figure 3.12: Similar to Fig.3.11 but with a Gumbel distribution for the luminosity function.

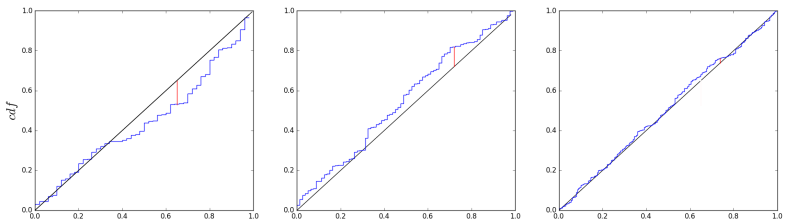

Figure 3.13: Three cdf testing uniform distribution with Kolmogorov-Smirnov test.

Afterwords, we compute analytically the cdf $F_w(M)$ defined in Eq.3.26. The maximum deviations between the continuous cdf $F_w(M)$ and the empirical cdf $F_w^{st}(M)$ are computed as follows:

$$D_{max} = Max(|F_w(M) - F_w^{st}(M)|) \tag{3.33}$$

If a Gaussian hypothesis for $f(M)$ is likely i.e the null hypothesis is accepted by the KS test for a significance level, one can estimate the characteristics of the Gaussian shape of $f(M)$: The standard deviation σ_M which is defined in Eq.3.32 and the mean M_0:

$$M_0 = \langle M \rangle + \frac{\beta \ln(10)}{5} \sigma_M^2 \tag{3.34}$$

The assumption of the completeness of the sample up to the limiting apparent magnitude m_{lim} leads to a technological function $\phi(m)$ like a Heaviside function

$\theta(m_{lim} - m)$. The calculation of Eq.3.27 using Eq.3.25 gives us the following theoretical cdf of $\phi_w(m)$:

$$\Phi_w(m) = 1 + \theta(m_{lim} - m)(10^{\frac{-\beta(m_{lim}-m)}{5}} - 1) \tag{3.35}$$

This last allows us to obtain the maximum deviations with respect to the empirical cdf $\Phi_w^{st}(m)$:

$$D_{max} = Max(|\Phi_w(m) - \Phi_w^{st}(m)|) \tag{3.36}$$

This test allows us to decide whether these deviations are statistical fluctuations.

3.5 The V/V$_{max}$ test

The V/V_{max} test is well known statistical approaches that have been used in cosmology. The random variable V/V_{max} has a uniform distribution between 0 to 1. Herein, we apply this test as described by [G. Bigot & R. Triay 1991]. We define the uniform random variable:

$$h(z, m) = \frac{V_0(z)}{V_m(M)} \tag{3.37}$$

where $V_0(z)$ is the comoving volume at redshift z and $V_m(M)$ is the comoving volume that the source of absolute magnitude M remains visible up to a redshift z_{max} at a limiting apparent magnitude m_{lim} of the survey, it corresponds to $V(z_{max})$ defined in Eq.2.8 [Schmidt M., 1968]. The probability density of a complete sample reads:

$$\mathrm{d}P_{obs} = \frac{1}{A}\theta(m_{lim} - m)\theta(z)\theta(z_{form} - z)f(M)\mathrm{d}M\,\mathrm{d}V \tag{3.38}$$

where A denotes the normalization factor, z_{form} the redshift of the formation epoch and θ the Heaviside function. A range of redshift is defined by the product of the Heaviside functions in the probability density in which a source of absolute magnitude M is observed. Following Eq.2.17 we defined this range by $\Pi_M(z)$:

$$\Pi_M(z) = \theta(m_{lim} - M - \zeta(z))\theta(z)\theta(z_{form} - z) \tag{3.39}$$

A little algebra shows that the probability density of M and h reads:

$$\mathrm{d}P \propto V_m(M)\, f(M)\mathrm{d}M\,\mathrm{d}h \tag{3.40}$$

After obtaining a set of candidate models (the NCC), we apply the KS test to test to these candidate models. That requires the calculation of: the absolute magnitude M_k, the maximum of redshift z_{max} (which corresponds to the limited apparent magnitude m_{lim}), the maximum of volume $V(z_{max})$ and the volume $V_0(z_k)$ according to Eqs.2.17, 2.7, 2.8 and 1.37, respectively.

3.5.1 Calculation of the V/V$_{max}$ terms

The calculation of V/V_{max} is straightforward, but for a positive curvature parameter, needs one pays attention to its calculation. In such a case, the redshift range $\Pi_M(z)$ might consist in several intervals, as in models with positive curvature. In that cases, the function $\zeta(z)$ is not monotonic and the inverse function $\zeta^{-1}(m_{lim} - M)$ does not exist. Therefore, to compute the terms $V_0(z)$ and $V_m(M)$ andt determine the redshift domain $\Pi_M(z)$, i.e. the regions where the object with luminosity M is observable. Let $z^\dagger$ be the redshift for which ζ reaches its maximum. The domain $\Pi_M(z)$ is not connected if $z^\dagger < z_{form}$. In such a case, Eq.2.17 has two roots: z_1 and z_2. Let us define the following magnitudes:

$$M^\dagger = m_{lim} - \zeta(z^\dagger) \tag{3.41}$$

$$M_{form} = m_{lim} - \zeta(z_{form}) \tag{3.42}$$

The sources with absolute magnitude M which satisfy the condition $M^\dagger < M < M_{form}$ has a visibility redshift window defined by a union of disjoint redshift intervals: $[0, z_1] \cup [z_2, z_{form}]$ (see Fig.3.14). To summarize, the calculation of $h(z, m)$ in case of a positive curvature model distinguished in two cases. Firstly, if Eq.2.17 has a single root then we have:

$$V_0(z) = V(z) \tag{3.43}$$

$$V_m(M) = V(min\{z_{form}, z_{max}\}) \tag{3.44}$$

Secondly, if Eq.2.17 has two roots then $h(z, m)$ is calculated with the following terms:

$$V_0(z) = \begin{cases} V(z) & \text{if } z < z_1 \\ V(z_1) + V(z) - V(z_2) & \text{if } z > z_2 \end{cases} \tag{3.45}$$

$$V_m(M) = V(z_1) + V(z_{form}) - V(z_2) \tag{3.46}$$

A similar issue occurs also in the presence of the k-correction term in Eq.2.17 (because the emission lines make this function solely invertible by part). We note that the V/V_{max} test can be applied on subsamples defined with criteria: $m_{min} < m < m_{max}$ and $z_{min} < z < z_{max}$. Therefore, $h(z, m)$ is calculated as follows:

$$h(z, m) = \frac{V_0(z) - max\{\varpi_1(M), V(z_{min})\}}{min\{\varpi_2(M), V(z_{max})\} - max\{\varpi_1(M), V(z_{min})\}} \tag{3.47}$$

where $\varpi_j(M)$ are given by Eqs.3.44 and 3.46 substituting m_{lim} into Eq.2.17, by m_{min} for j = 1, or by m_{max} for j=2.
Once the terms of variable $h(z, m)$ are determined, we compute its cumulative distribution function as follows:

$$F_h(x) = \frac{1}{N} \sum_{k=1}^{N} \theta(x - h(z_k, m_k)) \tag{3.48}$$

and therefore, we compare it to the cdf of theoretical uniform distribution between 0 and 1 (the linearity) using the KS test as follows:

$$D_{max} = Max(|F_h(x) - x|) \tag{3.49}$$

For each model on the NCC, we obtain a value of D_{max}. The lower the D_{max} value, the more the agreement between the two distributions. Thus, the most likely values of cosmological parameters correspond to the minimum of D_{max} over the NCC. The V/V_{max} test is applied, on the NCC in Fig.3.15 with $\Omega_\circ = 0.2$, and $\lambda_\circ = 0.5$. The values of D_{max} is given for each model on the curve. The yellow curve gives D_{max} as a function of $\lambda_\circ$ (Fig.3.15 in top right and left). The minimum is reached at value of $\lambda_\circ$ chosen for the simulated sample. Similarly, the magenta curve gives D_{max} as a function of $\Omega_\circ$, and we obtain the same result, the value of $\Omega_\circ$ chosen for the simulation (Fig.3.15 in top right and in bottom right). We measure that the likelihood of this result is estimated at at 99% significance level.

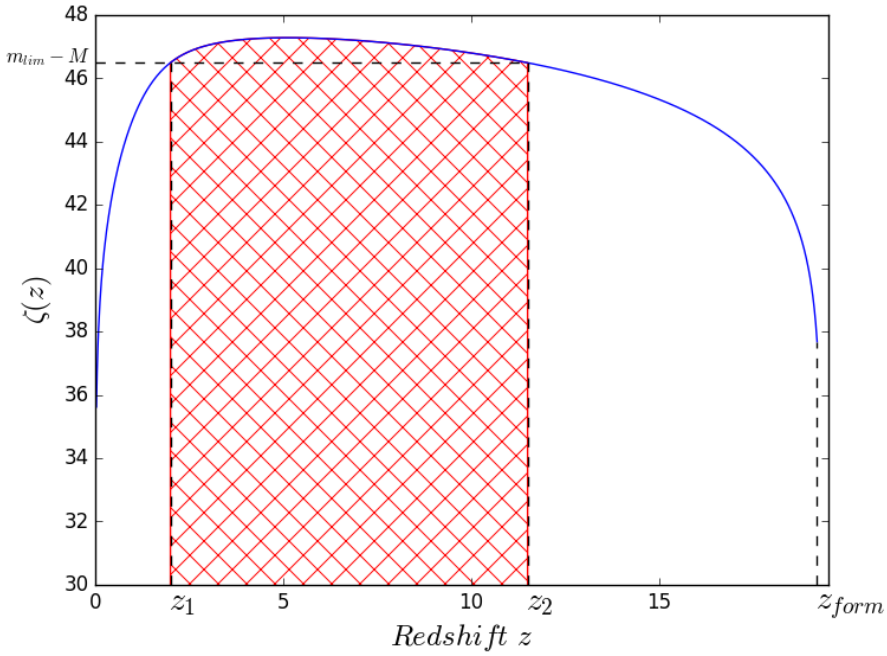

Figure 3.14: The redshift range is not connected for this model with positive curvature $\kappa_\circ = 0.4$. The distance modulus $\zeta(z)$ of a source with absolute magnitude M has most likely two solutions and it cannot be observed in the hatched area.

3.6 Conclusion

We had described, an innovative statistical method that does not require the knowledge of the luminosity function and which is free from the Malmquist bias. It consists on a first step which uses the null correlation technique to obtain a set of models which agree with data. The accuracy of estimates improves with the increasing of number of objects. Moreover, one estimates the luminosity and the selection functions.
A second step uses V/V_{max} test, with a little modification of the usual definition. It provides us with better estimates of cosmological parameters.

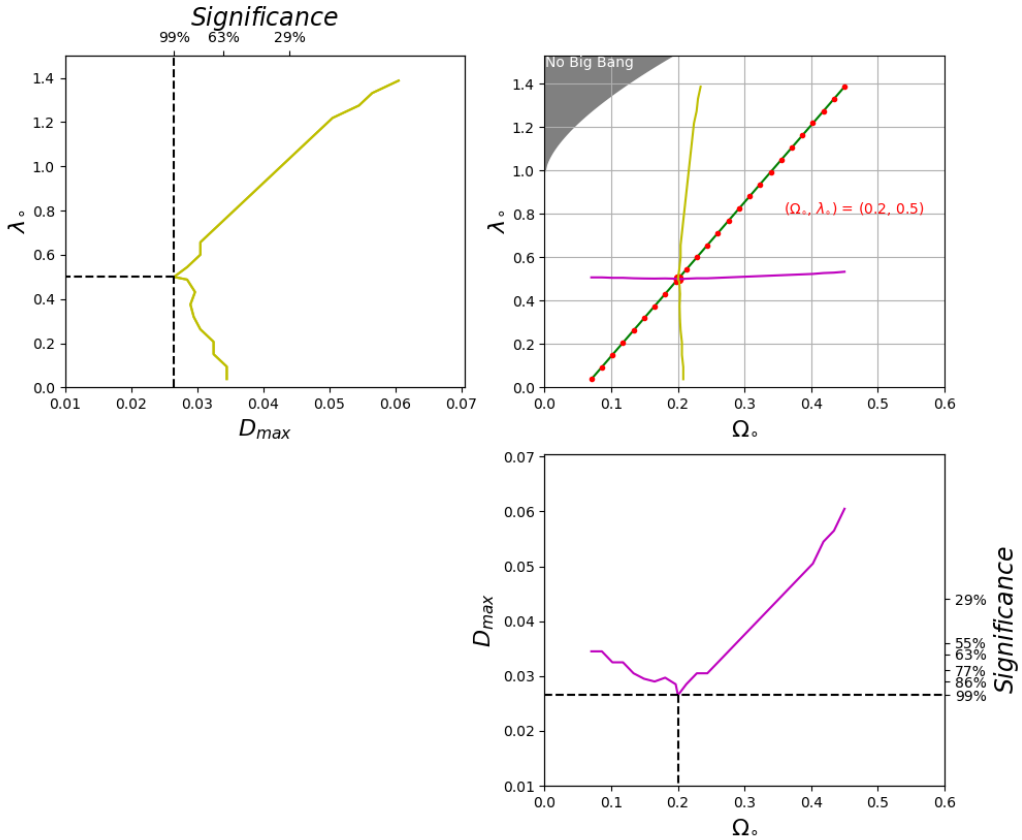

Figure 3.15: Kolmogorov- Smirnov test (Likelihood of candidates). Search for the minimum of D_{max} (top left) as a function of $\lambda_\circ$, and (bottom right) as a function of $\Omega_\circ$, on the NCC (top right).

CHAPTER 4

Application to quasars data

Contents

4.1 Introduction **51**

4.2 The Sloan Digital Sky Survey data **52**

4.2.1 The k-correction 53

4.3 Results **54**

4.3.1 The null correlation test 54

4.3.2 The V/V$_{max}$ test 57

4.3.3 Estimation of the luminosity function and the selection function 60

4.4 Inferences on cosmological expansion based on QSOs 61

4.5 Conclusion **79**

4.1 Introduction

The largest homogeneous sample of QSOs ever found, are provided by public data releases of SDSS. Hereafter, we proceed to a statistical analysis of these samples with the aim to apply the null correlation method for inferring cosmological information. For such a purpose, we use the absolute magnitude diagram and the V/V_{max} test.

4.2 The Sloan Digital Sky Survey data

The Sloan Digital Sky Survey is one of the well known surveys specialized in the identification of the QSOs and galaxies for mapping the Universe. Since 2000 the SDSS has evolved in two editions: SDSS-I (up to 2005), SDSS-II (2005-2008) followed by the SDSS-III in 2008 which mainly detects the characteristic scale imprinted by baryon acoustic oscillations (BAO) in the early Universe through the SDSS's Baryon Oscillation Spectroscopic Survey Project (BOSS). The SDSS telescope with diameter 2.5m is located at Apache Point Observatory, in Southeast New Mexico (USA), using multi-band with a photometric system of five filters (r, i, u, z, and g based on the AB magnitude system as explained in Sect.1.10.3) and covering about 11,600 deg^2 of the sky in Northern Hemisphere. It is also associated with a pair of spectrographs with optical fiber feed, which measure the spectra of selected objects.

We have used several catalogs to apply the null correlation test. We focused

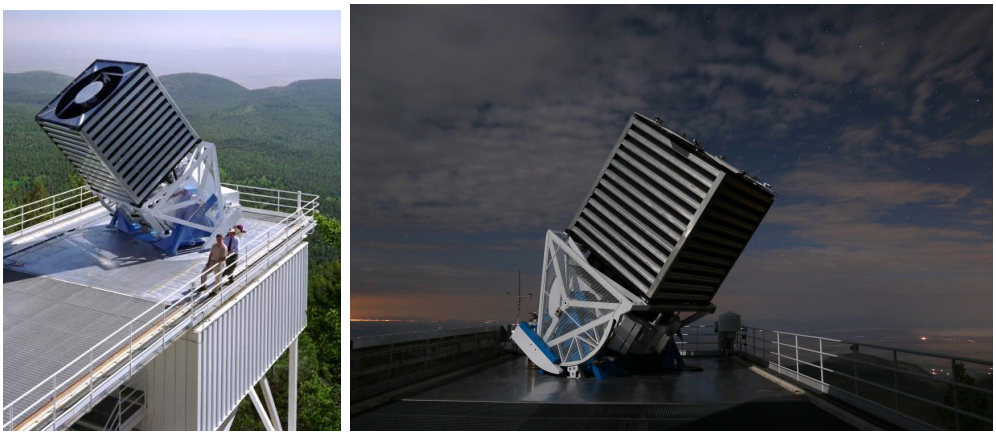

Figure 4.1: The Sloan foundation 2.5m telescope Ritchey-Chretien type located at Apache Point Observatory, in south east New Mexico.

on the samples from SDSS-I and SDSS-II. Since our investigation requires statistical properties such that the homogeneity of the sample, we were unable to perform the test on the SDSS-III samples. This is due to the selection of objects which was dependent on the redshift (more specifically for the nineth data release DR9-BOSS). In the DR9 sample, the QSOs were selected in order to measure the BAO scale in the Lyman-α forest at redshift ≈ 2.5. Thus, most of the QSOs in this sample span a range of redshifts: $2.5 < z < 3.5$ [Pâris et al 2010]. For the reason of this selection based on redshift, as seen in the absolute magnitude-volume diagram of DR9 (see Sect.4.4-§3.1 for more description and analysis of this diagram), we did not use this sample for the application of the null correlation test. However, the two editions I/II grow increasingly with a huge number of quasars (QSOs) and goodness of the quality of the selection

target candidates.
Firstly, we applied the test to the first edition of SDSS quasar catalog, the Early Data Release (EDR). It consists of 3,814 QSOs with redshifts ranging from 0.15 to 5.03. The survey reaches a flux limit of $i \approx 19$ for objects with $u-v < 1.5$. This limit becomes $i \approx 20$ for objects with $u-v > 1.5$ [Schneider et al 2002]. Secondly, we chose from SDSS-II, the first and third data releases (DR1 and DR3 respectively) where the latter covers all the area of the former with more than three times of quasars. Finally, we used a sample where the number of QSOs is much higher. It is the latest sample of SDSS-II, the seventh data release DR7, and is two times more than the DR3 cited above.
Here, I present the different characteristics of each sample (DR1, DR3 and DR7). The main difference between DR1 and DR3, is the number of quasars selected in each. The DR1 catalog contains 16,713 QSOs with redshift from 0.08 up to 5.41, and spans a range of apparent i magnitude between 15.15 and 21.79. While the DR3 catalog consists of 46,420 QSOs (three times more quasars than DR1) covering the full area of DR1, an area of 4188 deg^2. The DR3 sample is distinguished from DR1 due to the several modifications in the criteria of the selection candidates. Interestingly, due to new techniques used for this sample, the DR3 has more accuracy than the previous data releases in determining the signal/noise ratio used to determine the redshift. This allows to improve the localization of the selected quasars with more precision. Moreover, a good improvement of the photometric measurement and the imaging data are also released. The selected QSOs in DR3 have a redshift range from $z = 0.078$ to 5.414 where 520 quasars have redshifts greater than 4, of which 17 are at redshifts greater than 5. This sample extends from $i = 15$ to 21.78 ($i = 19.1$ is the first limit on the apparent magnitude at $z < 3$ and $i = 20.2$ for $z > 3$). Among this sample, only 160 QSOs have brightness fainter than 20.5 in the i band, for which only five QSOs have $i > 21.0$ [Schneider et al 2005].
The DR7 is the final data release for SDSS-II, it contains 105,783 spectroscopically confirmed QSOs which represent the entire set of QSOs from SDSS-I and SDSS-II Quasar survey. The catalog covers an area of 9380 deg^2. The range of redshift in this catalog is from 0.065 to 5.461 with apparent magnitude from $i = 14.86$ to 22.36. This sample has 1248 QSOs with redshifts larger than 4, of which 56 have redshifts above 5 [Schneider et al 2010].
All of the QSOs in these catalogs are selected with luminosities larger than $M = -22$ in the i band (calculated with the cosmological model: $\Omega_\circ = 0.3$, $\lambda_\circ = 0.7$ and $H_\circ = 70\ Km.Mpc^{-1}.s^{-1}$), as well as with a full width at half maximum (FWHM) of lines from the broad line region greater than 1000 $km.s^{-1}$. It is worth to mention that applying a limit on the absolute magnitude (which is a variable depends on the cosmological parameters) is prohibited because it makes a bias on the estimation of the parameters. However, the value $M = -22$ corresponds to $z \leq 0.06$, then its effect is not significant and therefore ignored.

4.2.1 The k-correction

As mentioned in Sect.2.5.3, the k-correction makes the absolute magnitude M centered at the same wavelength for all objects at any redshift. The dependence of the k-correction on the overall quasar Spectral Energy Distribution (SED) necessitates the study of its component, usefully by separating between the continuum (K_{cont}) and the emission lines (K_{em}). The quasar SED can be represented by assuming a power law distribution $f_\nu \propto \nu^{\alpha_\nu}$. Then, the K_{cont} is given, as traditionally, at redshift zero by the following:

$$K_{cont} = -2.5(1 + \alpha_\nu) log_{10}(1 + z) \tag{4.1}$$

According to [Richards et al 2006] paper, the continuum slopes appear correlated with the observed relative $g - i$ color, while the true correlation is not found yet, notably for high redshift. Then, it is useful to change the rest-frame's redshift which avoids the mentioned correlation. Therefore, a redshift close to the median redshift of the DR3 sample is chosen for the K_{cont} with a constant continuum slope $\alpha_\nu = -0.5$, i.e, the continuum k-corrections are zero at $z = 2$, which reduces the systematic error (This error incurred when using a fixed spectral index for all the bluest and reddest objects at high redshift). Transferring the zero point of the k-correction to $z = 2$, significantly reduces the systematic error incurred by extrapolating the wrong spectral index to high redshift (see [Richards et al 2006] for more details). k-correcting the part of emission lines, K_{em}, is established with a selection of the flux limit. This limit has been settled in the i band at $z = 2$ due to the fact that the i-band is relatively free of strongly peaked emission lines at this redshift. Note that, the Lyα forest does not include the i band until much higher redshift. The contribution of host galaxies is likely to be small in this analysis. Fig.4.2 shows the total k-correction, K_{cont} and K_{em}, in the i band.

4.3 Results

4.3.1 The null correlation test

The null correlation curves found with the samples and subsamples described above are very close to each other, and they coincide in the region of the low density matter in the $(\Omega_\circ, \lambda_\circ)$ diagram (see Fig 4.3). These results are in a good agreement with the results of [H. Fliche & J. M. Souriau 1979] who first applied this test on the QSOs. However, it must be noted that the NCC of the EDR sample (red curve in Fig 4.3) shows a decreasing shape which gives different results. This issue is due to the bad quality of the selection data of EDR sample. Indeed, it has been notified that original version of the quasar target selection algorithm used in the EDR data did a particularly poor job of selecting quasars with redshifts close to $z = 3.5$ [Richards et al 2006].

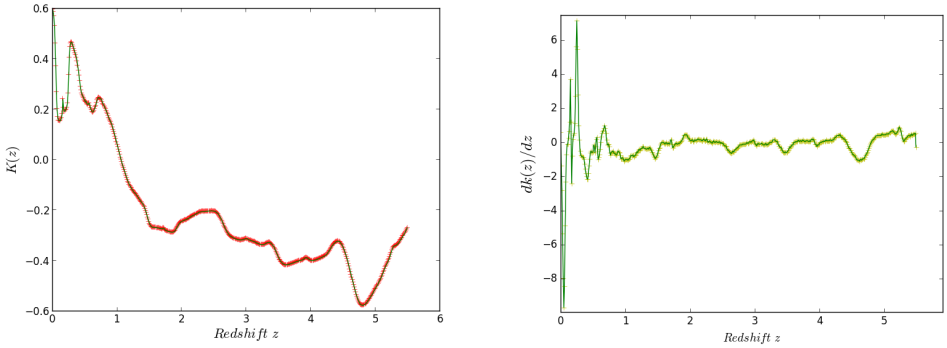

Figure 4.2: Left: The k-correction of the SDSS-DR3 sample in the i-band including both the emission-line and continuum components, normalized at $z = 2$ with a fixed spectral index $\alpha_\nu = -0.5$. Right: The numerical derivative of k-correction with respect to the redshift z.

Therefore, this curve is excluded. The model with zero curvature (defines a flat universe, $\Omega_\circ = 0.6$) is not a good candidate (see Sect.4.4-§3.2).

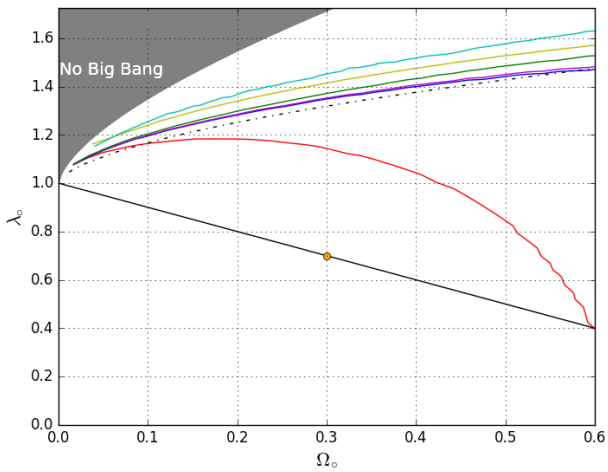

Figure 4.3: The null correlation curves corresponding to EDR, DR1, DR3, DR7 samples and DR3 subsamples. The curves are located in the region with positive curvature $\kappa_\circ > 0$ (above the straight line). All the curves give close candidate values for cosmological parameters excepted the one of EDR sample (red curve).

The V/V_{max} test provide us with more likely values of the cosmological parameters in agreement with the working hypotheses. Its application suggest

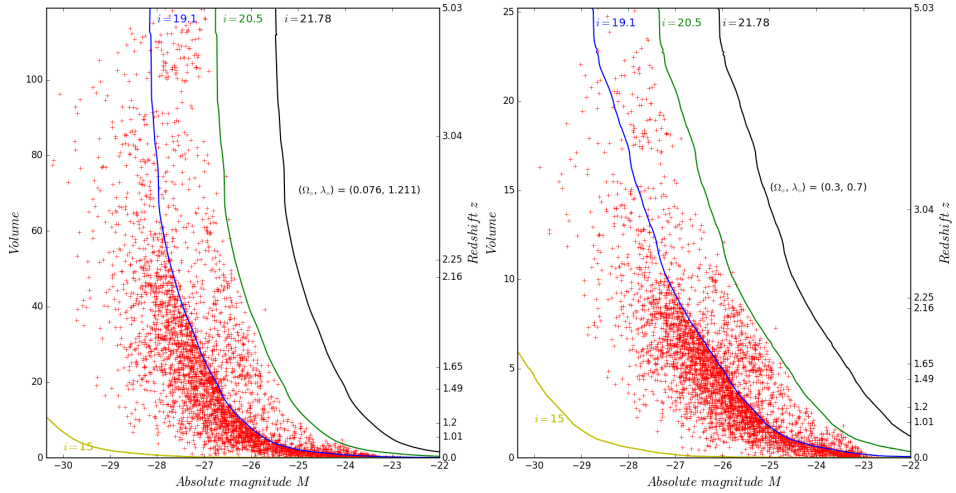

Figure 4.4: The absolute magnitude-volume diagram of the EDR sample. The left panel with $\Omega_\circ = 0.076$, $\lambda_\circ = 1.211$. The right panel with $\Omega_\circ = 0.3$, $\lambda_\circ = 0.7$. The domains corresponding to limiting magnitudes $i = 15$, 19.1, 20.5 and 21.78 are delimited by the corresponding curves (yellow, blue, green and black). The second ordinate axis represents the redshift values.

the most likely candidate defined by $\Omega_\circ = 0.076$, $\lambda_\circ = 1.211$. Hereafter, we use those values in the diagrams and graphics for the discussion of results. Afterward, we plot the absolute magnitude-volume diagram that will be named afterwards FS diagram (for Fliche and Souriau diagram). It is worth to note that two limiting apparent magnitude, $i = 19.1$ and $i = 20.5$, are present in this diagram that correspond to two distinct set of observations. In Figs. 4.4, 4.5, 4.6, 4.7 and 4.8 we show the difference between the FS diagrams built by a determined candidate model (left) and the model of the standard flat universe (right) for the samples EDR, DR1, DR3, the homogeneous subsample of DR3 and DR7. It is clear that the FS diagram of EDR sample suffers from the weakness of the size with respect to other catalogs. For the other catalogs, we noticed that objects are missing in the FS diagrams at redshifts $z = 2.7$ and $z = 3.5$. The obvious reason of this selection effect is because the SDSS colors of quasars at these redshifts are similar to the colors of their stars (host galaxies), which makes difficult to distinguish quasars from stars. Furthermore, we remark a lack of bright QSOs in the bottom-left of the FS diagram (white zone, which began more significant with flat universe) compared to the simulated diagram in Fig.4.9 (built with model $\Omega_\circ = 0.076$, $\lambda_\circ = 1.211$; the volume-redshift and distance modulus-redshift diagrams are represented in Figs4.10 and 4.11 respectively, this last enables one to understand the decreasing of the luminosity at high redshift in the simulation sample). This is

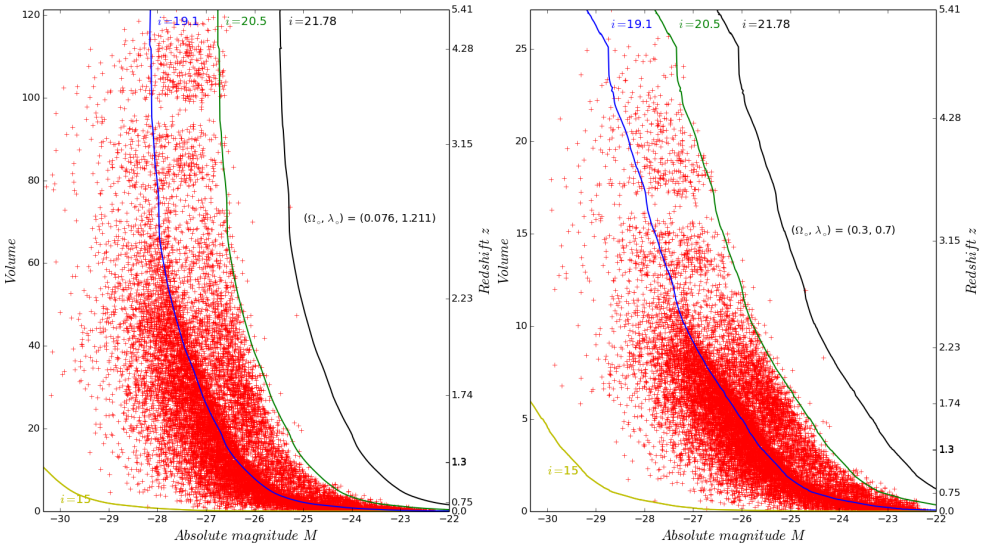

Figure 4.5: Similar to Fig.4.4: the absolute magnitude-volume diagram of the DR1 sample.

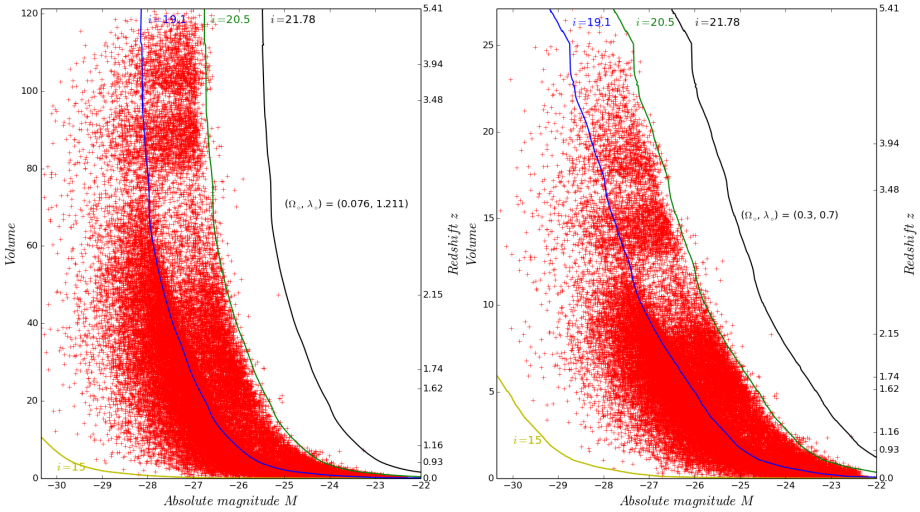

Figure 4.6: Similar to Fig.4.4: the absolute magnitude-volume diagram of the DR3 sample.

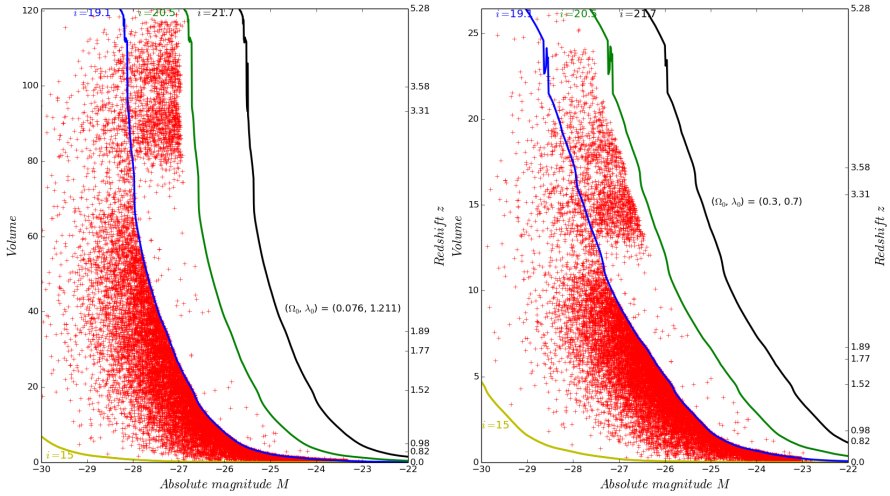

Figure 4.7: Similar to Fig.4.4: the absolute magnitude-volume diagram of the uniform statistical subsample of the DR3 (SUBDR3).

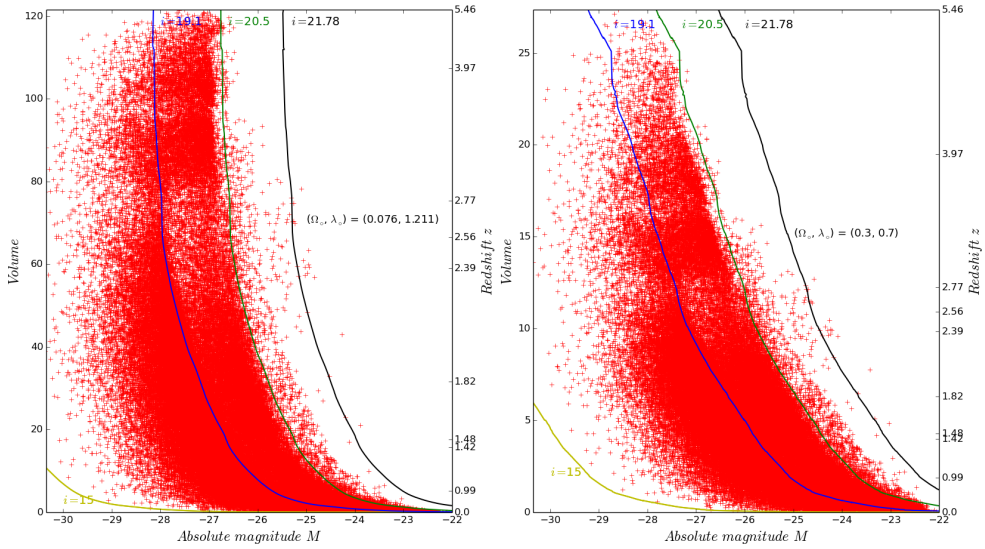

Figure 4.8: Similar to Fig.4.4: the absolute magnitude-volume diagram of the SDSS-DR7 sample.

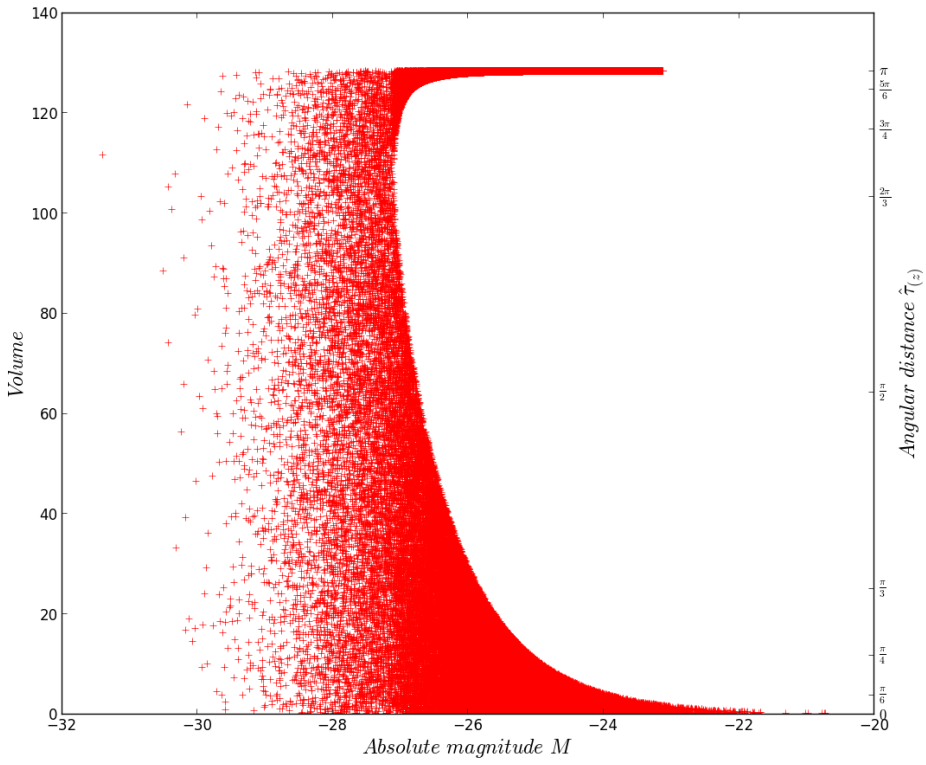

Figure 4.9: The absolute magnitude-volume diagram of a simulated sample which consists of 46,420 objects with a Gaussian luminosity function with $M_0 = -25$, $\sigma_M = 1.2$, a limiting magnitude $m_{lim} = 19.1$, and a maximum redshift $z_{max} = 13.6$ in the model $\Omega_\circ = 0.076$, $\lambda_\circ = 1.211$.

due to the selection of bright QSOs i.e. a limit on the apparent magnitude has been applied to select the brightest objects, $i = 15$, as mentioned above, in addition to a rarity of QSOs at low redshift (details are given in Sect.4.4-§3.2). Fig.4.12 (right panel) shows how the k-correction intervenes the weighting factor and its dependence on the cosmological model with the data (the red curves) and with a simulation (the blue curves) where variation between the curves is due to the changes of $\lambda_\circ$. The negative values (see left panel of Fig.4.12) are artefacts that appear when the distance-modulus is no longer invertible at high redshift, which concern solely 10 objects (0.02% of the sample size).

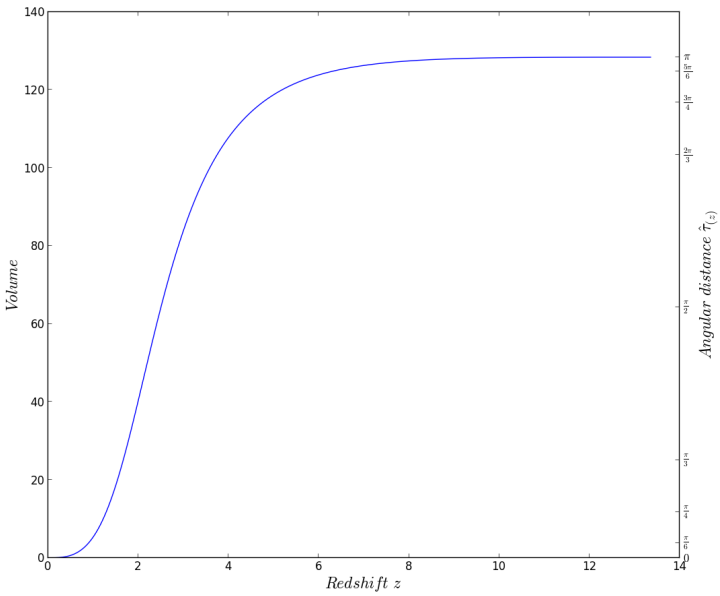

Figure 4.10: The volume-redshift diagram in the model $\Omega_\circ = 0.076$, $\lambda_\circ = 1.211$. The graduation on the ordinate is translated into angular distance on the right hand side axis.

4.3.2 The V/V_{max} test

Because the V/V_{max} test requires the most possible homogeneous data set, we focus on the DR3 and we use the subset of QSOs that were selected uniformly as described in [Richards et al 2006]. This subsample, noted SUBDR3, contains 15343 QSOs, where 90% of QSOs are fainter than the notably limit of the apparent magnitude, $i = 19.1$. Until this point, we have used only samples provided by their authors but the application of the V/V_{max} test requires complete samples [G. Bigot & R. Triay 1991], see details in Sect.3.5. The FS diagram enables one to check whether a sample staisfies such a property. As visible on Figures, they appear not homogenous, which forces us to identify complete subsamples. The theory allows one to apply a cutoff on the apparent magnitude ($m_{min} < m < m_{max}$) as well as a cutoff on the redshift ($z_{min} < z < z_{max}$). We have applied this test with several subsamples chosen by selecting domains on redshift and apparent magnitude to candidate models as given by the NCC. The method is iterative, it consists in delimiting domains for which the subsample appears homogeneous. Then, by means of the selection function determined by Eq.3.30, one identifies the apparent magnitude range for which the subsample shows to be complete. Hence, the KS test is applied to the corresponding subsample, which provides us with the likelihood level of the cosmological parameters.

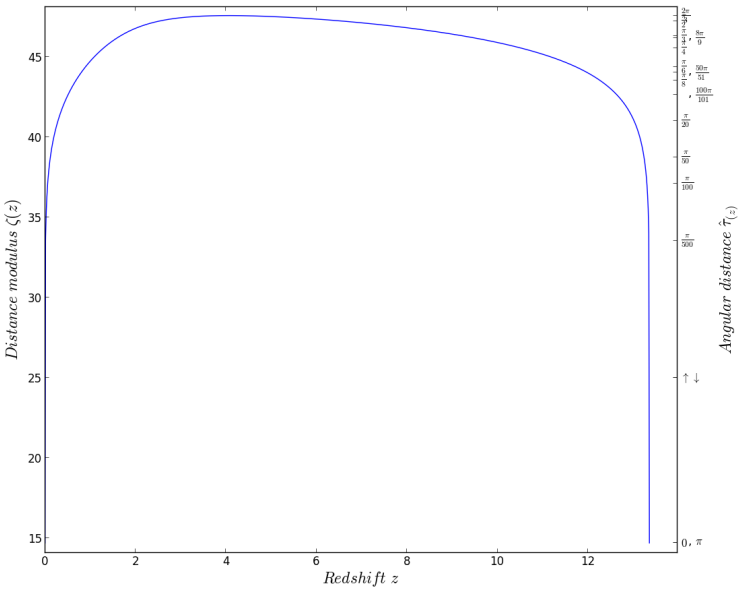

Figure 4.11: The distance modulus $\zeta(z)$-redshift diagram in the model $\Omega_\circ = 0.076$, $\lambda_\circ = 1.211$, showing the angular distance on the right hand side axis. The maximum of $\zeta(z)$ corresponds to $\tilde{\tau} = \frac{2\pi}{3}$.

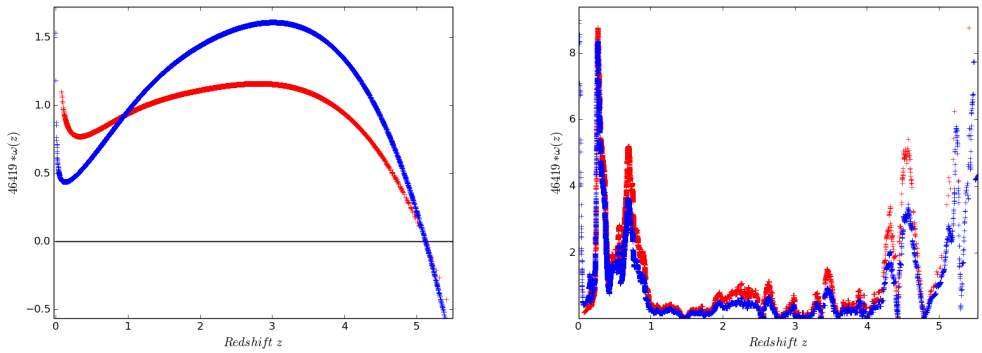

Figure 4.12: Weighting factor applied to DR3 sample and simulation sample without (left) and with (right) k-correction. Red curve with ($\lambda_\circ = 1.275$, $\Omega_\circ = 0.132$) and blue with ($\lambda_\circ = 1.229$, $\Omega_\circ = 0.132$). The disturbed shape of the curve is due to the contribution of the emission lines.

We start by applying the test to SUBDR3 sample using the corresponding NCC (the yellow curve in Fig.4.3). The results for each subsample are given

as follows:

- $18.65 \leq m \leq 19.1, \quad 0.04 \leq z \leq 2.45 : \Omega_\circ = 0.132, \lambda_\circ = 1.275$, at 35% significance level.

- $18.65 \leq m \leq 19.1, \quad 1.8 \leq z \leq 2.4 : \Omega_\circ = 0.076, \lambda_\circ = 1.211$, at 70% significance level.

They are shown in Figs.4.14 and 4.15.
The overdensity in the top of the FS diagram of SUBDR3 at redshift ≈ 3 is noticeable in Fig.4.13. Indeed, this may can upset the result of the null correlation test and then the V/V_{max} test. For this, we select a subsample of SUBDR3 limited at an apparent magnitude 19.1, which contains 13828 QSOs, getting rid the package in top. Therefore, we apply the null correlation test on this subsample which provids us a NCC (in cyan color) in Fig.4.3. Hence, we perform the V/V_{max} test on a subsample limited by:

- $18 \leq m \leq 19.1, \quad 1.8 \leq z \leq 2.4 : \Omega_\circ = 0.0305, \lambda_\circ = 1.1180$, at 77% significance level.

details about these results is presented in Sect.4.4-§3.3.

We select a subsample of DR7 in the following domain:

- $m_{min} = 18.65$, $m_{max} = 19.1$, $z_{min} = 1.8$, $z_{max} = 2.4$.

The application of V/V_{max} test suggests ($\Omega_\circ = 0.0169$, $\lambda_\circ = 1.079$) at 59% significance level (Figs.4.16 and 4.17. These selection criteria have been chosen to ensure the sample completeness within the largest magnitude range, accordingly to application requirements of the test. This is confirmed with the selection function $\phi(m)$ which is roughly constant in this interval and close to 1 (Fig 4.20 - see next section).

Error on the cosmological paramaters

The measurement errors on the apparent magnitude are available only for the DR3 sample (46419 QSOs), this sample was used to measure the fluctuations of the null correlation curve according to these errors. Fig.4.18 shows two curves that confine the estimates of the cosmological parameters corresponding to the taking into account of these errors. This allows us to estimate the error on the cosmological paramaters. We found for $\Omega_\circ = 0.132$, $\lambda_\circ = 1.229$: $\delta\Omega_\circ = \pm 0.003$, $\delta\lambda_\circ = \pm 0.0025$.

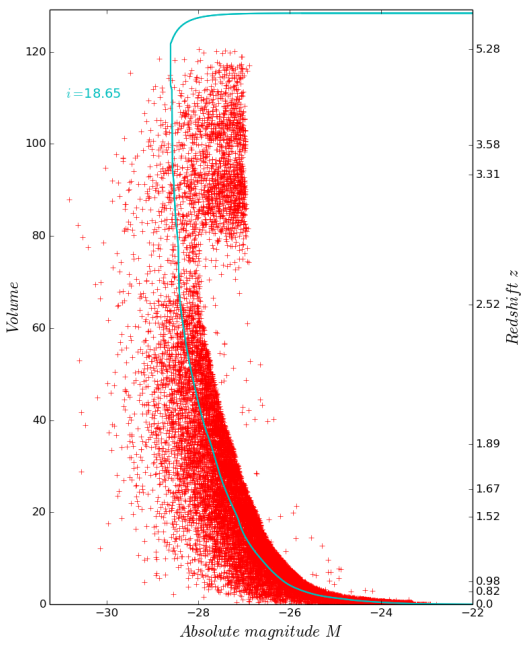

Figure 4.13: We represent the apparent magnitude limits on the FS diagram of the homogeneous statistical subsample, SUBDR3, chosen to apply the V/V_{max}: $18.65 < m < 19.1$

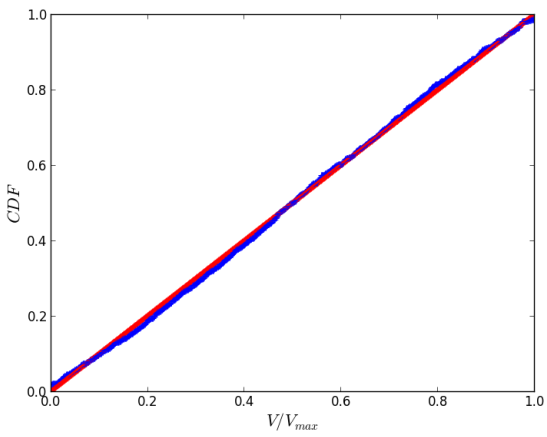

Figure 4.14: The cdf of V/V_{max} compared to a uniform distribution, for a SUBDR3 subsample with $\Omega_\circ = 0.076$ and $\lambda_\circ = 1.211$.

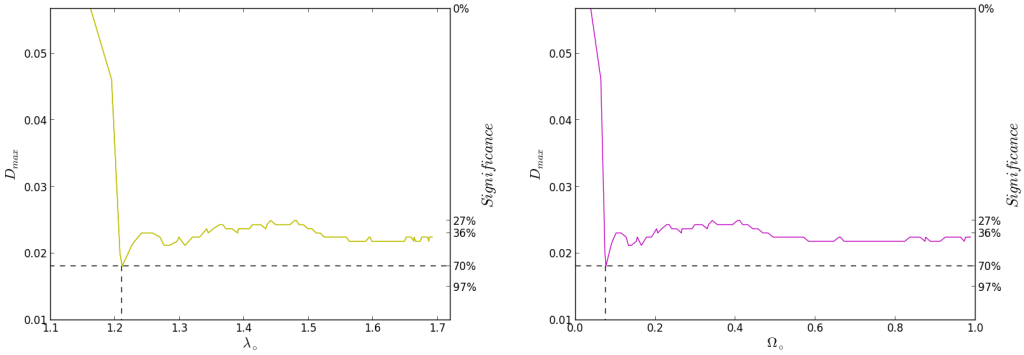

Figure 4.15: Distance between the empirical cdf and theoretical cdf (D_{max}), testing a uniform distribution of V/V_{max} values, for candidates cosmological models on the NCC corresponding to SUBDR3. Left panel: D_{max} as a function of $\lambda_\circ$. Right panel: D_{max} as a function of $\Omega_\circ$. In both panels, the values of D_{max} on the ordinate axis is translated into significance level on the right hand side axis.

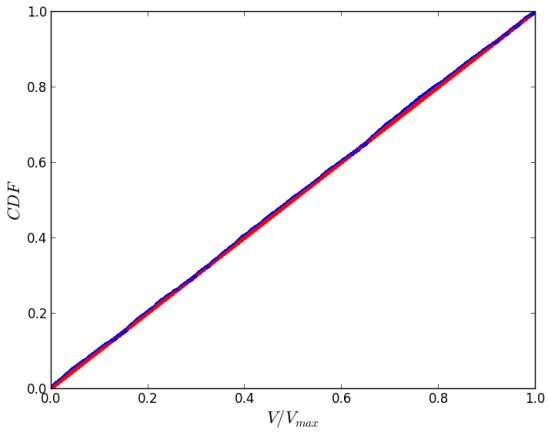

Figure 4.16: The cdf of V/V_{max} compared to a uniform distribution, for a DR7 subsample with ($\Omega_\circ = 0.0169$ and $\lambda_\circ = 1.079$).

4.3.3 Estimation of the luminosity function and the selection function

The null correlation approach enables us to evaluate the luminosity function $f(M)$ and the selection function $\phi(m)$ (for details of calculation see Sect.3.3). The cosmological parameters used for these estimations are ($\Omega_\circ = 0.0305$, $\lambda_\circ = 1.1180$). The luminosity function shows approximately Gaussian for the

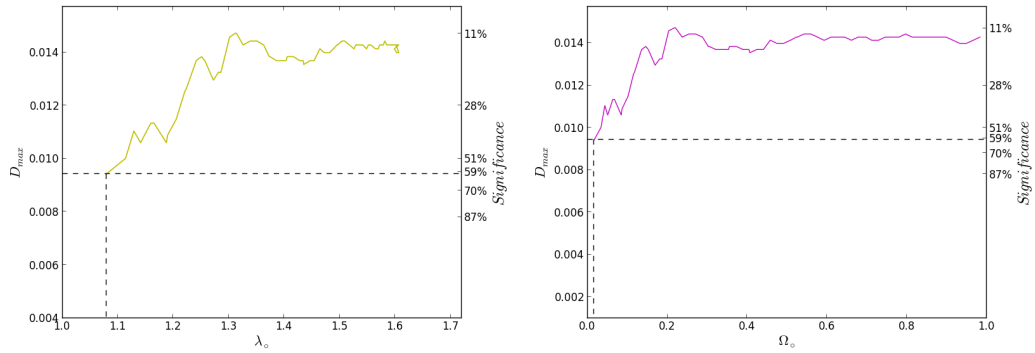

Figure 4.17: Similar to Fig.4.15 : D_{max} with respect to $\lambda_\circ$ (left) and ($\Omega_\circ$ (right) as candidates given by the null correlation curve of DR7.

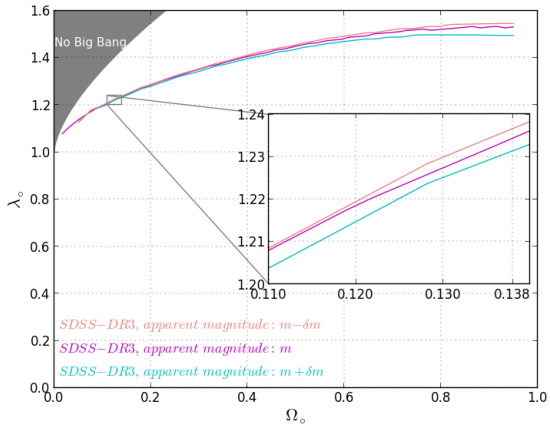

Figure 4.18: Contribution of measurement errors to NCC corresponding to DR3

brightest objects, whilst it becomes constant for the faintest objects (Fig.4.19 represents $f(M)$ of the subsample of SUBDR3 limited at 19.1 of apparent magnitude. For the other samples, see the Sect.4.4-§3.4). The completeness of the sample at a limited apparent magnitude is estimated in the simulation with 95% significance. As a point of fact, this is not suitable for the entire chosen sample. We found that the function $\phi(m)$ obtained from the SDSS data increases as an exponential function for the brightest objects (quasars are very rare at low redshift), while it clusters around $\phi(m) = 1.4$ from 18.65 to 19.1 of apparent magnitudes. In this range of magnitude, the QSOs are easily identified in the i band, thanks to the Lyα emission line which is more likely to be observed in this band. Above the first limit i=19.1, the function $\phi(m)$

decreases quickly as the deficiency of QSOs is important. But, $\phi(m)$ becomes constant until reaching the second apparent magnitude limit $i = 20.2$ (Fig.4.20 represents $\phi(m)$ of the subsample described above. For the other samples, see the Sect.4.4-§3.4). The shape of the $\phi(m)$ suggests that the SDSS samples are constituted of at least two apparent magnitude limits, and of regions where the emission lines of QSOs are easily identified in the i band. The bottom panel represents $\phi(m)$ with an increasing shape until i=18.65. This function becomes constant and close to $\phi(m) = 1.4$ up to the limit $i = 19.1$ where it starts to decrease at this limit. The top panel represents the zoom on $\phi(m)$ between the range from 17.9 to 19.1 where the function begin to be close to 1. This trend is due to the rare bright QSOs (the nearby QSOs) and to the easy identification of QSOs in this range.

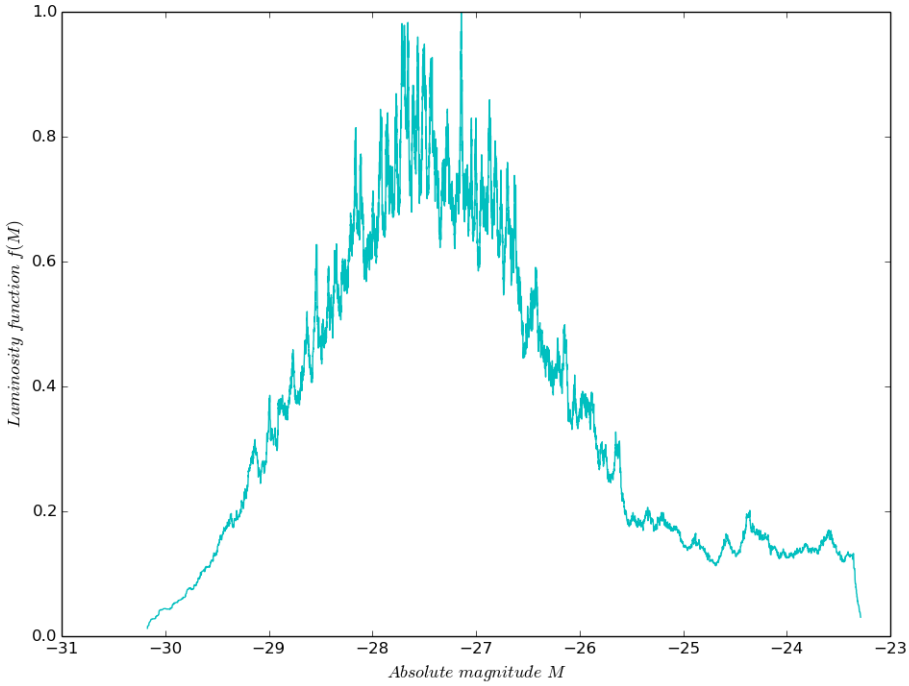

Figure 4.19: The luminosity function $f(M)$ of the subsample of SUBDR3 with ($\Omega_\circ = 0.0305$, $\lambda_\circ = 1.1180$).

4.4 Pub: Inferences on cosmological expansion based on QSOs, D. Chbib, R. Triay, JCAP (2017)

Prepared for submission to JCAP

Inferences on cosmological expansion based on QSOs

D. Chbib[a] **and R. Triay**[a]

[a]Aix Marseille Univ, Université de Toulon, CNRS, CPT, Marseille, France

E-mail: dyaa.chbib@cpt.univ-mrs.fr, triay@cpt.univ-mrs.fr

Abstract. By assuming that the evolutionary effects are negligible, SDSS QSO data favour a Friedmann-Lemaître model with a positive scalar curvature. Such a result is obtained by using a null correlation technique, which has the advantage of being independent of the luminosity function of sources and free from the Malmquist bias, what interprets as a robustness criteria in estimating the cosmological paramaters.

Keywords: dark energy, cosmological parameters, quasars

ArXiv ePrint: X.X

Contents

1 Introduction **1**

2 The null correlation technique **1**
- 2.1 The Friedman-Lemaître-Gamov model 2
- 2.2 Statistical modeling of data 3
- 2.3 Probing the geometry of spacetime with weighting factors 4
- 2.4 Luminosity function and Selection function 5
- 2.5 The FS diagram 6
- 2.6 Refining the determination 6
- 2.7 A comparison with the Hubble diagram 8
- 2.8 Simulations techniques 8
- 2.9 The methodology when using the null correlation method 9

3 Application to QSOs samples **9**
- 3.1 The Sloan Digital Sky Survey (SDSS) data 9
- 3.2 The null correlation test 11
- 3.3 Refining the cosmological parameter's estimates 14

4 Conclusion **15**

1 Introduction

In the 80's, because the estimation of cosmological parameters is more reliable when the sources are remote, one had expected that the use of the Hubble diagram was the most promising approach by using QSOs. However, such a viewpoint has been abandoned because of the large dispersion in their luminosity distribution and possible evolutionary effects of these sources. Nevertheless, despite of their weak capacity of being standard candles, an innovative statistical approach, known as the null correlation technique, provided us with the earliest estimates of the cosmological constant that accounts for the acceleration of the cosmological expansion. This approach has been introduced by Fliche and Souriau [11, 12] (FS) and later adapted with additional features to brightest cluster galaxies [17–19]. Our aim is to perform such an approach to QSOs data sets from the Sloan Digital Sky Survey (SDSS), in view of inferring cosmological informations..

2 The null correlation technique

Statistical analysis in observational cosmology is faced to the problem of selection effects, which makes the derivation of unbiased inferences a major challenge, e.g. see the Malmquist bias [14–16, 20], among others. One of the interesting features of the null correlation technique is indeed to contribute in solving such problems in the determination of cosmological parameters.

In the following sub-sections, we remind the geometry of the standard model with the cosmological constant (no dark energy) and define quantities used herein, with their notations. We show how to probe the geometry of spacetime through a statistical modelling of the

Hubble law by means of weighting factors. Then, we remind the definitions of statistics which provide us with estimates of the luminosity function and of the selection function, for cosmological models that agree with the working hypotheses, and how to test them by means of the FS diagram. Then, we show the appropriate use of the $V/V_{\max}$ test for refining the estimation of cosmological parameters. A comparison to the usual fitting technique in Hubble diagram, shows up the benefits of this approach. With respect to simulation techniques, an advantageous algorithm that provides complete samples up to a given apparent magnitude is described.This chapter concludes with the methodology of the null correlation test, that we use in the next section.

2.1 The Friedman-Lemaître-Gamov model

In Friedman-Lemaître-Gamov (FLG) model [10], the space-time is described by a RW metric

$$\mathrm{d}s^2 = \mathrm{d}t^2 - a^2(t)\mathrm{d}\sigma^2 \tag{2.1}$$

where t is the cosmic time, $a(t)$ is the (dimensionless) *expansion parameter* and $\mathrm{d}\sigma^2$ is the metric element on an homogeneous 3-dimensional manifold V_3 (namely, the *comoving space*). It corresponds to the space-time events from where the CMB is observed as an isotropic Black-Body Radiation at (a given) temperature T. It is characterized by its scalar curvature K and the Hubble parameter H, which specifies a *scale*. Nowadays, value of the CMB temperature is $T_\circ = T(t_\circ) = 2.73°\mathrm{K}$, and by setting $a_\circ = a(t_\circ) = 1$, these models[1] can be parametrized by the Hubble constant $H_\circ = H(t_\circ)$ and the following cosmological parameters

$$\lambda_\circ = \frac{1}{3}\Lambda H_\circ^{-2}, \quad \kappa_\circ = K_\circ H_\circ^{-2} = \lambda_\circ + \Omega_\circ + \alpha_\circ - 1, \quad \Omega_\circ = \frac{8}{3}\pi G\rho_\circ H_\circ^{-2} > 0 \tag{2.2}$$

$$\alpha_\circ = \frac{8}{45}\pi^3 \mathrm{G} k_\mathrm{B} T_\circ^4 \hbar^{-3} H_\circ^{-2} \approx 2.5\,10^{-5} h^{-2}, \quad h = H_\circ/(100\,\mathrm{km\,s^{-1}Mpc^{-1}}) \tag{2.3}$$

These are dimensionless quantities that stand respectively for the present values of the reduced versions of the cosmological constant Λ, the scalar curvature K of the comoving space, the matter density, ρ being the specific density of massive particles (dark matter included), G is the Newton's constant, and the radiation energy density[2], which accounts of CMB photons as sources of gravity, k_B is the Boltzmann constant, and $\hbar$ is the Planck constant; the deceleration parameter reads $q = \alpha + \frac{\Omega}{2} - \lambda$. These notations, for time dependent quantities of a different origins, are more appropriated than the usual ones $\Omega_\Lambda \equiv \lambda_\circ$, $\Omega_K \equiv -\kappa_\circ$, $\Omega_M \equiv \Omega_\circ$ and $\Omega_\gamma \equiv \alpha_\circ$, for preserving their own meaning (in particular, for the sign of the scalar curvature).

The dimensionless expressions of the geometrical quantities used hereafter are :

- the *comoving distance*[3] of a source at redshift z,

$$\tau(z) = \int_{(1+z)^{-1}}^{1} \frac{\mathrm{d}a}{\sqrt{P(a)}}, \quad P(a) = \lambda_\circ a^4 - \kappa_\circ a^2 + \Omega_\circ a + \alpha_\circ, \quad P(1) = 1 \tag{2.4}$$

[1] The V_3 homogeneity being related to the distribution of the gravitational sources, because of the presence of large scale structures in the universe, one agrees that this model describes an anamorphosis of the galaxies distribution that is smoothed at scale $\approx 100\,\mathrm{Mpc}$. The Sun is moving at speed $369\ \mathrm{km\,s^{-1}}$ from such an event.

[2] Although $\alpha_\circ$ is negligible today, it provides us with a better description of the Universe at recombination epoch than describing the radiation-dominated era and the matter-dominated era separately.

[3] The comoving distance reads $\tau/H_\circ$

- the comoving volume of a sphere of radius $\tau = \tau(z)$,

$$V(\tau) = \pi \times \begin{cases} (2\hat{\tau} - \sin(2\hat{\tau}))\,\kappa_\circ^{-3/2} & \text{if } \kappa_\circ > 0 \\ \frac{4}{3}\tau^3 & \text{if } \kappa_\circ = 0 \\ (\sinh(2\hat{\tau}) - 2\hat{\tau})\,(-\kappa_\circ)^{-3/2} & \text{if } \kappa_\circ < 0 \end{cases} \tag{2.5}$$

where $\hat{\tau} = \tau\sqrt{|\kappa_\circ|}$ for $(\kappa_\circ \neq 0)$.

2.2 Statistical modeling of data

A class of luminous objects, described intrinsically by an absolute magnitude M and a position in the comoving space, can be used to probe the space-time geometry, with even more precision than magnitude dispersion is small (standard candles). For those that can be observed, their world lines intercept the observer's past lightcone, one measures their redshift z and their apparent magnitude

$$m = M + \zeta(z) \tag{2.6}$$

where the distance modulus $\zeta(z)$ reads in term of cosmological parameters. For broad-band photometric measurements expressed in magnitudes, the estimation of rest frame luminosities requires a K-correction term $K(z)$. Hence, the distance modulus reads

$$\zeta(z) = 5\log\frac{d_{\rm L}}{10pc} + K(z) + A, \qquad d_{\rm L} = (1+z)\begin{cases} \sin\hat{\tau}/\sqrt{\kappa_\circ} & \text{if } \kappa_\circ > 0 \\ \tau & \text{if } \kappa_\circ = 0 \\ \sinh\hat{\tau}/\sqrt{-\kappa_\circ} & \text{if } \kappa_\circ < 0 \end{cases} \tag{2.7}$$

where $d_{\rm L}$ is the luminosity distance and A quantifies the foreground extinction.

According to FLG model, the spatial distribution of gravitational sources being uniform in V_3, their corresponding volume $V = V(\tau)$, of a sphere of comoving radius τ centered at the observer location, stands for a uniform random variable. If (one assumes that) these objects are permanent, the redshit z of those within the even horizon can be measured, (the visible part of) the comoving space is representatively sampled[4] by mean of their comoving distance $\tau = \tau(z)$. If the related sample shows a luminosity function $f(M)$ then the probability density of the random variables (M, V) reads[5]

$$\mathrm{d}P_{\rm th} \propto f(M)\mathrm{d}M\,\mathrm{d}V \tag{2.8}$$

If the selection effects depend solely on m, the probability density of observed objects reads

$$\mathrm{d}P = \frac{1}{P_{\rm th}(\phi)}\phi(m)f(M)\mathrm{d}M\,\mathrm{d}V, \qquad P_{\rm th}(\phi) = \int \phi(m)f(M)\mathrm{d}M\,\mathrm{d}V \tag{2.9}$$

where ϕ is a *selection function* that describes the difficulties to identify/collect the sources and/or the selection criteria, it works as a filter response (i.e., $0 \leq \phi(m) \leq 1$). According to eqs. (2.4),(2.5),(2.6),(2.7), it works as a correlation function of the random variables (M, V).

[4]When reasoning in the conformal spacetime diagram, this property becomes obvious since the past light cone of the observer intercept the worldlines of objects at the same angle of 45°.

[5]The absence of evolutionary effects is a requirement for being considered as standard candles.

2.3 Probing the geometry of spacetime with weighting factors

According to eq.(2.9), the probability density of random variables (M, m) can be written as

$$\mathrm{d}P = \frac{1}{P_{\mathrm{th}}(\phi)}\phi(m)f(M)\frac{\partial V}{\partial m}\mathrm{d}M\,\mathrm{d}m \tag{2.10}$$

which shows that the random variables (M, m) are correlated, because of the correlation fonction $\frac{\partial V}{\partial m}$. Hence, by weighting the data with the function

$$\omega_\beta(z) = \left(\frac{\partial V}{\partial m}\right)^{-1} 10^{\frac{\beta}{5}(m-M)} = \frac{\mathrm{d}\zeta}{\mathrm{d}z}\left(\frac{\mathrm{d}V}{\mathrm{d}z}\right)^{-1} 10^{\frac{\beta}{5}\zeta} \geq 0 \tag{2.11}$$

the random variables (M, m) become independent for the true values of cosmological parameters, which stands for the principle of the null correlation test.

For a sample $\{(z_k, m_k)\}_{k=1,N}$, one defines the normalized weighting factors as follows

$$\omega_k = \frac{\omega_\beta(z_k)}{\sum_{k=1,N}\omega_\beta(z_k)} \tag{2.12}$$

where the value of the parameter β is chosen to minimize the difference[6] between the weights

$$\omega_{\min} = \min_{k=1,N}\{\omega_\beta(z_k)\}\,, \quad \omega_{\max} = \max_{k=1,N}\{\omega_\beta(z_k)\} \tag{2.13}$$

and hence to diminish the lose of information. Figure 1 shows the weighting factors (scaled by the factor N) for the SDSS-DR3 sample calculated by assuming $(\Omega_\circ = 0.132, \lambda_\circ = 1.275)$ (bottom-left panel) and $(\Omega_\circ = 0.3, \lambda_\circ = 0.7)$ (bottom-right panel).

Let us emphasise that the K-correction term, which intervenes through the distance modulus ζ, plays an important rule in the weighting. Indeed, the comparison between the upper panels (without K-correction term) to the bottom ones of figure 1, shows that its effect in the weighting is not negligible with respect to that of cosmological parameters. It takes into account that a source is more easily detectable when an emission line of its spectrum overlaps with the observed wavelength window of the filter. Ignoring this effect necessarily produces biased estimates of cosmological parameters.

Therefore, the (weighted) correlation coeficient of random variables (M, m), which reads

$$\Gamma(\Omega_\circ, \lambda_\circ) = \sum_{k=1,N}\omega_k\frac{(M_k - \langle M\rangle_\omega)(m_k - \langle m\rangle_\omega)}{\sigma_\omega(M)\sigma_\omega(m)}, \quad M_k = m_k - \zeta(z_k) \tag{2.14}$$

where the weighted statistics of the mean and variance are defined by substituting X by M or m in the following equations

$$\langle X\rangle_\omega = \sum_{k=1,N}\omega_k X_k, \quad \sigma_\omega(X)^2 = \frac{N}{N-1}\sum_{k=1,N}\omega_k\left(X_k - \langle X\rangle_\omega\right)^2 \tag{2.15}$$

has a vanishing expectation for the true values of cosmological parameters. Hence, the *candidate model* is defined by those values that satisfy the equation[7]

$$\Gamma(\Omega_\circ, \lambda_\circ) = 0 \tag{2.16}$$

[6] It can be also the relative difference $\hat{\Delta}_\omega = \frac{\omega_{\max}-\omega_{\min}}{\omega_{\max}+\omega_{\min}}$.

[7] Note that if one limits solely to obtain these roots one can use the (weighted) covariance instead.

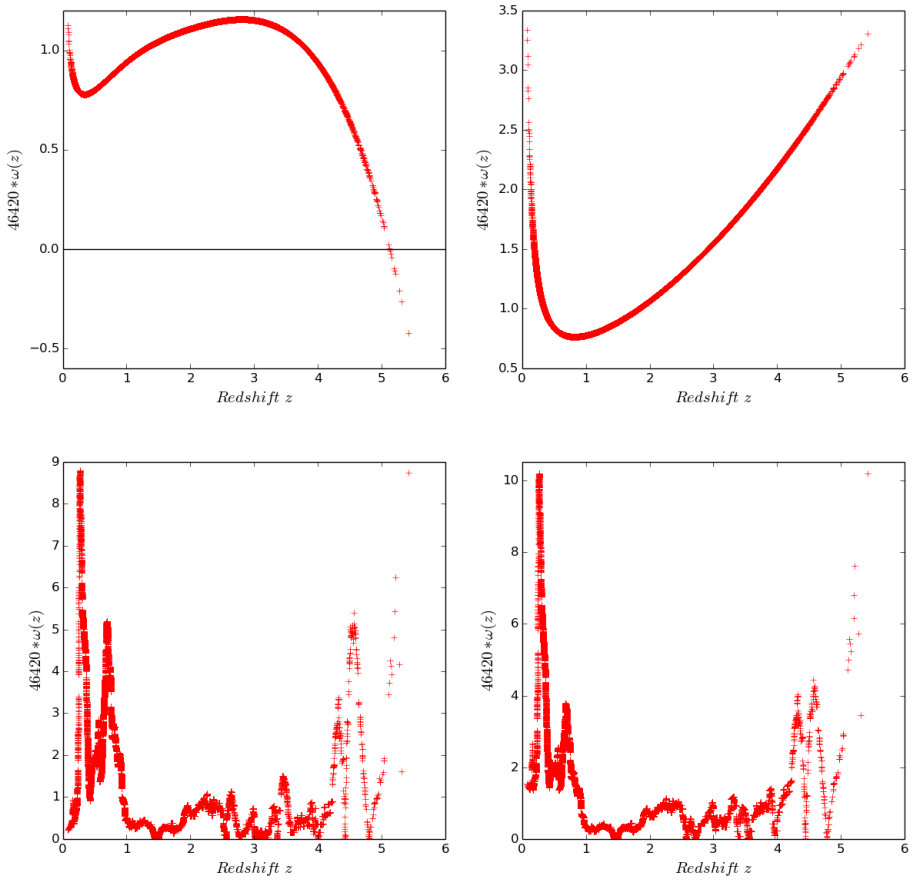

Figure 1. The weighting factors (scaled values by a factor $\times N$) for the SDSS-DR3 sample without K-correction (upper panels) and with K-correction (bottom panels), by assuming $(\Omega_\circ = 0.132, \lambda_\circ = 1.275)$ (left panels) and $(\Omega_\circ = 0.3, \lambda_\circ = 0.7)$ (right panels).

which provides us with a curve in the $\Omega_\circ$-$\lambda_\circ$ diagram, because of statistical characteristics of data and the degeneracy in the Hubble law. To avoid cumbersome calculations, the accuracy on the determination of cosmological parameters is estimated by applying the same procedure to simulations generated by assuming these candidate value.

According to working hypothesess, the null correlation test can be applied to any sub-sample selected in terms of the apparent magnitude[8]. It must be also noted that this method does not require to specify the selection function $\phi(m)$ and the luminosity function $f(M)$ of sources, which advantageously characterizes the robustness of our estimates.

2.4 Luminosity function and Selection function

For the candidate model, the weighted probability density that describes the sample reads

$$\mathrm{d}P_\omega \propto f_\omega(M)\mathrm{d}M\, \phi_\omega(m)\mathrm{d}m \tag{2.17}$$

[8] e.g., the sources whose apparent magnitude stand within the interval $[m_{\min}, m_{\max}]$, or any sampling, as long as it is free from selection effects on redshift.

as a product of two probability density functions, namely

$$f_\omega(M) \propto f(M)10^{-\frac{\beta}{5}M}, \qquad \phi_\omega(m) \propto \phi(m)10^{\frac{\beta}{5}m} \tag{2.18}$$

For large N, their cumulative distributions functions can be approched as follow

$$F_\omega(M) \approx \hat{F}_w(M) = \sum_{k=1}^{N} \omega_k \theta(M - M_k), \quad \Phi_\omega(m) \approx \hat{\Phi}_w(m) = \sum_{k=1}^{N} \omega_k \theta(m - m_k) \tag{2.19}$$

where θ stands for the Heaviside step function. Hence, from discrete derivatives of statitstics, one obtains estimates of the luminosity function and the selection function

$$f(M) \propto \frac{\Delta \hat{F}_w(M)}{\Delta M} 10^{\frac{\beta}{5}M}, \qquad \phi(m) \propto \frac{\Delta \hat{\Phi}_w(m)}{\Delta m} 10^{-\frac{\beta}{5}m} \tag{2.20}$$

2.5 The FS diagram

A graphic representation of the data in the (M, V) diagram, hereafter named FS diagram [11], enables one to detect inconsistencies with the working hypotheses as artifacts in the distribution. A complete sample up to a limiting apparent magnitude m_{lim} contains all the sources in the field whose absolute magnitude $M < M_{\text{max}}(z)$ at redshift z, where

$$M_{\text{max}}(z) = m_{\text{lim}} - \zeta(z) \tag{2.21}$$

is either a decreasing function (if $\kappa_\circ \leq 0$) or has a minimum for $\hat{\tau}(z) = \frac{\pi}{2}$ (if $\kappa_\circ > 0$), in addition of bumps related to the K-correction term, see figure 3. In the FS diagram, these data are located to the left hand side of the curve

$$\mathcal{C} : (M_{\text{max}}(z), V(z)) \tag{2.22}$$

that characterizes the threshold at the apparent magnitude m_{lim}. For the true values of cosmological parameters, they are distributed uniformly along the V-axis and according to the luminosity distribution function along the M-axis.

It is obvious that one can have alterations of this idealist picture, such as a "smoothed cut off" at m_{lim} instead of a sharp one, which might be a closer description to the real situation. Moreover, we must also expect the existence of structures characterizing the presence of several surveys, bumps on the curve $\mathcal{C}$ which are related to emission lines in the spectrum, and others alterations that depend on the identification process of sources. These structures, related to the selection effects on the apparent magnitude, do not contradict the working hypotheses, they are characterized by shapes that are parallel to $\mathcal{C}$. Any other structure that cannot be described by the selection function $\phi(m)$ biases the null correlation test. With this in mind, and according to working hypotheses, the presence of any structure suggesting evolution with redshift invalidates the candidate model. Thanks to the power of the discernment of the eye, a simple visual analysis of the FS diagram makes it possible to verify whether the working hypotheses are satisfied and also to discern the artefacts from real structures.

2.6 Refining the determination

If the sample is (statiscally) complete up to a limiting apparente magnitude, then the results obtained by the null correlation test can be refined by using the V/V_{max} test. Indeed, for the candidate model, the data should be distributed uniformly along the V-axis. If the sample

shows such a property solely within a redshift range of values, this test applies to the related subsample.

For brevity, let us describe a case that does not account of coincidences of the filter with the emission lines of sources[9] and of the case $\kappa_\circ > 0$ for which the sample contains objects with redshift $z > z^\star$, that is a threshold at which the apparent magnitude increases with redshift[10]. Hence, the selection effects being described by a cutoff at a limiting apparent magnitude $m_{\rm lim}$, the selection function reads

$$\phi(m) = \theta(m_{\rm lim} - m) \tag{2.23}$$

A source with absolute magnitude M is visible up to a redshift $z_{\rm lim}$, as defined by

$$m_{\rm lim} = M + \zeta(z_{\rm lim}) \tag{2.24}$$

For the candidate model, namely the values of cosmological parameters that satisfy eq. (2.16), the random variable

$$v = \frac{V}{V_{\rm max}(M)} \in [0,1[, \qquad V_{\rm max}(M) = V(z_{\rm lim}) \tag{2.25}$$

is uniformly distributed[11] within the range $[0,1]$. The likehood of this assumption can estimated by the Kolmogorov-Smirnov (KS) test to the sample of values

$$v_k = v(z_k, m_k) = \frac{V(z_k)}{V_{\rm max}(m_k - \zeta(z_k))}, \qquad (k = 1, N) \tag{2.27}$$

If the working hypotheses are correct, the distance between the empirical $\hat{F}(x)$ and the theoretical $F(x)$ cumulative distribution functions, which is defined as follows

$$\hat{\delta} = \sup_{x\in[0,1]} |\hat{F}(x) - x|, \qquad \hat{F}(x) = \frac{1}{N}\sum_{k=1}^{N} \theta(x - v_k) \tag{2.28}$$

is a random variable with the KS cumulative distribution function $\mathrm{Prob}_N(\hat{\delta} < \delta)$[12].

[9] In that case, according that the K-correction term takes emission lines into account, see eq. (2.7), the distance modulus is not an invertible function, and the formulation of the null correlation test becomes slightly different. Indeed, if the spectrum shows $\hat{p}$ emission lines, then equation $M_{\rm max}(z) = M$ shows a first root $\hat{z}_0$ in addition (eventually) of $p \leq \hat{p}$ pairs of roots $\{\hat{z}_{2j-1}, \hat{z}_{2j}\}_{j=1,p}$, ranked by increasing values, that correspond to redshift ranges where the souce becomes visible. Hence, the uniform random variable as give in eq. (2.27) transforms as follows

$$v = \frac{1}{V_{\rm max}(M)}\left(V(z) - \sum_{j=0}^{p} \theta\left(z - \hat{z}_{2j+1}\right)\left(V(\hat{z}_{2j+1}) - V(\hat{z}_{2j})\right)\right), \qquad V_{\rm max}(M) = V(\hat{z}_0) + \sum_{j=1}^{p}\left(V(\hat{z}_{2j}) - V(\hat{z}_{2j-1})\right)$$

[10] The redshift dependance of the distance modulus, excepted that through the K-correction term, is given by "$\log(1+z) + \log\sin\hat{\tau}(z)$", see eq. (2.7). Hence, if $\kappa_\circ > 0$, the distance modulus decreases with redshit above a given value $z^\star > \hat{\tau}^{-1}(\frac{\pi}{2})$; what characterizes a spatially closed universe (i.e., the comoving space V_3 stands for the 3-sphere).

[11] Indeed, its cumulative distribution function reads

$$F(x) = \mathrm{Prob}(v < x) = \mathrm{Prob}(V < xV_{\rm max}(M)) = \frac{x}{P_{\rm th}(\phi)}\int V_{\rm max}(M) f(M) \mathrm{d}M = x \tag{2.26}$$

[12] In short, the value $\mathrm{Prob}_N(\hat{\delta} \geq \delta)$, the probability to obtain statistical fluctuations larger than δ (the one measured), stands for the likelihood that the working hypotheses are correct.

One can easily prove that the $V/V_{\max}$ test can be applied to sub-domains defined in apparent magnitude $m \in [m_{\min}, m_{\max}]$ and/or in redshift $z \in [z_{\min}, z_{\max}]$. Moreover, to avoid making inferences on the formation epoch of sources, one can use $z_{\max}$ corresponding to the largest redshift value in the sample, which is particularly useful if $\kappa_\circ > 0$.

If the selection function ϕ is known, or given by eq. (2.20), then the $V/V_{\max}$ test can be adapted for using the entire sample by substituting V and $V_{\max}$ in eq. (2.27) by $\tilde{V}$ and $\tilde{V}_{\max}$ defined as follows

$$\tilde{V} = \int_0^V \phi\left(M + \zeta(z)\right) \mathrm{d}V, \qquad \tilde{V}_{\max}(M) = \int_0^{V_{\max}(M)} \phi\left(M + \zeta(z)\right) \mathrm{d}V(z) \tag{2.29}$$

where $V_{\max}(M)$ is given by eq. (2.24).

2.7 A comparison with the Hubble diagram

In both approaches, the data sampled the cosmological expansion throughout cosmic time, and along the observer's past light cone. The sources are assumed to be permanent and not evolving (number density, luminosity, spectral). Hence, a K-correction is used (unless using bolometric magnitude), what requires a composite spectrum of sources. Unlike the FS diagram, the Hubble diagram (m, z) the coordinates do not depend on cosmological parameters, which facilitates the identification of selection effects in observation. The data are expected to lie around a model dependent curve that gives the apparent magnitude of a standard candle as a function of redshift. The goal is to fit that curve to data by means of a least squares method, for estimating the values of cosmological parameters. To perform such an approach, one is faced to the arbitrary choice of a distance between the data to their the predicted values, which often results from heuristic method with subjective reasoning. Moreover, in order to perform properly the Malmquist bias correction, one has to specify the selection function $\phi(m)$ and the luminosity function $f(M)$. Because of these requirements, the null correlation technique appears then more robust in testing the working hypotheses. Moreover, the uniformity on the spatial distribution of sources, as required by FLG models, is also tested. The crucial difference with the Hubble diagram is that the eq. (2.16) does not have necessarely a solution if the data do not fulfill the required properties that are induced by the working hypotheses.

The null correlation method could have being introduced solely as a search for the roots of the statistics defined in eq. (2.16) but the presentation in terms of weighted probabilities allows to highlight a property akin to a lessening of the statistical information contained in the sample. This one can be quantified as a (sample) number deficit $N\mathcal{L}$ defined by means of the Shannon's entropy $H(\omega)$ as follows

$$\mathcal{L} = 1 + \frac{1}{\ln N} H(\omega), \qquad H(\omega) = \sum_{k=1,N} \omega_k \ln \omega_k \tag{2.30}$$

2.8 Simulations techniques

Let us focus on the case of a sample complete up to an apparent magnitude $m_{\lim}$ that are uniformly distributed in space and with a luminosity function $f(M)$, in a given cosmological model $(\Omega_\circ, \lambda_\circ)$. It is clear that to simulate such a sample $\{(z_k, m_k)\}_{k=1,N}$ with a trial and error method, that keeps those (V_k, M_k) in agreement with selection effects, is extremely time consuming. In order to avoid such a difficulty, one needs to proceed in a different way.

The probability density is given in eq. (2.9), the selection effects in observation are solely described by a cutoff in apparent magnitude, as described by eq.(2.23). Hence, the cumulative distribution function[13] reads

$$G(x) = \frac{1}{P_{\rm th}(\phi)} \int_{-\infty}^{x} V_{\rm max}(M) f(M) {\rm d}M \tag{2.31}$$

For each object, two random values g_k and v_k are generated, both uniformly distributed within the interval $[0, 1]$. By inversing the functions given in eqs. (2.31) and (2.5), one obtains successively $M_k = G^{-1}(g_k)$, $V_k = v_k V_{\rm max}(M_k)$, $z_k = V^{-1}(V_k)$ and $m_k = M_k + \zeta(z_k)$.

2.9 The methodology when using the null correlation method

Since only the selection effects allowed in the data are the ones on the apparent magnitude, one has to verify that there is no of other kinds, and in particular those on the redshift. For this purpose, a visual inspection on the data distribution in the FS diagram enables us to check whether anomalies at constant V are present. At this point, let us emphasize that the overlapping of emission lines of the spectrum of a source with the observed wavelength window of the filter interprets as a selection effect on the apparent magnitude and not on redshift.

Among the roots of eq. 2.16, that define the null correlation curve, one can refine the estimate of cosmological parameters if (and only if) the sample is complete up to a given limiting apparent magnitude. Indeed, the most likely values that account for the data is the one for which the spatial distribution of (the observed) sources appears to be the most uniform in the comoving space. The completeness criteria of the data can be checked by means of the statistic given in eq. (2.20), which provides us with an estimate of the selection function $\phi(m)$; it must coincide with a Heaviside step function at a threshold $m_{\rm lim}$. In general, the samples do not show a sharp cutoff at the (apparent) threshold $m_{\rm lim}$ but a smoother one. In that case, a brighter limiting magnitude $m^{\star}_{\rm lim} < m_{\rm lim}$ has to be chosen to perform the $V/V_{\rm max}$ test. It is clear that such a step diminishes the sample size but to the benefit of an unbiased estimation of the Kolmogorov-Smirnov test on the uniformity of the spatial distribution of sources. If necessary, other subsampling criteria can be chosen, to test the distribution on specific part of the FS-diagram, as described in section 2.6.

3 Application to QSOs samples

3.1 The Sloan Digital Sky Survey (SDSS) data

The data releases of Sloan Digital Sky Survey (SDSS) (http://www.sdss.org/) contain a large number of QSOs data, whose the size and accuracy of samples increase with their release numbers. However, we have been forced to limit our investigation on the first ones, because of the required statistical properties for our investigation.

For example, the FS diagram of DR9-BOSS on figure 2 shows that the SDSS-III samples suffer from an inhomogeneous parcelling due to data processing. For a homogenous sample, one should have a regular distribution of dots situated at the left side of a curve (or below it) representing the limiting apparent magnitude. Such a border is present, although its sharpness is diminished because of an additional and sparse distribution of dots beyond it.

[13] If ϕ cannot not be identified to a Heaviside step function then $V_{\rm max}$ in eq. (2.31) has to be substituted by $\tilde{V}_{\rm max}$ as defined in the footnote of sec. 2.6.

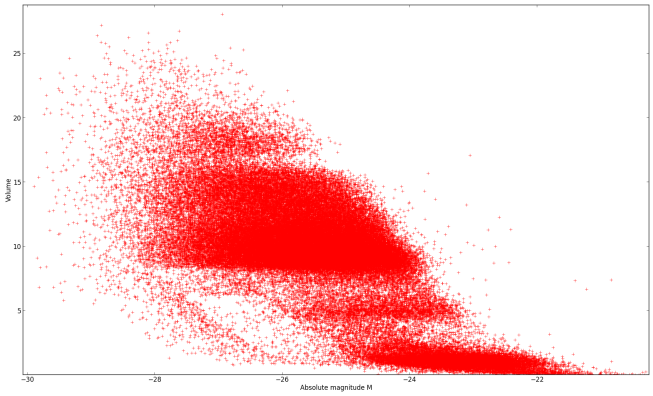

Figure 2. The FS diagram for the SDSS-III:DR9 sample by assuming $\Omega_\circ = 0.3$ and $\lambda_\circ = 0.7$.

Name	N	Δz	Δi-mag	ref
EDR	3,814	$[0.15, 5.03]$	$[15.16, 20.82]$	[2]
DR1	16,713	$[0.08, 5.41]$	$[15.15, 21.79]$	[3]
DR3	46,420	$[0.078, 5.414]$	$[15.10, 21.78]$	[5]
DR7	105,783	$[0.065, 5.461]$	$[14.86, 22.36]$	[8]

Table 1. QSOs samples

At the left side, and parrallel to it, two similar structures are also present. They probably account for surveys with brighter limiting magnitudes. Such features characterize surveys at different limiting apparent magnitudes. They can be treated globally by the null correlation technique, as long as selection effects on redshift are absent, which is not the case. Indeed, four prominent structures are present, the zones of higher density of dots with horizontal borders, and a sparse region (with a rhombus shape) at the bottom of the distribution, that characterize, as a matter of fact, selection effects on redshift. One of the reasons of such an inhomogeneity is that these QSOs have been selected with the aim to measure the BAO scale in the Lyman-α forest at redshift ≈ 2.5. Most of them span a range of redshift: $2.5 < z < 3.5$ [9].

Consequently, our choice has dropped to the SDSS Legacy Survey (i.e., SDSS-I and SDSS-II) which provides us with an "uniform and well-calibrated map of the Universe". These samples are described in table 1, characterized by their (number) size N and their range on the redshift Δz and the i magnitude Δi-mag.

Because of successive improvements of the data processing, these samples were made in different ways. For example, the differences between the DR1 and DR3 samples are due to several modifications in the selection criteria of candidates (on the efficiency of the S/N ratio to determine the redshift, on the constraint of the line width of the spectrum, new techniques are used for the photometric measurement and the data imaging.). Although it is recommended not to use previous versions to DR3 (see, http://classic.sdss.org/dr1/), we have performed the null correlation test to each of these samples, what enabled us to test the stability of this method versus measurement errors (and improvements in measurement). The K-correction term for the i-band used herein is described in [5, 6], it takes into account

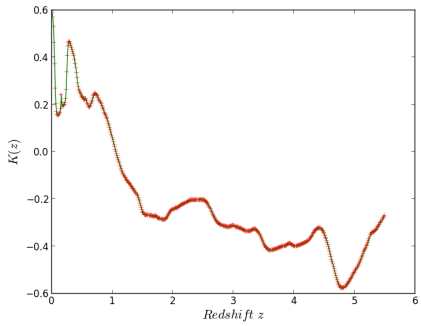

Figure 3. The K-correction of the SDSS-DR3 sample in the i-band, including both the emission-line and continuum components, normalized at $z = 2$ with a fixed spectral index $\alpha_\nu = -0.5$.

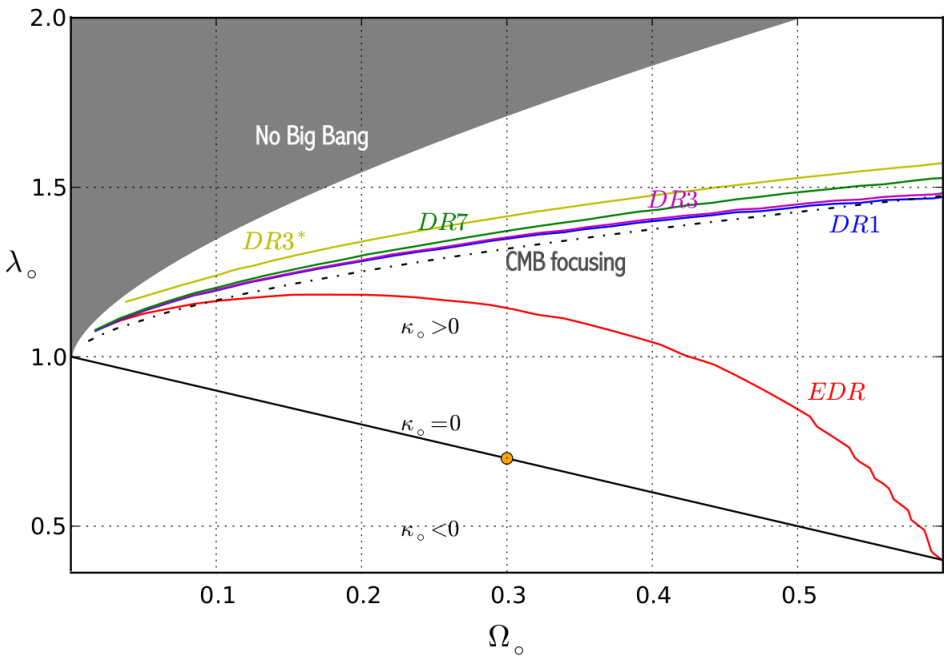

Figure 4. The null correlation curves in the $\Omega_\circ$-$\lambda_\circ$ diagram corresponding to samples : EDR, DR1, DR3 and DR7. They provide us with the candidate values of cosmological parameters which agree with the working hypotheses. The spatially closed cosmological models $\kappa_\circ > 0$ are located above the straight line, that corresponds to $\kappa_\circ = 0$, where the standard solution is represented by a yellow dot. The bottom curve corresponds to the EDR sample, these models are in complete disagreement with those derived from the other samples.

the continuum and the emission lines, see figure 3.

3.2 The null correlation test

The null correlation test has been applied to these four samples and the results are shown in the $\Omega_\circ$-$\lambda_\circ$ diagram, see figure 4. Each sample provides us with a null correlation curve that corresponds to candidate values in agreement with the working hypotheses.

The obvious result is that the candidate values obtained with the EDR sample are in

complete disagreement with those of other samples. As a matter of fact, "..., the original version of the quasar target selection algorithm used in the EDR data did a particularly poor job of selecting quasars with redshifts close to $z = 3.5$. (loc. cit., see [6]).

Hence, let us focus on the other null correlation curves. They slightly differ from each other, which is probably due to improved estimates of data and of different sample sizes. These candidate values lie rather above a straight line defined by $(\Omega_\circ \approx 0.04, \lambda_\circ \approx 1.1)$ and $(\Omega_\circ \approx 0.5, \lambda_\circ \approx 1.5)$, whose slope ≈ 0.52 indicates that estimates of $\lambda_\circ$ are twice as much accurated as those of $\Omega_\circ$. The unsettling result is that $\lambda_\circ > 1.1$ for all these candidate values, what does not match with the standard value of $\lambda_\circ \approx 0.7$; furthermore one obtains $\lambda_\circ \approx 1.3$ by choosing $\Omega_\circ \approx 0.3$.

We use the FS diagram of the samples DR3 and DR7 for evaluating the relevance of such a result, see figure 5. As representant, among these candidate models, we choose the one with the smallest scalar curvature $(\Omega_\circ = 0.076, \lambda_\circ = 1.211)$ (left panels), since it is common to these samples; their information deficit is $\mathcal{L} = 18.10^{-4}$ for DR3 and $\mathcal{L} = 17.10^{-4}$ for DR7, see eq. (2.30). These diagrams are compared to their versions with $(\Omega_\circ = 0.3, \lambda_\circ = 0.7)$ (right panels); their information deficit is $\mathcal{L} = 43.10^{-4}$ for DR3 and $\mathcal{L} = 50.10^{-4}$ for DR7. For purposes of the analysis, the graduation on the ordinate is translated into redshift on the right hand side axis. The curves, they correspond to the apparent i-magnitudes $m = \{15, 19.1, 20.5, 21.78\}$, give ranges on the magnitude. Let us keep in mind that, while the distribution along the vertical axis is expected to be uniform for a complete sample up to a limiting apparent magnitude, the presence of selection effects in apparent magnitude alters this characteristics, in addition of possible horizontal alterations due to selection effects by the redshift. With figure 2, one can note that the homogeneity of these samples has improved with respect to that of DR9 sample.

- FS diagram of DR3 sample :

  On the left panel, let us identify first the obvious structures which are produced by selection effects, they appear as discontinuities in the distribution of dots. It is clear that the low density region (hole) in the range $19.1 \leq m \leq 20.5$ and $2.7 \leq z \leq 3.1$ that extends (slightly) at brighter magnitudes at $z \approx 3.38$, is due to selection effects on the redshift. This attests of difficulties on identifying QSOs in the data processing. Mainly because the colors of quasars and the stars of their host galaxies are similar at these redshifts.

  Moreover, the distribution, which extends up to magnitude of $m = 21.78$ is very sparse down to i-magnitude $m = 20.5$ that confines more clearly the sample. A similar feature is also present at i-magnitude $m \approx 19$ characterizing a distinct survey. The region within $15 \leq m \leq 19.1$ could be splitted in two parts by a curve at constant i-magnitude, so to detach a sparse region of nearby sources. These low density regions on either side of the distribution are due to selection effects on apparent magnitude, while it is not the case for the hole.

  Hence, because of this inconsistency with the working hypothesis, these results can be questioned, unless the hole is (interpreted as) a statistical fluctuation.

  On the right panel, for an unbiased comparison with the left panel, the analysis of structures has to take in account their relative sizes with respect to the extend of the sample. With this in mind, the most prominent differences are that the size of the hole

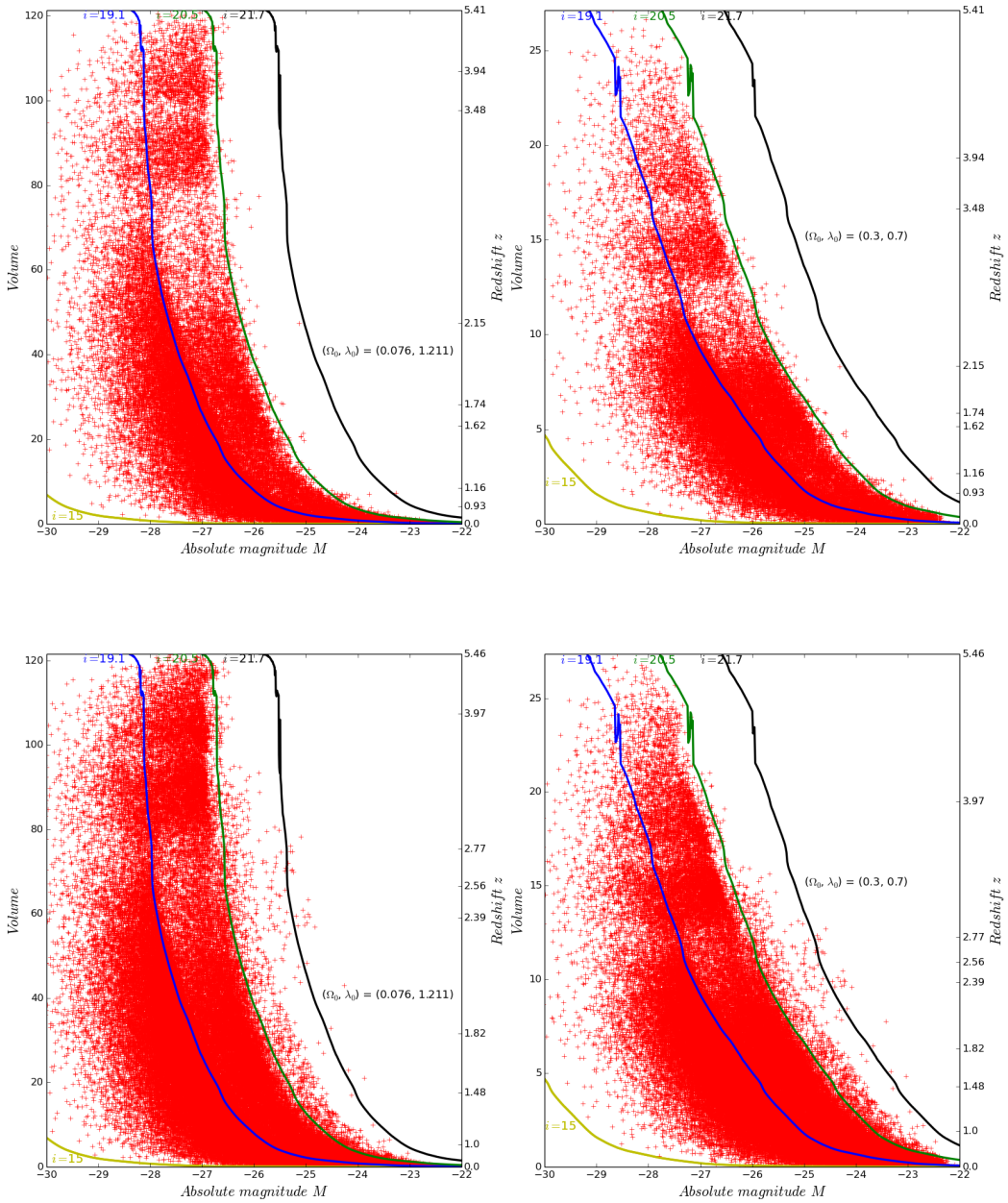

Figure 5. The FS diagram for the DR3 sample (upper panels) and the DR7 sample (bottom panels), by assuming ($\Omega_\circ = 0.076, \lambda_\circ = 1.211$) (left panels) and ($\Omega_\circ = 0.3, \lambda_\circ = 0.7$) (right panels). The curves correspond to the apparent i-magnitudes 15 (yellow), 19.1 (blue), 20.5 (green) and 21.78 (black). The graduation on the ordinate is translated into redshift on the right hand side axis.

has diminished and the zone where bright QSOs are missing at low redshift has enlarged significantly.

- FS diagram of DR7 sample :

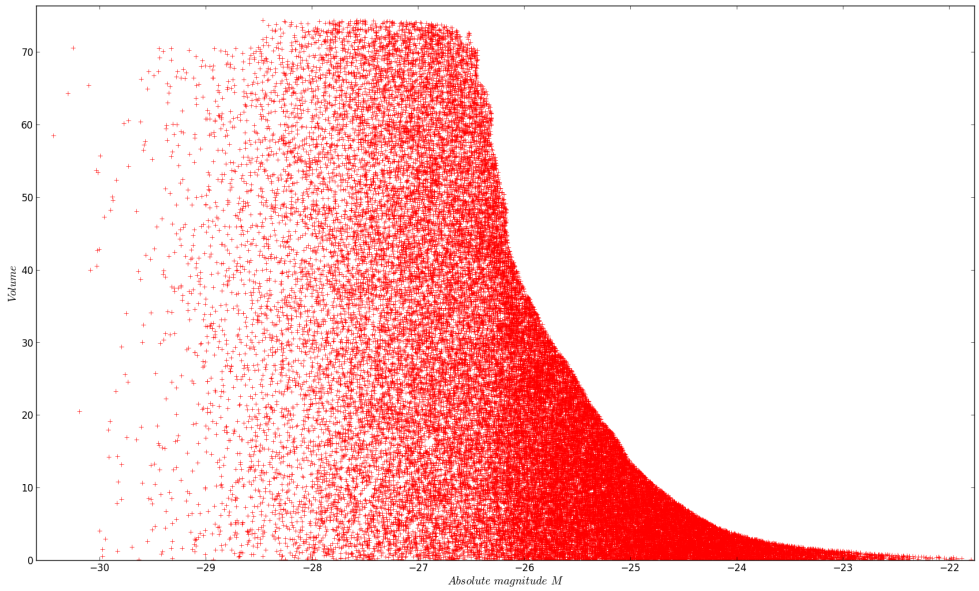

Figure 6. The bottom part of the FS diagram of a complete sample of 46,420 sources up to i-magnitue $m_{\text{lim}} = 21$, that was simulated by assuming $(\Omega_\circ = 0.132, \lambda_\circ = 1.275)$ with a Gaussian luminosity function of absolute meam i-magnitue $M_\circ = -25$ and standard deviation $\sigma_M = 1.2$.

On the left panel, compared to DR3, the distribution of dots is much more dense (since they are twice as much numerous and cover almost the same zone) and the void has been almost filled. At the right side of the curve $m = 20.5$, the sample shows a fainter limiting magnitude (well defined at lower redshift). Its number density decreases with z and vanishes at $z \approx 3.2$, which characterizes a selection effect on the redshift. An additional and sparse distribution is also present, that extends beyond $m = 21.78$.

On the right panel, the spatial distribution of bright QSOs appears less uniform compared to the the left panel, and the number of missing objects at low redshifts increases (statistically), which stands for as a significant issue.

3.3 Refining the cosmological parameter's estimates

The candidates models as obtained from DR3 and DR7 samples are not so differents from each other, that is the related null correlation curves coincide almost, see figure 4. With the aim to refine the cosmological parameter's estimates by mean of the V/V_{max} test we need complete subsamples.

The only comparison between the FS diagrams of DR3 and DR7 samples with a simulation on figure 6 shows that they are not complete, what is the required statistical property which enable us to refine these estimates of cosmological parameters by means of the V/V_{max} test.

We start by applying the test to subsamples using the corresponding NCC. The results for each subsample are given as follows:

90

- $18.65 \leq m \leq 19.1, \quad 0.04 \leq z \leq 2.45 : \Omega_\circ = 0.132, \lambda_\circ = 1.275$, at 35% significance level.
- $18.65 \leq m \leq 19.1, \quad 1.8 \leq z \leq 2.4 : \Omega_\circ = 0.076, \lambda_\circ = 1.211$, at 70% significance level.

4 Conclusion

The application of the null correlation and V/V_{max} tests to QSO samples of the SDSS survey allowed us to discriminate the candidates values for the cosmological parameters that agree with observations. We found a model with a positive scalar curvature with weak presence of dark matter.

References

[1] L. Wisotzki, *Quasar spectra and the K correction*, *Astron. & Astrophys.*, **353** (2000) 861

[2] D. P. Schneider *et al.*, *The sloan digital sky survey quasar catalog. I. Early Data Release*, *Astron. J.* **123** (2002) 567

[3] D. P. Schneider *et al.*, *The sloan digital sky survey quasar catalog. II. First Data Release*, *Astron. J.* **126** (2003) 2579

[4] K. Abazajian *et al.*, *The Third Data Release of the Sloan Digital Sky Survey*, *Astron. J.* **129** (2005) 1755

[5] D. P. Schneider *et al.*, *The sloan digital sky survey catalog. III. Third data release*, *Astron. J.* **130** (2005) 367

[6] G. T. Richards, *et al.*, *The SDSS Quasar Survey: Quasar Luminosity Function from Data Release Three*, *Astron. J.* **131** (2006) 2766

[7] K. Abazajian *et al.*, *The Seventh Data Release of the Sloan Digital Sky Survey*, *Astron. J. Suppl.* **182** (2009) 543

[8] D. P. Schneider *et al.*, *The sloan digital sky survey catalog. V. Seventh data release*, *Astron. J.* **139** (2010) 2360

[9] I. Pâris *et al.*, *The sloan digital sky survey catalog: ninth data release*, *Astron. & Astrophys.*, **548** (2012) 1

[10] J.M. Souriau, *Mécanique statistique, groupes de Lie et cosmologie*, in *Géométrie symplectique et physique mathématique*, (Colloq. Internat. CNRS No. 237, Aix-en-Provence, 1974) **237** (1975) 59

[11] H.H. Fliche, J.M. Souriau, *Quasars et cosmologie*, *Astron. & Astrophys.* **78** (1979) 87

[12] H.H. Fliche, *Evualuation des paramètres cosmologiques à l'aide des propriétés optiques des quasars. Fluctuations des modèles de Firedmann-Lemaître*, *Thèse d'état, Université de Provence* (1981)

[13] G. Bigot, H.H. Fliche, R. Triay, *A determination of $q_\circ$ by a technique of null correlation*, *Astron. & Astrophys.* **206** (1988) 1

[14] G. Bigot, R. Triay, *Comments on the Hubble diagram. I. The Malmquist bias*, *Phys. Lett. A* **150** (1990) 227

[15] G. Bigot, R. Triay, *Comments on the Hubble diagram. II. The technique of fitting*, *Phys. Lett. A* **150** (1990) 236

[16] G. Bigot, R. Triay, *The technique of fit in the Hubble diagram*, in *The quest for the fundamental constants in cosmology*, Proc. of the 24th Rencontre de Moriond (9th Moriond Astrophysics Meeting), (1990) 165

[17] G. Bigot, R. Triay, *A null correlation technique to determine* q_o, in *The quest for the fundamental constants in cosmology*, Proc. of the 24th Rencontre de Moriond (9th Moriond Astrophysics Meeting), (1990) 177

[18] G. Bigot, S. Rauzy, R. Triay, *Is evolution of radio sources necessary ?*, *Phys. Lett. A* **158** (1991) 282

[19] G. Bigot, R. Triay, *Comments of* $V/V_{\max}$ *test*, *Phys. Lett. A* **159** (1991) 201

[20] R. Triay, *Automatic biases correction*, *Astrophysical Letters and Communications* **31** (1995) 279

[21] Author, *Title*, *J. Abbrev.* **vol** (year) pg.

[22] Author, *Title*, arxiv:1234.5678.

[23] Author, *Title*, Publisher (year).

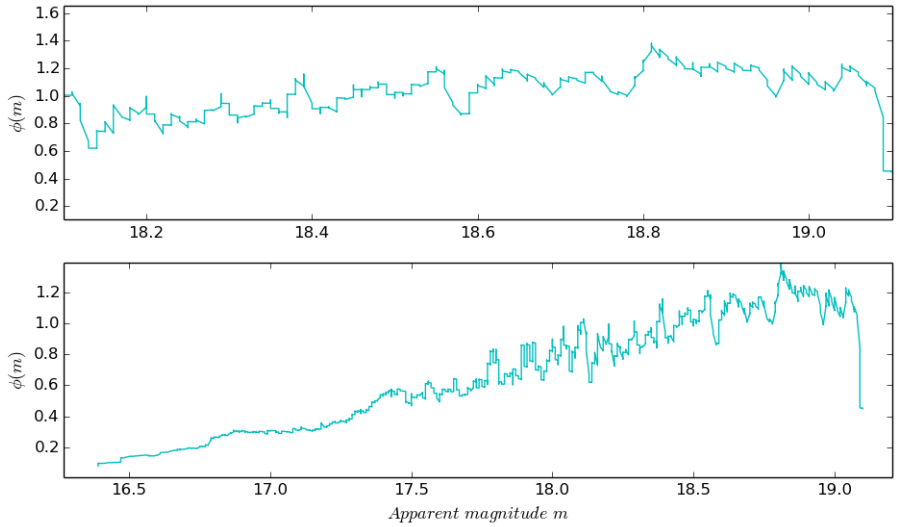

Figure 4.20: The selection function $\phi(m)$ of the SUBDR3 subsample with ($\Omega_\circ = 0.0305$, $\lambda_\circ = 1.1180$). The upper panel is an enlargement of the area in which the function is most constant.

4.5 Conclusion

The application of the null correlation and V/V_{max} tests to QSO samples of the SDSS survey allowed us to discriminate the candidates values for the cosmological parameters that agree with observations. We found a model with a positive scalar curvature with weak presence of dark matter.

CHAPTER 5

Application to supernovae type Ia sample

Contents

5.1 Introduction 81

5.2 Type Ia Supernovae as standard candles 82

5.2.1 The lightcurve of type-Ia SN 83

5.2.2 Standardisation of type-Ia SN 84

5.2.3 Modelling of the Supernova event 86

5.2.4 Sampling the light curve of type-Ia SN and selection effects 88

5.2.5 Calibration statistics 90

5.2.6 Simulation 94

5.3 The null correlation test on the supernova sample . 98

5.3.1 Luminosity function and Selection function 100

5.3.2 Precision and error 101

5.4 Application to the JLA sample 101

5.4.1 Description of samples 102

5.4.2 Results 103

5.5 Conclusion 107

5.1 Introduction

Historical records of supernovae have been found over the past two thousand years. The first SN in our own galaxy was observed and recorded by the Chi-

nese astronomers, dating back to 7 December 185 AD with a visibility of 20 months [Clark et al 1977]. This event was discovered by several missions (China, Japan, Korea, Arab and Europe) and followed by a three-year observation and recorder in 1006 AD as the earlier high luminous SN. The Crab Nebula is the remains of a SN which was occurred in AD 1054 and confirmed in 1968 to be associated with a pulsar, which is interesting to explain the energetics and structure of the whole supernovae remnant [Green et al 2003].
In this chapter, we describe a homogeneous class of supernova (type Ia) with a standardization method. A new modelling of supernova sample is detailed in Sect.5.2.3. Sect.5.2.4 presents a detailed description of the selection effects. The calibration of events is given in Sect5.2.5. Sect.5.3 shows an adaptation of the null correlation test to the type-Ia SN. The application of model to real data is presented in Sect.5.4.

5.2 Type Ia Supernovae as standard candles

The supernova (SN) is one of the most luminous objects in the universe discovered until today. It is the result of the explosion of massive stars at the end of its life. Its luminosity can match the one of its host galaxy in some cases, and they are observed at cosmological distances. The SNe are classified into groups, one of which can be used as standard candles for probing cosmological distances with high accuracy.

The spectral and photometric studies of SN points out two categories (Minkowski 1940) according to their properties, mainly based on the presence (type II) or not (type I) of Hydrogen elements in their spectra. The spectrum, is related to the photosphere phase (a few instants after explosion). The fast expansion of its envelope makes the medium opaque to radiation, causing the absorption lines to appear in the spectrum. Later, during the nebular phase (After a few weeks of growth) emission lines arise in the spectrum since the medium becomes transparent to radiation. For type I, the strong absorption feature at wavelength ≈ 6150 Å due to silicon II (SiII) characterizes the type Ia. In absence of SiII, the SN is classified depending on the presence/absence of Helium He element as a type Ib/Ic. This classification is summarized in Fig.5.1.

The photometric classification is based on the comparison of the evolution of luminosity with time i.e. the light curve of the SN. Fig.5.2 shows, the light curves of type II SNe which decline slowly in the B band. Two additional classes are distinguished from the type IIn, the SN type II-L that displays a linear light-curve, and the SN type II-P which displays a plateau light-curve. However, the SN type Ib decreases faster than the type II, it represents a similar light-curve to that of SN Ia. This last group is the brightest among the other types of SNe. According to [Cappellaro et al 1999], the SN type Ib, Ic,

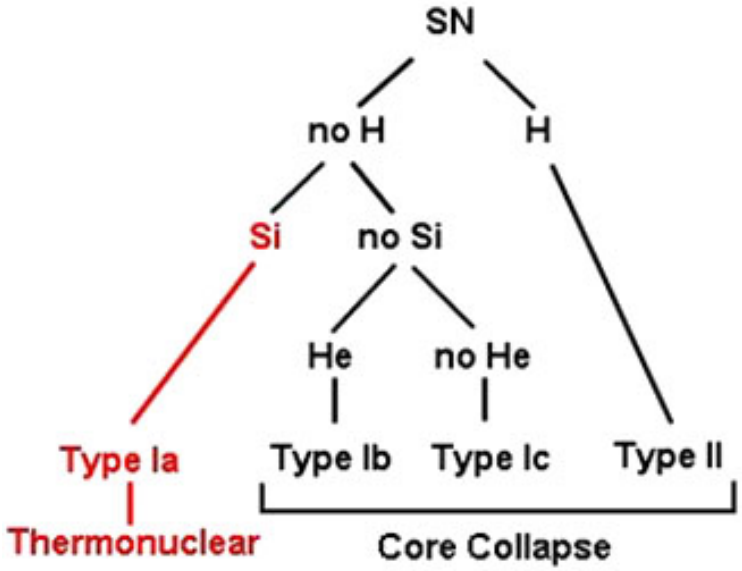

Figure 5.1: The supernova classification tree.

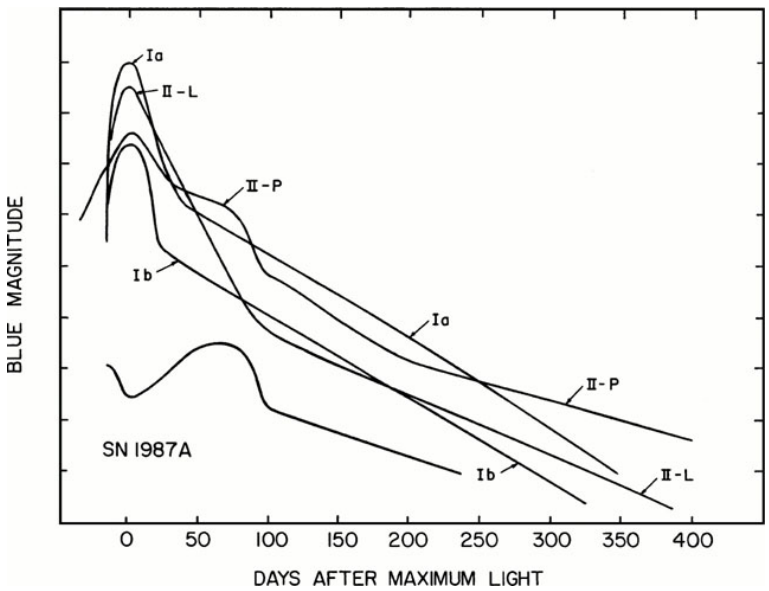

Figure 5.2: The light curves of different types of SNe in the blue band: the type Ia, Ib, II-L, II-P, and SN 1987A. The Curve of the SN Ia is brighter than all other SN types. Figure courtesy: [Wheeler 1990].

and II are the result of the explosion of massive stars in the framework of their core-collapse. These types are formed in the arms of spiral galaxies and they never had the possibility to be in the elliptical galaxies, where the rate of old stars is high. Contrastingly, the type-Ia SN can be in any type of galaxy, as

they are the result of the thermonuclear explosions of white dwarfs (Figs.5.3 & 5.4). The low-mass stars ($< 8M_{\odot}$)[1] evolve as their hydrogen combusts and

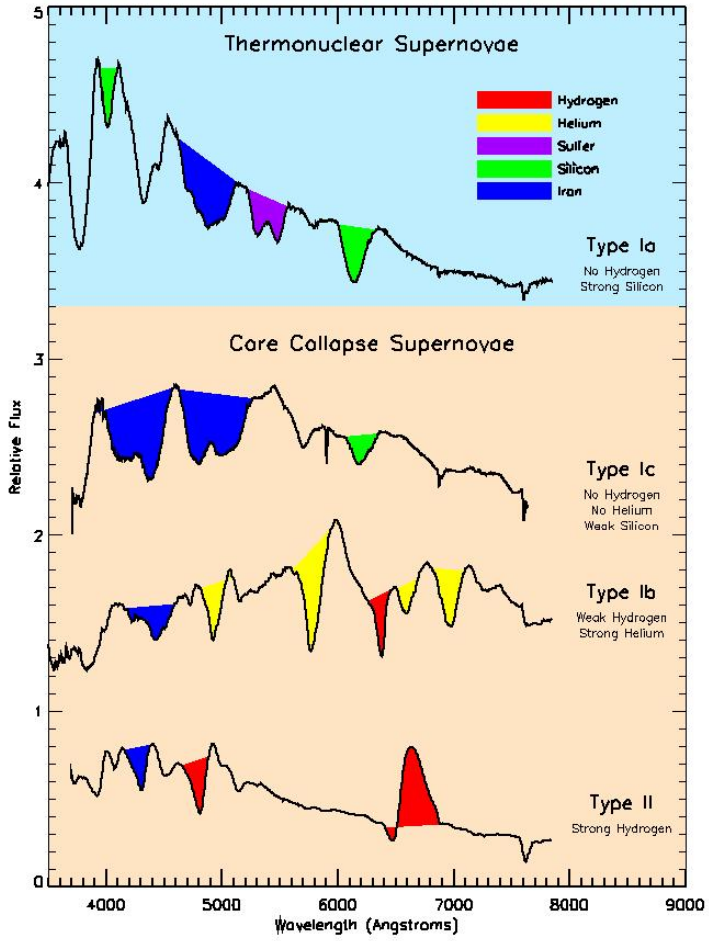

Figure 5.3: The supernova spectral Types. The gravitational supernovae is the progenitor of the supernovae type Ib, Ic and II. The progenitor of SN type Ia is a thermonuclear explosion of white dwarfs. Figure courtesy: Supernova Cosmology Project (SCP).

transforms into Helium, which is explodes with increasing the temperature to transform into carbon and oxygen. The most well-known model that describes the progenitor of the type-Ia SN as a low-mass star is that the one which becomes a white dwarf at the end of its life. This latter is accompanied with another star as a binary partner system (Fig.5.4) accreting matter on the white dwarf, and then increasing its mass until reaching the Chandrasekhar mass limit ($\approx 1.4M_{\odot}$). Consequently, the white dwarf explodes to produce the

[1] $M_{\odot}$ is the solar mass

type-Ia supernovae. The main characteristic of this class is the homogeneity of the SN spectra as shown in Fig.5.5.

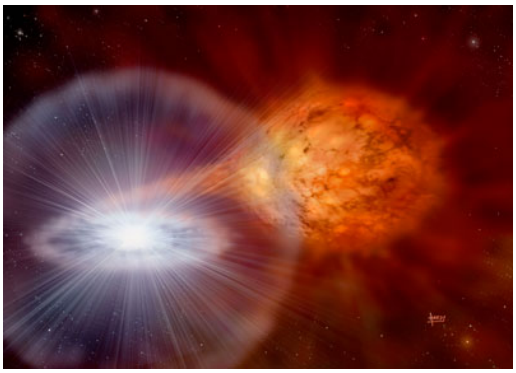

Figure 5.4: An artistic image of a white dwarf and a red geant star. Figure courtesy: STFC/David Hardy.

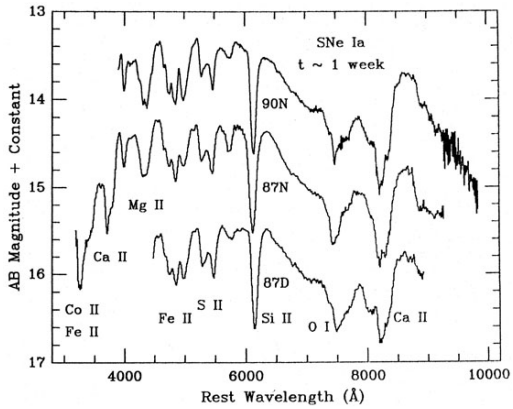

Figure 5.5: Spectra of three Type Ia supernovae, SN 1987D, SN 1987N, and SN 1990N, about one week after the maximum of their LC. Figure courtesy: [A. V. Filippenko 1997]

5.2.1 The lightcurve of type-Ia SN

The light curve (LC) represents the temporal evolution of the luminosity during the lifetime of SN. For objects that change their brightness, the LC is a major source of information and a valuable tool for studying these events. Fig.5.6 shows the SN 1998bu with almost similar or different LC in optical bands (referring to Bessel bands); e.g., note that two "bumps" appear in the I and R bands with a delay of the second bump by 21 to 30 days from the maximum in the B band. It is worth mentioning that among all types of SN, the LC in the B band of the type-Ia SN is almost the same for all of them (Fig.5.7 top panel). This feature makes them the most homogeneous family among the SN types with respect to LC. The decline of a SN Ia light curves after the maximum of luminosity correlates with the radioactive decay of ^{56}Ni to ^{56}Co for three to four weeks at the rate of $0.11 mag.day^{-1}$ and with the radioactive decay ^{56}Co to ^{56}Fe at the rate of $0.01 mag.day^{-1}$ more than one month.

5.2.2 Standardisation of type-Ia SN

In view to determine cosmological parameters, it is generally admitted that the LC of type-Ia SNe are good candidates to be used as standard candles, because the dispersion of luminosity at the maximum seems to be small, which is an

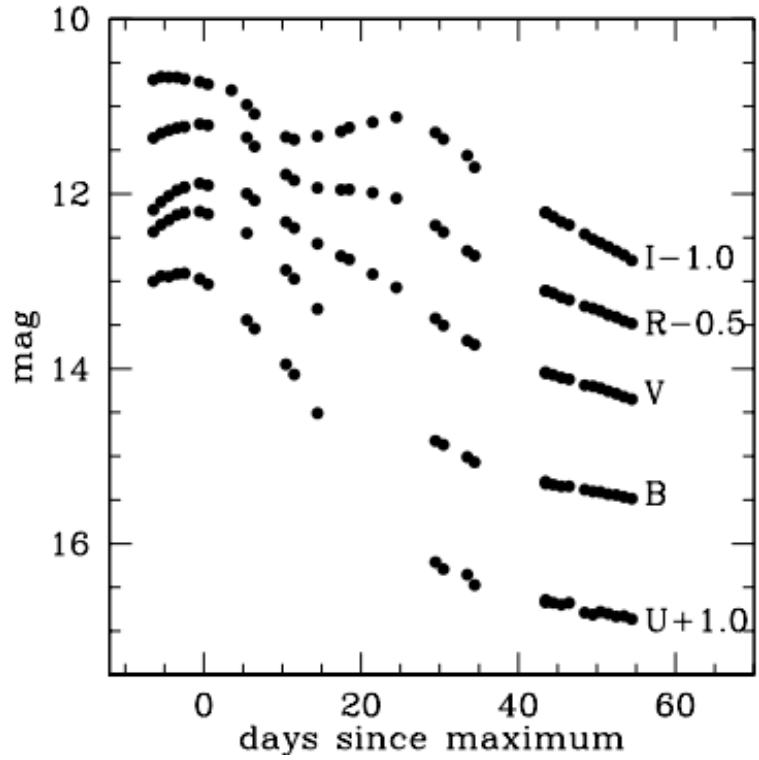

Figure 5.6: UBVRI light curves for SN 1998bu (Figure courtesy: [N. B. Suntzeff 1999])

obvious improvement compared to QSOs. [M. M. Phillips 1993]; [Hamuy et al. 1995], [1996a]; [Riess et al 1995], [1996a]; have shown up a correlation between the absolute magnitude, M_B, at the maximum of luminosity and the decline rate of luminosity after 15 days, noted Δm_{15} (Fig.5.8). This correlation enables one to estimate the absolute magnitude and hence the distance modulus. Several models have been applied to standardize their LCs in order to reduce the dispersion at the maximum of luminosity in the B band. Among these models, one has the MLCS (Multicolor Light Curve Shape), the MLCS2k2, the Stretch (stretching of the LC), the SiFTO, the SALT (Spectral Adaptive Lightcurve Template) and the SALT2 models which are the most widely used. These models standardize the SNe with: the apparent magnitude at maximum of luminosity (free from the k-correction), the (B-V) color at this maximum of luminosity and a shape parameter for describing the LC.

A brief description of SALT2 Model

The SALT2 model (for the second version of Spectral Adaptive Lightcurve Template) is an empirical model that determines the flux of type-Ia SNe as a

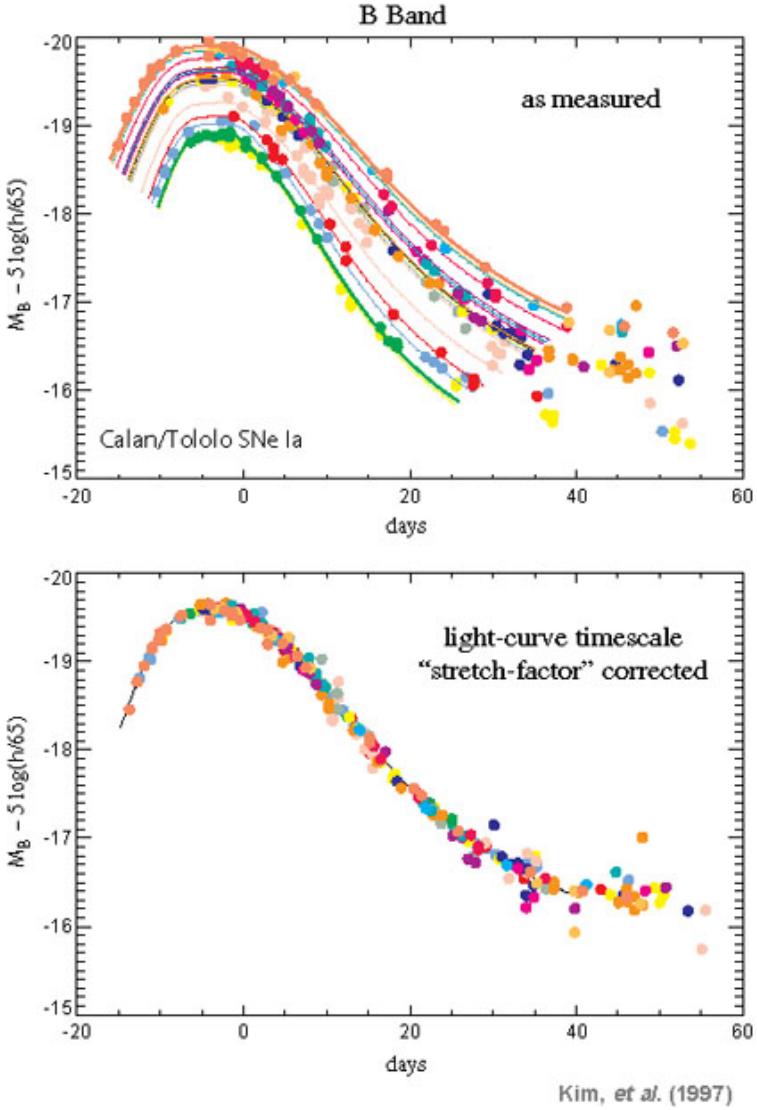

Figure 5.7: Light curve standard obtained. The B-band light-curves for a low-redshift SNe Ia from the Calan-Tololo survey (Figure courtesy: Hamuy et al. [1996a])

function of p (phase) and λ (wavelenghth), where p is defined as follows:

$$p = \frac{t_{obs} - t^*_{obs}}{1+z} \tag{5.1}$$

where t_{obs} stands for the date of observation and t^*_{obs} at maximum of luminosity in "rest frame". Similarly, t^* stands as the emission date at maximum of luminosity. This model is parameterized by: the normalization factor, the shape and the color parameters. It is based on modelling the spectral energy

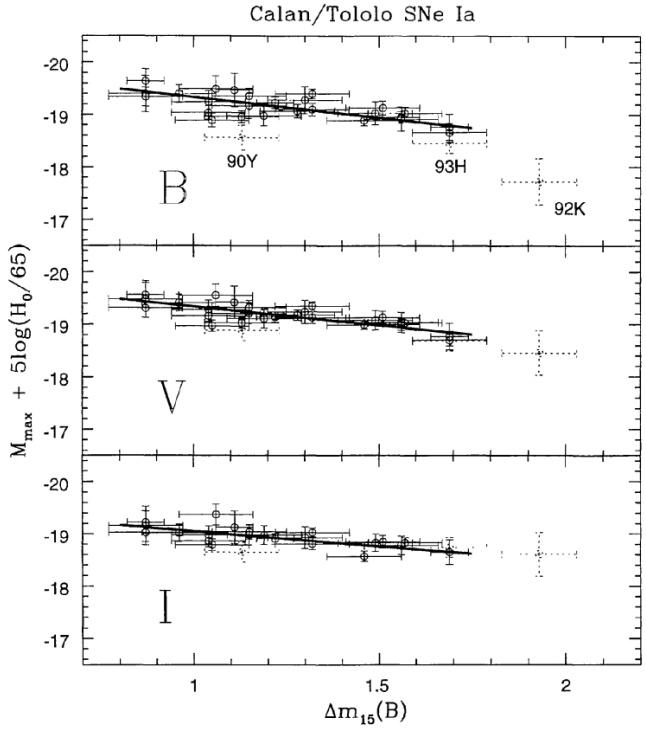

Figure 5.8: Correlation between the absolute magnitude with the decline rate Δm_{15} of the light-curve for low-redshift SN Ia from the Calan-Tololo survey (Figure courtesy: Hamuy et al. [1996a])

distribution:

$$F_{SN}(p,\lambda) = x_0 \times [S_0(p,\lambda) + x_1 S_1(p,\lambda) + ...] \times e^{[c \times CL(\lambda)]} \tag{5.2}$$

where x_0 is the global normalization in flux, x_1 is the shape parameter (equivalent to (s - 1) factor in Stretch method of standardization) which is used as an estimator of the absolute magnitude, and c the color of SN. The S_k are the spectral sequences: S_0 stands for the mean spectral sequence, S_1 stands for the first order deviation around S_0, etc...; B-splines functions are used to define them. CL stands for the phase-independent color-law. The SALT2 output provides us with : the apparent magnitude in B band free from (foreground) alterations $m_c^* = -2.5\log_{10}(x_0) + ZP$, the date at maximum of luminosity t^*_{obs}, the difference of color between B and V bands and the shape parameter x_1 [Guy et al 2010], [Betoule, M. et al 2014].

5.2.3 Modelling of the Supernova event

The SN Ia event translates to a powerful flash whose intrinsic luminosity varies with time. The light curve is characterized by the date t^* at which the luminosity reaches its maximum and by the corresponding absolute magnitude M^*.

The evolution of the absolute magnitude with time is parametrized by a shape parameter x_1, that acts for a dilation/contraction of a pattern curve. The lifetime of SN is shown to be linearly correlated with M^* (Fig.5.8 describes the apparent correlation between the absolute Magnitude and the decline rate Δm_{15}):

$$M^* = -\alpha x_1 + M_0 \tag{5.3}$$

where M_0 stands for the absolute magnitude of the pattern curve at maximum luminosity and $\alpha \geq 0$. The absolute magnitude at date t reads:

$$M(t) = -2.5 \log_{10}(F(t; t^*, M^*, x_1)/F_0) \tag{5.4}$$

where F_0 stands for the flux of the reference star and $F(t; t^*, M^*, x_1)$ the intrinsic flux; it is described by SALT2 model in the reference frame of the supernova.
The evolution of the apparent magnitude with time is given by the following:

$$m(t_{obs}) = M(t) + \zeta(z) \tag{5.5}$$

The absolute and the apparent magnitude at maximum luminosity satisfy:

$$m^* = M^* + \zeta(z) \tag{5.6}$$

The necessary property which is required for a SN to be observable is that its world-line intercepts the observer's past light cone, as described in Figs.2.4 and 5.9.

Herein, the SN event is defined by (M^*, t^*, x_1, V) with a probability density given by:

$$\mathrm{d}P_{th} = g(M^*, x_1)\mathrm{d}M^* \, \mathrm{d}x_1 \, \mathrm{d}t^* \, \mathrm{d}V \tag{5.7}$$

which describes a uniform distribution as much in (comoving) space as in (cosmic) time; where V stands for the comoving volume of a sphere centered at the observer location, and the comoving distance of the source as radius. Subsequently, we will limit ourselves to considering the random variable t^* as a parameter required in the SALT2 procedure, as usual.

5.2.4 Sampling the light curve of type-Ia SN and selection effects

Although the SNe are known to be used as standard candles, they could be affected by large uncertainties due to the limitations in SN observation. Similarly to QSOs, the selection effects must be taken into account in deriving inferences, e.g. the one responsible of the Malmquist bias. However, in this

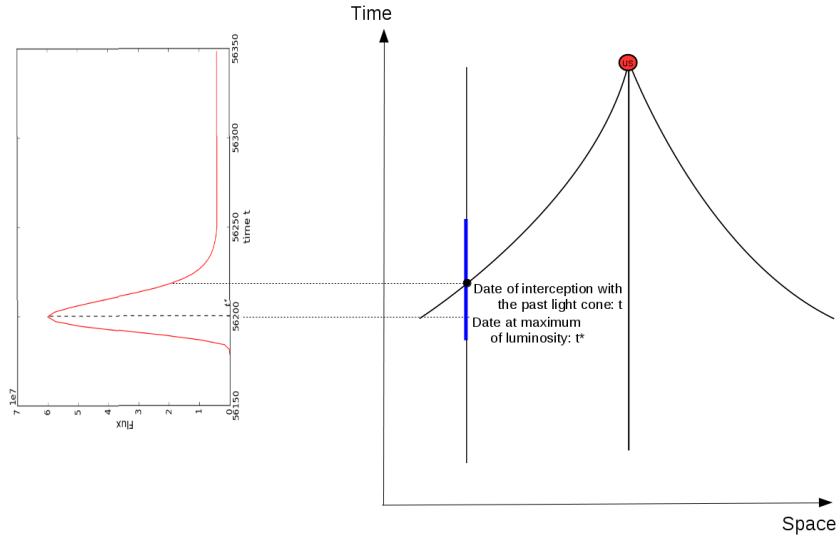

Figure 5.9: Left: a schematic of intrinsic light curve of a SN. Right: the interception of the world-line of the SN with the past light cone.

respect SN differs from QSO, mainly because it is not perenial.
SN candidate are firstly identified among variable light sources by comparing two images of the same field taken at different times. Then, spectroscopic monitoring allows to identify the candidate and determine their redshifts. Finally, if it turns out to be a type-Ia SN (based on the presence of identified absorption lines), a photometric monitoring is performed, that privides us with a light curve. The drawback in searching of type-Ia SNe (or any non-perennial object) is the loss of many objects due to the bad weather conditions or a delay in spectroscopic and photometric observations. In the aim to increase the time and the field of observation, the rolling search method (developed in the framework of the SuperNova Legacy Survey (SNLS) project) is followed to observe this type of events. This method consists of four observation fields during several regular time intervals and in different filters. This technique enables one to discover and monitor several SNe simultaneously in four bands (g', r', i', z'); it is used in SDSS, referring to the Smith catalog (2002) and based on the AB system of magnitude[2]. Using multiple bands can cover a wide wavelength range, which makes possible the observation of SN Ia at high redshifts. An other advantage of using several filters is that the flux in the reference of the SN in the B band can be estimated by an interpolation from the color of the SN measured in two other bands (at least).
Each field is observed during 3-4 days and the successive images are compared by subtracting their pixels [Pritchet 2004]. In the case of a significant

[2]Which can be converted to Johnson-Cousins bands system (B, V, R, I) referring to the Landolt catalog (1992) based on the Vega system of magnitude.

difference between the pixels, a photometric measurement is recorded. This technique allows to obtain a good sampling of the light curve. In ideal cases, a SN with lifetime $\sim$ 80 days (the average for the SNe lifetime) might have $\sim$ 20 photometric measurements, which provides us with an accurate fit of the SN light curve. For instance, Fig.5.10 shows the SN SNLS-04D3gx light curve in the i band sampled with 17 photometric measurements. The sampling of SN curves needs photometric measurements in particular phases p, as described in [Guy et al 2010]. Namely, the SNe are selected according to the following requirements:

- they must show at least:
  1. four measurements at different epochs ranging within -10 $<$ p $<$ +35 days.
  2. one measurement in early epoch ranging within -10 $<$ p $<$ +5 days.
  3. one measurement ranging within +5 $<$ p $<$ +20 days.
  4. two bands, with one measurement or more in the range -8 $<$ p $<$ +10 days to ensure a genuine estimation of luminosity peak and color.

A SN with a light curve poorly sampled is discarded from the sample. According to [Guy et al 2010], this effect is not significant for SNLS sample (SNe with high redshifts), while the SN SDSS-II sample (SNe with low redshifts) is affected significantly [Betoule, M. et al 2014].
Fig.5.11 shows light curves that help to understand the standardization method, see [S. Perlmutter et al. 1999]. They are described by referring to a pattern curve (dashed, the master light curve) with a stretch s_p, a color c_p and an absolute magnitude at maximum luminosity M_p. The SNe with light curves lying above the master curve are characterized by : $s > s_p$ and $c < c_p$. They are brighter (a long lifetime), showing a slow decreases and bluer ($f_B > f_V$)[3]. Conversely, the ones below the master curve are characterized by : $s < s_p$ and $c > c_p$. They are fainter (a short lifetime), showing a fast decreases and less bluer ($f_B < f_V$). We note that the color of SN at maximum of its luminosity is more negative (resp., positive) for the SNe with light curves above (resp., below) the one of the master curve.

The opportunity to detect a supernova requires that the event lies in the past light cone of the observer and that its apparent luminosity is brighter than a given threshold f_{lim}, let m_{lim} be the corresponding limiting apparent magnitude that characterizes a device, see the red line in Fig.5.11. Because the brighter the object the longer the lifetime, as a first approximation, a single

[3] c = B - V = -2.5log$_{10}$($\frac{f_B}{f_V}$)

selection criteria on the magnitude accounts for both. Moreover, the SN light curve requires to show a sufficient time to fulfill the selection criteria based on the phase. Hence, the threshold of selection has to be brighter than m_{lim}.

The light curve must show a significant gap between m_{lim} and m^*, and a small Δm_{15} to have a good sampling in accordance with the detection technique described above. With this in mind, we might idealize a "threshold" light curve in term of m^*_{lim} and $\Delta m_{15,lim}$ which fulfills the aforementioned criteria (see Fig.5.12). It is clear that a selection on m^*, which takes into account the lifetime, also describes a Malmquist bias (see Fig.5.13). Then, the probability density of observed event reads:

$$\propto \phi_B(m^*)\mathrm{d}P_{th} \tag{5.8}$$

where $\phi_B(m^*)$ stands for a selection function on the peak of apparent magnitude in the B band. Although such a representation of the selection effects is the most commonly accepted, it is clear that an improvement taking into account the lifetime of the events is necessary. However, because the longer the lifetime the brighter the supernova, the correction to this representation can be expected to be small. A work is in progress to enable us to ensure this quantitatively.
The color stands for a correction to decrease the scatter of the distribution of the absolute magnitude at maximum luminosity M^*. The corrected absolute magnitude M^*_c satisfies the relation:

$$M^* = M^*_c - \beta c; \quad \beta \geq 0 \tag{5.9}$$

which makes brighter the object the bluer. Hence, according to Eq.5.8, the probability density of observed SN transforms:

$$\propto \phi_B(m^*)\, g_G(c; 0, \sigma_c)\mathrm{d}c\, \mathrm{d}P_{th} \tag{5.10}$$

5.2.5 Calibration statistics

The calibration of the Brighter-Slower (BS) relation assumed as a linear correlation between M^* and x_1 as described by the probability density that reads:

$$\propto g(M^*, x_1)\mathrm{d}M^*\, \mathrm{d}x_1 \tag{5.11}$$

We assume that the error in estimating M^* from x_1, as given by:

$$M^* = ax_1 + b + \epsilon \tag{5.12}$$

is a a random variable with a Gaussian distribution function $g_G(\epsilon; 0, \sigma_\epsilon)$, see Fig.5.14. The estimation of parameters a and b (calibration), can be performed either :

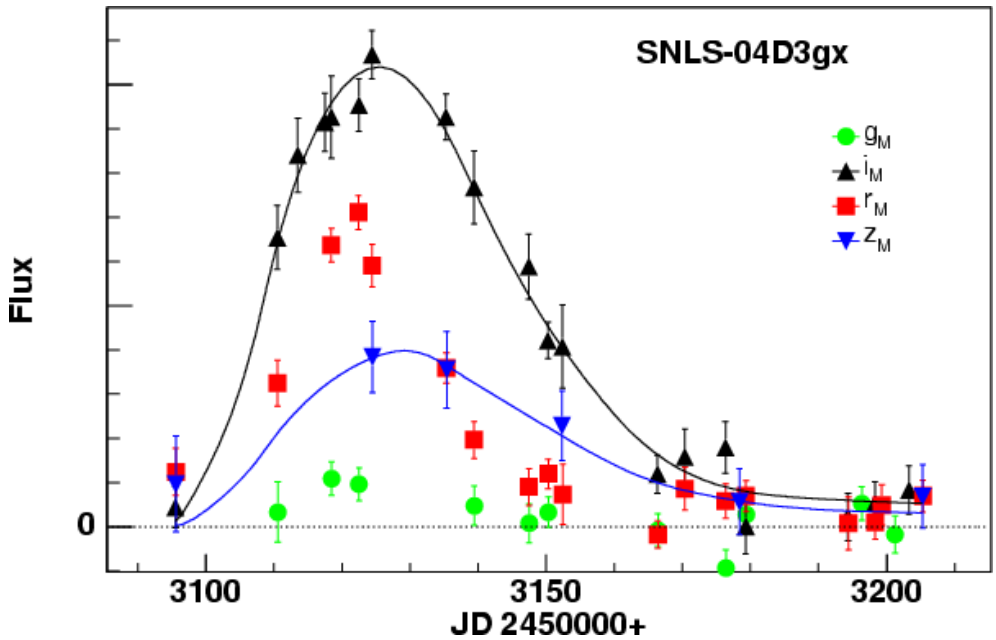

Figure 5.10: Light curve of SN SNLS-04D3gx. This figure shows a light curve well sampled by observations which help to characterize its parameters (x_0, t^*_{obs}, x_1, c) without biases. Figure courtesy: [Astier P. et al, 2006]

- with the direct brighter-slower relation (DBS):

$$g(M^*, x_1)\mathrm{d}M^*\,\mathrm{d}x_1 \approx g_{M^*}(x_1)\mathrm{d}x_1\, g_G(\epsilon; 0, \sigma_\epsilon^{DBS})\mathrm{d}\epsilon \tag{5.13}$$

  where :

$$M^* = a^{DBS}x_1 + b^{DBS} + \epsilon \tag{5.14}$$

- or with the indirect brighter-slower relation (IBS):

$$g(M^*, x_1)\mathrm{d}M^*\,\mathrm{d}x_1 \approx g_{x_1}(M^*)\mathrm{d}M^*\, g_G(\epsilon; 0, \sigma_\epsilon^{IBS})\mathrm{d}\epsilon \tag{5.15}$$

  where :

$$x_1 = a^{IBS}M^* + b^{IBS} + \epsilon \tag{5.16}$$

The estimates of corresponding parameters are denoted a^{DBS}, b^{DBS}, σ_ϵ^{DBS}, a^{IBS}, b^{IBS} and σ_ϵ^{IBS}.
As usual, we proceed with the maximum likelihood (ML) technique as described in [Triay et al 1994]. With a nearby objects used for calibration, we can safely assume a uniform diestribution in an euclidian space. Hence, the probability density that describes the calibration sample reads:

$$\propto \phi_B(m^*)g(M^*, x_1)\mathrm{d}M^*\,\mathrm{d}x_1\, g_G(c; 0, \sigma_c)\mathrm{d}c\,\mathrm{d}t^*\,\mathrm{e}^{\gamma\zeta}\mathrm{d}\zeta \tag{5.17}$$

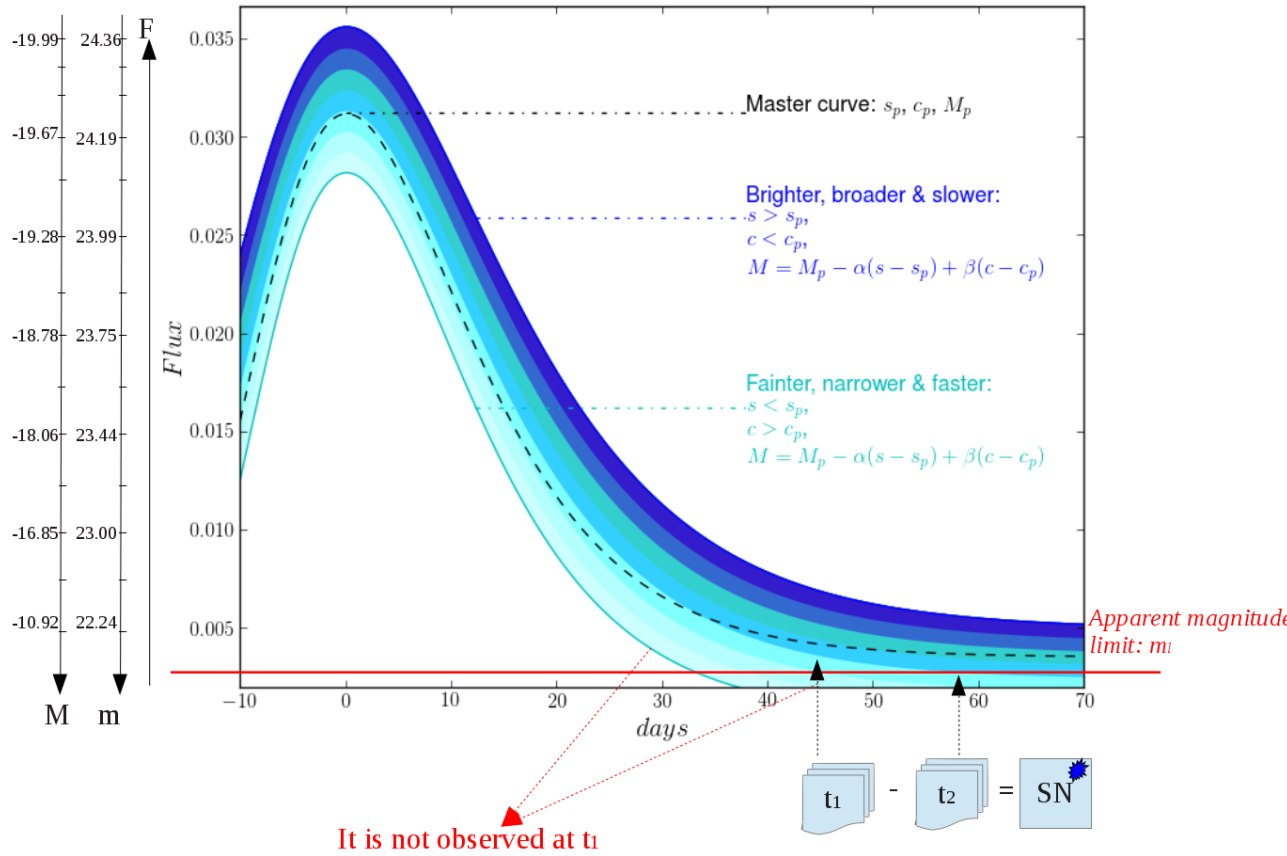

Figure 5.11: A representative figure of the SN Ia light curves in the aim to explain the selection effects. The dashed curve represents the master curve where the entire light curves must coincide. The highest blue curve represents the light curve of the SN Ia brighter, broader, slower and bluer than the master curve. The cyan curve (the lowest) represents the light curve of the SN Ia fainter, narrower, faster and less bluer than the master curve. The t_1 and t_2 are two observation dates for which a candidate of SN is detected by subtracting the images taken at these dates.

where $\gamma = \frac{3ln(10)}{5}$. Depending on the method used, as given by Eqs.5.13 and 5.15, the sample can be described by the corresponding probability densities:

$$\mathrm{d}P_{obs} = \frac{1}{P_{th}(\phi_B)}\phi_B(m^*)g_{M^*}(x_1)dx_1 g_G(c;0,\sigma_c)dcdt^* \mathrm{e}^{\gamma\zeta}d\zeta \times g_G(\epsilon;0,\sigma_\epsilon)d\epsilon \tag{5.18}$$

$$dP_{obs} = \frac{1}{P_{th}(\phi_B)}\phi_B(m^*)g_{x_1}(M^*)\mathrm{d}M^*\, g_G(c;0,\sigma_c)\mathrm{d}c\,\mathrm{d}t^*\,\mathrm{e}^{\gamma\zeta}\mathrm{d}\zeta \times g_G(\epsilon;0,\sigma_\epsilon)\mathrm{d}\epsilon \tag{5.19}$$

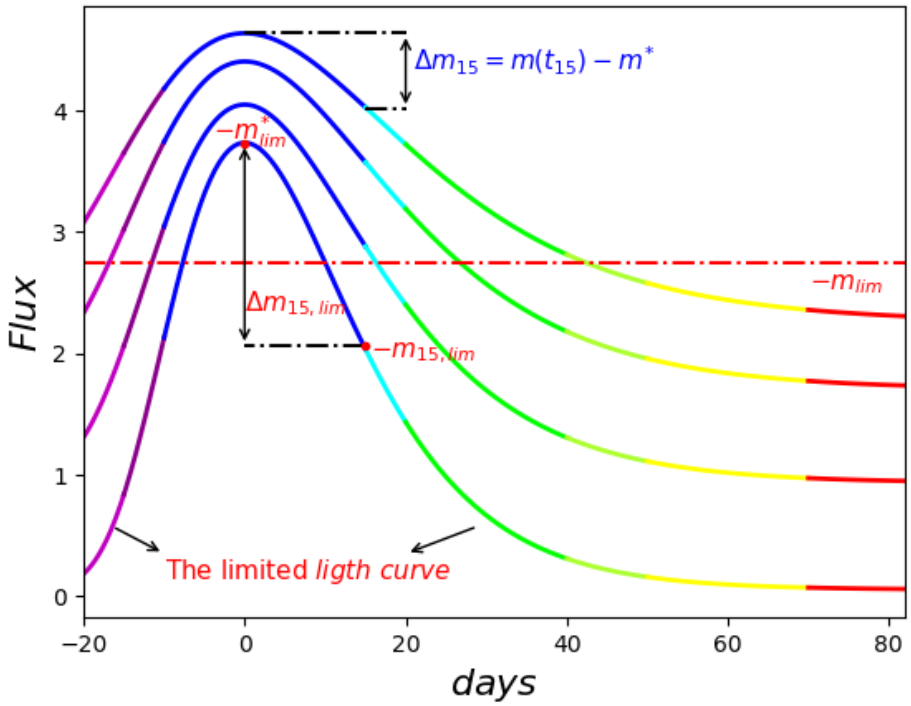

Figure 5.12: The selection of SNe depends on two characteristics: the maximum of luminosity m^* and the decline rate Δm_{15}. The lowest light curve is the threshold light curve characterized by m^*_{lim} and $\Delta m_{15,lim}$ which are used as the selection criteria. A SN with a decline rate $\Delta m_{15} < \Delta m_{15,lim}$ is observed as long as its apparent magnitude at maximum luminosity $m^* < m^*_{lim}$.

where the normalization factor reads :

$$P_{th}(\phi_B) = \int \phi_B(ax_1 + b + \zeta) g_{M^*}(x_1) \mathrm{d}x_1 \mathrm{e}^{\gamma\zeta} \mathrm{d}\zeta \times \mathrm{d}t^* g_G(c; 0, \sigma_c) \mathrm{d}c g_G(\epsilon; 0, \sigma_\epsilon) \mathrm{d}\epsilon \tag{5.20}$$

$$P_{th}(\phi_B) \propto \int \phi_B(ax_1 + b + \zeta) g_{M^*}(x_1) \mathrm{d}x_1 \mathrm{e}^{\gamma\zeta} \mathrm{d}\zeta \tag{5.21}$$

The statistics of parameters a, b and σ_ϵ are determined by following the order of their rating as follows:

- for the DBS relation :

$$a^{DBS} = \frac{Cov(x_1, M^*)}{\sigma^2_{x_1}} \tag{5.22}$$

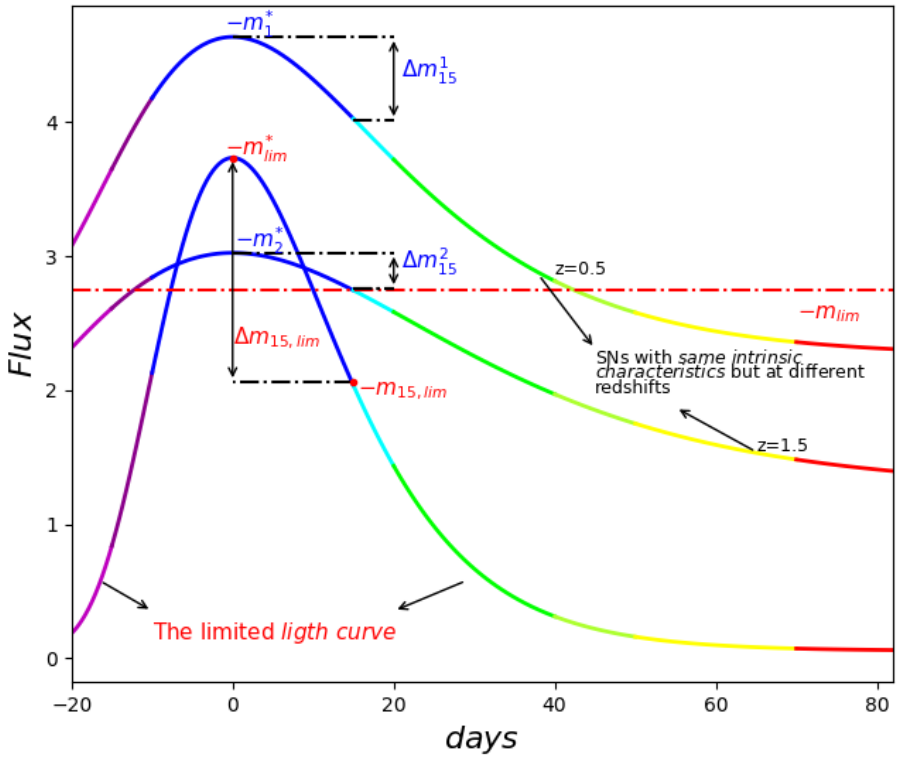

Figure 5.13: Two SNe with the same intrinsic characteristics at different redshifts. Although the light curve of the SN of the highest redshift ($z = 1.5$) has a small decline rate $\Delta m_{15}^2 < \Delta m_{15,lim}$ due to the dilation of time, this SN will not be considered in the sample because it has not a sufficient time to have a good sampling of its light curve. The selection of SN is done only if $m^* < m_{lim}^*$.

$$\sigma_\epsilon^{DBS} = \sigma_{M^*}\sqrt{1-\rho^2(x_1, M^*)} \tag{5.23}$$

where $\rho(x_1, M^*)$ is the correlation coefficient.

$$b^{DBS} = \langle M^* \rangle - a^{DBS}\langle x_1 \rangle + \gamma\sigma_\epsilon^{DBS^2} \tag{5.24}$$

- for the IBS relation:

$$a^{IBS} = \frac{\sigma_{x_1}^2}{Cov(x_1, M^*)} \tag{5.25}$$

$$b^{IBS} = \langle M^* \rangle - a^{IBS}\langle x_1 \rangle \tag{5.26}$$

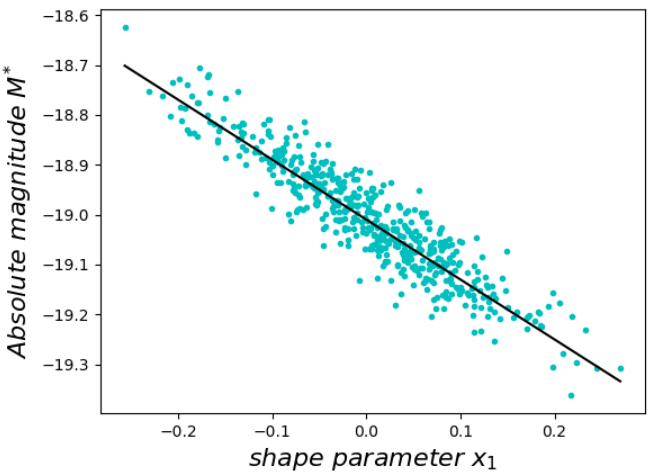

Figure 5.14: The brighter-slower relation (absolute magnitude versus shape parameter)

$$\sigma_\epsilon^{IBS} = \sigma_{M^*}\sqrt{\frac{1}{\rho^2(x_1, M^*)} - 1} \tag{5.27}$$

It is worth to mention that the existence of the factor $\gamma\sigma_\epsilon^{DBS^2}$ in the estimation of b^{DBS} parameter stands for a bias correction. In the following, we use the IBS calibration method, because it is more robust (with respect to selection effects) than the DBS one [Triay et al 1994].

Because the calibration schema turns out to be identical to the correlation (M_c^*, c), one obtains similar equations, but this step requires the DBS method to estimate the absolute magnitude.

5.2.6 Simulation

We proceed similarly as for the simulations of quasars samples, see Sect.2.5.2, but by including the color correction with the probability density given in Eq.5.10 and the IBS relation, given in Eq.5.16. Then, one has the following probability density:

$$\propto \phi_B(m^*) g_{x_1}(M^*)\mathrm{d}M^*\, g_G(c; 0, \sigma_c)\mathrm{d}c\, g_G(\epsilon; 0, \sigma_\epsilon)\mathrm{d}\epsilon\, \mathrm{d}t^*\, \mathrm{d}V \tag{5.28}$$

where t^* is required in the SALT2 routine. Here, we assume that ϕ_B reads as a Heaviside function $\theta(m^*_{lim} - m^*)$ characterizing complete samples up to a limiting apparent magnitude m^*_{lim}.

The apparent magnitude in rest-frame B band obtained with standardization of SNe (free from the k-correction) is given by:

$$m_c^* = M_c^* + \zeta(z) \tag{5.29}$$

where

$$M_c^* = \begin{cases} ax_1 + b + \beta c & \text{if } M^a_{stellar} < 10^{10} M_\odot \\ ax_1 + b + \beta c + \delta & \text{otherwise} \end{cases} \tag{5.30}$$

δ stands for a correction that depends on the host stellar mass $M^a_{stellar}$ [Sullivan, M. et al 2010], [Conley et al 2011]. Its value has been evaluated in [Betoule, M. et al 2014] $\delta = -0.070 \pm 0.023$ by using the joint light-curve analysis sample of 740 SNe. It is used in this investigation.
To simulate a sample free from (foreground) alterations, we used M_c^* instead of M^*, then Eq.5.28 reads:

$$\propto \phi_B(m^*)\, f(M_c^*) \mathrm{d}M_c^*\, g_G(c; 0, \sigma_c) \mathrm{d}c\, \mathrm{d}V \tag{5.31}$$

where $f(M_c^*)$ is the distribution function of M_c^*. Let us define the cumulative distribution function of the random variable M_c^* as follows

$$\hat{G} \equiv G(x) = \frac{1}{P_{th}(\phi_B)} \int_{-\infty}^{x} f(M_c^*)\, Q(M_c^*)\, \mathrm{d}M_c^* \tag{5.32}$$

where

$$P_{th}(\phi_B) = \int \phi_B(m^*)\, f(M_c^*) \mathrm{d}M_c^*\, g_G(c; 0, \sigma_c) \mathrm{d}c\, \mathrm{d}V \tag{5.33}$$

and

$$Q(M_c^*) = \int \theta(m^*_{lim} - M_c^* + \beta c - \zeta(z)) g_G(c; 0, \sigma_c) \mathrm{d}c\, \mathrm{d}V \tag{5.34}$$

For a given value of M_c^*, the probability density of random variables c and V is defined as follows

$$dP^{(1)} = \frac{1}{P^{(1)}_{th}(\phi_B)} \theta(m^*_{lim} - M_c^* + \beta c - \zeta(z)) g_G(c; 0, \sigma_c) \mathrm{d}c\, \mathrm{d}V \tag{5.35}$$

where

$$P^{(1)}_{th}(\phi_B) = \int \theta(m^*_{lim} - M_c^* + \beta c - \zeta(z)) g_G(c; 0, \sigma_c) \mathrm{d}c\, \mathrm{d}V \tag{5.36}$$

The cdf of the random variable c reads

$$\hat{C} \equiv C(x) = \frac{1}{P^{(1)}_{th}(\phi_B)} \int_{-\infty}^{x} \theta(m^*_{lim} - M_c^* + \beta c - \zeta(z)) g_G(c; 0, \sigma_c) \mathrm{d}c\, \mathrm{d}V \tag{5.37}$$

The simulation scheme consists in the following trials

$$M_c^* \longrightarrow c \longrightarrow V \tag{5.38}$$

Let us remind that $\hat{G} \in [0,1]$ and $\hat{C} \in [0,1]$ are uniform random variables. Each generated random values for $\hat{G}$ and $\hat{C}$, provide $M_c^* = G^{-1}(\hat{G})$ and $c = C^{-1}(\hat{C})$ from the inverse functions, see Eq.5.32, 5.37. Then, with $M^* = M_c^* - \beta c$, one simulates a value of the uniform random variable $\hat{V} \in$[0, $\mathrm{V}_{max}(M^*)$], see Eq.2.8. The redshift is given by $z = V^{-1}(\hat{V})$ and the apparent magnitude at maximum of luminosity m_c^* by Eq.5.29. The shape parameter x_1 is determined either with Eq.5.16 for the calibration parameters a^{IBS} and b^{IBS} or with Eq.5.14 for a^{DBS} and b^{DBS}, and a value ϵ generated by a white noise, in accordance with working hypotheses. Let us analyze two samples of 240 objects which are simulated with the following characteristics and according the models of white noise as described in the calibration processes:

$$(\mathrm{A}):\begin{cases} \Omega_\circ = 0.3, \lambda_\circ = 0.7 \\ \sigma_{M_c^*} = 0.3, \sigma_c = 0.085 \\ \beta = 3.14, \sigma_\epsilon = 0.09 \\ a^{DBS} = -0.14, b^{DBS} = -19 \\ M_{c,0}^* = -19, m_{lim}^* = 25.04 \end{cases} \quad (\mathrm{B}):\begin{cases} \Omega_\circ = 0.3, \lambda_\circ = 0.7 \\ \sigma_{M_c^*} = 0.3, \sigma_c = 0.085 \\ \beta = 3.14, \sigma_\epsilon = 0.6 \\ a^{IBS} = -5, b^{IBS} = -95 \\ M_{c,0}^* = -19, m_{lim}^* = 25.04 \end{cases}$$

(5.39)

As expected, the FS diagrams in Fig.5.15 show that the distributions are upper bounded by the curve $V_{max}(M^*)$, characterizing the limiting apparent magnitude m_{lim}^*, uniformly distributed with respect to V, and Gaussian with respect to M_c^*. It can be noted that brighter objects have a more blue color. The Hubble diagrams as shown in Fig.5.16 provide us with a data distribution about the expected relation for a standard candel with $M_c^* = -19$ ($color = 0$). The selection effect at the limiting apparent magnitude, $m_{lim}^* = 25.04$, makes clearly the bound of the distribution. Because of such a feature, a least square fitting method requires horizontal estimates of distances to the expected curve. The characteristics of two samples (A) and (B) are described in four dimensional diagrams in Figs.5.17, 5.18. The likelihood of working hypotheses on the color and the shape parameter can be easily checked on these diagrams. That are the correlation between M_c^* and c (middle left panel), also between M^* and x_1 (top right panel).

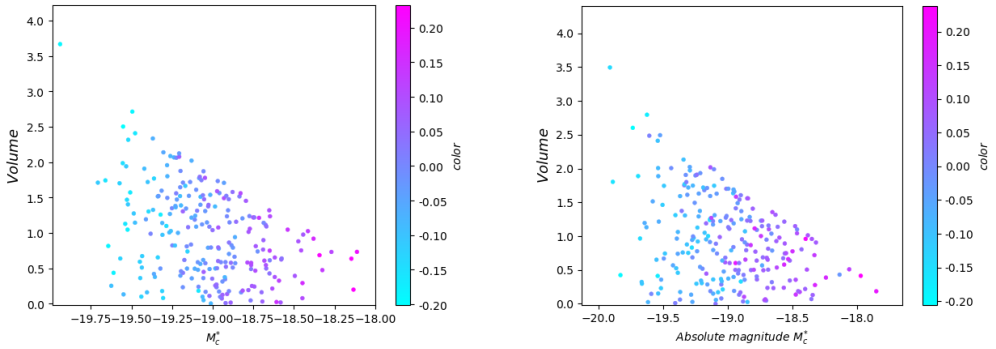

Figure 5.15: Absolute magnitude-volume diagram of simulated samples (A) (left) and (B) (right).

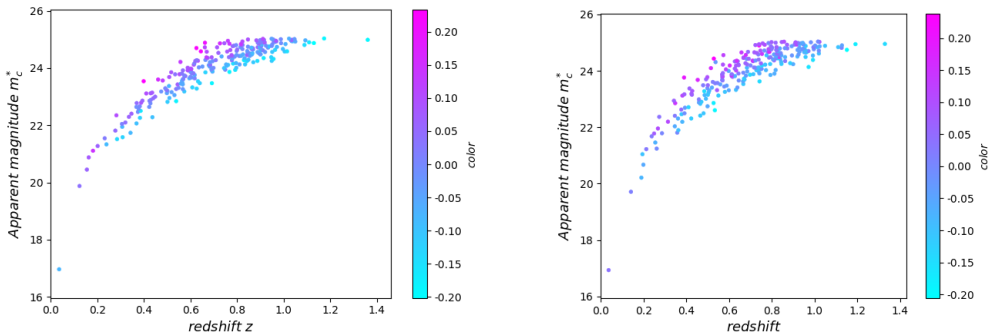

Figure 5.16: Hubble diagram of simulated samples (A) (left) and (B) (right).

5.3 The null correlation test on the supernova sample

Hereafter, we adapt the null correlation approach to SN samples for determining the cosmological parameters. The SN event is described in the (M_c^*, m_c^*) frame by the following probability density:

$$\propto \rho\, \phi_B(m^*)\, g_G(c; 0, \sigma_c) \mathrm{d}c\, f(M_c^*) \mathrm{d}M_c^*\, \mathrm{d}m_c^* \tag{5.40}$$

where $\rho = \rho(z) = \frac{\partial V}{\partial m_c^*}$ stands as a correlation function which depends on the cosmological parameters, see Eqs.3.13, 3.15 and 3.17. The weighting factor is defined by Eq.3.21, but where the distance modulus is given by:

$$\zeta_{est} = m_c^* - M_c^* \tag{5.41}$$

where the absolute magnitude M_c^* being estimated by x_1 and c. This is the major difference with the null correlation procedure above used with quasars.

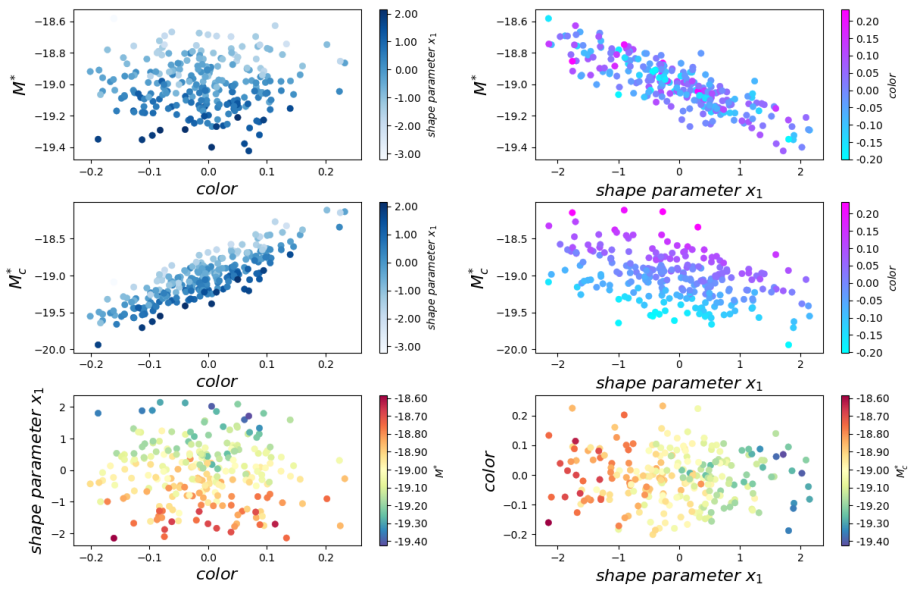

Figure 5.17: Four dimensional diagrams of characteristics of sample (A).

Hence, the weighting factor reads:

$$w_\mu(z) = \frac{1}{\frac{\partial V}{\partial m_c^*}} 10^{\frac{\mu}{5}\zeta_{est}} \tag{5.42}$$

where μ is determined by minimizing the quantity :

$$\Delta_w = \frac{max\{w_\mu(z)\} - min\{w_\mu(z)\}}{max\{w_\mu(z)\} + min\{w_\mu(z)\}} \tag{5.43}$$

It must be noted that the weighted correlation coefficient reads:

$$\Gamma(\Omega_\circ, \lambda_\circ) = \sum_{k=1}^{N} \frac{\omega_k (M_{c,k}^* - \langle M_c^* \rangle)(m_{c,k}^* - \langle m_c^* \rangle)}{\Sigma_{M_c^*} \Sigma_{m_c^*}} \tag{5.44}$$

where M_c^* is given by Eq.5.30 The statisctics of standard deviations $\sigma_{M_c^*}$ and $\sigma_{m_c^*}$ are defined by:

$$\Sigma_{M_c^*}^2 = \frac{N}{N-1} \sum_{k=1}^{N} \omega_k (M_{c,k}^* - \langle M_c^* \rangle)^2 \tag{5.45}$$

$$\Sigma_{m_c^*}^2 = \frac{N}{N-1} \sum_{k=1}^{N} \omega_k (m_{c,k}^* - \langle m_c^* \rangle)^2 \tag{5.46}$$

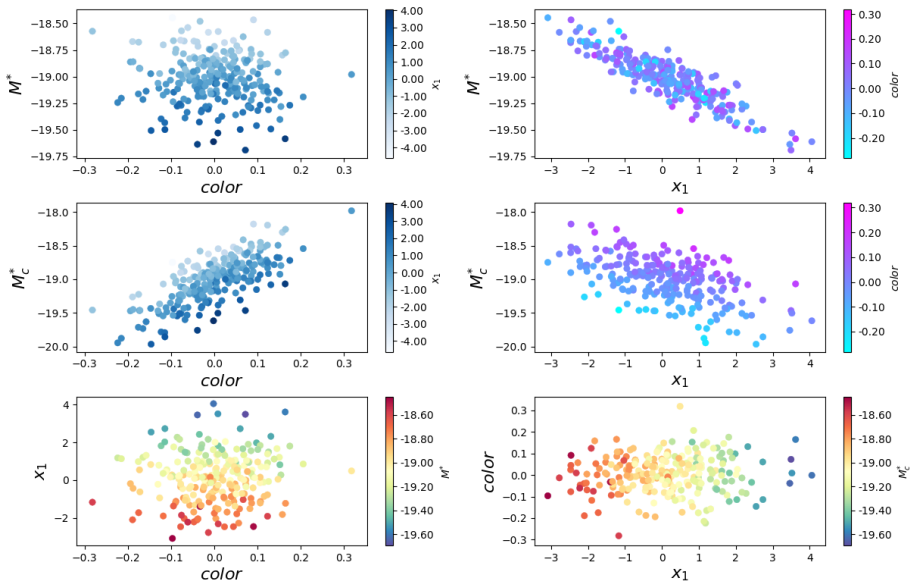

Figure 5.18: Four dimensional diagrams of characteristics of sample (B).

Fig.5.19 shows the NCCs of the two simulated samples described above. As expected, the values of the cosmological parameters used to generate the samples are roots of the statistic $\Gamma(\Omega_\circ, \lambda_\circ) = 0$. It will be seen that the differences in shape (e.g., the curvature) of the NCCs corresponding to these samples, obtained according to different calibrations, are of a random nature and do not reflect the calibration type.

To analyse the dependence of the shape of the NCC on the cosmological model and the sample characteristics, thirty samples are simulated similar to (B) but with different limiting apparent magnitude ($m^*_{lim} = 25.04$, $m^*_{lim} = 23$) and different sample sizes N. To illustrate the results, we have chosen two representative samples allowing us to describe them clearly, see Fig.5.20. The shape depends strongly on the sample characteristics (left panel). It is a matter of fact that the NCC retrieve the cosmological parameters used to simulate the samples, which shows the robustness of this approach. The degeneracy of the Hubble law is analyzed with two simulated samples having the same characteristics of (B) as follows: the first one is defined by ($\Omega_\circ = 0.3$, $\lambda_\circ = 0.7$) and the second one is chosen on the NCC of the first sample, ($\Omega_\circ = 0.4$, $\lambda_\circ = 1.03$). The corresponding NCCs deviate quite slightly from each other (right panel) which shows the need to use an additional statistic to disentangle the true model. The accuracy on the determination of the cosmological pa-

rameters which form the NCC can be estimated from statistical fluctuations specific to ten randomly generated samples with the same characteristics of (B), see Fig.5.21. We can have a hint of this precision from a square that covers the edges of this distribution of curves, and we obtain $\Delta\Omega_\circ \approx 0.02$ and $\Delta\lambda_\circ \approx 0.125$, that correspond roughly to 3σ error.

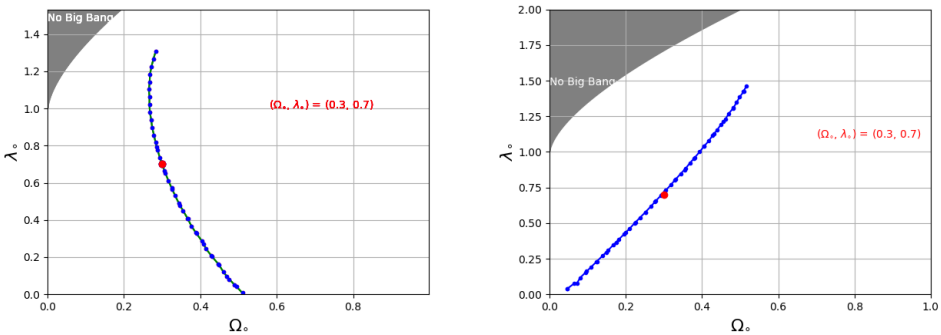

Figure 5.19: The NCC corresponding to (A) sample (left) and the one corresponding to (B) sample (right).

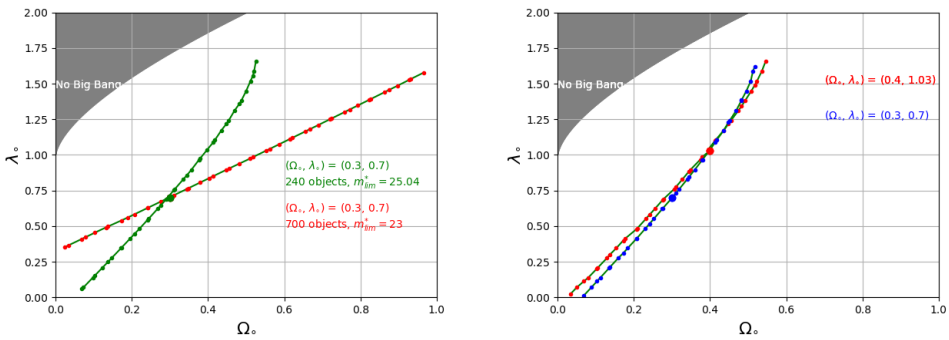

Figure 5.20: Shape of the NCC with respect to the characteristics of sample and cosmological model.

The sample is described, after the determination of the color, as follows:

$$\mathrm{d}P \propto \theta(m^*_{lim} - m^*) f(M^*_c)\mathrm{d}M^*_c\,\mathrm{d}V \tag{5.47}$$

Hence, we applied the V/V_{max} test, see Sec.3.5.1. The model used for the simulation shows 97% significance level as it is shown in Fig.5.22.

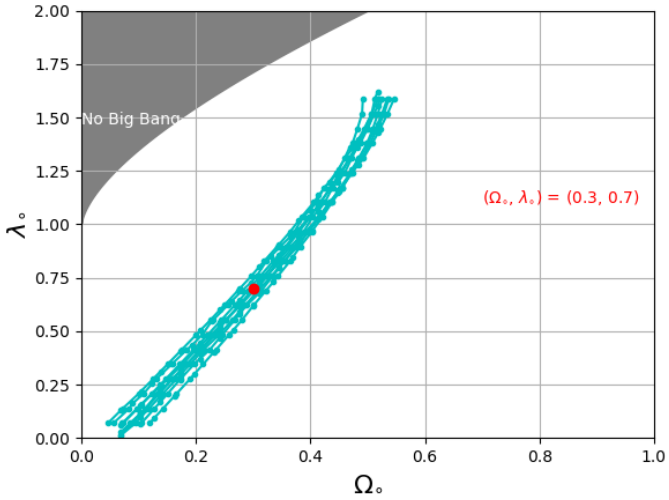

Figure 5.21: NCC of ten randomly generated samples with the same characteristics in the standard cosmological model.

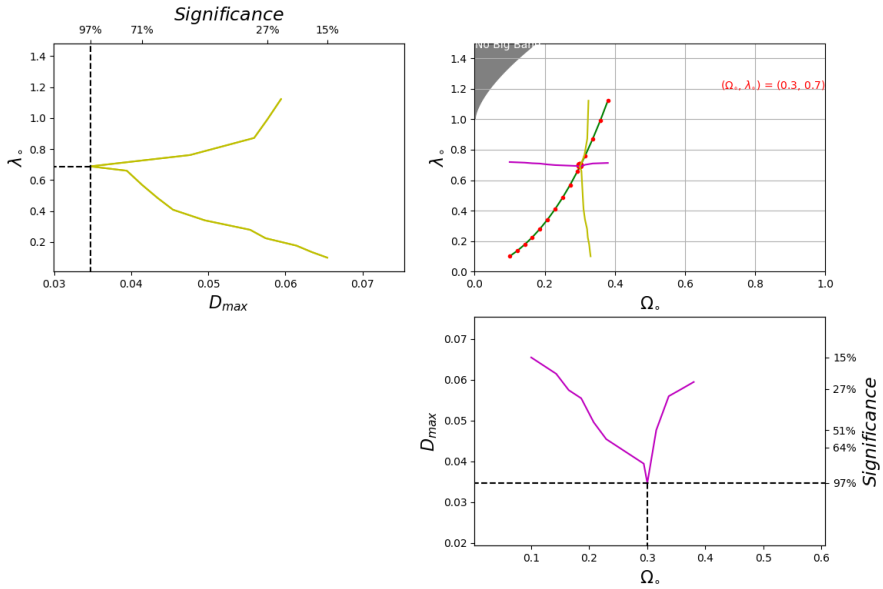

Figure 5.22: Search for the minimum of KS test, D_{max}, (top left) as a function of $\lambda_\circ$, and (bottom right) as a function of $\Omega_\circ$, on the NCC (top right).

5.3.1 Luminosity function and Selection function

One of the advantages of the null correlation approach is to estimate the luminosity function and the selection function. Since the color is determined by means of SALT2 routine, the sample can be described by the weighted probability density that reads:

$$\mathrm{d}P_\omega \propto f_\omega(M_c^*)\mathrm{d}M_c^*\,\phi_{B,\omega}(m^*)\mathrm{d}m_c^* \tag{5.48}$$

Let us emphasize that $\phi_B(m*)$ stands as a correlation function of c and m_c^*, since $m^* = m_c^* - \beta c$. The probability density functions reads as a product of two independent functions, the color correction being performed

$$f_\omega(M_c^*) \propto f(M_c^*)10^{-\frac{\mu}{5}M_c^*}, \qquad \phi_{B,\omega}(m_c^* - \beta c) \propto \phi_B(m_c^* - \beta c)10^{\frac{\mu}{5}m_c^*} \tag{5.49}$$

For large N, their cumulative distributions functions can be approximated by the step-functions:

$$F_\omega(M_c^*) \approx \hat{F}_\omega(M_c^*) = \sum_{k=1}^{N} \omega_k \theta(M_c^* - M_{c,k}^*) \tag{5.50}$$

$$\Phi_{B,\omega}(m_c^* - \beta c) \approx \hat{\Phi}_{B,\omega}(m_c^* - \beta c) = \sum_{k=1}^{N} \omega_k \theta(m_c^* - \beta c - (m_{c,k}^* - \beta c_k)) \tag{5.51}$$

where θ is the Heaviside step function. Therefore, the derivatives of $\hat{F}_\omega(M_c^*)$ and $\hat{\Phi}_{B,\omega}(m_c^* - \beta c)$ allow to estimate the luminosity function and the selection function

$$f(M_c^*) \propto \frac{\Delta\hat{F}_\omega(M_c^*)}{\Delta M_c^*}10^{\frac{\mu}{5}M_c^*}, \qquad \phi_B(m_c^* - \beta c) \propto \frac{\Delta\hat{\Phi}_{B,\omega}(m_c^* - \beta c)}{\Delta m_c^*}10^{-\frac{\mu}{5}m_c^*} \tag{5.52}$$

Figs.5.23, 5.24 show the estimation of the functions $f(M_c^*)$ and $\phi_B(m_c^* - \beta c)$ with simulated sample in which $f(M_c^*)$ is a Gaussian function with an average $M_{c,0}^* = -19$ and a standard deviation $\sigma_{M_c^*} = 0.25$. These statistics have been validated by tens simulated samples, the figures show that the assumed profiles of functions are retrieved, they have not been smoothed from statistical fluctuations and those due to the numerical derivate method, human eyes being more efficient estimators than automatic methods.

5.3.2 Precision and error

In order to estimate the error budget around the best model of the cosmological parameters, we performed a simulation of 500 samples using the caracteristics

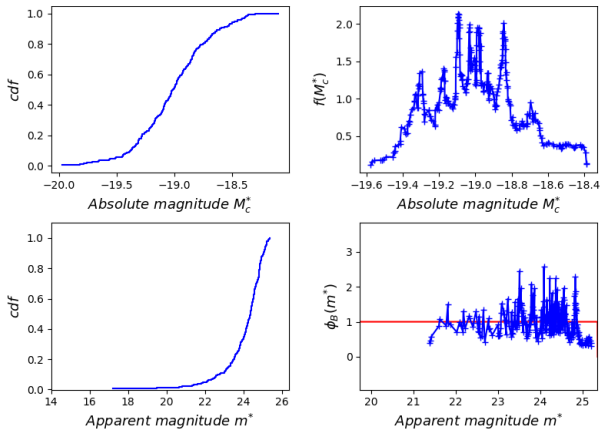

Figure 5.23: Statistics of the luminosity function (upper panels) and the selection function (lower panels)

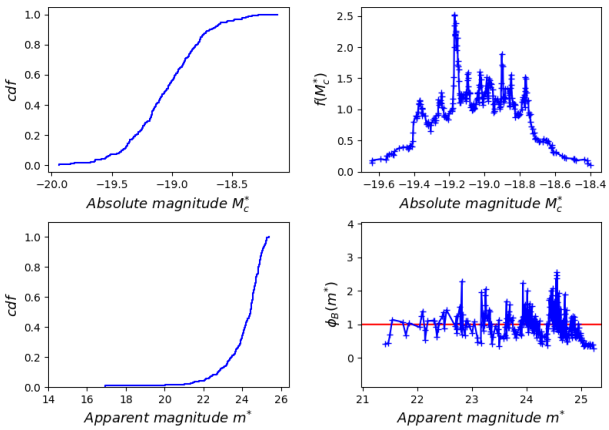

Figure 5.24: Similar to Fig.5.23

listed in the (B) case of Eq.5.39. Each sample consists of 500 SN events. Firstly, we applied the null correlation test to the 500 samples and we determined their NCCs, see Fig.5.25. In this figure, we can see the effect of the statistical fluctuations for the determination of the true cosmological model. Then, we performed the V/V_{max} test which provided us a set of models considered as best estimates at a given significance level (between 86% and 97%). Therefore, we split the area of models in squares (10 x 10) and we determined the density of points in each square. This allowed us to determine the probability density function on the $\Omega_\circ$ and $\lambda_\circ$ axes, see Fig.5.26. As a result, we obtained: $\Omega_\circ = 0.3 \pm 0.03$, $\lambda_\circ = 0.7 \pm 0.01$ at 68% confidence level.

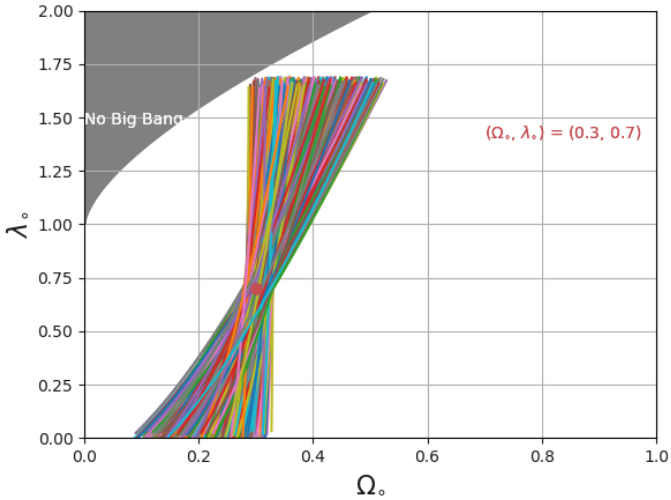

Figure 5.25: The NCCs of the 500 simulated samples.

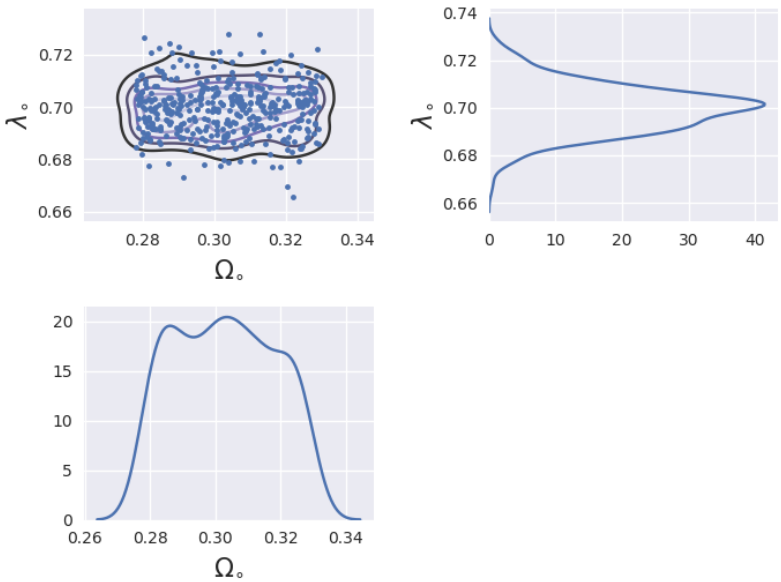

Figure 5.26: Set of the best candidates of the cosmological model with the likelihood contours (top left). The probability density functions with respect to $\lambda_\circ$ (top right) and with respect to $\Omega_\circ$ (left bottom).

5.4 Application to the JLA sample

It is generally acknowledged that the type-Ia SN stands for a good standard candle to constrain the cosmological parameters. Nevertheless, the nowadays catalogs suffer from their small size. The joint light-curve analysis (JLA)[4] sample, published in [Betoule, M. et al 2014], consists of 740 type-Ia SNe confirmed spectroscopically. It includes two main samples: the SDSS-II (374 SNe) and SNLS3 (239 SNe) samples on which the present analysis is performed, see table 5.1.

5.4.1 Description of samples

The FS diagram of JLA sample is described in Fig.5.27. Let us remind that, according to the working hypotheses, the V-distribution should be uniform and limited by a curve related to a limiting apparent magnitude. It is clear that this distribution does not meet this expectation. Indeed, the three points at $V \geq 3$ are significantly detached from the rest of the distribution. They belong to the HST sample, which shows inhomogeneities in selecting objects, see Fig5.28. Hence it must be excluded, in accordance with the requirement of the null correlation approach. The red distribution in the FS diagram of JLA represents the SDSS-II sample (objects with redshift less than 0.4). This concentration is due to the difference between the observation conditions with other surveys, mainly the SNLS3 sample (the blue points), SDSS-II has a limiting apparent magnitude smaller than the one used for SNLS3. For this reason, we decided to use the subsamples of JLA separately. The FS diagram of low-z sample is represented in Fig.5.29 where the threshold on apparent magnitude appears obviously. The FS diagram of SDSS-II supernova sample is shown in Fig.5.30 , such a structure is detected in this diagram within the volume interval $[0, 0.04]$ for $M_c^* < -19$. In this region, there is a concentration of objects. Upper to this cloud of points, we find a rectangular white space. This shows that the SDSS-II sample is not uniformly distributed in volume axis and then it is not consistent with the working hypotheses.
Fig.5.31 represents the FS diagram of SNLS3 sample which contains objects up to high redshift ($z = 1.06$). This sample shows a uniform distribution and does not suffer from significant selection effects, apart from the limitation in apparent magnitude. Consequently, this sample is more suitable to be used in our approach.

5.4.2 Results

The calibration of data is performed with respect to the steps detailed in Sect.5.2.5. Since the calibration method suggests to use a cosmological model

[4] http://supernovae.in2p3.fr/sdss_snls_jla/ReadMe.html

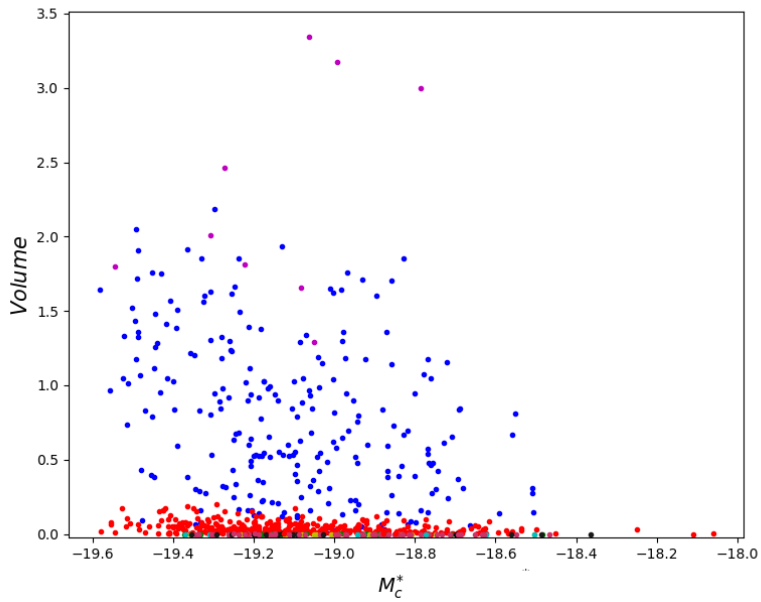

Figure 5.27: The FS diagram of JLA sample build with the model: $\Omega_\circ = 0.3$, $\lambda_\circ = 0.7$. The red dots represent the SDSS-II data, and the blue ones represent those of SNLS3. The rest is represented with multicolor.

with zero scalar curvature (we used $\Omega_\circ = 0.3$, $\lambda_\circ = 0.7$), it will be more reasonable to use a sample at low redshift where the effect of cosmological parameters can be ignored. For this, we carried out the calibration for the low-z sample which contains objects up to z = 0.08. We obtained: $a = -0.138$, $b = -19.043$ and $\beta = 2.641$. The correlation between the variables for SNLS3 sample is shown in Fig5.32.

Once the absolute magnitude is estimated by using Eq.5.30, the null correlation test is applied on both SNLS3 and SDSS-II samples. The NCC was not found for the latter. In accordance with the above analysis on the FS diagram (Fig.5.30), this sample turns out indeed not compatible with the working hy-

Name	N	Δz	ΔB-mag
JLA	740	$[0.01, 1.29]$	$[14.14, 26.04]$
SNLS3	239	$[0.12, 1.06]$	$[19.75, 25.03]$
SDSS-II	374	$[0.036, 0.4]$	$[17.32, 22.42]$
low-z	118	$[0.01, 0.08]$	$[14.14, 18.47]$
HST	9	$[0.84, 1.29]$	$[24.36, 26.04]$

Table 5.1: SNe Ia samples.

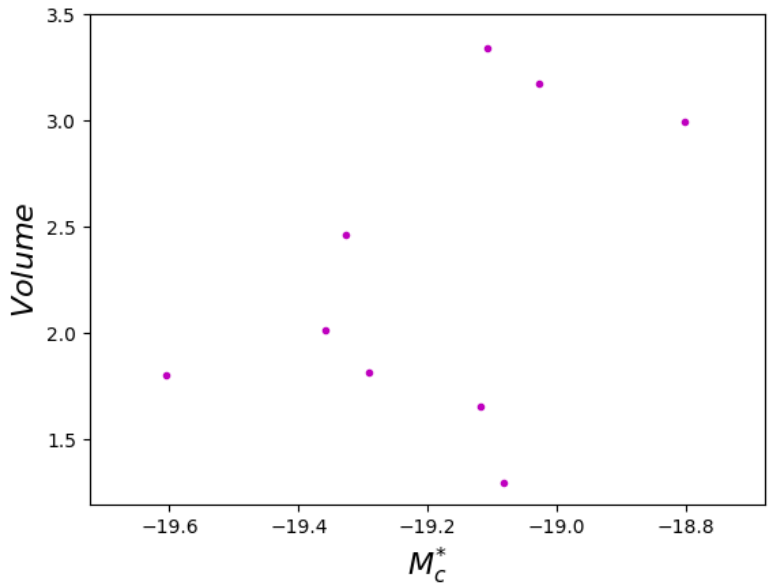

Figure 5.28: The FS diagram of HST sample build with the model ($\Omega_\circ = 0.3$, $\lambda_\circ = 0.7$).

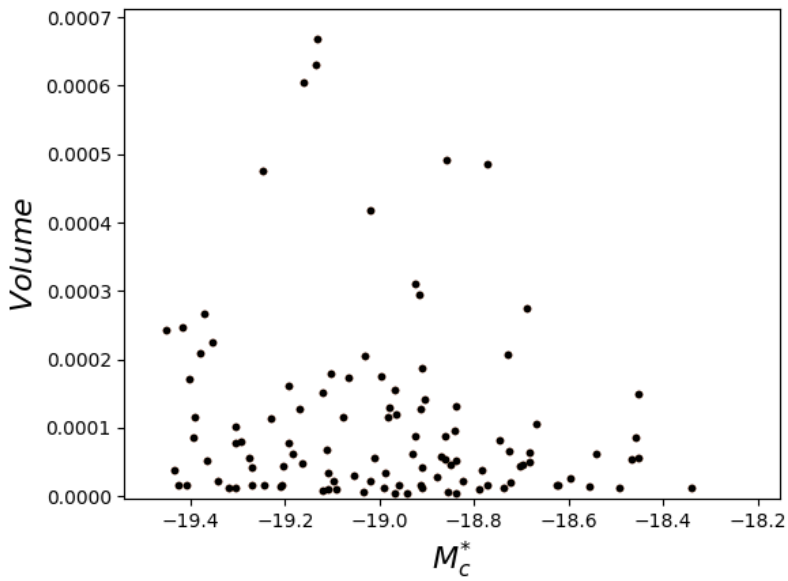

Figure 5.29: The FS diagram of low-z sample build with the model ($\Omega_\circ = 0.3$, $\lambda_\circ = 0.7$).

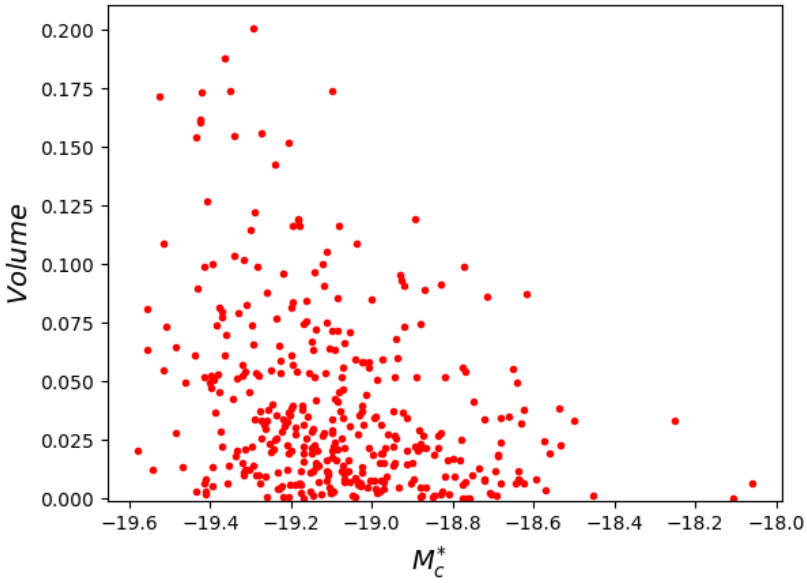

Figure 5.30: The FS diagram of SDSS-II sample build with the model: $\Omega_\circ = 0.3$, $\lambda_\circ = 0.7$.

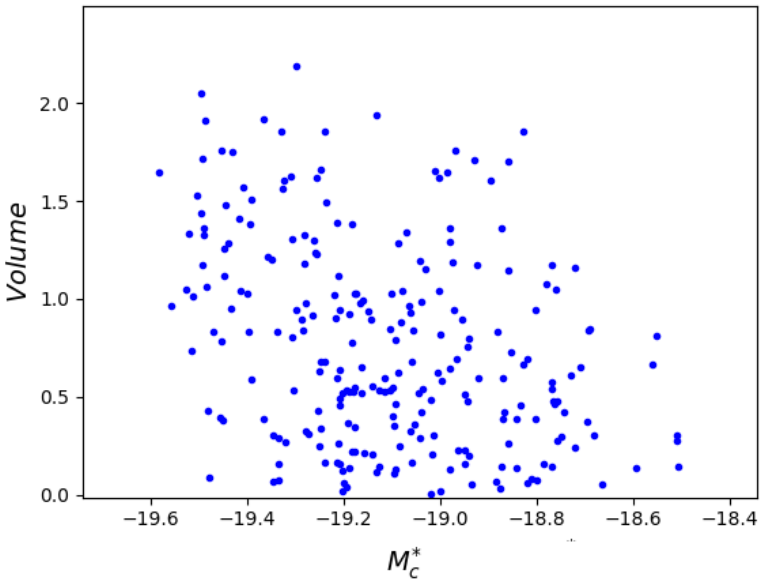

Figure 5.31: The FS diagram of SNLS3 sample build with the model: $\Omega_\circ = 0.3$, $\lambda_\circ = 0.7$.

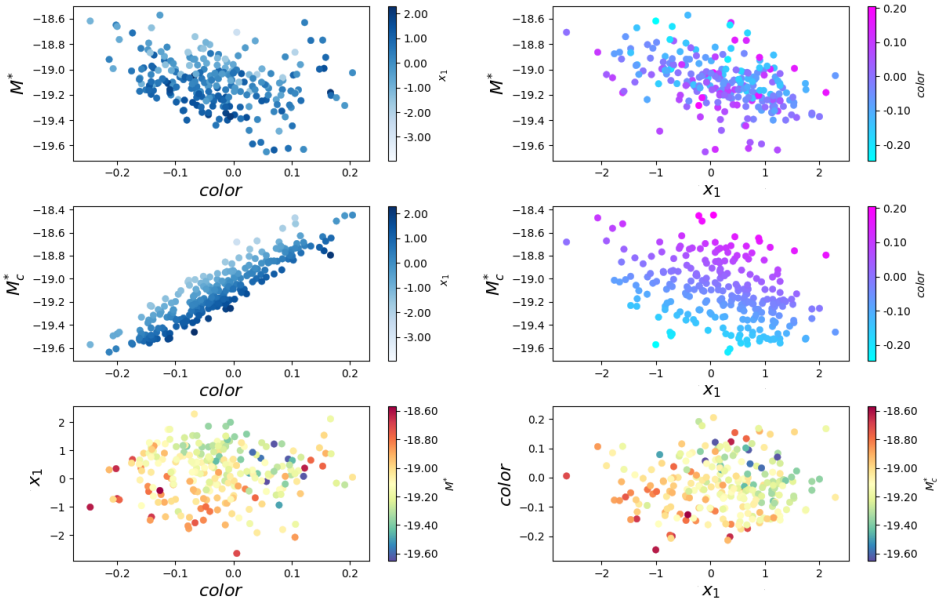

Figure 5.32: Similar to Fig.5.17 for SNLS3 sample with calibration of standardization coefficients with respect to the low-z sample.

potheses. On the other hand, the NCC has been determined with the SNLS3 sample, as shown in Fig.5.33.

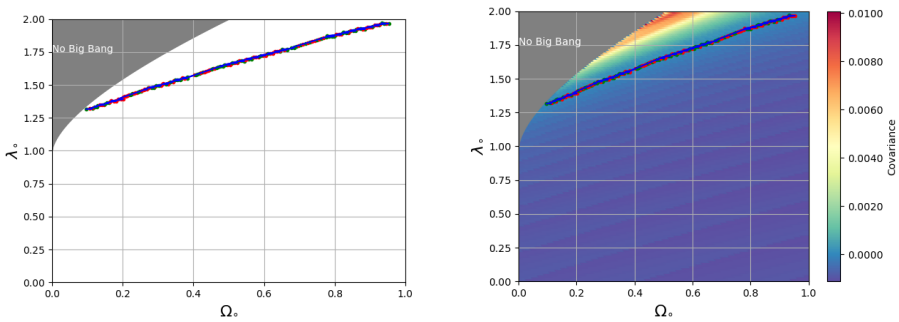

Figure 5.33: The null correlation curve in the $\lambda_\circ - \Omega_\circ$ diagram corresponding to SNLS3 sample.

This NCC is obviously coherent with the results obtained with the SDSS-II QSO samples, which favor a cosmological model with positive curvature (see Fig.5.34).

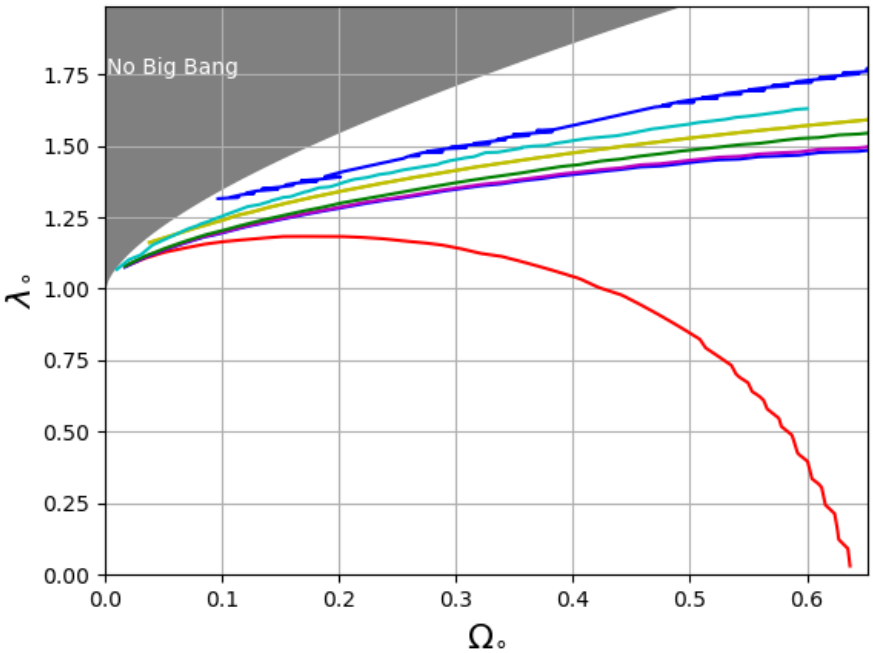

Figure 5.34: The null correlation curves in the ($\Omega_\circ$, $\lambda_\circ$) diagram that correspond to QSO samples and SNLS3 sample (the highest).

The application of the V/V_{max} test on the NCC provides us with cosmological parameters estimates ($\Omega_\circ = 0.11$, $\lambda_\circ = 1.32$) at 40% significance level (Fig.5.35). It must be noted that because of the weak sample size, we have not selected subsamples complete to a limiting apparent magnitude for performing properly the V/V_{max} test, but we did to the entire sample, which reduces inevitably the significance level.

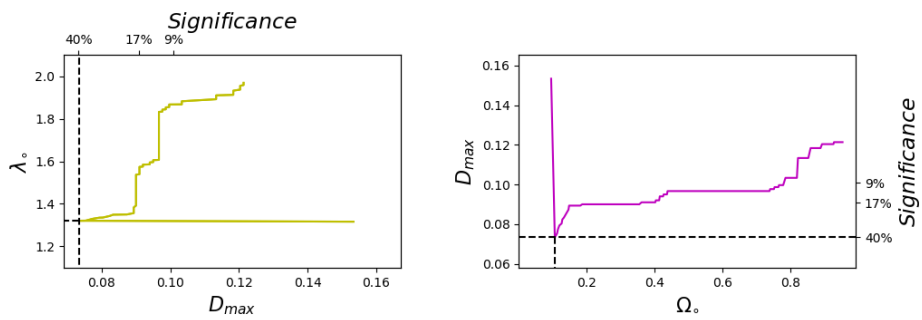

Figure 5.35: D_{max} with respect to $\lambda_\circ$ (left) and $\Omega_\circ$ (right) as candidates given by the NCC of SNLS3.

Figs.5.36, 5.37 show the FS diagrams for SDSS-II and SNLS3 samples,by assuming these values. It is clear that the SNLS3 sample appears more uniformly distributed in V-axis than the standard one, see Fig.5.31 with this cosmological model ($\Omega_\circ = 0.3$, $\lambda_\circ = 0.7$).

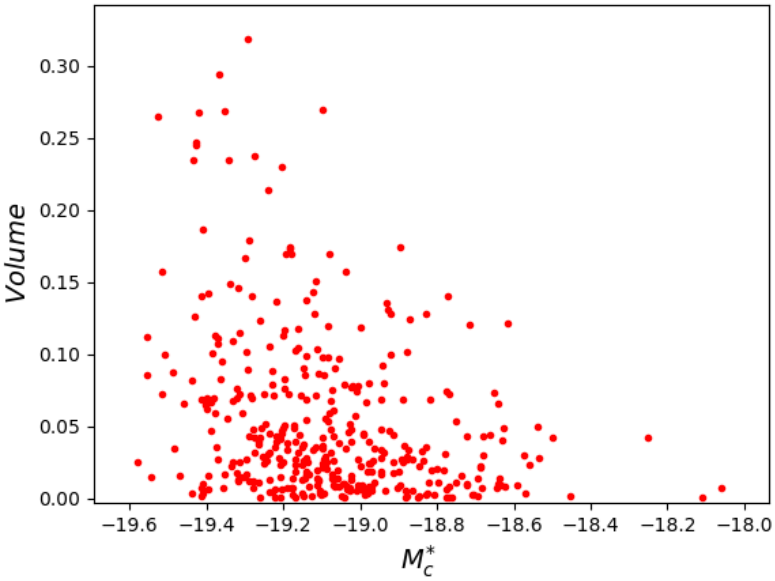

Figure 5.36: The FS diagram of SDSS-II sample build with the model ($\Omega_\circ = 0.11$, $\lambda_\circ = 1.32$).

By using the estimation method for the luminosity function and selection function, described in Sect.5.3.1, we obtained almost a Gaussian luminosity function for the SNLS3 sample, see Fig.5.38 (left panel). The average and standard deviation $\sigma_{M_c^*}$ is estimated using Eq.5.45. This yields an average $M_{c,0}^* \approx -19.139$ and $\sigma_{M_c^*} \approx 0.19$. Fig.5.38 (right panel) shows that the selection function $\phi_B(m^*)$ is compatible with a Heaviside function up to a magnitude of 24 and decreases. This result gives evidence of the difficulties in sampling the light curve of faint magnitude objects.

We determined the error on the the cosmological parameters by perfoming a perturbation of the apparent magnitude with a Gaussian white noise characterized by a standard deviation of 0.03. Therefore, we found the corresponding NCCs and we applied the V/V_{max} test. We performed this process for 200 times. The obtained candidates are determined within 35% and 43% significance level. Fig5.39 shows the results of the tests within their error in-

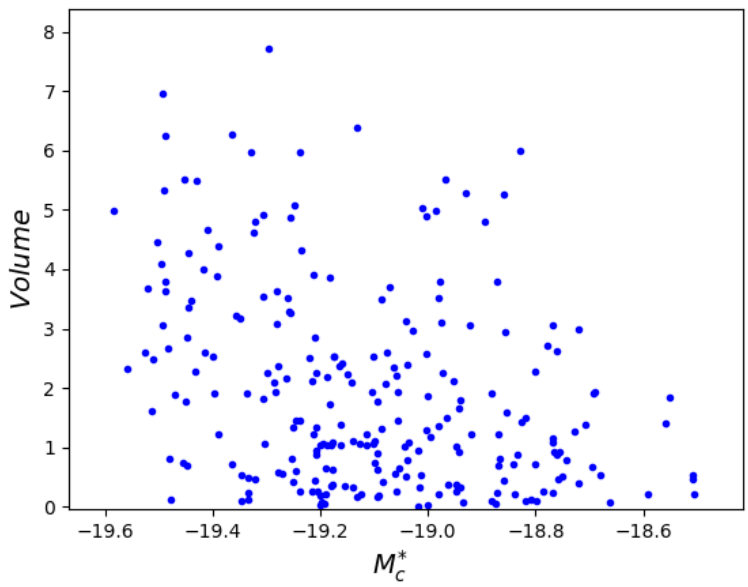

Figure 5.37: The FS diagram of SNLS3 sample build with the model ($\Omega_\circ = 0.11$, $\lambda_\circ = 1.32$).

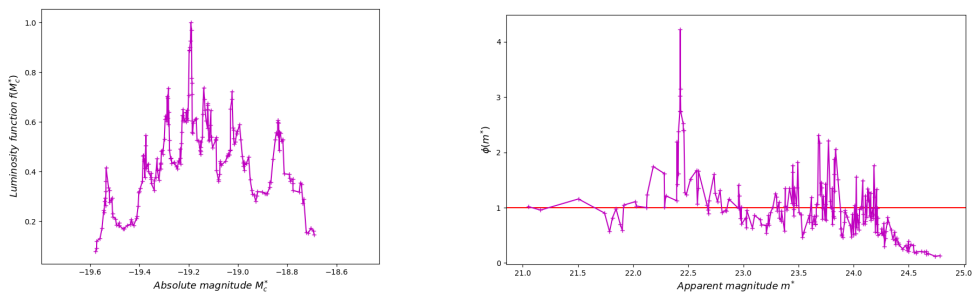

Figure 5.38: Luminosity function (left panel) and selection function (right panel) built with the model ($\Omega_\circ = 0.11$, $\lambda_\circ = 1.32$), corresponding to SNLS3 sample.

tervals with the probability density functions. This work brought the result: $\Omega_\circ = 0.13 \pm 0.02$, $\lambda_\circ = 1.34 \pm 0.01$.

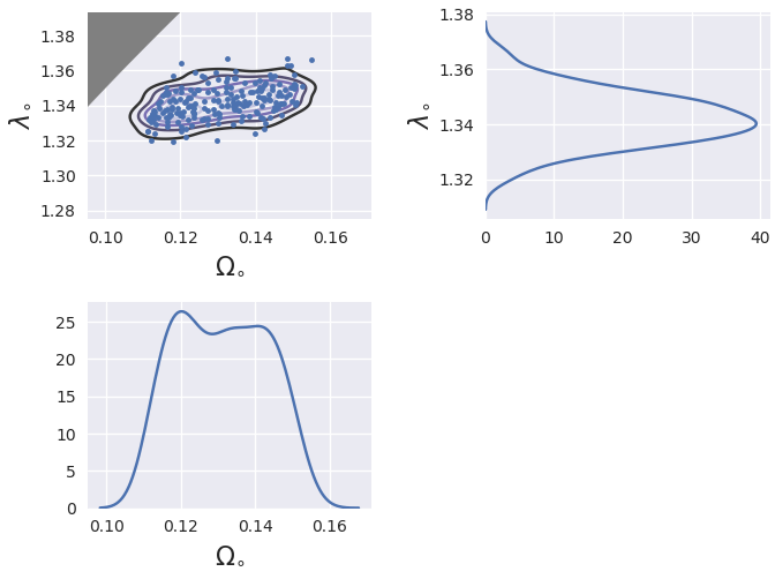

Figure 5.39: Similar to Fig.5.26

5.5 Conclusion

We studied the type-Ia supernovae events to infer the cosmological parameters by means of their light curves which are good candidates to be used as standard candles. Such a feature that provides us an estimation of the absolute magnitude at maximum of luminosity thanks to its correlation with the shape parameter of the light curve. This is an advantage over the QSO investigation. The selection of SNe does not depend solely on the observation of the object at a given date, but also on the sampling of the light curve, which makes the selection of objects more difficult. For this purpose, we analyzed the selection effect and we determined a selection criterion (m^*_{lim}) that is a characteristic of a fictive limiting light curve.
In a first step, we simulated supernovae samples taking into account the correlation between the absolute magnitude and the shape parameter. The null correlation test was adapted to these samples.
In a second step, we studied the JLA sample which consists of 740 SNe. Unfortunately, we found that this sample is not consistent with our approach. Therefore, we applied the null correlation test to its subsamples, SDDSS-II and SNLS3. The SNLS3 sample provided a null correlation curve close to the ones found by using the QSO samples. This result favors a model with positive scalar curvature with a weak presence of dark matter.

Important improvement can be considered to extend this work. An improvement in the description of the selection function that takes into account the lifetime of events can provide more accurate results.

In the future, this work will be a strong initiative to study the Gamma Ray Bursts (GRBs), the most powerful explosive events ever observed in the Universe. The GRBs are extragalactic objects distributed in a wide redshift range reaching $z = 8.3$ (GRB 090423, [Tanvir, N. R. et al 2009]). The study of GRBs using the statistical approach proposed in this thesis will allow to infer the cosmological information more accurately.

Résumé en français

CHAPTER 6

Résumé en français

Contents

6.1 La cosmologie moderne 115

6.2 Simulation d'échantillon de quasar 118

6.3 La technique de corrélation nulle 120

6.4 Résultats avec les données quasars 121

6.5 Modélisation d'échantillon de supernova et résultats sur les données de SDSS-II/SNLS3 122

Un siècle après le modèle d'univers de Friedmann-Lemaître, les observations le confortent avec une constante cosmologique Λ et une composante de matière sombre (noire) sans pression (poussière) et froide dominant celle baryonique, communément appelé Modèle "Lambda Cold Dark Matter" (ΛCDM) ou encore modèle standard. L'accélération de l'expansion de l'Univers confirmée par le diagramme de Hubble des supernovae en 1998 impose une valeur positive à la constante cosmologique.

Mes travaux de thèse se focalisent sur l'estimation des valeurs de paramètres cosmologiques du modèle standard en utilisant la technique de corrélation nulle. Cette approche présente l'avantage d'être plus robuste que les techniques usuelles. En particulier, il n'est pas requis de préciser la fonction de luminosité, celle-ci est déduite par cette méthode. De plus, elle prend en compte le biais de Malmquist due à la limitation en magnitude apparent. Ce travail a consisté aussi à modéliser des échantillons de l'événement quasar ainsi que l'événement supernova, une extrapolation adaptée du premier. Ce qui a permis de générer des échantillons conformes aux hypothèses des modèles, afin

de valider les approches statistiques. Pour ce qui concerne les quasars, nous avons utilisé le Sloan Digital Sky Survey (SDSS) d'une part, et pour les supernovae le SuperNova Legacy Survey (SNLS) et SDSS-II d'autre part. Les inférences statistiques de ces données ont conduit à un univers spatialement fermé et une présence de matière noire plus faible.

Dans le cadre d'une prochaine application de cette technique, elle pourra être utilisée pour contraindre les modèles d'énergie noire. De même, l'utilisation des amas de galaxies observées grâce à l'effet de Sunyaev Zel'dovich, servira naturellement comme échantillon cosmologique. Une telle étude pourra contribuer à apporter un élément de réponse à la validité du rôle supposé des neutrinos massifs dans la formation des amas dans l'ère primordiale de l'Univers.

Mots Clés : Cosmologie, Matière noire, Énergie noire, paramètres cosmologiques, statistiques, simulation, quasars, supernovae, diagramme de Hubble.

6.1 La cosmologie moderne

La cosmologie moderne est basé sur le principe cosmologique, qui favorise les hypothèses de l'homogénéité et de l'isotropie de l'univers. En effet, le principe copernicien a proposé qu'il n'y a pas de place privilégiée dans l'univers. En outre, l'hypothèse de l'isotropie de ce dernier signifie que chaque point de l'Univers possède des propriétés identiques dans des directions différentes, alors l'Univers semble homogène (l'isotropie de chaque point implique l'homogénéité). L'observation dans des différentes directions avec la même angle solide ont conduit à un résultat identique. Ceci implique que, à grande échelle, nous pouvons décrire l'univers observable comme étant spatialement homogène et isotrope. Cela nous amène à la description de l'espace-temps avec la métrique Friedmann-Lemaître-Robertson-Walker (FLRW):

$$\mathrm{d}s^2 = \mathrm{d}t^2 - a^2(t)\mathrm{d}\sigma^2 \tag{6.1}$$

où t est le temps cosmique, $a(t)$ est le *paramètre d'expansion* (sans dimension) et $\mathrm{d}\sigma^2$ est l'élément métrique de l'espace homogène tridimensionnel V_3 (nommé par, *espace comobile*).

Malgré l'inhomogénéité de l'Univers à petites échelles, la métrique FLRW décrit l'espace-temps à grandes échelles, à partir de plus de 100 Mpc, où les hypothèses cosmologiques sont valables comme les a montré la distribution des quasars à grande échelle avec le sondage Baryon Oscillation Spectroscopic Survey (BOSS).

En 1948, Gamow, Alpher et Herman ont prédit le fond diffus cosmologique, ils ont proposé un modèle de Big Bang chaud en supposant un univers primordial composé uniquement de neutrons (qui se désintègrent ensuite en protons) [P. J. E. Peebles 2014], [V. Alpher 2014]. Dans ce modèle (connu sous le nom de BBN pour Big Bang Nucleosynthesis), l'Univers primordial était composé d'un plasma de photons, fermions et quarks extrêmement chaud et dense. L'Univers a ensuite montré une expansion où sa densité, ainsi sa température ont diminué, favorisant la nucléosynthèse primitive, c'est-à-dire la formation des premiers noyaux faibles (Hydrogène, hélium, deutérium, lithium). Environ 380 000 ans après le Big Bang, la température est devenue assez faible ($\sim$ 3000°K) pour que les premiers atomes se forment à travers un processus appelé recombinaison (bien que les atomes n'aient jamais été combinés avant). à cette époque, les photons ont découplé de baryons et la lumière a commencé à se propager librement. Ce rayonnement, qui a été simplement refroidi pendant l'évolution de l'univers, est connu sous le nom de fond diffus cosmologique (CMB pour Cosmic Microwave Background en anglais). Les observations ont confirmé le modèle BBN, une fois lorsque Penzias et Wilson ont détecté le CMB. Ce rayonnement a presque un spectre de corps noir parfait avec une

température moyenne de 2.73°K produit par les photons de l'Univers primordial. La température de CMB est isotrope et homogène à des variations de l'ordre de 10^{-5}. Et une autre fois par les mesures de l'abondance des éléments légers dans l'univers, en tant que deuxième preuve, qui sont en excellent accord avec les prédictions de la nucléosynthèse primordiale [G. Steigman 2004]. Cela inclut l'abondance massive d'Hélium He4 prédite entre 23% et 30%, avec un accord parfait avec les observations [C. A. Bertulani, et al. 2016]. Le contenu de l'univers est considéré comme un fluide parfait qui se caractérise par les propriétés du tenseur énergie-impulsion avec la pression P et la densité d'énergie dans l'univers ρ. En effet, les équations de Friedmann nous permettent de définir le polynôme suivant:

$$P(a) = \lambda_\circ a^4 - \kappa_\circ a^2 + \Omega_\circ a + \alpha_\circ; \quad P(1) = 1 \tag{6.2}$$

où les coefficients sont des paramètres sans dimension, et ils sont défini comme suivant:

$$\lambda_\circ = \frac{1}{3}\Lambda H_\circ^{-2}, \quad \kappa_\circ = K_\circ H_\circ^{-2} = \lambda_\circ + \Omega_\circ + \alpha_\circ - 1, \quad \Omega_\circ = \frac{8}{3}\pi G \rho_\circ H_\circ^{-2} > 0 \tag{6.3}$$

$$\alpha_\circ = \frac{8}{45}\pi^3 \mathrm{G} k_\mathrm{B} T_\circ^4 \hbar^{-3} H_\circ^{-2} \approx 2.5\,10^{-5} h^{-2}, \quad h = H_\circ/(100\,\mathrm{km\,s^{-1}Mpc^{-1}}) \tag{6.4}$$

Ce sont des quantités qui se situent respectivement pour les valeurs actuelles des versions réduites de la constante cosmologique Λ, la courbure scalaire K de l'espace, la densité de la matière, ρ étant la densité spécifique des particules massives (Matière noire incluse), G est la constante de Newton, la densité d'énergie du rayonnement et la constante de Hubble.

Ces paramètres satisfont la formule:

$$\lambda_\circ - \kappa_\circ + \Omega_\circ + \alpha_\circ = 1 \tag{6.5}$$

Par la suite, nous estimons les paramètres: $\lambda_\circ$ et $\Omega_\circ$.

Ce que Hubble a mené à la découverte de sa loi célèbre était la mesure de la distance et de la vitesse des galaxies dans l'Univers proche. Il a découvert que les galaxies semblaient reculer à une vitesse qui augmentait proportionnellement avec leur distance. Ce phénomène se reflète dans La loi de Hubble:

$$v = H_\circ d \tag{6.6}$$

Avec les coordonnées comobile des galaxies, on peut définir la *distance comobile* τ entre l'observateur et la source de lumière à redshift z:

$$\tau(z) = \int_{\frac{1}{1+z}}^{1} \frac{\mathrm{d}a}{\sqrt{P(a)}} \tag{6.7}$$

La distance de luminosité, d_L, est défini comme le rayon d'une sphère centrée sur la source lumineuse dont son énergie lumineuse est distribué sur la surface de cette sphère. La lumière reçue par unité de temps représente le flux (la luminosité apparente) de cette source qui diminue avec le carré de la distance, par la loi d'inverse carré :

$$f = \frac{L}{4\pi d_L^2} \tag{6.8}$$

où L est la luminosité intrinsèque de l'objet. Il s'avère que la distance de luminosité est liée à la distance comobile et elle s'écrit comme suit:

$$d_L = \frac{c}{H_\circ}(1+z)\begin{cases} \frac{sin(\tilde{\tau})}{\sqrt{\kappa_0}} & \text{if } \kappa_0 > 0 \\ \tau & \text{if } \kappa_0 = 0 \\ \frac{sinh(\tilde{\tau})}{\sqrt{|\kappa_0|}} & \text{if } \kappa_0 < 0 \end{cases} \tag{6.9}$$

où $\tilde{\tau} = \tau\sqrt{|\kappa_0|}$ est la distance angulaire.
En astronomie, le système de magnitude est fréquemment utilisé pour décrire la luminosité d'un objet. La magnitude est une échelle utilisée pour classer les étoiles en fonction de leur luminosité. Les étoiles les plus brillantes ont la plus faible amplitude pour lesquelles un degré de magnitude correspond à une différence de 2,51 fois de luminosité. En utilisant la définition de la magnitude apparente m, nous pouvons introduire la magnitude absolue M d'un objet. Ce dernier est une mesure de la luminosité intrinsèque de l'objet et est défini comme il apparaîtrait à un observateur hypothétique à une distance de 10pc. La magnitude apparente d'un objet à redshift z est liée à la magnitude absolue (suivant Eq.6.8), on peut écrire:

$$m = M + \zeta(z) \tag{6.10}$$

où $\zeta(z)$ est le module de distance qui dépend des paramètres cosmologiques. La meilleure mesure ou estimation de cette dernière distance représente la clé pour contraindre les perles de diagramme de Hubble, c.à.d les paramètres cosmologiques $\lambda_\circ$ et $\Omega_\circ$.

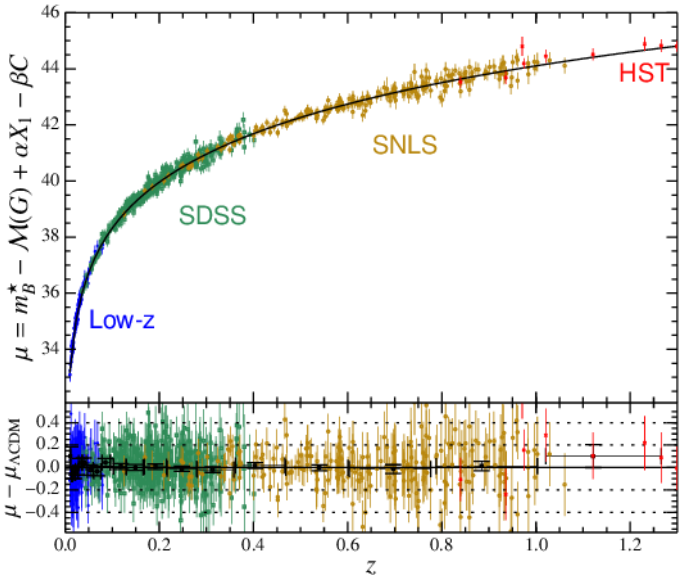

Figure 6.1: Le diagramme de Hubble des échantillons de Supernovae avec SNLS, SDSS, HST et plusieurs sondages low-z. Figure tirée de [Betoule, M. et al 2014]

6.2 Simulation d'échantillon de quasar

Conformément aux hypothèses de l'homogénéité et de l'isotropie de l'univers, les objets dans l'espace sont censés d'être uniformément répartis. Les quasars (QSOs, pour Quasar stellar Objects en anglais) supposés d'être des objets permanents pour sonder la géométrie de l'espace-temps. Ils sont caractérisés intrinsèquement d'une magnitude absolue M et une distance comobile τ (le rayon de volume V centré à la position de l'observateur avec une répartition uniforme dans l'espace comobile). Si la magnitude absolue M est répartie selon la fonction de luminosité f(M), l'échantillon de QSO est décrit avec le produit de deux densités de probabilité indépendantes comme suit:

$$dP_{th} \propto f(M)dM.dV \tag{6.11}$$

En supposant que les effets de sélection dépendent uniquement de la magnitude apparente m, nous utilisons une fonction de sélection $\phi(m)$ dans la densité de probabilité dans le but de prendre en compte le processus de sélection en observation. Par conséquent, la densité de probabilité des variables observables sont décrites par:

$$dP_{obs} = \frac{\phi(m)dP_{th}}{P_{th}(\phi)} \tag{6.12}$$

où P_{th} est un facteur de normalisation. Nous définissons la fonction de répartition en terme de la variable aléatoire de magnitude absolue M comme

l'intégrale de l'équation 6.12. La fonction de répartition est une variable aléatoire uniforme entre 0 et 1. L'échantillon simulé est réalisé par la recherche de la solution de l'inverse de la fonction de répartition en déterminant les deux quantités intrinsèque, la magnitude absolue M et le volume V. Ensuite, le redshift z est déterminé par la solution de l'inverse de Volume V^{-1}. Enfin, la magnitude apparente est calculé en utilisant l'Eq.6.10.

Le diagramme de magnitude absolue-volume $(M-V)$ est représenté comme une dérivation du diagramme de Hubble. Alors que ce diagramme ne montre pas les effets de sélection, le diagramme $M-V$ donne une illustration claire des effets de sélection.

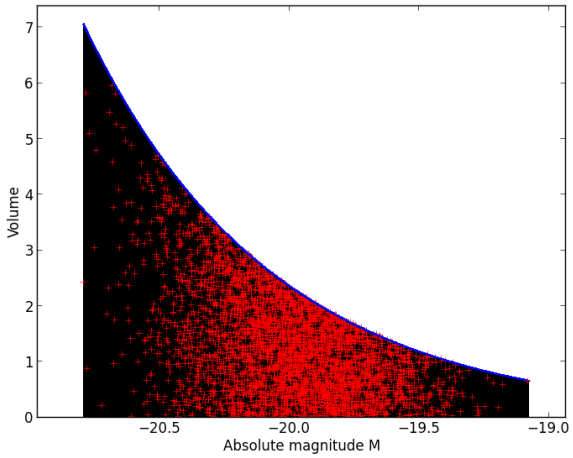

Figure 6.2: Le diagramme magnitude absolue-volume de l'échantillon simulé présenté en rouge. La courbe bleue est le volume en fonction de la magnitude absolue à une magnitude apparente limite donnée. Cet échantillon a été généré avec un univers plat $(\Omega_\circ, \lambda_\circ = 0.3, 0.7)$. Une répartition uniforme apparaît sur l'axe vertical et une distribution gaussienne sur l'axe horizontal tel qu'ils ont été choisi initialement dans la simulation.

Ces simulations nous permettent d'obtenir des échantillons de QSO similaires aux données réelles, qui peuvent être utilisés avec le test de corrélation nulle.

6.3 La technique de corrélation nulle

La méthode statistique habituelle, au moyen de l'ajustement du moindre carré, consiste à adapter les données de l'échantillon observable au modèle théorique supposé. En d'autres termes, les paramètres cosmologiques sont définis de telle sorte que les données montrent la dispersion minimale du comportement

théorique. Cependant, le biais de Malmquist empêche à estimer correctement la magnitude d'une telle dispersion à moins qu'on connaisse la fonction de luminosité et les effets de sélection de l'observation.

Avec la technique de corrélation nulle, nous sommes exemptés de fournir ces caractéristiques. Néanmoins, les effets de sélection ne doivent pas dépendre du redshift mais uniquement de la magnitude apparente. Selon la formule 6.12, un échantillon simulé sous le modèle $(\Omega_\circ, \lambda_\circ = 0.3, 0.7)$ est effectué, nous avons utilisé une fonction de luminosité gaussienne. Cet échantillon a été utilisé comme référence pour vérifier la performance de la technique statistique.

La technique de corrélation nulle est une méthode statistique robuste qui n'exige pas la connaissance de la fonction de luminosité a priori. De plus, cette technique est exempte du biais de Malmquist. La technique de corrélation nulle nous permettre d'obtenir un ensemble de modèles qui sont considéré comme les meilleurs candidats qui s'accordent avec les données.

L'échantillon observé est représenté dans le plan (M, m) par la densité de probabilité suivante:

$$dP_{(M,m)} = \rho(z)\phi(m)f(M)dM.dm; \quad \rho(z) = \frac{\partial V}{\partial m} \tag{6.13}$$

où $\rho(z)$ est une fonction de corrélation entre M et m. Pour les vraies valeurs des paramètres cosmologiques $(\Omega_\circ, \lambda_\circ)$, la corrélation entre les variables aléatoires M et m disparaissent en divisant chaque événement par la fonction de corrélation $\rho(z)$. Cette corrélation est donnée par la covariance pondérée de M et m, elle dépend des paramètres cosmologiques et s'écrit comme suivant:

$$\Gamma(\Omega_\circ, \lambda_\circ) = \sum_{k=1}^{N} \omega_k (M_k - \langle M \rangle)(m_k - \langle m \rangle) \tag{6.14}$$

où ω_k est le facteur de pondération qui est inversement proportionnel à $\rho(z)$. Les moyennes pondérées de M et m sont notées $\langle M \rangle$ et $\langle m \rangle$ respectivement, elles sont définies par les formules suivantes:

$$\langle M \rangle = \sum_{k=1}^{N} \omega_k M_k \tag{6.15}$$

$$\langle m \rangle = \sum_{k=1}^{N} \omega_k m_k \tag{6.16}$$

La solution de l'équation $\Gamma(\Omega_\circ, \lambda_\circ) = 0$ donne les valeurs candidates de $\Omega_\circ$ et $\lambda_\circ$, au moyen de la courbe de corrélation nulle dans le plan $(\Omega_\circ, \lambda_\circ)$ (Fig.6.3).

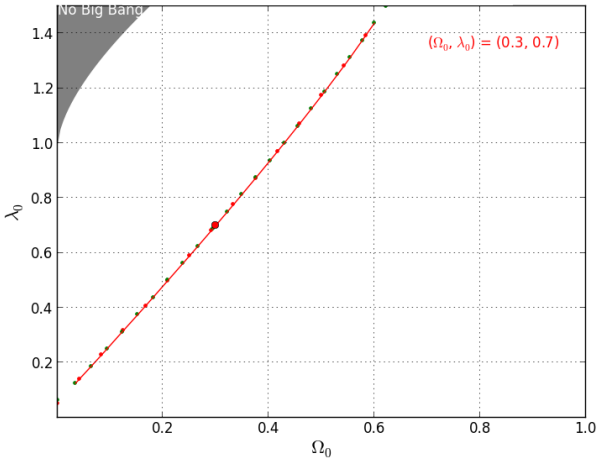

Figure 6.3: La courbe de corrélation nulle dans le plan $(\Omega_\circ, \lambda_\circ)$. La courbe retrouve le modèle cosmologiques utilisé pour effectuer la simulation de l'échantillon.

L'exactitude de cette technique a été montré en étudiant les fluctuation statistiques qui diminuent avec l'augmentation du nombre d'objets. D'autre part, l'approche de corrélation nulle nous a permis de déterminer la fonction de luminosité et la fonction de sélection.

Un deuxième test a été établi, au moyen du test V/V_{max}, avec une petite modification de la définition habituelle. Nous avons affiné les résultats en appliquant ce test sur la courbe de corrélation nulle dans le but d'obtenir les meilleurs candidats des paramètres cosmologiques.

6.4 Résultats avec les données quasars

Nous avons appliqué le test de corrélation nulle et celui de V/V_{max} sur plusieurs échantillons et sous-échantillons de QSO fournis par les données du sondage SDSS. Nous avons obtenu plusieurs courbes de corrélation nulles qui nous ont permis de discriminer les meilleurs candidats qui s'accordent avec les hypothèses de travail. En outre, nous avons affiné les résultats en vérifiant la répartition spatiale uniforme des QSO en utilisant le test V/V_{max}, en particulier sur le sous-échantillon le plus homogène. Ces deux tests nous ont permis de déterminer une constante cosmologique positive avec une faible valeur de densité de matière pour une courbure positive (Fig6.4).

Grâce aux techniques statistiques utilisées dans ce travail, les QSOs ont des inférences de l'accélération cosmique bien qu'elles ne soient pas classées comme des bougies standard.

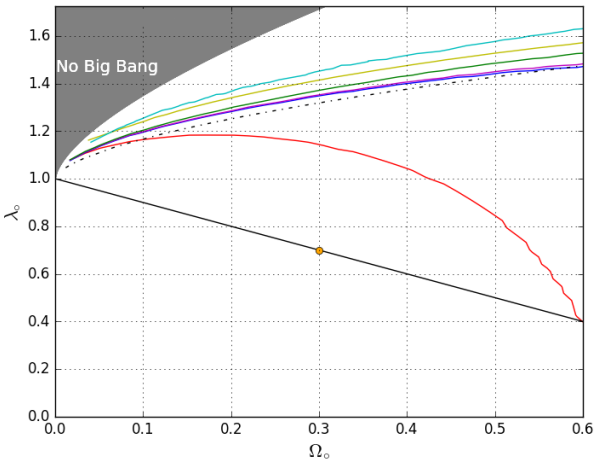

Figure 6.4: Les courbes de corrélation nulles dans le diagramme($\Omega_\circ$, $\lambda_\circ$) correspondant aux échantillons EDR, DR1, DR3, DR7 et aux sous-échantillons DR3. Les courbes sont situées dans la région avec une courbure positive $\kappa_\circ > 0$ (au-dessus de la ligne droite). Toutes les courbes sont en accord et proches l'une de l'autre, sauf la courbe rouge qui correspond à l'échantillon EDR.

6.5 Modélisation d'échantillon de supernova et résultats sur les données de SDSS-II/SNLS3

La supernova (SN) est l'un des objets les plus lumineux dans l'univers découvert jusqu'aujourdâhui. Ce type d'objet est le résultat de l'explosion des étoiles massives avec une intensité phénoménale. Cette explosion est le signe du changement d'état d'une étoile à la fin de sa vie. La SN est un objet très lumineux (galactique et extragalactique) avec une luminosité qui peut correspondre à celle de sa galaxie hôte dans certains cas. Grâce à leurs luminosités intrinsèques, les SNe sont observés à des distances cosmologiques. Elles ont été classées et distinguées en groupes, dont l'une est considérée comme une famille de bougies standard.

Puisque la dispersion de la luminosité au maximum de la courbe de lumière (CL) des SNe du type Ia est susceptible d'être faible, elles sont considérées comme de bons candidats des bougies standard, ce qui en fait les meilleurs outils pour estimer les distances cosmologiques et ensuite contraindre les paramètres cosmologiques avec une grande précision. [M. M. Phillips 1993], [Hamuy et al. 1995], [1996a], [Riess et al 1995] et [1996a] ont démontré la corrélation entre un paramètre de la CL et la magnitude absolue, M_B, au maximum de luminosité. Ce paramètre est le taux de déclin de la CL, noté

Δm_{15} ou x_1, sachant que la notation et la signification du paramètre de forme dépendent de la méthode de standardisation choisi. On mentionne spécialement, x_1 utilisé avec le modèle de standardisation SALT2.

La description des événements avec une durée de vie finie[1], comme c'est le cas pour les SNe de type Ia, nécessite une détermination sensible de leurs quantités (variables) intrinsèques. L'événement SN Ia est un flash puissant caractérisé par sa courbe de lumière, c'est-à-dire l'évolution de sa luminosité intrinsèque avec le temps. La courbe de lumière est identifiée par la date au maximum de luminosité, notée t^*, et par la magnitude absolue qui correspond à ce maximum, noté M^*. Ces deux variables intrinsèques caractérisent l'évolution de la magnitude absolue avec le temps, M(t), qui est également paramétré par un paramètre de forme x_1, c'est-à-dire la dilatation ou la contraction de la durée de vie par rapport à un courbe patron. Le paramètre de forme x_1 représente la durée de vie de chaque SN et il est supposé d'être linéairement corrélé avec M^*.

Pour prendre en compte les effets de sélection, nous avons étudié le comportement des courbes de lumière d'un échantillon de SN donné afin de souligner un critère général qui peut être utilisé pour distinguer les SNe et, par conséquent, éliminer les SNe avec des courbes de lumière de mauvais échantillonnage. Un supernova a une courbe de lumière bien échantillonnée si elle a eu suffisamment du temps pour montrer une évolution de sa luminosité au-dessus du flux limite f_{lim} qui correspond au flux de la magnitude apparente limite m_{lim}.

Il faut rappeler que la courbe de lumière observée se caractérise par la magnitude apparente au maximum de luminosité m^* et par le taux de déclin Δm_{15} (de plus Δm_{15} est grand, de plus la diminution de la courbe de lumière est vite). La courbe de lumière doit présenter un écart significatif entre la magnitude apparente limite de m_{lim} et son pic de magnitude apparente m^* d'une part, et d'autre part un petit Δm_{15} pour avoir un temps suffisant pour échantillonner la courbe de lumière. Dans cette vision, les techniques d'observation susmentionnées permettent de déterminer une courbe de lumière, définie comme une courbe de lumière limite, pour laquelle les exigences minimales sont assurées. Cette courbe limite dépend fortement de la capacité des techniques d'observation de chaque enquête et elle se caractérise par m^*_{lim} et $\Delta m_{15,lim}$. En conclusion, cette courbe de lumière limite est utilisée pour juger la sélection des SNe en fonction du pic de la magnitude apparente m^*, où une SN est observée avec succès et sélectionnée si son $m^* < m^*_{lim}$. Avec ce critère de sélection, nous incluons non seulement le biais de Malmquist, mais

[1]Un objet non pérenne

aussi les biais qui dues au mauvais échantillonnage des courbes de lumière, en particulier pour les SNe avec des courtes durées de vie.

Avec cette description des effets de sélection, nous avons introduit dans la densité de probabilité des objets observés, une fonction technologique $\phi_B(m^*)$ qui dépend du pic de la magnitude apparente dans la bande B:

$$dP_{obs} = \phi_B(m^*)g(M^*, x_1)dM^*dx_1dt^*dV \tag{6.17}$$

La couleur est utilisée pour rendre la distribution de la magnitude absolue au maximum de luminosité plus étroite. Ensuite, nous notons M_c^* pour la valeur corrigée de la magnitude absolue:

$$M^* = M_c^* - \beta c \tag{6.18}$$

où β est un coefficient correctif positif. Par conséquent, la couleur doit être prise en compte dans la loi sur la densité de probabilité de l'événement. Alors, Eq.6.17 est écris:

$$dP_{obs} = \phi_B(m^*)g(M^*, x_1)dM^*dx_1g_G(c; 0, \sigma_c)dcdt^*dV \tag{6.19}$$

où M_c^* s'écris:

$$M_c^* = \begin{cases} ax_1 + b - \beta c & \text{if } M^a_{stellar} < 10^{10}M_\odot \\ ax_1 + b - \beta c + \delta & \text{otherwise} \end{cases} \tag{6.20}$$

où δ est le coefficient de corrélation entre la magnitude absolue et la masse stellaire de la galaxie hôte $M^a_{stellar}$ [Sullivan, M. et al 2010], [Conley et al 2011]. Le coefficient de standardisation hôte-masse est évalué dans [Betoule, M. et al 2014] pour la valeur $\delta = -0.070 \pm 0.023$ en utilisant l'analyse de l'échantillon JLA (pour Joint Light-curve Analysis) qui se compose de 740 SNe.

Les paramètres a, b et σ_ϵ sont calculés selon les formules suivantes:

$$a = \frac{Cov(x_1, M^*)}{\sigma^2_{x_1}} \tag{6.21}$$

$$\sigma_\epsilon = \sigma_{M^*}\sqrt{1 - \rho^2(x_1, M^*)} \tag{6.22}$$

où $\rho(x_1, M^*)$ est le coefficient de correlation.

$$b = \langle M^* \rangle - a\langle x_1 \rangle + \gamma {\sigma_\epsilon}^2 \tag{6.23}$$

Les mêmes étapes de calibration sont effectuées pour déterminer les paramètres de corrélation linéaire dans le plan (M_c^*, c).

Nous avons adapté le test de corrélation nulle pour un échantillon de supernova. Nous avons appliqué ce test sur les échantillons de SDSS-II et SNLS. On a trouvé que l'échantillon de SN de SDSS-II n'est pas approprié avec les hypothèses de travail. Autrement-dit, le diagramme magnitude absolue-volume ne montre pas une distribution uniforme sur l'axe de volume, on a remarqué un structure et une concentration sur ce diagramme. Par conséquent, le test de corrélation nulle avec cet échantillon n'a pas trouvé des candidats pour les paramètres cosmologiques (c.à.d on n'a pas trouvé la courbe de corrélation nulle). En revanche, l'application de ce test à l'échantillon de SNLS nous a permis d'obtenir un ensemble de candidats de modèles cosmologiques où les données s'accordent avec les hypothèses de travail. La courbe de corrélation nulle obtenu avec l'échantillon de SNLS conforte les résultats obtenus avec les échantillons de QSOs de SDSS (Fig.6.5).

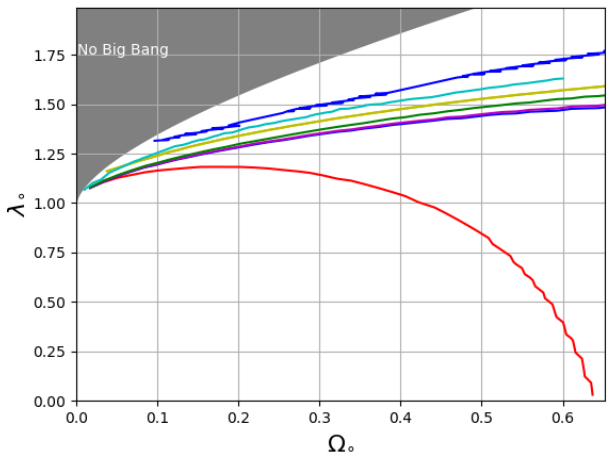

Figure 6.5: Les courbes de corrélation nulles dans le diagramme ($\Omega_\circ$, $\lambda_\circ$) qui correspondent aux échantillons QSO et à l'échantillon SNLS (le plus élevé).

Dans ce travail, nous avons effectué une nouvelle modélisation d'un échantillon de supernova du type Ia en tenant compte de la corrélation entre la magnitude absolue et le paramètre de forme de la courbe de lumière. L'application du test de corrélation nulle à l'échantillon de SNLS a confirmé un modèle cosmologique avec une courbure positive et une présence faible de la matière noire.

Appendices

APPENDIX A

Probability density functions

- The probability density function (pdf) of a Gaussian distribution with a standard deviation σ_x and an average x_0, is defined by:

$$g_G(x; x_0, \sigma_x) = \frac{1}{\sqrt{2\pi\sigma_x^2}} \mathrm{e}^{\frac{-(x-x_0)^2}{2\sigma_x^2}} \tag{A.1}$$

- The probability density function for the Gumbel (named for German mathematician Emil Julius Gumbel) distribution is:

$$p(x; x_0, \gamma_x) = \frac{e^{-(x-x_0)/\gamma_x}}{\gamma_x} e^{-e^{-(x-x_0)/\gamma_x}}, \tag{A.2}$$

  where x_0 is the mode, a location parameter, and γ_x is the scale parameter. The pdf has a mean of $x_0 + 0.57721\gamma_x$ and a variance of $\frac{\pi^2}{6}\gamma_x^2$

APPENDIX B

Calculation of the weighting factor

With Eq.1.37, one computes the weighting factors depending of the sign of the reduced curvature, and the intermediate results are given as follows

- For the case of the close Universe $\kappa_\circ > 0$:

$$\begin{aligned}\frac{\partial V}{\partial z} &= \frac{\pi}{\kappa_\circ^{\frac{3}{2}}}[2\kappa_\circ^{\frac{1}{2}}\frac{\partial \tau}{\partial z} - 2\kappa_\circ^{\frac{1}{2}}\frac{\partial \tau}{\partial z}\cos(2\kappa_\circ^{\frac{1}{2}}\tau)] \\ &= \frac{2\pi}{\kappa_\circ}\frac{\partial \tau}{\partial z}[1-\cos(2\kappa_\circ^{\frac{1}{2}}\tau)] \\ &= \frac{2\pi}{\kappa_\circ}\left[\frac{1-\cos(2\kappa_\circ^{\frac{1}{2}}\tau)}{(1+z)^2\sqrt{P(\frac{1}{1+z})}}\right]\end{aligned} \tag{B.1}$$

$$\begin{aligned}\frac{\partial \zeta}{\partial z} &= \frac{5}{\ln(10)}\frac{\frac{\partial((1+z)\sin(\kappa_\circ^{\frac{1}{2}}\tau))}{\partial z}}{(1+z)\sin(\kappa_\circ^{\frac{1}{2}}\tau)} \\ &= \frac{5}{\ln(10)}\left[\frac{1}{(1+z)} + \frac{\kappa_\circ^{\frac{1}{2}}\cot(\kappa_\circ^{\frac{1}{2}}\tau)}{(1+z)^2\sqrt{P(\frac{1}{1+z})}}\right] \\ &= \frac{5}{\ln(10)}\left[\frac{(1+z)\sqrt{P(\frac{1}{1+z})} + \kappa_\circ^{\frac{1}{2}}\cot(\kappa_\circ^{\frac{1}{2}}\tau)}{(1+z)^2\sqrt{P(\frac{1}{1+z})}}\right]\end{aligned} \tag{B.2}$$

Then, we obtain:

$$\frac{\partial V}{\partial \zeta} = \frac{2\pi \ln(10)}{5\kappa_\circ} \frac{(1-\cos(2\kappa_\circ^{\frac{1}{2}}\tau))}{[(1+z)\sqrt{P(\frac{1}{1+z})} + \kappa_\circ^{\frac{1}{2}} \cot(\kappa_\circ^{\frac{1}{2}}\tau)]} \tag{B.3}$$

- With the similar calculation for the negative $\kappa_\circ$, we obtain:

$$\frac{\partial V}{\partial \zeta} = \frac{2\pi \ln(10)}{5|\kappa_\circ|} \frac{(\cosh(2|\kappa_\circ|^{\frac{1}{2}}\tau) - 1)}{[(1+z)\sqrt{P(\frac{1}{1+z})} + |\kappa_\circ|^{\frac{1}{2}} \coth(|\kappa_\circ|^{\frac{1}{2}}\tau)]} \tag{B.4}$$

APPENDIX C

Calculation of V(M)

Here, we detail the determination of the curve of the equation $m(M, V) = m_{lim}$. In other words, the volume V as a function of M at a limiting apparent magnitude m_{lim}. We note that the absolute magnitude M is replaced by the reduced absolute magnitude for reasons of simplicity in the calculation.

- For $\kappa_\circ = 0$:

$$\tau^3 = \frac{1}{(1+z_{lim})^3} 10^{\frac{3(m_{lim}-M)}{5}} \tag{C.1}$$

  where

$$z_{lim} = \zeta^{-1}(m_{lim} - M) \tag{C.2}$$

  the source of absolute magnitude M remains visible up to a redshift z_{lim} under a given limited apparent magnitude m_{lim}, therefore, using Eqs.1.37 and C.1, the volume becomes:

$$V(M; m_{lim}, z_{lim}) = \frac{4\pi}{3} \frac{1}{(1+z_{lim})^3} 10^{\frac{3(m_{lim}-M)}{5}} \tag{C.3}$$

- For $\kappa_\circ > 0$:

$$V(z) = \frac{\pi}{\kappa_\circ^{3/2}} (2\tau\kappa_\circ^{1/2} - \sin(2\tau\kappa_\circ^{1/2})) \tag{C.4}$$

$$d_l = \frac{(1+z)\sin(\tau\kappa_\circ^{1/2})}{\kappa_\circ^{1/2}} \tag{C.5}$$

therefore, one obtains:

$$\sin(\tau\kappa_{\circ}^{1/2}) = \frac{\kappa_{\circ}^{1/2}}{(1+z_{lim})}\,10^{\frac{(m_{lim}-M)}{5}} \tag{C.6}$$

$$\tau\kappa_{\circ}^{1/2} = \arcsin\left[\frac{\kappa_{\circ}^{1/2}}{(1+z_{lim})}\,10^{\frac{(m_{lim}-M)}{5}}\right] \tag{C.7}$$

since from the trigonometric relations we have, $\sin(2\alpha) = 2\sin(\alpha)\cos(\alpha)$ and $\cos(\arcsin(\alpha)) = \sin(\arccos(\alpha)) = \sqrt{1-\alpha^2}$ where $\alpha \in$ [-1,1], so:

$$V(M; m_{lim}, z_{lim}) = \frac{\pi}{\kappa_{\circ}^{3/2}}\left(2\tau\kappa_{\circ}^{1/2} - 2\sin(\tau\kappa_{\circ}^{1/2})\cos(\tau\kappa_{\circ}^{1/2})\right) \tag{C.8}$$

$$V(M; m_{lim}, z_{lim}) = \frac{\pi}{\kappa_{\circ}^{3/2}}\left[2\arcsin(\alpha_l) - 2\alpha_l\sqrt{1-\alpha_l^2}\right] \tag{C.9}$$

where:

$$\alpha_l \equiv \alpha(M; m_{lim}, z_{lim}) = \frac{\kappa_{\circ}^{1/2}}{(1+z_{lim})}\,10^{\frac{(m_{lim}-M)}{5}} \tag{C.10}$$

- For $\kappa_{\circ} < 0$:

$$V(z) = \frac{\pi}{|\kappa_{\circ}^{3/2}|}(\sinh(2\tau|\kappa_{\circ}|^{1/2}) - 2\tau|\kappa_{\circ}|^{1/2}) \tag{C.11}$$

$$d_l = \frac{(1+z)}{|\kappa_{\circ}|^{1/2}}\sinh(2\tau|\kappa_{\circ}|^{1/2}) = 10^{\frac{(m_{lim}-M)}{5}} \tag{C.12}$$

$$\sinh(\tau|\kappa_{\circ}|^{1/2}) = \frac{|\kappa_{\circ}|^{1/2}}{(1+z_{lim})}\,10^{\frac{(m_{lim}-M)}{5}} \tag{C.13}$$

$$\tau|\kappa_{\circ}|^{1/2} = \left[\frac{|\kappa_{\circ}|^{1/2}}{(1+z_{lim})}\,10^{\frac{(m_{lim}-M)}{5}}\right] \tag{C.14}$$

$$\alpha_l \equiv \alpha(M; m_{lim}, z_{lim}) = \frac{|\kappa_{\circ}|^{1/2}}{(1+z_{lim})}\,10^{\frac{(m_{lim}-M)}{5}} \tag{C.15}$$

the trigonometric relations allow us to write: $\sinh(2\alpha) = 2\sinh(\alpha)\cosh(\alpha)$ and $\cosh((\alpha)) = \sqrt{1+\alpha^2}$, then:

$$V(M; m_{lim}, z_{lim}) = \frac{\pi}{|\kappa_{\circ}|^{3/2}}\left[2\alpha_l\sqrt{1+\alpha_l^2} - 2(\alpha_l)\right] \tag{C.16}$$

APPENDIX D

Code Python

```
#!/usr/bin/python2.7.3
# -*- coding: latin-1 -*-

#=================================
#author            :Dyaa Chbib
#date              :2014_11_28
#version           :0.1
#python_version    :2.7.3
#=================================

from pylab import *
import pylab as pl
import matplotlib.pyplot as plt
from numpy import *
import numpy as np
from mpl_toolkits.mplot3d import Axes3D
from random import *
import scipy.integrate as si
import math
import os
import sympy
import socket

import Methods
from Methods import Functions
from Cosmological_Model import Model

H_0 = 70.0 #Km.s-1.Mpc-1
LightVelocity = 2.99792458*10**5.0 # Km.s-1

class ApparentMagnitude:
```

```python

def __init__(self, z, lambda_0, omega_0, M, Kcorrection, redsh_k, k_z):

    self.Kcorrection = Kcorrection
    self.redsh_k = redsh_k
    self.k_z = k_z

    self.param = Functions(lambda_0, omega_0)
    self.z = z
    self.M = M
    self.cosmoModel = Model(lambda_0, omega_0)
    self.d_L = self.cosmoModel.curvature(self.z, lambda_0, omega_0, M)[2]
    self.comobileDistance = self.cosmoModel.curvature(self.z, lambda_0, omega_0, M)[0]
    #---------K-correction----
    if self.Kcorrection == 'Kcorrection_OK':

      dkcorr = []

      for i in range(len(redsh_k)):
        if i==0 or i==(len(redsh_k)-1):
          dkcorr.append(k_z[i])
        else:
          dkcor = (k_z[i+1] - k_z[i-1])/(redsh_k[i+1] - redsh_k[i-1])
          dkcorr.append(dkcor)

      dkcorr = array(dkcorr)

      d_kcorr = []
      kcorr = []
      for i in range(len(self.z)):
        k_cor = Functions(lambda0, omega0).Nonlinear_Interpolation(k_z, redsh_k, self.z[i])
        kcorr.append(k_cor)

      for i in range(len(self.z)):
        d_k_cor = Functions(lambda0, omega0).Nonlinear_Interpolation(dkcorr, redsh_k, self.z[i])
        d_kcorr.append(d_k_cor)

      #alfa_nu = -0.5

      #self.kcorr = kcorr_con + kcorr_em
      self.kcorr = array(kcorr)

      self.d_kcorr = array(d_kcorr)
                #-----------------------
    elif self.Kcorrection == 'Kcorrection_NO':
      pass
```

```
    else:
      print "You must determine the condition of the Kcorrection as 'Kcorrection_OK' or 'Kcorrection_NO'. ", "\n"
    #-------------------------

  def m_theor(self, z, lambda_0, omega_0, M):

    if self.Kcorrection == 'Kcorrection_OK':

      m_theorie = self.M + 5.*np.log10(self.d_L/10.0) + self.kcorr

    elif self.Kcorrection == 'Kcorrection_NO':

      m_theorie = self.M + 5.*np.log10(self.d_L/10.0)

    else:
      print "You must determine the condition of the Kcorrection as 'Kcorrection_OK' or 'Kcorrection_NO'. ", "\n"

    return m_theorie


  #============Jacobian_1============


  def Jacobian(self, z):

    if self.Kcorrection == 'Kcorrection_OK':

      tau = self.comobileDistance

      if self.param.kappa_0 == 0.0:
        jac_1 = (1./(tau**2.))*( (1. + self.z)*sqrt(self.param.P(1./(1. + self.z))) + (1./tau) + self.d_kcorr*sqrt(self.param.P(1./(1. + self.z)))*(1. + self.z)**2. )


      elif self.param.kappa_0 > 0.0:

        epsilon = 2*tau*sqrt(self.param.kappa_0)

                                jac_1 = ((1. + self.z)*sqrt(self.param.P(1./(1. + self.z))) + (sqrt(self.param.kappa_0)/((sin(epsilon/2.0))/cos(epsilon/2.0) ) ) + ((((1. + self.z)**2.)*sqrt(self.param.P(1./(1. + self.z))))*self.d_kcorr))/(1. - cos(epsilon))

      elif self.param.kappa_0 < 0.0 :
        epsilon = 2.*tau*sqrt(abs(self.param.kappa_0))

        jac_1 = ((1. + self.z)*sqrt(self.param.P(1./(1. + self.z))
```

```
) + (sqrt(abs(self.param.kappa_0))/tanh(epsilon/2.0)) + ((((1.
+ self.z)**2.)*sqrt(self.param.P(1./(1. + self.z))))*self.
d_kcorr))/(cosh(epsilon) - 1.)

      else:
        pass


    elif self.Kcorrection == 'Kcorrection_NO':

      tau = self.comobileDistance

      if self.param.kappa_0 == 0.0:
        jac_1 = (1./(tau**3.))*( tau*(1. + self.z)*sqrt(self.param
.P(1./(1. + self.z))) + 1. )


      elif self.param.kappa_0 > 0.0:

        epsilon = 2*tau*sqrt(self.param.kappa_0)

        jac_1 = ((1. + self.z)*sqrt(self.param.P(1./(1. + self.z))
) + (sqrt(self.param.kappa_0)/((sin(epsilon/2.0))/cos(epsilon
/2.0) ) ))/(1. - cos(epsilon))


      elif self.param.kappa_0 < 0.0 :
        epsilon = 2.*tau*sqrt(abs(self.param.kappa_0))

        jac_1 = ((1. + self.z)*sqrt(self.param.P(1./(1. + self.z))
) + (sqrt(abs(self.param.kappa_0))/tanh(epsilon/2.0)))/(cosh(
epsilon) - 1.)


      else:
        pass
    else:
      print "You must determine the condition of the Kcorrection
as 'Kcorrection_OK' or 'Kcorrection_NO'. ", "\n"

    return jac_1

#=======Weighting factor==========


  def Weightingfactor(self, z, beta):

    tau = self.comobileDistance

    if self.Kcorrection == 'Kcorrection_OK':

      if self.param.kappa_0 == 0.0:
```

```
        weighing = self.Jacobian(z)*( ((1. + z)*tau*10.**(self.kcorr))**beta )

      elif self.param.kappa_0 > 0.0:
        epsilon = tau*sqrt(self.param.kappa_0)
        weighing = self.Jacobian(z)*( ((1. + z)*abs(sin(epsilon))*10.**(self.kcorr)/sqrt(self.param.kappa_0))**beta )

      elif self.param.kappa_0 < 0.0 :
        epsilon = tau*sqrt(abs(self.param.kappa_0))
        weighing = self.Jacobian(z)*( ((1. + z)*sinh(epsilon)*10.**(self.kcorr)/sqrt(abs(self.param.kappa_0)))**beta )
      else:
        pass


    elif self.Kcorrection == 'Kcorrection_NO':

      if self.param.kappa_0 == 0.0:
        weighing = self.Jacobian(z)*( ((1. + z)*tau)**beta )


      elif self.param.kappa_0 > 0.0:

        epsilon = tau*sqrt(self.param.kappa_0)
        weighing = self.Jacobian(z)*( ((1. + z)*sin(epsilon)/sqrt(self.param.kappa_0))**beta )

      elif self.param.kappa_0 < 0.0 :

        epsilon = tau*sqrt(abs(self.param.kappa_0))
        weighing = self.Jacobian(z)*( ((1. + z)*sinh(epsilon)/sqrt(abs(self.param.kappa_0)))**beta )
      else:
        pass

    else:
      print "You must determine the condition of the Kcorrection as 'Kcorrection_OK' or 'Kcorrection_NO'. ", "\n"

    return weighing


  def VOLUME(self, M, zz, ZETA, m_l):

    z_l = self.param.Nonlinear_Interpolation(zz, ZETA, m_l - M)

    if self.param.kappa_0 == 0.0:
      mu = M + 5*log10(((LightVelocity*10**6.0)/(10.*H_0)))
      if self.Kcorrection == 'Kcorrection_OK':
        V = (4.*pi/3.)*((1/(1. + z_l))**3.)*10**(3.*(m_l - mu - self.kcorr)/5.)
```

```
      elif self.Kcorrection == 'Kcorrection_NO':
        V = (4.*pi/3.)*((1/(1. + z_l))**3.)*10**(3.*(m_l - mu)/5.)
      else:
        print "You must determine the condition of the Kcorrection as 'Kcorrection_OK' or 'Kcorrection_NO'. ", "\n"

    elif self.param.kappa_0 > 0.0:

      mu = M + 5*log10(((LightVelocity*10**6.0)/(10.*H_0)))

      if self.Kcorrection == 'Kcorrection_OK':

        alfa_l = (sqrt(self.param.kappa_0)/(1 + z_l))*(10**((m_l - mu - self.kcorr)/5.))
      elif self.Kcorrection == 'Kcorrection_NO':

        alfa_l = (sqrt(self.param.kappa_0)/(1 + z_l))*(10**((m_l - mu)/5.))
      else:
        print "You must determine the condition of the Kcorrection as 'Kcorrection_OK' or 'Kcorrection_NO'. ", "\n"

      V = (pi/self.param.kappa_0**(3./2))*(2*arcsin(alfa_l) - 2*alfa_l*sqrt(1 - alfa_l**2.))

    elif self.param.kappa_0 < 0.0 :

      mu = M + 5*log10(((LightVelocity*10**6.0)/(10.*H_0)))
      alfa_l = (sqrt(abs(self.param.kappa_0))/(1 + z_l))*(10**((m_l - mu)/5.))

      if self.Kcorrection == 'Kcorrection_OK':

        alfa_l = (sqrt(abs(self.param.kappa_0))/(1 + z_l))*(10**((m_l - mu - self.kcorr)/5.))
      elif self.Kcorrection == 'Kcorrection_NO':

        alfa_l = (sqrt(abs(self.param.kappa_0))/(1 + z_l))*(10**((m_l - mu)/5.))
      else:
        print "You must determine the condition of the Kcorrection as 'Kcorrection_OK' or 'Kcorrection_NO'. ", "\n"

      V = (pi/abs(self.param.kappa_0)**(3./2))*(2*alfa_l*sqrt(1 + alfa_l**2.) - 2*arcsinh(alfa_l))

    else:
      pass

    return V

```

```
class Model:

  def __init__(self, lambda_0, omega_0):

    self.param = Functions(lambda_0, omega_0)

  def curvature(self, z, lambda_0, omega_0, M):

    zz = self.param.LowerBound(z)
    comobileDistance = self.param.Trapeze(self.param.FunctiontoIntegrate, zz, 1.0)
    lookback_time = self.param.Trapeze(self.param.FunctiontoIntegrate2, zz, 1.0)
    if self.param.kappa_0 > 0.0:

      epsilon = comobileDistance*sqrt(self.param.kappa_0)
      volume = pi*(2.0*epsilon - sin(2.0*epsilon))/(self.param.kappa_0**(3./2.))
      d_L = (LightVelocity*10**6.0)*(1. + z)*(sin(epsilon))/(H_0*sqrt(self.param.kappa_0))


    elif self.param.kappa_0 < 0.0:

      epsilon = comobileDistance*sqrt(-self.param.kappa_0)
      volume = pi*(sinh(2.0*epsilon) - 2.0*epsilon)/((-self.param.kappa_0)**(3./2.))

      d_L = (LightVelocity*10**6.0)*(1. + z)*sinh(epsilon)/(H_0*sqrt(-self.param.kappa_0))

    elif self.param.kappa_0 == 0.0:

      volume = 4.*pi*(comobileDistance**3.0)/3.

      d_L = (LightVelocity*10**6.0)*(1. + z)*comobileDistance/H_0
    else:

      pass


    return comobileDistance, volume, d_L, lookback_time




class SIMULATED:

  def __init__(self, lambda_0, omega_0):

```

```
    self.param = Functions(lambda_0, omega_0)

  def Sample(self, M_0, sigma, m_lim, zform, z_max, z_min,
   Sizeofsample, NumbOfSamples, Kcorrection, redsh_k, k_z):

    lambda0, omega0 = self.param.lambda_0, self.param.omega_0
    kappa0 = self.param.kappa_0
    print "kappa0 = ", kappa0, "\n"
    print Functions(lambda0, omega0).NoBigBang(omega0, 'permission
   ')

    Betalist = linspace(np.float64(0.01), np.float64(6), 600)
    Beta = array([array([a]) for a in Betalist])

    #==========K-correction======

          t = asc.read('/SDSS-DR3/K-correction.dat', guess=False)

    #redsh_k, k_z = t['redsh'], t['kcorre']

    dkcorr = []

    for i in range(len(redsh_k)):
      if i==0 or i==(len(redsh_k)-1):
        dkcorr.append(k_z[i])
      else:
        dkcor = (k_z[i+1] - k_z[i-1])/(redsh_k[i+1] - redsh_k[i
   -1])
        dkcorr.append(dkcor)

    dkcorr = array(dkcorr)

    zz = np.linspace(z_min, zform, 10**4)
    if Kcorrection == 'Kcorrection_NO':
      redsh_k_l, k_z_l = [], []
      pass
    elif Kcorrection == 'Kcorrection_OK':
      List_of_Poly = []
      for i in range(int(len(t['kcorre'])/5)):
          j = i*5
          fit4 = np.polyfit(t['redsh'][j:j+5+1], t['kcorre'][j:j
   +5+1], int(len(t['kcorre'][j:j+5+1])))
          fit_fn = np.poly1d(fit4)
          List_of_Poly.append((min(t['redsh'][j:j+5+1]), max(t['
   redsh'][j:j+5+1]), fit_fn))

      def Fit_of_Kcorrection(List_of_Poly, z):
        i = 0
        Condition = z>List_of_Poly[i][1]
        while Condition == True and i<=len(List_of_Poly)-2:
          i = i+1
          Condition = z>List_of_Poly[i][1]
```

```
        if Condition == True:
          value = -0.2135964
        else:
          value = List_of_Poly[i][2](z)
        return value

      redsh_k_l = []

      for i in range(len(zz)):
          if i==0 or i==(len(zz)-1):
        redsh_k_l.append(Fit_of_Kcorrection(List_of_Poly, zz[i]))
          else:
        redsh_k_l.append((Fit_of_Kcorrection(List_of_Poly, zz[i+1])-Fit_of_Kcorrection(List_of_Poly, zz[i-1]))/(zz[i+1]-zz[i-1]))

      redsh_k_l = array(redsh_k_l)

      k_z_l = []

      for i in range(len(zz)):
        k_z_l.append(Fit_of_Kcorrection(List_of_Poly, zz[i]))

      k_z_l = array(k_z_l)
    else:
      print "You must determine the condition of the Kcorrection as 'Kcorrection_OK' or 'Kcorrection_NO'. ", "\n"
    #==========================

    ZETA = ApparentMagnitude(zz, lambda0, omega0, 0.0, Kcorrection, redsh_k_l, k_z_l).m_theor(zz, lambda0, omega0, 0.0)

    paths_of_samples = []

    for bb in range(0, NumbOfSamples):

      Number_of_simulation = bb

      m_app = []
      redshift = []
      redred  = []

      Mlist, Volume, Volume_l, redshift_l = [], [], [], []

      HH = np.random.uniform(low=0.0, high=1, size=(Sizeofsample))
      Mlist1 = linspace(-30, -22., 2*Sizeofsample)

      F_M = []

      F_th = quad(Functions(lambda0, omega0).Pro_DensityFunction, -70, 70, args=(z_min, m_lim, M0, sigma))[0]
      for i in range(2*Sizeofsample):
```

```
        z_l = Functions(lambda0, omega0).Nonlinear_Interpolation(zz, ZETA, m_lim - Mlist1[i])
        f_M = quad(Functions(lambda0, omega0).Pro_DensityFunction, -70, Mlist1[i], args=(z_l, m_lim, M0, sigma))[0]

        F_M.append(f_M)

      F_M = array(F_M)/F_th
      #F_M = array(F_M)/max(F_M)

      for i in range(Sizeofsample):
        F_cap = np.random.uniform(low=0.0, high=1, size=(1))[0]
        M_k = Functions(lambda0, omega0).Nonlinear_Interpolation(Mlist1, F_M, F_cap)
        Mlist.append(M_k)

      Mlist = array(Mlist)
      plt.hist(Mlist, bins=50, histtype='step', normed=False, color='r')
      plt.show()

      #================

      if Kcorrection == 'Kcorrection_NO':

        if kappa0 > 0:

          Angular_distance = Model(lambda0, omega0).curvature(np.linspace(z_min, 1100, 10**4), lambda0, omega0, 0.0)[0]*sqrt(kappa0)
          z_pi = Functions(lambda0, omega0).Nonlinear_Interpolation(np.linspace(z_min, 1100, 10**4), Angular_distance, pi)
          zz = np.linspace(z_min, z_pi, 10**4)
          ZETA_pi = ApparentMagnitude(zz, lambda0, omega0, 0, Kcorrection, 0, 0).m_theor(zz, lambda0, omega0, 0)

          M_star = m_lim - max(ZETA_pi)
          ZETA_form = ApparentMagnitude(z_pi, lambda0, omega0, 0.0, Kcorrection, 0, 0).m_theor(z_pi, lambda0, omega0, 0.0)
          M_form = m_lim - ZETA_form

          for ii in range(Sizeofsample):
            M_k = Mlist[ii]
            mu_lim = m_lim - M_k

            if M_k>M_star and M_k<M_form:

              ZETA_jj = ZETA*1.0
              zz_jj = zz*1.0
              z_l_jj = []
              for jj in range(10):
```

```
                z_ljj = Functions(lambda0, omega0).Nonlinear_Interpolation(zz_jj, ZETA_jj, mu_lim)
                z_l_jj.append(z_ljj)
                index_of_mu_lim = list(abs(ZETA_jj - mu_lim)).index(min(abs(ZETA_jj - mu_lim)))
                ZETA_jj = list(ZETA_jj*1)
                zz_jj = list(zz_jj*1)
                ZETA_jj.remove(ZETA_jj[index_of_mu_lim])
                zz_jj.remove(zz_jj[index_of_mu_lim])
                ZETA_jj = array(ZETA_jj*1)
                zz_jj = array(zz_jj*1)

            z_l_jj = array(z_l_jj)
            z_l_jj.sort()
            Distanguish_of_solutions = [str(gg)[0:5] for gg in z_l_jj]
            z_l_l = []
            z_l_l.append(z_l_jj[0])
            for i in range(1, len(z_l_jj)-1):
                condition = (Distanguish_of_solutions[i]==Distanguish_of_solutions[i-1])
                if condition == False:
                    z_l_l.append(z_l_jj[i])
                else:
                    pass

            Distanguish_of_solutions = [str(gg)[0:4] for gg in z_l_l]
            z_l = []
            z_l.append(z_l_l[0])
            for i in range(1, len(z_l_l)):
                condition1 = (Distanguish_of_solutions[i]==Distanguish_of_solutions[i-1])
                condition2 = (abs(float(Distanguish_of_solutions[i]) - float(Distanguish_of_solutions[i-1]))>= 0.06)
                if condition1 == False and condition2 == True:
                    z_l.append(z_l_l[i])
                else:
                    pass

            if (len(z_l) % 2 == 0): #even
                print "len(z_l)", len(z_l)
                z_l.append(zform)
                z_l.sort()
                z_l = array(z_l)
                Volume_list = list(Model(lambda0, omega0).curvature(z_l, lambda0, omega0, 0.0)[1])
                V_l = Volume_list[0]
                RandomChoiceList_of_Volume = []
                for i in range(1, int((len(Volume_list)-1)/2)+1):
                    V_l += Volume_list[2*i] - Volume_list[2*i-1]

```

```
                Volume_l.append(V_l)

                ZoneProhibited_of_Volume = []
                ZoneProhibited_of_redshift = []
                for i in range(int(len(Volume_list)/2)):
                  ZoneProhibited_of_Volume.append((Volume_list[2*i], Volume_list[2*i+1]))
                  ZoneProhibited_of_redshift.append((z_l[2*i], z_l[2*i+1]))

                HH_list = []
                condition_on_HH = (len(HH_list) == 0)
                ij = -1
                V_z_list = []
                condition_on_V_z = (len(V_z_list) == 0)
                while condition_on_V_z == True and condition_on_HH == True:
                  ij = ij + 1
                  if ij > len(HH)-1:
                    break
                  else:
                    V_K = HH[ij]*V_l
                    V_z = V_K
                    RandomChoiceList_of_Volume.append(V_z)
                    for i in range(len(Volume_list)-1):
                      if (i % 2 == 0):
                        V_z += - Volume_list[i]
                      else:
                        V_z += Volume_list[i]
                        RandomChoiceList_of_Volume.append(V_z)

                    for dd in range(len(RandomChoiceList_of_Volume)):
                      V_z = RandomChoiceList_of_Volume[dd]

                      for i in range(len(ZoneProhibited_of_Volume)):
                        condition = (V_z > min(ZoneProhibited_of_Volume[i]) and V_z < max(ZoneProhibited_of_Volume[i]))
                        if condition == True:
                          continue
                        else:
                          if V_z > max(ZoneProhibited_of_Volume[i]):
                            continue
                          else:
                            V_z_list.append(V_z)
                            HH_list.append(HH[ij])
                            HH.remove(HH[ij])
                            break
                      condition_on_HH = (len(HH_list) == 0)
```

```
                        condition_on_V_z = (len(V_z_list) == 0)
                        if condition_on_V_z == True and condition_on_HH == True:
                          continue
                        else:
                          pass

                        V_z = V_z_list[0]
                        Volume.append(V_z)
                        Mlistlist.append(Mlist[ii])

                else: #odd
                  z_l.sort()
                  z_l = array(z_l)
                  Volume_list = list(Model(lambda0, omega0).curvature(z_l, lambda0, omega0, 0.0)[1])
                  V_l = Volume_list[0]
                  RandomChoiceList_of_Volume = []
                  for i in range(1, int((len(Volume_list)-1)/2)+1):
                    V_l += Volume_list[2*i] - Volume_list[2*i-1]

                  Volume_l.append(V_l)

                  ZoneProhibited_of_Volume = []
                  ZoneProhibited_of_redshift = []
                  for i in range(int(len(Volume_list)/2)):
                    ZoneProhibited_of_Volume.append((Volume_list[2*i], Volume_list[2*i+1]))
                    ZoneProhibited_of_redshift.append((z_l[2*i], z_l[2*i+1]))

                  HH_list = []
                  condition_on_HH = (len(HH_list) == 0)
                  ij = -1
                  V_z_list = []
                  condition_on_V_z = (len(V_z_list) == 0)
                  while condition_on_V_z == True and condition_on_HH == True:
                    ij = ij + 1
                    if ij > len(HH)-1:
                      break
                    else:
                      V_K = HH[ij]*V_l
                      V_z = V_K
                      RandomChoiceList_of_Volume.append(V_z)
                      for i in range(len(Volume_list)-1):
                        if (i % 2 == 0):
                          V_z += - Volume_list[i]
                        else:
                          V_z += Volume_list[i]
                          RandomChoiceList_of_Volume.append(V_z)

```

```
                    for dd in range(len(RandomChoiceList_of_Volume)):
                      V_z = RandomChoiceList_of_Volume[dd]

                      for i in range(len(ZoneProhibited_of_Volume)):
                        condition = (V_z > min(ZoneProhibited_of_Volume[i]) and V_z < max(ZoneProhibited_of_Volume[i]))
                        if condition == True:
                          continue
                        else:
                          if V_z > max(ZoneProhibited_of_Volume[i]):
                            continue
                          else:
                            V_z_list.append(V_z)
                            HH_list.append(HH[ij])
                            HH.remove(HH[ij])
                            break
                      condition_on_HH = (len(HH_list) == 0)
                      condition_on_V_z = (len(V_z_list) == 0)
                      if condition_on_V_z == True and condition_on_HH == True:
                        continue
                      else:
                        pass

                      V_z = V_z_list[0]
                      Volume.append(V_z)
                      Mlistlist.append(Mlist[ii])


          else:

            z_l = Functions(lambda0, omega0).Nonlinear_Interpolation(zz, ZETA, mu_lim)
            redshift_l.append(z_l)
            V_l = Model(lambda0, omega0).curvature(z_l, lambda0, omega0, 0.0)[1]
            Volume_l.append(V_l)
            V_K = HH[ii]*V_l
            Volume.append(V_K)
            Mlistlist.append(Mlist[ii])

      else:
        for ii in range(Sizeofsample):
          M_k = Mlist[ii]
          mu_lim = m_lim - M_k

          z_l = Functions(lambda0, omega0).Nonlinear_Interpolation(zz, ZETA, mu_lim)
```

```
            redshift_l.append(z_l)
            V_l = Model(lambda0, omega0).curvature(z_l, lambda0, omega0, 0.0)[1]
            Volume_l.append(V_l)
            V_K = HH[ii]*V_l
            Volume.append(V_K)
            Mlistlist.append(Mlist[ii])

      elif Kcorrection == 'Kcorrection_OK':

        if kappa0 > 0:

          Angular_distance = Model(lambda0, omega0).curvature(np.linspace(z_min, 1100, 10**4), lambda0, omega0, 0.0)[0]*sqrt(kappa0)
          z_pi = Functions(lambda0, omega0).Nonlinear_Interpolation(np.linspace(z_min, 1100, 10**4), Angular_distance, pi)

          M_star = m_lim - max(ZETA)
          k_z_zform = Fit_of_Kcorrection(List_of_Poly,zform)
          ZETA_form = ApparentMagnitude(zform, lambda0, omega0, 0.0, Kcorrection, 0, k_z_zform).m_theor(zform, lambda0, omega0, 0.0)
          M_form = m_lim - ZETA_form

          for ii in range(Sizeofsample):
            M_k = Mlist[ii]
            mu_lim = m_lim - M_k

            if M_k>M_star and M_k<M_form:

              ZETA_jj = ZETA*1.0
              zz_jj = zz*1.0
              z_l_jj = []
              for jj in range(20):
                z_ljj = Functions(lambda0, omega0).Nonlinear_Interpolation(zz_jj, ZETA_jj, mu_lim)
                z_l_jj.append(z_ljj)
                index_of_mu_lim = list(abs(ZETA_jj - mu_lim)).index(min(abs(ZETA_jj - mu_lim)))
                ZETA_jj = list(ZETA_jj*1)
                zz_jj = list(zz_jj*1)
                ZETA_jj.remove(ZETA_jj[index_of_mu_lim])
                zz_jj.remove(zz_jj[index_of_mu_lim])
                ZETA_jj = array(ZETA_jj*1)
                zz_jj = array(zz_jj*1)

              z_l_jj = array(z_l_jj)
              z_l_jj.sort()
              Distanguish_of_solutions = [str(gg)[0:5] for gg in z_l_jj]
```

```
            z_l_l = []
            z_l_l.append(z_l_jj[0])
            for i in range(1, len(z_l_jj)-1):
              condition = (Distanguish_of_solutions[i]==
Distanguish_of_solutions[i-1])
              if condition == False:
                z_l_l.append(z_l_jj[i])
              else:
                pass

            Distanguish_of_solutions = [str(gg)[0:4] for gg in
z_l_l]
            z_l = []
            z_l.append(z_l_l[0])
            for i in range(1, len(z_l_l)):
              condition1 = (Distanguish_of_solutions[i]==
Distanguish_of_solutions[i-1])
              condition2 = (abs(float(Distanguish_of_solutions[i
]) - float(Distanguish_of_solutions[i-1]))>= 0.06)
              if condition1 == False and condition2 == True:
                z_l.append(z_l_l[i])
              else:
                pass

            if (len(z_l) % 2 == 0): #even

              print "len(z_l)", len(z_l)
              z_l.append(zform)
              z_l.sort()
              z_l = array(z_l)
              Volume_list = list(Model(lambda0, omega0).
curvature(z_l, lambda0, omega0, 0.0)[1])
              V_l = Volume_list[0]
              RandomChoiceList_of_Volume = []
              for i in range(1, int((len(Volume_list)-1)/2)+1):
                V_l += Volume_list[2*i] - Volume_list[2*i-1]

              Volume_l.append(V_l)

              ZoneProhibited_of_Volume = []
              ZoneProhibited_of_redshift = []
              for i in range(int(len(Volume_list)/2)):
                ZoneProhibited_of_Volume.append((Volume_list[2*i
], Volume_list[2*i+1]))
                ZoneProhibited_of_redshift.append((z_l[2*i], z_l
[2*i+1]))

              HH_list = []
              condition_on_HH = (len(HH_list) == 0)
              ij = -1
              V_z_list = []
              condition_on_V_z = (len(V_z_list) == 0)
```

```
                    while condition_on_V_z == True and condition_on_HH == True:
                      ij = ij + 1
                      if ij > len(HH)-1:
                        break
                      else:
                        V_K = HH[ij]*V_l
                        V_z = V_K
                        RandomChoiceList_of_Volume.append(V_z)
                        for i in range(len(Volume_list)-1):
                          if (i % 2 == 0):
                            V_z += - Volume_list[i]
                          else:
                            V_z += Volume_list[i]
                            RandomChoiceList_of_Volume.append(V_z)

                        for dd in range(len(RandomChoiceList_of_Volume)):
                          V_z = RandomChoiceList_of_Volume[dd]

                          for i in range(len(ZoneProhibited_of_Volume)):
                            condition = (V_z > min(ZoneProhibited_of_Volume[i]) and V_z < max(ZoneProhibited_of_Volume[i]))
                            if condition == True:
                              continue
                            else:
                              if V_z > max(ZoneProhibited_of_Volume[i]):
                                continue
                              else:
                                V_z_list.append(V_z)
                                HH_list.append(HH[ij])
                                HH.remove(HH[ij])
                                break
                          condition_on_HH = (len(HH_list) == 0)
                          condition_on_V_z = (len(V_z_list) == 0)
                          if condition_on_V_z == True and condition_on_HH == True:
                            continue
                          else:
                            pass

                          V_z = V_z_list[0]
                          Volume.append(V_z)
                          Mlistlist.append(Mlist[ii])

                else: #odd

                  print "len(z_l)", len(z_l)
                  z_l.sort()
```

```
                z_l = z_l[0]
                redshift_l.append(z_l)
                V_l = Model(lambda0, omega0).curvature(z_l, lambda0, omega0, 0.0)[1]
                Volume_l.append(V_l)
                V_K = HH[ii]*V_l
                Volume.append(V_K)
                Mlistlist.append(Mlist[ii])
            else:

              ZETA_jj = ZETA*1.0
              zz_jj = zz*1.0
              z_l_jj = []
              for jj in range(20):
                z_ljj = Functions(lambda0, omega0).Nonlinear_Interpolation(zz_jj, ZETA_jj, mu_lim)
                z_l_jj.append(z_ljj)
                index_of_mu_lim = list(abs(ZETA_jj - mu_lim)).index(min(abs(ZETA_jj - mu_lim)))
                ZETA_jj = list(ZETA_jj*1)
                zz_jj = list(zz_jj*1)
                ZETA_jj.remove(ZETA_jj[index_of_mu_lim])
                zz_jj.remove(zz_jj[index_of_mu_lim])
                ZETA_jj = array(ZETA_jj*1)
                zz_jj = array(zz_jj*1)

              z_l_jj = array(z_l_jj)
              z_l_jj.sort()
              Distanguish_of_solutions = [str(gg)[0:5] for gg in z_l_jj]
              z_l_l = []
              z_l_l.append(z_l_jj[0])
              for i in range(1, len(z_l_jj)-1):
                condition = (Distanguish_of_solutions[i]==Distanguish_of_solutions[i-1])
                if condition == False:
                  z_l_l.append(z_l_jj[i])
                else:
                  pass

              Distanguish_of_solutions = [str(gg)[0:4] for gg in z_l_l]
              z_l = []
              z_l.append(z_l_l[0])
              for i in range(1, len(z_l_l)):
                condition1 = (Distanguish_of_solutions[i]==Distanguish_of_solutions[i-1])
                condition2 = (abs(float(Distanguish_of_solutions[i]) - float(Distanguish_of_solutions[i-1]))>= 0.06)
                if condition1 == False and condition2 == True:
                  z_l.append(z_l_l[i])
                else:
```

```
                    pass

                if (len(z_l) % 2 == 0): #even
                  z_l = z_l[0]
                  redshift_l.append(z_l)
                  V_l = Model(lambda0, omega0).curvature(z_l, lambda0, omega0, 0.0)[1]
                  Volume_l.append(V_l)
                  V_K = HH[ii]*V_l
                  Volume.append(V_K)
                  Mlistlist.append(Mlist[ii])

                else: #odd

                  z_l.sort()
                  z_l = array(z_l)
                  Volume_list = list(Model(lambda0, omega0).curvature(z_l, lambda0, omega0, 0.0)[1])
                  V_l = Volume_list[0]
                  RandomChoiceList_of_Volume = []
                  for i in range(1, int((len(Volume_list)-1)/2)+1):
                    V_l += Volume_list[2*i] - Volume_list[2*i-1]

                  Volume_l.append(V_l)

                  ZoneProhibited_of_Volume = []
                  ZoneProhibited_of_redshift = []
                  for i in range(int(len(Volume_list)/2)):
                    ZoneProhibited_of_Volume.append((Volume_list[2*i], Volume_list[2*i+1]))
                    ZoneProhibited_of_redshift.append((z_l[2*i], z_l[2*i+1]))

                  HH_list = []
                  condition_on_HH = (len(HH_list) == 0)
                  ij = -1
                  V_z_list = []
                  condition_on_V_z = (len(V_z_list) == 0)
                  while condition_on_V_z == True and condition_on_HH == True:
                    ij = ij + 1
                    if ij > len(HH)-1:
                      break
                    else:
                      V_K = HH[ij]*V_l
                      V_z = V_K
                      RandomChoiceList_of_Volume.append(V_z)
                      for i in range(len(Volume_list)-1):
                        if (i % 2 == 0):
                          V_z += - Volume_list[i]
                        else:
                          V_z += Volume_list[i]
```

```
                        RandomChoiceList_of_Volume.append(V_z)

                    for dd in range(len(RandomChoiceList_of_Volume)):
                      V_z = RandomChoiceList_of_Volume[dd]

                      for i in range(len(ZoneProhibited_of_Volume)):
                        condition = (V_z > min(ZoneProhibited_of_Volume[i]) and V_z < max(ZoneProhibited_of_Volume[i]))
                        if condition == True:
                          continue
                        else:
                          if V_z > max(ZoneProhibited_of_Volume[i]):
                            continue
                          else:
                            V_z_list.append(V_z)
                            HH_list.append(HH[ij])
                            HH.remove(HH[ij])
                            break
                      condition_on_HH = (len(HH_list) == 0)
                      condition_on_V_z = (len(V_z_list) == 0)
                      if condition_on_V_z == True and condition_on_HH == True:
                        continue
                      else:
                        pass

                      V_z = V_z_list[0]
                      Volume.append(V_z)
                      Mlistlist.append(Mlist[ii])


        else:
          for ii in range(Sizeofsample):
            M_k = Mlist[ii]
            mu_lim = m_lim - M_k

            ZETA_jj = ZETA*1.0
            zz_jj = zz*1.0
            z_l_jj = []
            for jj in range(20):
              z_ljj = Functions(lambda0, omega0).Nonlinear_Interpolation(zz_jj, ZETA_jj, mu_lim)
              z_l_jj.append(z_ljj)
              index_of_mu_lim = list(abs(ZETA_jj - mu_lim)).index(min(abs(ZETA_jj - mu_lim)))
              ZETA_jj = list(ZETA_jj*1)
              zz_jj = list(zz_jj*1)
              ZETA_jj.remove(ZETA_jj[index_of_mu_lim])
```

```
                zz_jj.remove(zz_jj[index_of_mu_lim])
                ZETA_jj = array(ZETA_jj*1)
                zz_jj = array(zz_jj*1)

            z_l_jj = array(z_l_jj)
            z_l_jj.sort()
            Distanguish_of_solutions = [str(gg)[0:5] for gg in z_l_jj]
            z_l_l = []
            z_l_l.append(z_l_jj[0])
            for i in range(1, len(z_l_jj)-1):
                condition = (Distanguish_of_solutions[i]==Distanguish_of_solutions[i-1])
                if condition == False:
                    z_l_l.append(z_l_jj[i])
                else:
                    pass

            Distanguish_of_solutions = [str(gg)[0:4] for gg in z_l_l]
            z_l = []
            z_l.append(z_l_l[0])
            for i in range(1, len(z_l_l)):
                condition1 = (Distanguish_of_solutions[i]==Distanguish_of_solutions[i-1])
                condition2 = (abs(float(Distanguish_of_solutions[i]) - float(Distanguish_of_solutions[i-1]))>= 0.06)
                if condition1 == False and condition2 == True:
                    z_l.append(z_l_l[i])
                else:
                    pass

            if (len(z_l) % 2 == 0): #even
                z_l = z_l[0]
                redshift_l.append(z_l)
                V_l = Model(lambda0, omega0).curvature(z_l, lambda0, omega0, 0.0)[1]
                Volume_l.append(V_l)
                V_K = HH[ii]*V_l
                Volume.append(V_K)
                Mlistlist.append(Mlist[ii])
            else: #odd
                z_l.sort()
                z_l = array(z_l)
                Volume_list = list(Model(lambda0, omega0).curvature(z_l, lambda0, omega0, 0.0)[1])
                V_l = Volume_list[0]
                RandomChoiceList_of_Volume = []
                for i in range(1, int((len(Volume_list)-1)/2)+1):
                    V_l += Volume_list[2*i] - Volume_list[2*i-1]

                Volume_l.append(V_l)
```

```
            ZoneProhibited_of_Volume = []
            ZoneProhibited_of_redshift = []
            for i in range(int(len(Volume_list)/2)):
              ZoneProhibited_of_Volume.append((Volume_list[2*i], Volume_list[2*i+1]))
              ZoneProhibited_of_redshift.append((z_l[2*i], z_l[2*i+1]))

            HH_list = []
            condition_on_HH = (len(HH_list) == 0)
            ij = -1
            V_z_list = []
            condition_on_V_z = (len(V_z_list) == 0)
            while condition_on_V_z == True and condition_on_HH == True:
              ij = ij + 1
              if ij > len(HH)-1:
                break
              else:
                V_K = HH[ij]*V_l
                V_z = V_K
                RandomChoiceList_of_Volume.append(V_z)
                for i in range(len(Volume_list)-1):
                  if (i % 2 == 0): #even
                    V_z += - Volume_list[i]
                  else: #odd
                    V_z += Volume_list[i]
                    RandomChoiceList_of_Volume.append(V_z)

                  for dd in range(len(RandomChoiceList_of_Volume)):
                    V_z = RandomChoiceList_of_Volume[dd]

                    for i in range(len(ZoneProhibited_of_Volume)):
                      condition = (V_z > min(ZoneProhibited_of_Volume[i]) and V_z < max(ZoneProhibited_of_Volume[i]))
                      if condition == True:
                        continue
                      else:
                        if V_z > max(ZoneProhibited_of_Volume[i]):
                          continue
                        else:
                          V_z_list.append(V_z)
                          HH_list.append(HH[ij])
                          HH.remove(HH[ij])
                          break
                    condition_on_HH = (len(HH_list) == 0)
                    condition_on_V_z = (len(V_z_list) == 0)
```

```
                        if condition_on_V_z == True and condition_on_HH == True:
                          continue
                        else:
                          pass

                        V_z = V_z_list[0]
                        Volume.append(V_z)
                        Mlistlist.append(Mlist[ii])

      else:
        print "You must determine the condition of the Kcorrection as 'Kcorrection_OK' or 'Kcorrection_NO'. ", "\n"


      Mlistlist = np.asarray(Mlistlist)
      Mlist = Mlistlist*1.0
      Volume = np.asarray(Volume)

      Mlist_second = []
      Volume_second = []
      Volume_l_second = []
      redshift_l_second = []
      V = Model(lambda0, omega0).curvature(zz, lambda0, omega0, 0.0)[1]
      for ii in range(Sizeofsample):

        red = Functions(lambda0, omega0).Nonlinear_Interpolation(zz, V, Volume[ii])
        redshift.append(red)
        redred.append(red)
        Mlist_second.append(Mlist[ii])

      Mlist = array(Mlist_second)
      Sizeofsample = len(redshift)
      redshift = array(redshift)
      #======K-corrections======
      if Kcorrection == 'Kcorrection_NO':
        redsh_k, k_z = [0]*Sizeofsample, [0]*Sizeofsample
        pass
      elif Kcorrection == 'Kcorrection_OK':
        redsh_k, k_z =  t['kcorre'], t['redsh']
        kcorr = []
        d_kcorr = []
        for i in range(len(redshift)):
          #print i
          k_cor = Functions(lambda0, omega0).Nonlinear_Interpolation(t['kcorre'], t['redsh'], redshift[i])
          kcorr.append(k_cor)

        for i in range(len(redshift)):
          d_k_cor = Functions(lambda0, omega0).
```

```
Nonlinear_Interpolation(dkcorr, t['redsh'], redshift[i])
        d_kcorr.append(d_k_cor)


      kcorr = array(kcorr)
      d_kcorr = array(d_kcorr)

    else:
      print "You must determine the condition of the Kcorrection as 'Kcorrection_OK' or 'Kcorrection_NO'. ", "\n"
    #==========================

    m_app = ApparentMagnitude(redshift, lambda0, omega0, Mlist, Kcorrection, redsh_k, k_z).m_theor(redshift, lambda0, omega0, Mlist)

    #==========================
    redred.sort()
    Mlist = np.asarray(Mlist)
    m_app = np.asarray(m_app)
    redred = np.asarray(redred)
    redshift = np.asarray(redshift)

    print "max(redshift) = ", max(redshift)
    print "max(m_app) = ", max(m_app)

    Mlist1 = Mlist*1.0
    m_app1 = m_app*1.0
    Mlist1.sort()
    m_app1.sort()

    #=====weighting factor====
    WeightingManifold = ApparentMagnitude(redshift, lambda0, omega0, 0.0, Kcorrection, redsh_k, k_z).Weightingfactor(redshift, Beta)

    WeightingSum = [a/sum(a) for a in WeightingManifold]
    DetermineBeta = [abs(max(b) - min(b)) for b in WeightingSum]
    beta = Beta[DetermineBeta.index(min(DetermineBeta))][0]
    Weighting = ApparentMagnitude(redshift, lambda0, omega0, 0.0, Kcorrection, redsh_k, k_z).Weightingfactor(redshift, beta)

    SumWeighting = sum(Weighting)
    factorWeighting = array(Weighting)/SumWeighting
    #==========================

    #=======saving data=====

    filename = 'SimulationData_'+str(lambda0)+'-'+str(omega0)+'_NbOfObjects'+str(Sizeofsample)+'_limitMag'+str(m_lim)+'_NbOfSimulation'+str(Number_of_simulation)+'Beta'+str(beta)+'.dat'
```

```
        listofarrays = [Mlist, m_app, redshift, redshift_l, Volume, Volume_l, Weighting, factorWeighting, redred, z1, redsh_k, k_z]
        stringlistofarrays = ['Mlist', 'm_app', 'redshift', 'redshift_l', 'Volume', 'Volume_l', 'Weighting', 'factorWeighting', 'redred', 'z1', 'redsh_k', 'k_z']

        Save(listofarrays, stringlistofarrays, filename).ReadWrite(True, 'work')
        path = Save(listofarrays, stringlistofarrays, filename).ReadWrite(True, 'work')
        paths_of_samples.append(path)
        #=========================
        print "Number_of_simulation = ", Number_of_simulation, "\n"
        print "path = ", path, "\n"

    return paths_of_samples


class NullCorrelation:
  """NullCorrelation Method to seek the cosmological parameters"""
  def __init__(self):
    #self, Booleen
    #self.Booleen = Booleen
    pass


  def SeekOfParameters(self, m_app, redshift, lambda0_Model, omega0_Model, couleur, Kcorrection, redsh_k, k_z):


    omegalist = linspace(np.float64(10**-6), np.float64(1.0), 30) #20
    lamdalist = linspace(np.float64(10**-6), np.float64(1.5), 30) #20
    #omegalist = linspace(np.float64(10**-6), np.float64(0.2), 50) #20
    #lamdalist = linspace(np.float64(1.0), np.float64(1.4), 50) #20

    Betalist = linspace(np.float64(0.01), np.float64(3.9), 150)
    #Betalist = linspace(np.float64(0.01), np.float64(3.9), 100)

    Beta = array([array([a]) for a in Betalist])
    All_models = []

    for i in range(len(lamdalist)):
        for j in range(len(omegalist)):
          All_models.append((lamdalist[i], omegalist[j]))


    def func(a, z, bet):      # a = All_models;  z = redhsift;  bet
```

```
= Beta
    aa=[]

    for i in range(len(a)):

        Bounced_limit = Functions(a[i][0],a[i][1]).NoBigBang(a[i][1], 'permission')

        if Bounced_limit==0:
            aa.append(int(0))
        else:

            WeightingManifold = ApparentMagnitude(z, a[i][0],a[i][1], 0.0, Kcorrection, redsh_k, k_z).Weightingfactor(z, bet) # a[i][0],a[i][1] = (lamda, omega)
            WeightingSum = [b/sum(b) for b in WeightingManifold]
            DetermineBeta = [abs(max(b) - min(b)) for b in WeightingSum]
            beta = Beta[DetermineBeta.index(min(DetermineBeta))][0]
            #L_1_Manifold = [1.0 + (1./np.log(len(b))*sum(b*np.log(b))) for b in WeightingSum]
            #beta = Beta[L_1_Manifold.index(min(L_1_Manifold))][0]

            w_k = ApparentMagnitude(z, a[i][0],a[i][1], 0.0, Kcorrection, redsh_k, k_z).Weightingfactor(z, beta)/sum(ApparentMagnitude(z, a[i][0],a[i][1], 0.0, Kcorrection, redsh_k, k_z).Weightingfactor(z, beta))
            Mlist_tild = m_app - ApparentMagnitude(z, a[i][0],a[i][1], 0.0, Kcorrection, redsh_k, k_z).m_theor(z, a[i][0],a[i][1], 0.0)

            COVA_riance = sum(w_k*(Mlist_tild - sum(w_k*Mlist_tild))*(m_app - sum(w_k*m_app)))
            COR_elation = (1./(sqrt(sum(w_k*(Mlist_tild - sum(w_k*Mlist_tild))**2.0))*sqrt(sum(w_k*(m_app - sum(w_k*m_app))**2.0))))*COVA_riance
            #COR_elation = COVA_riance
            aa.append(COR_elation)

            #aa.append((w_k, Mlist_tild))
            """
            plt.figure(4)
            z2 = z*1.0
            z2.sort()
            ww = ApparentMagnitude(z2, a[i][0],a[i][1], 0.0).Weightingfactor(z2, beta, 0.0)
            wk = ww/sum(ww)
            plt.plot(z2, len(z2)*wk)

            plt.figure(5)
            L_1 = 1.0 + (1./np.log(len(wk))*sum(wk*np.log(wk)))
            plt.plot(a[i][0], L_1, marker='+', color='g')
```

```
            plt.plot(a[i][1], L_1, marker='+', color='r')

            plt.figure(6)
            V = Model(a[i][0], a[i][1]).curvature(z2, a[i][0],a[i][1], 0.0)[1]
            plt.plot(z2, V)
            """
        return aa




    Cov_All_Models = func(All_models,redshift , Beta)

    #print "Cov_All_Models = ", Cov_All_Models, "\n"
    print "len(Cov_All_Models) = ", len(Cov_All_Models), "\n"

    print "len(All_models) = ", len(All_models), "\n"

    All_models = np.asarray(All_models)
    Cov_All_Models = np.asarray(Cov_All_Models)

    #***********grid of covariance****************
    # figure of 3D(surface)

    #All_models[:,0] is a liste of lamda
    #All_models[:,1] is a liste of omega

    fig = plt.figure(7)
    ax = fig.add_subplot(111)

    col = plt.scatter(All_models[:,1], All_models[:,0], marker='.', s=150, c=Cov_All_Models, linewidths=0.3, cmap=plt.cm.Spectral_r)
    #for vv, ww, dd in zip(All_models[:,1], All_models[:,0], Cov_All_Models):
    # pl.text(vv, ww, '%.2f' % dd, ha='center', va='bottom')
    plt.plot([omega0_Model],[lambda0_Model], marker='o', color='m')

    # Add a colourbar.
    #cax = fig.colorbar(col, orientation='vertical',format='%.30f')
    cax = fig.colorbar(col, orientation='vertical',format='%.2f')
    cax.set_label('Covariance')

    plt.xlabel('$\\Omega_{\\circ}$', fontsize=14)
    plt.ylabel('$\\lambda_{\\circ}$', fontsize=14)

    #============For the save of the data================
    OmegaOfGrid = All_models[:,1]*1.0
    LambdaOfGrid = All_models[:,0]*1.0
```

```
    CorrCoefficient = Cov_All_Models*1.0
    #==========================================================


    #plt.figure(8)
    #for i in range(len(Cov_All_Models)):
    # plt.plot(Cov_All_Models[i], All_models[i][0], marker='o', color='r')

    #n, bins, patches = plt.hist(Cov_All_Models,40,normed='True')
    #(mu_hist, sigma_hist) = norm.fit(array(Cov_All_Models))
    #y = mlab.normpdf( bins, mu_hist, sigma_hist)
    #plt.plot(bins, y, 'r--', linewidth=2)
    #plt.title(r'$\rho_{0}=%.7f,\ \sigma_{0}=%.3f$' %(mu_hist, sigma_hist), color='r')
    #plt.xlabel('Correlation coefficient', fontsize=14)

    #*************************************

    Covariance_Vert = []
    Covariance_Hor = []

    omega0Covariance_Vert = []
    lambda0Covariance_Vert = []
    q0Covariance_Vert = []

    omega0Covariance_Hor = []
    lambda0Covariance_Hor = []
    q0Covariance_Hor = []

    # make the array as matrix to search the null correlation curve on the grid!
    Cov_All_Models = Cov_All_Models.reshape(int(sqrt(len(All_models[:,1]))), int(sqrt(len(All_models[:,0]))))

    All_modelslambda = All_models[:,0].reshape(int(sqrt(len(All_models[:,0]))), int(sqrt(len(All_models[:,0])))) # For matrix of lambda
    All_modelsomega = All_models[:,1].reshape(int(sqrt(len(All_models[:,1]))), int(sqrt(len(All_models[:,0])))) # For matrix of omega

    #To make the contours of confidence levels
    #CS = pl.contour(All_modelsomega, All_modelslambda, abs(Cov_All_Models), 3, linewidths=np.arange(.5, 4, .5), colors=('r', 'green', 'blue', (1,1,0), '#afeeee', '0.5'))
    #plt.clabel(CS, inline=1, fontsize=10)
    #plt.show()

    #search of covariance zero by HORIZONTAL interpolation
    for i in range(len(omegalist)):
      #----------------
```

```
        Condition_1 = any(Cov_All_Models[i] == 0.0)
        if Condition_1 == True:
          rr = Cov_All_Models[i]
          bb = All_modelsomega[i]
          while Condition_1 == True:
            rr = list(rr)
            bb = list(bb)

            bb.remove(bb[rr.index(0.0)])
            rr.remove(0.0)

            rr = array(rr)
            bb = array(bb)

            Condition_1 = any(rr == 0.0)

        else:
          rr = Cov_All_Models[i]
          bb = All_modelsomega[i]


        rr = array(rr)
        bb = array(bb)

        Condition_2 = all(sign(rr)> 0)
        Condition_3 = all(sign(rr)< 0)

        if Condition_1 == False and Condition_2 == False:
          Cov_0 = 0.0
          lambda0 = All_modelslambda[i][0]
          omega0 = Functions(0.7, 0.3).Nonlinear_Interpolation(bb, rr, Cov_0)
          q0 = omega0/2. - lambda0

          Covariance_Hor.append(Cov_0)
          omega0Covariance_Hor.append(omega0)
          lambda0Covariance_Hor.append(lambda0)
          q0Covariance_Hor.append(q0)

        else:
           pass

        #----------------

      #search of covariance zero by VERTICAL interpolation
      for i in range(len(lamdalist)):

        #----------------

        Condition_1 = any(Cov_All_Models[:,i] == 0.0)
        if Condition_1 == True:
```

```
        rr = Cov_All_Models[:,i]
        bb = All_modelslambda[:,i]

        while Condition_1 == True:
          rr = list(rr)
          bb = list(bb)

          bb.remove(bb[rr.index(0.0)])
          rr.remove(0.0)

          rr = array(rr)
          bb = array(bb)

          Condition_1 = any(rr == 0.0)

      else:
        rr = Cov_All_Models[:,i]
        bb = All_modelslambda[:,i]


      rr = array(rr)
      bb = array(bb)

      Condition_2 = all(sign(rr)> 0)
      Condition_3 = all(sign(rr)< 0)

      if Condition_1 == False and Condition_2 == False:
        Cov_0 = 0.0
        lambda0 = Functions(0.7, 0.3).Nonlinear_Interpolation(bb, rr, Cov_0)
        omega0 = All_modelsomega[:,i][0]
        q0 = omega0/2. - lambda0

        Covariance_Vert.append(Cov_0)
        omega0Covariance_Vert.append(omega0)
        lambda0Covariance_Vert.append(lambda0)
        q0Covariance_Vert.append(q0)

      else:
         pass

      #----------------


    #plt.figure(9)

    Y_Fit, X_Fit = [], []
    lambda0Covariance = lambda0Covariance_Hor + lambda0Covariance_Vert
    omega0Covariance = omega0Covariance_Hor + omega0Covariance_Vert
    lambda0Covariance1 = list(array(lambda0Covariance)*1.0)
```

```
    omega0Covariance1 = list(array(omega0Covariance)*1.0)

    print "lambda0Covariance1 = ", lambda0Covariance1
    print "omega0Covariance1 = ", omega0Covariance1

    for i in range(len(lambda0Covariance_Vert)):
      plt.plot(omega0Covariance_Vert[i], lambda0Covariance_Vert[i], marker='.', color='r')

    for i in range(len(lambda0Covariance_Hor)):
      plt.plot(omega0Covariance_Hor[i], lambda0Covariance_Hor[i], marker='.', color='g')

    for i in range(len(lambda0Covariance)):
      X_Fit.append(min(omega0Covariance1))
      Y_Fit.append(lambda0Covariance1[omega0Covariance1.index(min(omega0Covariance1))])

      lambda0Covariance1.remove(lambda0Covariance1[omega0Covariance1.index(min(omega0Covariance1))])
      omega0Covariance1.remove(min(omega0Covariance1))

    Y_Fit2, X_Fit2 = list(array(lambda0Covariance)*1.0), list(array(omega0Covariance)*1.0)
    X_Fit3, Y_Fit3 = [], []

    for i in range(len(X_Fit2)):
      if X_Fit2[i] == min(X_Fit2) or Y_Fit2[i] == min(Y_Fit2):
        pass
      elif X_Fit2[i] == max(X_Fit2) or Y_Fit2[i] == max(Y_Fit2):
        pass

      else:
        X_Fit3.append(X_Fit2[i])
        Y_Fit3.append(Y_Fit2[i])

    X, Y = [], []
    for i in range(len(X_Fit3)):
      Y.append(min(Y_Fit3))
      X.append(X_Fit3[Y_Fit3.index(min(Y_Fit3))])
      X_Fit3.remove(X_Fit3[Y_Fit3.index(min(Y_Fit3))])
      Y_Fit3.remove(min(Y_Fit3))

    print "len(X) = ", len(X)
    print "len(Y) = ", len(Y)

    print "X = ", X
    print "Y = ", Y
    if omega0_Model < min(X):
      omegalist2 = linspace(omega0_Model-0.02, max(X), 200)

    elif omega0_Model > max(X):
```

```
        omegalist2 = linspace(min(X), omega0_Model+0.02, 200)

    else:
        omegalist2 = linspace(min(X), max(X), 200)

    plt.plot(X, Y, color=couleur)

    Lamdalimit=[]
    omegalist = linspace(min(omegalist), max(omegalist), 200)

    for i in range(len(omegalist)):
        Lamdalimit.append(Functions(0.7, 0.3).NoBigBang(omegalist[i], 'limit'))

    plt.fill_between(omegalist, Lamdalimit, max(Lamdalimit), color=(0.5,0.5,0.5))
    plt.text(0.001, 1.468, 'No Big Bang', color='w')
    plt.text(0.7, 1.32, '($\\Omega_{\\circ}$, $\\lambda_{\\circ}$) = ('+str(omega0_Model)+', '+str(lambda0_Model)+')', color='r')

    plt.plot([omega0_Model],[lambda0_Model], marker='o', color='r')
    plt.xlabel('$\\Omega_{\\circ}$', fontsize=16)
    plt.ylabel('$\\lambda_{\\circ}$', fontsize=16)
    grid(True)

    plt.figure(9)

    Y_Fit, X_Fit = [], []
    lambda0Covariance = lambda0Covariance_Hor + lambda0Covariance_Vert
    omega0Covariance = omega0Covariance_Hor + omega0Covariance_Vert
    lambda0Covariance.append(lambda0_Model)
    omega0Covariance.append(omega0_Model)

    lambda0Covariance1 = list(array(lambda0Covariance)*1.0)
    omega0Covariance1 = list(array(omega0Covariance)*1.0)

    print "lambda0Covariance1 = ", lambda0Covariance1
    print "omega0Covariance1 = ", omega0Covariance1

    for i in range(len(lambda0Covariance_Vert)):
        plt.plot(omega0Covariance_Vert[i], lambda0Covariance_Vert[i], marker='.', color='r')

    for i in range(len(lambda0Covariance_Hor)):
        plt.plot(omega0Covariance_Hor[i], lambda0Covariance_Hor[i], marker='.', color='g')

    for i in range(len(lambda0Covariance)):
        X_Fit.append(min(omega0Covariance1))
```

```
        Y_Fit.append(lambda0Covariance1[omega0Covariance1.index(min(omega0Covariance1))])

        lambda0Covariance1.remove(lambda0Covariance1[omega0Covariance1.index(min(omega0Covariance1))])
        omega0Covariance1.remove(min(omega0Covariance1))

    Y_Fit2, X_Fit2 = list(array(lambda0Covariance)*1.0), list(array(omega0Covariance)*1.0)
    X_Fit3, Y_Fit3 = [], []

    for i in range(len(X_Fit2)):
        if X_Fit2[i] == min(X_Fit2) or Y_Fit2[i] == min(Y_Fit2):
            pass
        elif X_Fit2[i] == max(X_Fit2) or Y_Fit2[i] == max(Y_Fit2):
            pass

        else:
            X_Fit3.append(X_Fit2[i])
            Y_Fit3.append(Y_Fit2[i])

    X, Y = [], []
    #---------
    for i in range(len(X_Fit3)):
        Y.append(min(Y_Fit3))
        X.append(X_Fit3[Y_Fit3.index(min(Y_Fit3))])
        X_Fit3.remove(X_Fit3[Y_Fit3.index(min(Y_Fit3))])
        Y_Fit3.remove(min(Y_Fit3))

    """
    for i in range(len(X_Fit3)):
        X.append(min(X_Fit3))
        Y.append(Y_Fit3[X_Fit3.index(min(X_Fit3))])
        Y_Fit3.remove(Y_Fit3[X_Fit3.index(min(X_Fit3))])
        X_Fit3.remove(min(X_Fit3))
    """
    #------

    print "len(X) = ", len(X)
    print "len(Y) = ", len(Y)

    print "X = ", X
    print "Y = ", Y
    if omega0_Model < min(X):
        omegalist2 = linspace(omega0_Model-0.02, max(X), 200)

    elif omega0_Model > max(X):
        omegalist2 = linspace(min(X), omega0_Model+0.02, 200)

    else:
        omegalist2 = linspace(min(X), max(X), 200)

```

```
    plt.plot(X, Y, color=couleur)

    Lamdalimit=[]
    omegalist = linspace(min(omegalist), max(omegalist), 200)

    for i in range(len(omegalist)):
      Lamdalimit.append(Functions(0.7, 0.3).NoBigBang(omegalist[i
    ], 'limit'))

    plt.fill_between(omegalist, Lamdalimit, max(Lamdalimit), color
    =(0.5,0.5,0.5))
    plt.text(0.001, 1.468, 'No Big Bang', color='w')
    plt.text(0.7, 1.35, '($\\Omega_{\\circ}$, $\\lambda_{\\circ}$)
    = ('+str(omega0_Model)+', '+str(lambda0_Model)+')', color='r')

    plt.plot([omega0_Model],[lambda0_Model], marker='o', color='r'
    )
    plt.xlabel('$\\Omega_{\\circ}$', fontsize=16)
    plt.ylabel('$\\lambda_{\\circ}$', fontsize=16)
    grid(True)

    return OmegaOfGrid, LambdaOfGrid, CorrCoefficient, X, Y

class Save:
  """Registration of all lists and arrays in one file"""
  def __init__(self, listofarrays, stringlistofarrays, filename):

    self.listofarrays = listofarrays
    self.stringlistofarrays = stringlistofarrays
    self.filename = filename

  def ReadWrite(self, header, private_pc):


    path = str(self.filename)

    f = open(path, 'w')
    if header == True:

      for l in range(len(self.stringlistofarrays)):

        listname = self.stringlistofarrays[l]
        listname = str(listname)
        f.write(listname)
        f.write("                    ")

      f.write("\n")

    elif header == False:

      pass
```

```
    length = [len(a) for a in self.listofarrays]
    for i in range(max(length)):

      for l in range(len(self.listofarrays)):

        if i < len(self.listofarrays[l]):
          element = self.listofarrays[l][i]
          element = str(element)
          f.write(element)
          f.write("        ")
        else:
          f.write("Nan")
          f.write("        ")

      f.write("\n")


    f.close()

    print path, "\n"
    return path
```

Listing D.1: Python example

Bibliography

[L. Gerrit 1937] Gerrit L. Verschuur, Interstellar Matters, Essays on Curiosity and Astronomical Discovery, Bowie, MD 20715, USA, Library of Congress Cataloging-in-Publication Data, 1937

[N. Pastorello 2013] N., Pastorello, M., Sarzi, M., Cappellari, E., Emsellem, et al., The planetary nebulae population in the nuclear regions of M31: the SAURON view, Monthly Notices of the Royal Astronomical Society, Volume 430, 2013 ADS-2013MNRAS.430.1219P

[J. B., Kaler 1976] J. B., Kaler, A catalog of relative emission line intensities observed in planetary and diffuse nebulae, Astrophysical Journal Supplement Series, vol. 31, 1976 ADS-1976ApJS...31..517K

[I. Ribas 2005] I. Ribas, C. Jordi, F. Vilardell, et al., First Determination of the Distance and Fundamental Properties of an Eclipsing Binary in The Andromeda Galaxy, Astrophys.J.635:L37-L40,2005 arxiv-0511045

[M.S. Longair 2013] Malcolm S. Longair, Springer Science Business Media, page 4, 14 mars 2013

[E. R. Harrison 1989] Harrison, E. R., The Galactic and Extragalactic Background Radiation. Proceedings of the 139th. Symposium of the International Astronomical Union, held in Heidelberg, FRG, June 12-16, 1989. ADS-1990IAUS..139....3H

[T. Plotner 2008] T. Plotner, The Night Sky Companion, A Yearly Guide to Sky-Watching 2008-2009, 2008

[E. Harrison 2000] Edward Harrison, Cosmology: The Science of the Universe, Cambridge University Press, page 333, 16 mars 2000

[I. Appenzeller 2013] I. Appenzeller, Introduction to Astronomical Spectroscopy, Cambridge university press, 2013

[J. D. Fernie 1969] Fernie, J. D., The period-luminosity relation: A historical review, Publications of the Astronomical Society of the Pacific, Vol. 81, No. 483, p.707, 1969 ADS-1969PASP...81..707F

[H. Nussbaumer 2014] Harry Nussbaumer, Einstein's conversion from his static to an expanding universe, Vol. 39, p. 37-62, European Physics Journal-History, 2014 arxiv-1311.2763

[A. Einstein and W. de Sitter 1932] A. Einstein and W. de Sitter, On the Relation between the Expansion and the Mean Density of the Universe, Proceedings of the National Academy of Sciences of the United States of America, 18, 213-214 (1932)

[G. Lemaitre 1927] G. Lemaitre, Un Univers homogene de masse constante et de rayon croissant rendant compte de la vitesse radiale des nebuleuses extragalactiques, Annales de la Societee Scientifique de Bruxelles, A47, p. 49-59, 1927 ADS-1927ASSB...47...49L

[E. Hubble 1929] E. Hubble, A Relation between Distance and Radial Velocity among Extra-Galactic Nebulae, Proceedings of the National Academy of Sciences of the United States of America, 1929 ADS-1929PNAS...15..168H

[Robert M. Wald 1984] Robert M. Wald., General Relativity. The University of Chicago Press, Chicago and London, 1984

[V. Alpher 2014] Ralph A Alpher, George Antonovich Gamow, and the Prediction of the Cosmic Microwave Background Radiation, Vol. 23, Asian Journal of physics, 2014 arxiv-1411.0172

[P. J. E. Peebles 2014] P. J. E. Peebles, Discovery of the hot Big Bang: What happened in 1948, physics.hist-ph, 2014 arxiv-1310.2146

[A. Coc 2016] A. Coc,, Primordial Nucleosynthesis, Nuclear Physics in Astrophysics VI (NPA6), Journal of Physics: Conference Series 665, 2016 arxiv-1208.4748

[D.J. Fixsen 1996] D.J. Fixsen, E.S. Cheng, J.M. Gales, J.C. Mather, R.A. Shafer, E.L. Wright, The Cosmic Microwave Background Spectrum from the Full COBE/FIRAS Data Set, 1996, Astrophys.J. 473 arxiv-9605054

[C. L. Bennett 2013] C. L. Bennett, D. Larson et al.,NINE-YEAR WILKINSON MICROWAVE ANISOTROPY PROBE (WMAP) OBSERVATIONS: FINAL MAPS AND RESULTS, 2013

[C. A. Bertulani, et al. 2016] C. A. Bertulani and T. Kajino,Frontiers in Nuclear Astrophysics, 2016 arxiv-1604.03197

[G. Steigman 2004] G. STEIGMAN, Big Bang Nucleosynthesis: Probing the First 20 Minutes, Carnegie Observatories Astrophysics Series, Vol. 2: Measuring and Modeling the Universe, ed. W. L. Freedman (Cambridge: Cambridge Univ. Press), 2004

[M. Colless 2003] M. Colless, et al., The 2dF Galaxy Redshift Survey: Final Data Release, Astrophysics (astro-ph), 2003 arxiv-0306581

[J. H. Oort 1932] J. H. Oort. The force exerted by the stellar system in the direction perpendicular to the galactic plane and some related problems. Bull. Astron. Inst. Netherlands, 6 :249, August 1932

[F. Zwicky 1937] F. Zwicky. On the Masses of Nebulae and of Clusters of Nebulae. Astrophysical Journal, Vol. 86, p.217, 1937

[E. Hubble 1934] E. Hubble. The distribution of extra-galactic Nebulae. Astrophysical Journal, vol. 79, p.8, 1934 ADS-1934ApJ....79....8H

[F. Zwicky 1933] F. Zwicky. Republication of: The redshift of extragalactic nebulae, General Relativity and Gravitation, Volume 41, Issue 1, pp.207-224, (original publication: Helvetica Physica Acta, Vol. 6, p. 110-127, 1933) ADS-2009GReGr..41..207E

[Planck Collaboration I (2015)] Planck collaboration, Planck 2015 results. I. Overview of products and scientific results, Astronomy Astrophysics, August 11, 2015 arxiv-1502.01582v2

[Planck Collaboration XIII (2015)] Planck collaboration, Planck 2015 results. XIII. Cosmological parameters, Astronomy Astrophysics, June 20, 2016 arxiv-1502.01589

[A. G. Riess et al. 1998] A. G. Riess et al., Observational Evidence from Supernovae for an Accelerating Universe and a Cosmological Constant. AJ, 116 : 1009-1038, 1998 arxiv-9805201v1

[S. Carroll 2001] Sean M. Carrol., The Cosmological Constant. Living Reviews in Relativity, 4 :1, 2001

[S. Carroll 2004] Carroll, S. M., Why is the Universe Accelerating ? 235-+ Pages of Freedman, W. L. (ed), Astronomical Journal, 2004 Measuring and Modeling the Universe.

[S. Weinberg 1989] Weinberg, S. 1989. The cosmological constant problem. Reviews of Modern Physics, 61 (Jan. 1989), 1-23

[S. Perlmutter et al. 1999] S. Perlmutter et al. and Supernova Cosmology Project. Measurements of Omega and Lambda from 42 High-Redshift Supernovae. ApJ, 517 :565-586, June 1999

[B. Ratra 1988] Ratra, B., and Peebles, P. J. E., Cosmological Consequences of a Rolling Homogeneous Scalar Field, Phys. Rev., 1988 ADS-1988PhRvD..37.3406R

[C. Wetterich 1988] Wetterich, C., Cosmology and the Fate of Dilatation Symmetry, Nucl. Phys., 1988 ADS-1988NuPhB.302..668W

[R. Caldwell 2002] Caldwell, R., A phantom menace? cosmological consequences of a dark energy component with super-negative equation of state, Phys.Lett. B545, 2002

[2003] Caldwell, R. R., Kamionkowski, M., and Weinberg, N. N., Phantom energy and cosmic doomsday, Phys.Rev.Lett. 91, 2003 arxiv-0302506

[T. Chiba et al. 2000] Chiba, T., Okabe, T., and Yamaguchi, M., Kinetically driven quintessence, Phys.Rev.D 62, 2000

[C. Armendariz-Picon 2000] Armendariz-Picon, C., et al., A dynamical solution to the problem of a small cosmological constant and late-time cosmic acceleration, Phys.Rev.Lett. 85, 2000

[2001] Armendariz-Picon, C., Mukhanov, V., and Steinhardt, P. J., Essentials of k-essence, Phys.Rev.D 63, 2001

[W. Hu 1997] Hu W., Sugiyama N. & Silk J., The Physics of Microwave Background Anisotropies, Nature, 386, 1997 arxiv-9604166v1

[Johnson and Morgan 1953] Johnson, H. L. & Morgan W. W., Fondamental stellar photometry for standards of spectral type on the revised system of the Yerkes spectral Atlas, ApJ, volume 117, 1953 ADS-1953ApJ...117..313J

[B. J. Taylor 1986] Taylot, B. J., Transformation equations and other aids for VRI photometry, ApJ, 60, 577-599, 1986 ADS-1986ApJS...60..577T

[D. S., Hayes et al. 1985] Hayes, D. S., Pasinetti, L. E., Philip, A. G. D., Calibration of fundamental stellar quantities, Proceedings of the Symposium, Como, Italy, 1985 ADS-1985IAUS..111.....H

[Bohlin et al. 2004] Bohlin, R. C., Gilliland, R. L., Hubble Space Telescope Absolute Spectrophotometry of Vega from the Far-Ultraviolet to the Infrared, AJ, 127, 2004 ADS-2004AJ....127.3508B

[Fukugita et al. 1996] Fukugita, M., Ichikawa, T., Gunn, J. E., Doi, M., Shimasaku, K., Schneider, D. P., The Sloan Digital Sky Survey Photometric System, AJ, v.111, 1996 ADS-1996AJ....111.1748F

[J. B. Oke et al. 1983] Oke, J. B., Gunn, J. E., Secondary standard stars for absolute spectrophotometry, AJ, v. 266, 1983 ADS-1983ApJ...266..713O

[Rubin et al. 1970] Rubin, Vera C., Ford, W. Kent, Jr., Rotation of the Andromeda Nebula from a Spectroscopic Survey of Emission Regions, Astrophysical Journal, vol. 159, p.379, 1970 ADS-1970ApJ...159..379R

[Triay, R. et al. 1990] G. Bigot, R. Triay, A null correlation technique to determine $q_\circ$, in The quest for the fundamental constants in cosmology, Proc. of the 24th Rencontre de Moriond (9th Moriond Astrophysics Meeting), (1990) 177

[K. Krisciunas 1993] Krisciunas, Kevin, Look Back Time, the Age of the Universe, and the Case for a Positive Cosmological Constant, J. Roy. Astron. Soc. Canada, volume 87, pages 223, 1993 Measuring and Modeling the Universe. arxiv-9306002

[Betoule, M. et al 2014] Betoule, M. et al, Improved cosmological constraints from a joint analysis of the SDSS-II and SNLS supernova samples, Astron. Astrophys, volume 568, pages A22, 2014 arxiv-1401.4064?

[A. G. Petschek 1990] Albert G. Petschek, department of physics, New Mexico Institute of Mining and Technology, USA, Astronomy and astrophysics library, 1990.

[Cappellaro et al 1999] Cappellaro, E. and Evans, R. and Turatto, M., A new determination of supernova rates and a comparison with indicators for galactic star formation, Astronomy & Astrophysics, Volume 351, p.459, 1999

[Lewis et al 2002] Lewis, Antony and Bridle, Sarah, Cosmological parameters from CMB and other data: A Monte Carlo approach, journal Phys. Rev., volume D66, 2002 arxiv-0205436

[Clark et al 1977] Clark, D.H. and Stephenson, F.R., The Historical Supernovae, Pergamon Press; New York, 1977

[Green et al 2003] Green D. A. and Stephenson, F. Richard, The Historical supernovae, Lect. Notes Phys., volume 598, p.7, 2003 arxiv-0301603

[A. V. Filippenko 1997] Alexei V. Filippenko, Optical spectra of supernovae, Annual Reviews, Astronomy and astrophysics, July 5, 1997.

[M. M. Phillips 1993] M. M. Phillips, The absolute magnitudes of Type IA supernovae, Astrophysical Journal, Part 2 - Letters (ISSN 0004-637X), vol. 413, no. 2, p. L105-L108, 1993 ADS-0301603

[Humason, Mayall, & Sandage 1956] Humason M. L., Mayall N. U., Sandage A. R., Redshifts and magnitudes of extragalactic nebulae, Astronomical Journal, Vol. 61, p. 97-162, 1956 ADS-1956AJ.....61...97H

[Oke & Sandage 1968] Oke J. B., Sandage A., Energy Distributions, K Corrections, and the Stebbins-Whitford Effect for Giant Elliptical Galaxies, Astrophysical Journal, vol. 154, p.21, 10-1968 ADS-1968ApJ...154...21O

[Hogg, D. W. 2002] Hogg, D. W., The K correction, astro-ph/0210394v1, 2002 arxiv-0210394v1

[Ross N. P. 2013] Ross N. P., The SDSS-III Baryon Oscillation Spectroscopic Survey: The Quasar Luminosity Function from Data Release Nine, Astrophysical Journal, Volume 773, Number 1, 2013

[Binney & Merrifield, 1998] Binney J., Merrifield M, Galactic Astronomy, Princeton University Press, page 111, 1998

[Colless M., 2005] Colless M., The New Cosmology, World Scientific, page 20, 28 Jun 2005

[Astier P. et al, 2006] Astier P. et al, The Supernova Legacy Survey: measurement of Ω_M, Ω_Λ and w from the first year data, Astronomy & Astrophysical Journal, Volume 447, p.31 - 48, Number 1, February III 2006 ADS-26A...447...31A

[H. Fliche & J. M. Souriau 1979] H.H. Fliche, J.M. Souriau, Quasars et cosmologie, Astron. & Astrophys. **78** (1979) 87

[Wheeler 1990] Wheeler JC., Wheeler et al pp. 1-93, 1990

[C. M. Urry, P. Padovani, 1995] Urry, C. M. and Padovani, P., Unified Schemes for Radio-Loud Active Galactic Nuclei, Publications of the Astronomical Society of the Pacific, v.107, p.803, 1995 ADS-1995PASP..107..803U

[M. Schmidt 1963] Schmidt, M., 3C 273 : A Star-Like Object with Large Red-Shift. Nature 197, 1963 ADS-1963Natur.197.1040S

[R. Antonucci 1993] Antonucci, R., Unified models for active galactic nuclei and quasars, A&A 31, 473-521, 1993

[J. Gunn and B. Peterson 1965] Gunn, J. E. and Peterson, B. A., On the Density of Neutral Hydrogen in Intergalactic Space. ApJ 142, 1633â1641, 1965 ADS-1965ApJ...142.1633G

[E. Momjian et al 2013] Momjian, E. and Carilli, C. L. and Walter, F. and Venemans, B., The Highest Redshift Quasar at $z = 7.085$: A Radio Quiet Source. Astron. J. 147, p.6, 2013 arxiv-1310.7960v1

[D. N. Spergel et al 2013] Spergel D. N. et al, Three-Year Wilkinson Microwave Anisotropy Probe (WMAP) Observations: Implications for Cosmology. Astrophysical Journal, Volume 170, p.377, 2007

[D. Berk, et al 2001] Spergel D. et al, Composite Quasar Spectra from the Sloan Digital Sky Survey. Astronomical Journal, Volume 122, p.549, 2001 ADS-2001AJ....122..549V

[Vicent J. Martinez et al] Vicent J. Martinez, Enn Saar, Enrique Martinez Gonzales, Maria Jesus Pons-Borderia, Data Analysis in Cosmology, 2009

[R. Sharp et al 2001] Sharp R., Hodgkin S., McMahon R., Irwin M., High Redshift Quasars in the ING Wide Field Survey. The ING newsletter, No. 4, p.13 March 2001

[Hamuy et al. 1995] Hamuy, Mario; Phillips, M. M.; Maza, Jose; Suntzeff, Nicholas B.; Schommer, R. A.; Aviles, R. Affiliation: A Hubble diagram of distant type Ia supernovae, Astronomical Journal, vol. 109, no. 1669, p. 1-13, 1995 ADS-1995AJ....109....1H

[1996a] Hamuy, M., Phillips, M. M., Suntzeff, N. B., Schommer, R. A., Maza, J., Aviles, R., The Absolute Luminosities of the Calan/Tololo type Ia Supernovae, Astronomical Journal, volume 112, p.2391, 1996 arxiv-9609059

[Riess et al 1995] Riess, Adam G.; Press, William H.; Kirshner, Robert P., Using type Ia supernova light curve shapes to measure the Hubble constant, Astrophysical Journal, vol. 438, no. 1, p. L17-L20, 1995 arxiv-9410054

[1996a] Riess, Adam G., Press, William H., Kirshner, Robert P., A Precise Distance Indicator: Type Ia Supernova Multicolor Light-Curve Shapes, Astrophysical Journal, volume 473, p.88, 1996 arxiv-9604143

[M. M. Phillips 1999] Phillips, M. M.; Lira, Paulina; Suntzeff, Nicholas B.; Schommer, R. A.; Hamuy, Mario; Maza, José, The Reddening-Free Decline Rate Versus Luminosity Relationship for type Ia Supernovae, Astronomical Journal, Volume 118, Issue 4, page 1766-1776, 1999 arxiv-9907052

[N. B. Suntzeff 1999] Suntzeff Nicholas B., et al Optical Light Curve of the type Ia Supernova 1998BU in M96 and the Supernova Calibration of the Hubble Constant, Astronomical Journal, Volume 117, Issue 3, pp. 1175-1184, 1999 arxiv-9811205

[R. B. Nelsen 1999] Roger B. Nelsen, An Introduction to Copulas, Springer Science Business Media, 1999

[C. Meyer 2009] Christian Meyer, The Bivariate Normal Copula, 15 Dec 2009 arxiv-0912.2816

[G. Bigot & R. Triay 1991] G., Bigot, R.,Triay, "Comments on the V/Vmax test", Physics Letters A, Volume 159, October, 1991

[Schmidt M., 1968] Schmidt, M., Space Distribution and Luminosity Functions of Quasi-Stellar Radio Sources, Astrophysical Journal, vol. 151, p.393, 1968 ADS-1968ApJ...151..393S

[Triay et al 1991] Triay R., Rauzy S., Bigot G., Is evolotion of radio sources necessary?, Physics Letters A, volume 158, p.282-290, 12 July 1991

[Schneider et al 2002] D. P. Schneider et al., The sloan digital sky survey quasar catalog. I. Early Data Release, Astron. J., 123, (2002) 567

[Schneider et al 2003] D. P. Schneider et al., The sloan digital sky survey quasar catalog. II. First Data Release, Astron. J., 126, (2003) 2579

[Abazajian et al 2005] K. Abazajian et al., The Third Data Release of the Sloan Digital Sky Survey, Astron. J., 129, (2005) 1755

[Schneider et al 2005] D. P. Schneider et al., The sloan digital sky survey catalog. III. Third data release, Astron. J., 130 (2005) 367

[Richards et al 2006] G. T. Richards et al., The SDSS Quasar Survey: Quasar Luminosity Function from Data Release Three, Astron. J., 131, (2006), 2766

[Abazajian et al 2009] K. Abazajian et al., The Seventh Data Release of the Sloan Digital Sky Survey, Astron. J. Suppl., 182, (2009) 543

[Schneider et al 2010] D. P. Schneider et al., The sloan digital sky survey catalog. V. Seventh data release, Astron. J., 139, 2010, 2360

[Pâris et al 2010] I. Pâris et al., The sloan digital sky survey catalog: ninth data release, Astron. & Astrophys., 548, 2012

[Guy et al 2010] J. Guy et al., SNLS collaboration, The Supernova Legacy Survey 3-year sample: Type Ia Supernovae photometric distances and cosmological constraints, Astronomy & Astrophysics Journal, Volume 523, 2010, A7 arxiv-1010.4743

[Pritchet 2004] Pritchet, Chris J., SNLS collaboration, The Supernova Legacy Survey, ASP Conf. Ser., Volume 339, pages 60, March 18-20, 2005 arxiv-0406242

[Triay et al 1994] Triay, R., Lachièze-Rey, M., Rauzy, S., On the Malmquist bias in the determination of H_0 and of distances of galaxies, Astronomy & Astrophysics Journal, volume 289, p.19-34, 1994

[Conley et al 2011] Conley, A. et al., SNLS collaboration, Supernova Constraints and Systematic Uncertainties from the First 3 Years of the Supernova Legacy Survey, Astrophysics Journal, volume 192, p. 1, 2011, arxiv-1104.1443

[Sullivan, M. et al 2010] Sullivan, M. et al., SNLS collaboration, The Dependence of Type Ia Supernova Luminosities on their Host Galaxies, Monthly Notices of the Royal Astronomical Society, volume 406, p.782-802, 2010 arxiv-1003.5119

[Tanvir, N. R. et al 2009] Tanvir, N. R. et al., A γ-ray burst at a redshift of z~8.2 , NAT Journal, volume 461, p.1254-1257, 2009 Natur.461.1254T